An Investigation into the Tropospheric Chemistry of Acidic Aerosols and Ammonia in the laboratory

A thesis submitted to
THE NATIONAL UNIVERSITY OF IRELAND

for the degree of
DOCTOR OF PHILOSOPHY

by

Thomas Michael Townsend

Based on research carried out at

Centre for Research into Atmospheric Chemistry
Department of Chemistry
University College Cork

under the supervision of
Prof. John R. Sodeau

Head of Department
Prof. Jeremy D. Glennon

November 2009

Table of Contents

Dedication

'Mammy and Daddy'

'Going with the Flow-Tube'

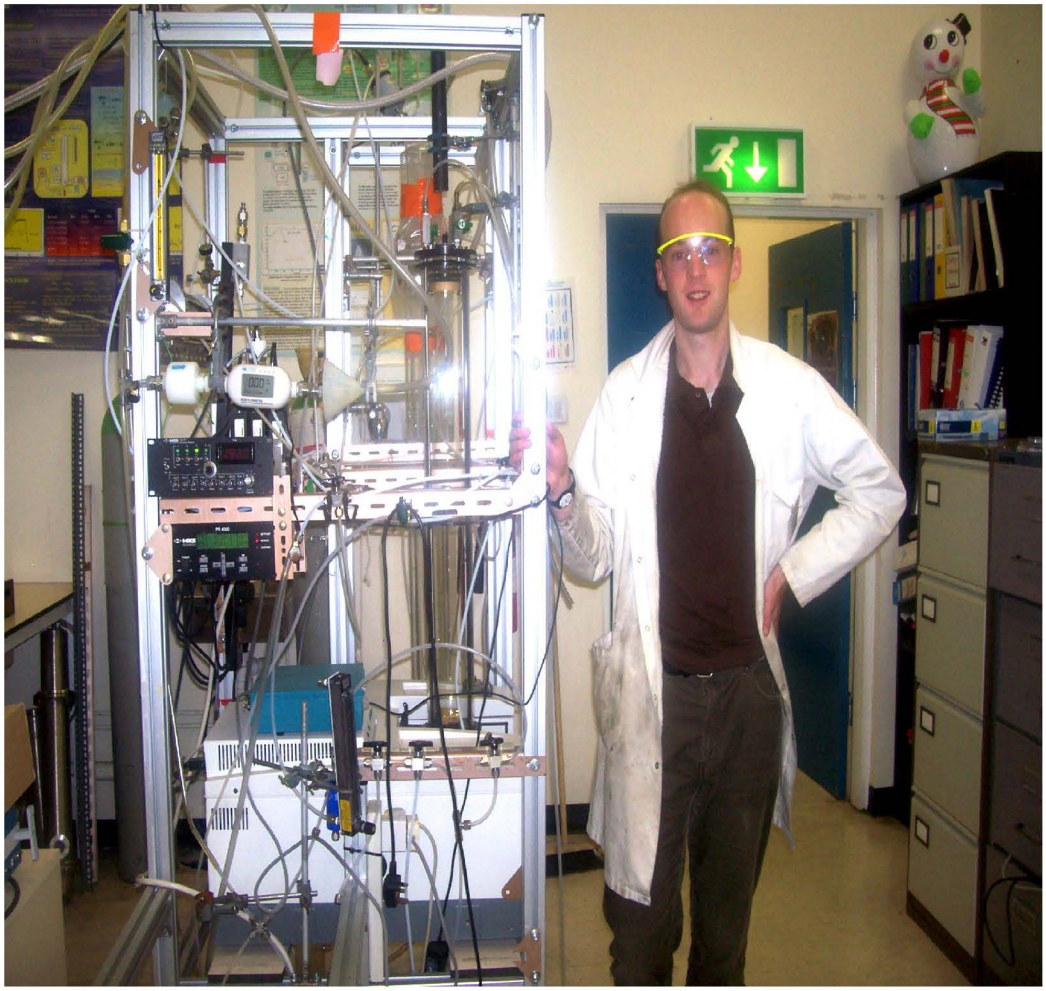

Acknowledgements

So to begin with, I'd like to thank Prof. JRS for his offering of a PhD at the CRAIC Lab, not sure what the 'I' stands for... Also for his assistance, motivation, guidance... no this isn't a joke! ;-) I did learn a lot about research from him though and the world of academia, both highs and lows!!! It's interesting though that he doesn't advertise at NewScientist anymore where I found him!

Now to the labateers, where to start? Well first and foremost Colette for showing me the ropes at the very beginning and helping me tie it all up at the very end. Also Arnaud for the design of the flow-tube and a few useful things here and there towards the end of the work. The other postdocs too were good in their own ways; Stig, Brice, Andy, Jose, Emma I suppose, Virginia, Ivan, Shuming, Iusti and the newly transformed ones: Dave, my fellow Ercan and Rob. Then we have the rest of the Sodeau's, Eoin, Brian, even Paul, that sly snake Ian, Danny sure, the other Dave, Ruairi, Keith and MacGillyCuddyReek. The Wenger bunch fronted by the other John with a foreign surname were a pleasant antidote, we have Ger?, Grainne, Margaret, Perla, Micheal, my counterpart Trevor, Kristine, Mary who I beat to the line, Jenny (who tops the current ranking) and Yang. All the students from home and abroad added to the mix. I mustn't forget the administrative staff, especially Christine, the technical staff for their gossip exchanges and the rest of the academics, most of whom I met only in fancy dress!

My friends who were doing PhDs at the same time were great to have in the same boat (Sairu, Ev and Ruairdri) along with my other pals and housemates from all walks of life who took me away from it all and made me feel human!

Finally my family of course, my sisters Jenny and Rosie, brothers-in-laws Faisal and John, nieces Roisin, Niamh and Laura, nephews Zia and Sam and of course Mammy and Daddy who kept me going during the tough times and doing what parents do.

That's it!

Declaration

I declare that the work contained in this thesis, submitted by me for the degree of Doctor of Philosophy, is my own work, except where due reference is made to other authors, and has not been previously submitted by me for any other degree at this or any other university.

Abstract

This thesis describes a broad range of experiments based on an aerosol flow-tube system to probe the interactions between atmospherically relevant aerosols with trace gases. This apparatus was used to obtain simultaneous optical and size distribution measurements using FTIR and SMPS measurements respectively as a function of relative humidity and aerosol chemical composition. Heterogeneous reactions between various ratios of ammonia gas and acidic aerosols were studied in aerosol form as opposed to bulk solutions. The apparatus is unique, in that it employed two aerosol generation methods to follow the size evolution of the aerosol while allowing detailed spectroscopic investigation of its chemical content. A novel chemiluminescence apparatus was also used to measure [NH_4^+].

$SO_2.H_2O$ is an important species as it represents the first intermediate in the overall atmospheric oxidation process of sulfur dioxide to sulfuric acid. This complex was produced within gaseous, aqueous and aerosol SO_2 systems. The addition of ammonia, gave mainly hydrogen sulfite tautomers and disulfite ions. These species were prevalent at high humidities enhancing the aqueous nature of sulfur (IV) species. Their weak acidity is evident due to the low [NH_4^+] produced. An increasing recognition that dicarboxylic acids may contribute significantly to the total acid burden in polluted urban environments is evident in the literature. It was observed that speciation within the oxalic, malonic and succinic systems shifted towards the most ionised form as the relative humidity was increased due to complete protonisation. The addition of ammonia produced ammonium dicarboxylate ions. Less reaction for ammonia with the malonic and succinic species were observed in comparison to the oxalic acid system. This observation coincides with the decrease in acidity of these organic species. The interaction between dicarboxylic acids and 'sulfurous'/sulfuric acid has not been previously investigated. Therefore the results presented here are original to the field of tropospheric chemistry. SHO_3^-; $S_2O_5^{2-}$; HSO_4^-; SO_4^{2-} and $H_{1,3,5}C_{2,3,4}O_4^-$; $C_{2,3,4}O_4^{2-}$ were the main components found in the complex inorganic-organic systems investigated here. The introduction of ammonia produced ammonium dicarboxylate as well as ammonium disulfite/sulfate ions and increasing the acid concentrations increased the total amount of [NH_4^+].

Chapter 1

Introduction

1.1 Overview

The notion that human activities may endanger the Earth's environment has emerged as a leading societal challenge in the post-industrial era. Under the ever increasing pressures of population growth and economic development, the problems of air pollution have now become matters of both local and global challenge. Sources of man-made pollution have become competitive with nature's own cycles and are threatening to perturb long-established ecological balances at a rapid pace. Smog, acid rain, ozone holes, the greenhouse effect and global warming have become household words and an intense public policy debate about the cost and benefits of environmental protection continues. There is a growing realisation that the consequences of air pollution can be felt in unpredictable ways in near and faraway places. Many cities, such as Kuala Lumpur, now suffer from haze, and ozone depletions are the largest in the Antarctic stratosphere. Over the last three decades many countries have instituted ambient air quality standards designed to mitigate problems of health and welfare associated with the release of chemicals such as sulfur dioxide, nitrogen oxides, hydrocarbons, carbon monoxide and particulate matter. Global agreements to prevent the depletion of the ozone layer and to slow down climatic change are therefore being actively debated and formulated.

All life on planet Earth is dependant on the atmosphere. As well as filtering out harmful UV radiation, it also serves to maintain the ambient temperature by balancing incoming UV with outgoing IR radiation. The main constituents of air are the gases, nitrogen, oxygen, and, to a smaller extent, argon, comprising 99.9% by volume [(1)]. Human activity therefore does not affect the bulk gas concentrations to any significant degree but it is the trace species and aerosols that the influence on humanity is most pronounced. The other atmospheric components include carbon dioxide, whose concentration has been observed to increase significantly in historic times owing to anthropogenic causes. Two centuries of industrial activity have caused a significant shift in the carbon cycle

(approximately 0.04% of the atmosphere), resulting in a 30% increase in carbon dioxide and a more than 100% increase in methane, which is another important trace gas. Water vapour, a particularly variable atmospheric constituent, resides almost entirely in the lower and middle troposphere [(2)]. Other trace gases include ozone, oxides of nitrogen and halocarbons. 'London' smog, as a result of acidic aerosols and soot leading to severe respiratory problems along with excess deaths in the 1950s was a major precursor for atmospheric chemical studies. This was complimented by the 'Los Angeles' haze due to ozone and photochemical oxidants produced in the 1940s that resulted in strongly oxidising, eye-watering and plant-killing pollutants. Today's atmosphere contains a wide range of aerosols and the total tropospheric aerosol burden is thought to be on the increase since pre-industrial times [(3)]. Destruction of stratospheric ozone caused by relatively small atmospheric concentrations of chlorofluorocarbons has vividly illustrated the capacity of human activity to alter our atmosphere in a manner that has significant and far-ranging effects.

During the past two decades, the critical role played by heterogeneous processes, involving trace gas interactions with aerosols and cloud droplets has been a key theme of atmospheric chemistry research. Indeed, heterogeneous processing is now recognised as an important component of the chemistry characterising major environmental issues such as acid deposition (acid rain), stratospheric ozone depletion, tropospheric ozone production and oxidative capacity, along with the formation and growth of tropospheric aerosols. In addition, all of the above are known to impact greatly upon both climate and human health [(1)]. Periods of high mortality and morbidity have been linked to elevated levels of pollution [(4)]. Climate change over the last number of years is assumed to be caused mainly by several anthropogenic perturbations of the atmospheric radiative balance with the increase in greenhouse gases being the dominating process [(3)]. Atmospheric aerosols can directly and indirectly affect the Earth's climate (climate forcing). Direct forcing is induced by scattering and absorption of solar radiation from the particle themselves, giving the atmosphere a 'hazy' appearance and therefore loss

of visibility. The concentration, size and water solubility of cloud condensation nuclei (CCN) have an immediate influence on the concentration and size of water droplets, which in turn determine the radiative properties of clouds indirectly [5] as well as affecting their formation and lifetime. Anthropogenic sulfate aerosols and smoke from biomass burning dominate man-made albedo increases of clouds. However, soot incorporated in sufficient amounts into cloud droplets can reduce albedo [6].

The interaction of trace gaseous species in aqueous acid aerosols and cloud droplets clearly plays a major role in important issues, which have been discussed above, concerning the atmospheric environment. However, an uncertainty in the nature and formation rates of atmospheric particles leads to difficulties in calculating the effects of such particles on these issues. The complexity is compounded by the difficulty in characterising the chemical and physical properties of atmospheric heterogeneous surfaces before performing suitable computational or experimental simulations in the laboratory [7]. Therefore, the need for reliable laboratory measurements, using appropriate mimics and modern equipment, is undeniably clear and it is in this context that the results detailed in this thesis are presented.

1.2 Characteristics of the Atmosphere

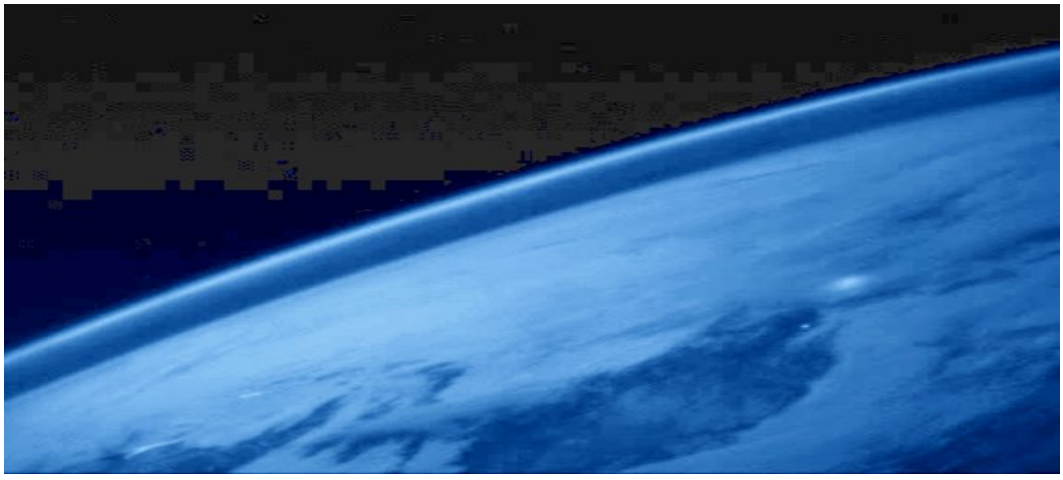

Figure 1.1: The Earth's atmosphere (thin blue line on the horizon).

It is of interest to put the atmosphere in perspective with respect to the size of the Earth itself. The Earth's average diameter is 12,742 km, yet, Earth possesses an atmosphere that extends upwards of only about 120 km and appears as a thin blue line on the horizon when viewed from space as shown in Figure 1.1. (less than 0.4% of the Earth's diameter)! Clearly, the atmosphere is a very thin, fragile shield upon which life depends. The temperature structure of the atmosphere is such that it is often considered to be stratified in the vertical into several layers although integrated between each other by a combination of dynamic and radiative transfer processes (see Figure 1.2) [8].

Extending from the surface to a height of 10 − 15 km, the troposphere is characterised by strong vertical mixing due to the hot lighter air under colder, denser air; species emitted at the surface can rise to the tropopause in a matter of a few days depending on meteorological conditions. Approximately all of the atmospheric water vapour, clouds (including aerosols) and precipitation are found in the Earth's troposphere, which provides an important mechanism for scavenging pollutants from the atmosphere. The lowest part of the troposphere, to be influenced on a daily basis, is called the planetary boundary layer. As its name suggests, its properties are a function of those of the underlying surface.

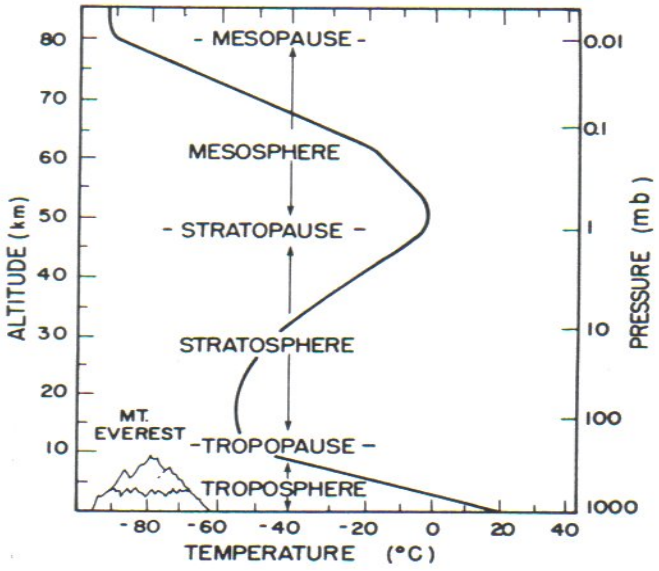

Figure 1.2: Temperature profile of the Earth's atmosphere, adapted from *Way*ne [8].

The tropopause (located at a height of 10 – 15 km depending on latitude and time of year) marks the troposphere's upper boundary, above which lies the stratosphere. Even though in some earlier studies the tropopause was perceived as being a 'barrier' between the lower and upper atmospheres, it has become increasingly clear that the troposphere and stratosphere are intimately connected. This is a quiescent region of the atmosphere, where vertical transport of materials is slow and radiative transfer of energy dominates. An increase in temperature is observed here due to a critical series of reactions involving ozone and molecular oxygen that absorb thermal energy. Subsequent absorption of solar radiation by ozone serves to enhance this effect. In fact, it is in the stratosphere that the bulk of the Earth's ozone content resides, forming a layer that absorbs much of the sun's UV radiation, thereby shielding the Earth's surface below from its effects which would otherwise be damaging to life at the surface.

Above ~ 50 km, the ozone producing reaction becomes unfavourable due to the low density of the atmosphere and the temperature decreases again. This signals the beginning of the mesosphere which extends to an altitude of ~ 90 km and is a region of temperature extremes and strong turbulent motion over large spatial scales. Beyond this, in the thermosphere and the ionosphere, ionisation of the remaining atmospheric species by high energy solar radiation leads to a warming until such time as the atmosphere dissipates completely. In these higher regions, matter exists in an ionised state and becomes particularly reactive with the solar radiation.

1.3 Chemistry of the Troposphere

Although the Earth's atmosphere is predominantly gaseous, with 90% of the atmosphere's bulk residing in the troposphere [(9)], the observations of phenomena such as acid rain and photochemical smogs confirm the role of aerosols in mediating important atmospheric chemical reactions [(10)]. Condensed-phase reactions in the bulk of an aerosol particle and heterogeneous reactions on the

particle surface can provide alternative reaction mechanisms to those which occur in the homogeneous gas-phase. For aerosol chemistry to play a significant role in influencing the chemical balance of the atmosphere there are a number of processes that must occur efficiently when compared to the rates of the corresponding homogeneous gas-phase reactions. These include: {1} the diffusion of reagents in the gas-phase to the particle surface, {2} their subsequent heterogeneous reaction and {3} release of the products from the particle surface into the gas-phase.

Aerosols are defined as stable suspensions of solid or liquid particles in a gas [(1)]. Thus aerosols differ from solid or liquid particles in that an aerosol includes both the particles and the gas in which they are suspended. They are produced in vast numbers by human activity (anthropogenic) but are unmatched on a global scale by natural sources and are subsequently modified by a multitude of complex processes. Aerosols play an important role in air pollution, which is defined as the presence in the atmosphere of a substance in such small amounts as to adversely affect humans, animals, vegetation or materials [(11)]. They are known to be crucially important to many issues that directly affect everyday life (including respiratory health issues, turbidity, visibility, clouds, rainfall, atmospheric chemistry and global and regional climate as well as intensifying the toxic effects of gases such as SO_2 and NO_x) but they also comprise one of the most poorly understood aspects of the atmosphere. These shortcomings in understanding are partly due to the small sizes involved, typically in the order of microns (10^{-6} m) or less, making aerosols difficult to study experimentally. In addition, the processes involved are quite complex due to their wide ranging, composition, varying surface/volume ratio areas and multiphase nature.

1.3.1 Sources, Transformations and Sinks of Aerosols

Aerosols are derived from a number of human activities, mainly, transportation, fuel combustion, industrial processes and solid waste. Construction activity and

agricultural operations also produce significant amounts of airborne particles. Natural sources include mainly wind-blown dust, plant pollen, wildfires, sea spray and volcanoes. Particles may be either directly emitted into the atmosphere or formed there by chemical reactions; these are referred to as primary and secondary particles, respectively. Primary sources include wind-driven erosion, anthropogenic activities, volcanoes and biomass burning, while gas to particle conversion gives rise to secondary particles.

Particles from biomass combustion can be emitted into buoyant plumes and may thus be carried substantial distances. An important source of very small particles in the atmosphere is the conversion of gases. This process is usually accomplished by accretion onto pre-existing tiny particles but can sometimes occur by direct nucleation from the gas-phase. The sulfate ion from sulfuric acid is usually the most abundant species resulting from gas to particle conversion. Because of its extremely low equilibrium vapour pressure, sulfuric acid condenses onto cloud droplets and aerosol particle surfaces. The formation of secondary particulate matter in various size ranges by chemical reactions in the atmosphere may occur by a number of mechanisms. These include {1} reactions of gases to form low vapour pressure products (e.g. reaction of aromatics with OH to form multifunctional oxygenated products) followed by homogeneous nucleation to form new particles or condensation on pre-existing particles along with coagulation between particles, {2} heterogeneous condensation of gases on the surfaces of existing particles to form condensed-phase products (e.g. the reaction of gaseous HNO_3 with sea salt particles to form $NaNO_3$), and {3} chemical reactions within the aqueous phase in fogs, clouds, or aerosol particles (e.g. SO_2 oxidation to sulfate).

The ultimate fate of most particles is their removal from the atmosphere by wet and dry deposition. Acid rain is a form of wet deposition resulting from the atmospheric oxidation of the oxides of sulfur and nitrogen to sulfuric acid and nitric acid, respectively, with atmospheric aerosols playing a significant role in

this process [9]. The oxidation and deposition processes can occur over relatively short distances from the primary pollutant sources or at distances of a 1000 km or more. Aerosols may also act as sinks for new reactive species. As a result of these widespread implications, understanding their direct sources, their formation from chemical reactions in air, their fates, and how their physical and chemical properties determine health, climate and visibility impacts is critical.

1.3.2 Processes and Properties of Aerosols

In the troposphere, man-made sulfate particles and smoke particles from biomass burning are now recognised to have global radiative effects [12] in a term known as 'global cooling' that may have significantly offset the warming induced by the greenhouse gases released in industrial times [13]. They decrease visibility in both urban and rural areas, and they contribute to acid deposition. In addition, atmospheric aerosols may cause adverse health effects and also have a significant affect on human mortality rates. Aerosol particles in the lower troposphere exhibit an average residence time of roughly one week, a sufficient period to allow transport on continental to intercontinental scales, with important resultant influences on global atmospheric processes. Particles may act as sinks for reactive species such as the hydroperoxyl radical, particularly in remote regions, hence affecting the chemistry of the gas-phase as well.

There are a number of properties of particles that control their role in atmospheric processes. These include particle size, chemical composition and morphology. Of these, size is the most fundamental; it is related not only to the source of the particles but also to their effects on health, visibility and climate. In addition, particles can be either dry solid or deliquescent, depending on relative humidity. According to their surface properties, aerosol particles are suspected, and in a number of cases have been shown, to interact with gaseous environmental chemicals, radicals and other reactive intermediates. Knowledge of the physical

state and composition of these particles is of great importance due to the role they play in important atmospheric processes.

1.3.2.1 Size

Particles, or particulate matter, may be solid or liquid, with diameters between ~ 0.002 and ~ 100 μm. The lower end of the size range is not sharply defined because there is no accepted criterion at which a cluster of molecules becomes a particle. The upper end corresponds to the size of fine drizzle or very fine sand; these particles are so large that they quickly fall out of the atmosphere and hence do not remain suspended for significant periods of time. The most important particles with respect to atmospheric chemistry are in the 0.002 – 10 μm range. Aerosols with diameters of 0.1 – 1.0 μm are most effective at extinguishing incoming solar radiation and causing haze. These aerosols are also more detrimental to human health. Some means of expressing the size of such particles is essential since many important properties of the particle such as volume, mass and settling velocity depend on the size. Although most particles are not spherical, it is convenient to designate the size of a particle by its *equivalent radius*, which is the radius of a sphere that experiences the same resistance to motion as the non-spherical particle [(1)]. Under this or any other definition, atmospheric particles cover a truly enormous size range, perhaps four or more orders of magnitude. The atmosphere, whether in remote or urban areas, always contains significant concentrations of particles, up to 10^8 cm^{-3}.

Atmospheric particles are normally separated into different classes according to their size, as ambient particles normally occupy one of four modes, related to their formation process and atmospheric age (Figure 1.3).

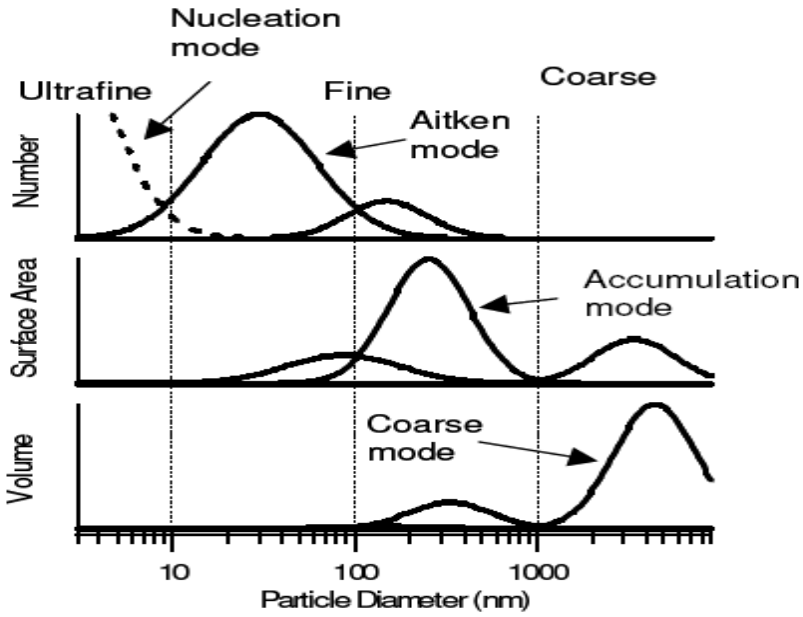

Figure 1.3: A representation of the different classes and types of particles commonly observed in ambient aerosol adapted from *Pitts and Finlayson-Pitts* [(1)]. The lower limit of this graph, 3 nm, is the smallest size observable by currently available commercial instrumentation.

Particles smaller than 0.1 μm are known as ultrafine particles. These are thought to be formed through nucleation processes directly from gas-phase species such as sulfuric acid [(14)]. Because of their small size and mass, these particles are very difficult to study but are normally produced in discrete bursts of very large numbers at their sources. Despite their very low mass, they are extremely significant further downwind when considering particle number concentrations, as these act as seeds for larger particles. Nucleation bursts can arise in the presence of either biogenic or anthropogenic emissions when accompanied by favourable local conditions and form a distinct 'nucleation mode' in the particle size

distribution. These particles diffuse rapidly due to their Brownian velocities and therefore stick easily to any available surfaces through random impactions.

Particles of diameters between 0.01 and 0.1 μm are often referred to as the Aitken mode. These are relatively young particles that can arise from the growth or coagulation of smaller particles. They are also produced in high numbers by primary combustion sources such as vehicle exhausts and are routinely observed as a distinct mode in airborne urban environments. Such particles often continue to grow to accumulation mode sizes through atmospheric processes. Collectively, accumulation and Aitken mode particles are often referred to as 'fine' particles.

The particles of diameters between 0.1 and 2.5 μm are known as the accumulation mode. Much of the accumulation mode mass comes from gas to particle conversion processes within the atmosphere. Accumulation mode particles are generally the most significant when considering gas-phase deposition and atmospheric heterogeneous chemistry, as the majority of the chemically active particulate surface area is normally contained within this mode. They also tend to have long atmospheric lifetimes and frequently act as the nuclei for cloud droplets.

Much of the total suspended particulate (TSP) matter in the atmosphere is composed of so-called coarse particles. These are typically classed as those particles of 2.5 μm (or greater) in diameter and are normally initially suspended in the air through mechanical processes. These origins include spray from bubbles bursting in the sea, dust suspended in the air through wind action and debris from vehicles. The particles in this class are frequently the most important when considering the optical properties of the atmosphere, due to their size. They generally have shorter lifetimes in the atmosphere, compared to other sizes of particle, as they are most readily lost through gravimetric settling, sedimentation and impaction.

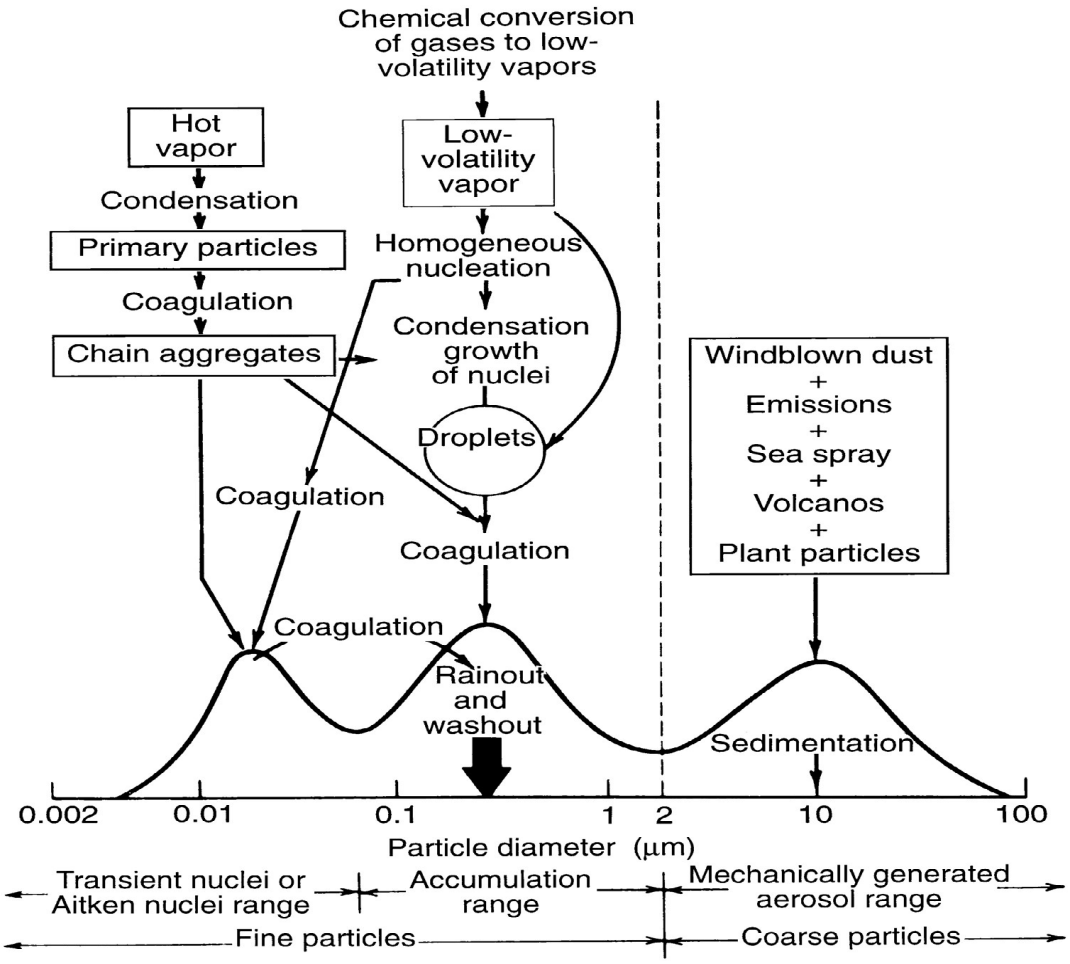

Figure 1.4: Sources, transformations and sinks of aerosol particles in the troposphere [(15)].

In short, particles in the atmosphere are now frequently treated in terms of the modes summarised in Figure 1.4, which shows the major sources and removal processes for each one. Although the vertical axis is not shown, it could in theory be any of the distributions discussed, that is, number, mass, surface area, or volume.

1.3.2.2 Composition

The composition and microphysical properties of aerosols are mainly determined by their sources although other factors contribute significantly such as ageing of the aerosols, relative humidity and the presence of other local aerosol sources and gas emissions. It is important to note that aerosol characteristics vary at different

locations such as urban, rural, forest, marine and remote areas and with meteorological conditions such as precipitation and wind directions. Generally, the smallest ultrafine particles are produced by homogeneous nucleation and tend to contain secondary species such as sulfate and likely organics. Aitken particles tend to be composed of water, inorganic salts, insoluble materials (dust, crustal material), organics (soot, volatile organic compounds (VOC)) and trace metals. The principal components of the fine (accumulation) mode are water; sulfate, nitrate and ammonium ions; organic compounds and black carbon soot. Inorganic salts comprise 25 – 50% of dry total fine aerosol mass [16] and together with water make up a significant portion of the total aerosol mass (especially in high relative humidity environments). The inorganic salts found are mainly those of ammonium, sodium, nitrate and chloride. Total particle concentrations are fairly uniform throughout the tropical regions, and range between 100 to 300 particles cm^{-3} [17]. Finally, because mechanical processes are largely responsible for coarse particles larger than about 2.5 μm, these larger particles typically contain sea salt and elements present in soil. Based on their major chemical composition, tropospheric aerosols can be divided into the following five main categories: sulfuric aerosols (mainly SO_4^{2-}); black and organic carbon aerosols; dust; sea salt; and nitrate containing aerosols. However, aerosols that are a mixture of the above-mentioned chemical components are commonly observed in the troposphere. The complexity is compounded by the difficulty in characterising the chemical and physical properties of atmospheric heterogeneous surfaces and then reproducing suitable simulations in the laboratory; concentration and pressure being two obvious problems [7].

With water being ubiquitous in the atmosphere, all aerosol particles contain an aqueous component. A general aerosol particle may consist of solid aggregates of solid salts in equilibrium with aqueous dissolved species. Surrounding these aggregates is the aqueous medium, which acts to hold the aggregates together. The water content of the aerosol is dependant on the relative humidity (RH), defined as the ratio of the water vapour density to the saturation water vapour

density and usually expressed as a percentage. When RH increases to a threshold value, crystalline aerosol salt particles spontaneously absorb water to form aqueous saline droplets of increased volume, a process referred to as deliquescence [18] in contrast to hygroscopicity which exhibits no phase change. Conversely, when RH decreases, aqueous saline aerosol particles firstly reduce in size, due to evaporation, and finally crystallise at a certain threshold value. This process is called efflorescence. The threshold values of deliquescence relative humidity (DRH) and efflorescence relative humidity (ERH) are not equal, leading to a hysteresis effect (a supersaturated solution) in which particles at a given humidity may be crystalline or aqueous depending on the atmospheric temperature and RH history of the air mass (see Figure 1.5). Sodium chloride has a deliquescence point of 75 %RH at which point it absorbs water forming a hydrated salt solution.

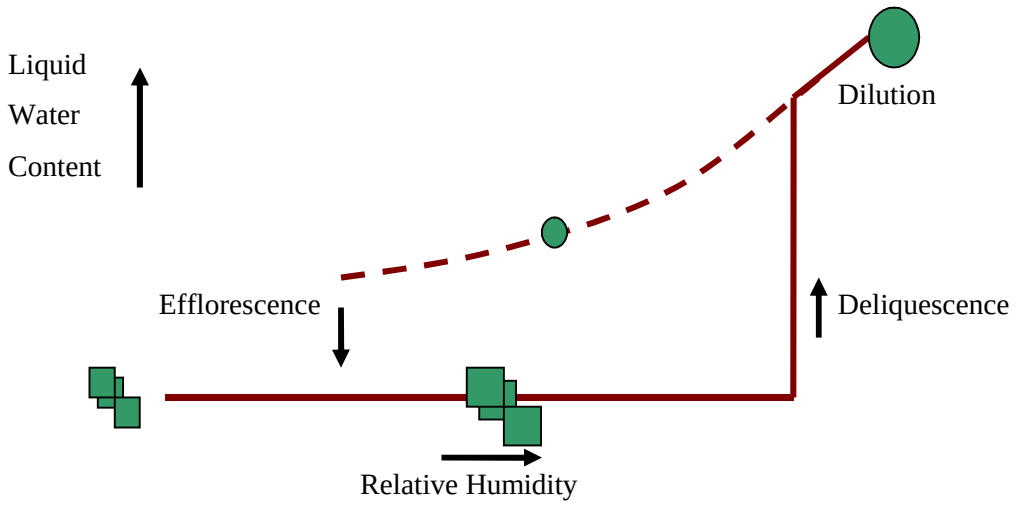

Figure 1.5: Generalised hysteresis curve for deliquescence and efflorescence adapted from *Reid* [10] .

1.3.2.3 Morphology

The physical state of aerosol particles is of substantial interest with regard to their microphysical aerosol behaviour. In atmospheric particles, the stoichiometry of the droplets is unlikely to correspond precisely to the crystallising solid, therefore,

liquid usually remains upon crystallisation. Most of the aerosol particles present in the troposphere are not expected to become totally dry and solid, but rather to form a mixed phase, containing a solid- and a remaining liquid-phase [19]. The morphologies of these particles may be complex and diverse. The principal morphological structures are illustrated in Figure 1.6 which displays a single crystal (I), an agglomerate of single crystals or a polycrystalline solid (II), a polycrystalline material with several open cavities filled with liquid (III), a solid polycrystalline shell with embedded liquid (IV), a solid single-crystalline shell with embedded liquid (V), a single crystal with surrounding liquid (VI), a polycrystalline solid with surrounding liquid (VII) and a totally liquid aerosol particle (VIII) [20]. Work using electron microscopy indicates that atmospheric aerosol particles indeed occur as complex aggregates with all kinds of different morphologies [21]. The morphology of particles have been observed by optical microscopy and various forms of electron microscopy, for example in combustion aerosols containing elemental carbon with traces of sorbed compounds, in fly-ash particles of characteristic morphology, in sea-salt particles with nitrate on the surface, and in solid graphitic or other core particles surrounded by sulfate containing droplets or crystalline layers. Direct observation of individual particles, their physical shape, and the heterogeneous nature of the distribution of species has provided both for identification of chemical species and some indication of the mechanisms by which they were formed.

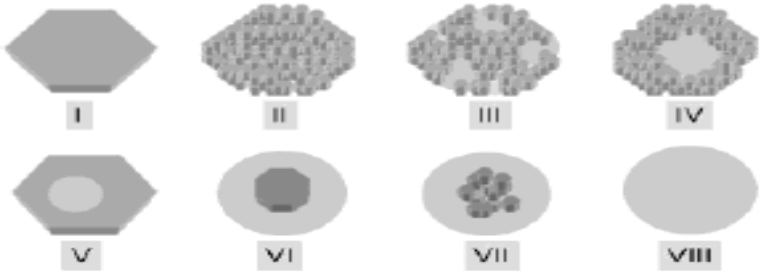

Figure 1.6: Possible structures of aerosol particles [19]. Morphological differences are displayed: (I) single crystal; (II) agglomerate of single crystals, respectively, a polycrystalline solid; (III) polycrystalline material with several open but liquid-filled cavities; (IV) solid polycrystalline shell with embedded liquid; (V) solid single-crystalline shell with embedded liquid; (VI) single crystal with surrounding liquid; (VII) polycrystalline solid with surrounding liquid; (VIII) liquid aerosol particle. It must be pointed out that the polycrystalline materials might contain different solids.

1.3.3 Atmospheric constituents

Most chemical constituents are emitted into the atmosphere at the Earth's surface through natural processes such as volcanoes and geochemical cycles and also, increasingly, through anthropogenic (agricultural and technological) activities. Generations of human beings, in all parts of the world, have been changing their environment through forest removal and many other kinds of land use. Today, industrial activities cause large perturbations on the chemistry of the atmosphere so that, for instance, worldwide emissions of sulfur and nitrogen compounds are now dominated by the burning of fossil fuels.

1.3.3.1 Sulfuric acid and Sulfates

The recognition of acid deposition, commonly called 'acid rain' has a long history. In his 1872 book *Air and Rain: The beginnings of a Chemical Climatology*, Robert Angus Smith coined the infamous term and described many of the factors affecting it, such as coal combustion and the amount and frequency of precipitation. The oxidation of SO_2 to sulfuric acid is potentially damaging to the environment, the two most serious influences appearing to be on fresh water fish and forest ecology as discussed by the British National Research Council [(22)]. Anthropogenic pollution, principally from fossil fuel combustion, is the dominant source of atmospheric SO_2, with natural sources only accounting for ~ 10% of the atmospheric concentration (volcanic eruptions and the oxidation of dimethyl sulfide ($S(CH_3)_2$) in the marine environment).

That the oxidation proceeds more rapidly under conditions of high humidity or when condensed water is available, suggests that oxidation can be mediated by aqueous atmospheric aerosol particles. The gas-phase oxidation of SO_2 is initated by reaction with hydroxyl radicals. Oxidation in the aqueous phase, present in the troposphere in the form of aerosol particles, clouds and fogs, is also important. SO_2 from the gas-phase dissolves in these water droplets and may be oxidised

within the droplet by such species as H_2O_2, O_3, O_2 and free radicals (involving transfer of sulfur dioxide and oxidant species to the droplet phase with subsequent liquid phase oxidation). A schematic diagram involving these oxidation processes is shown in Figure 1.7.

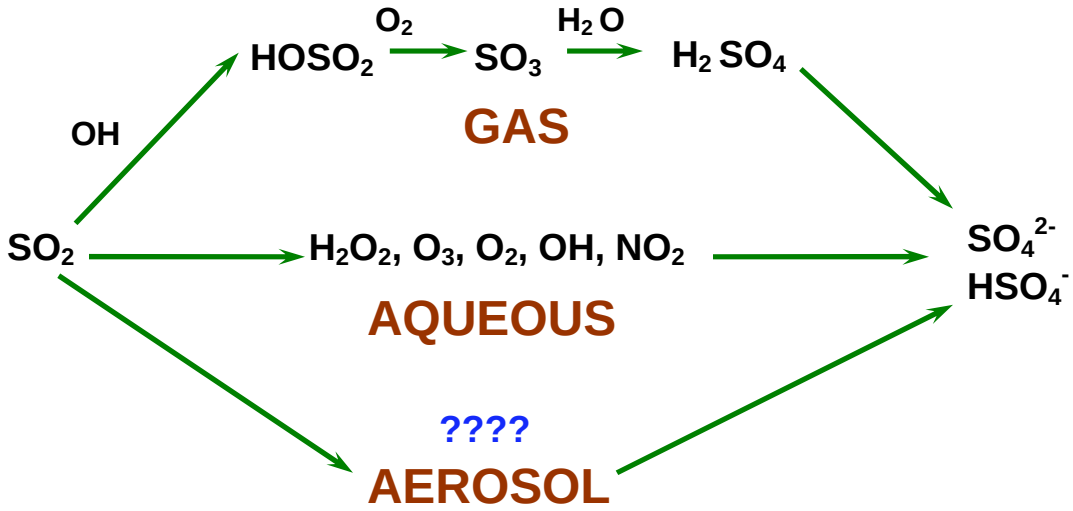

Figure 1.7: Schematic pathway illustrating the formation of sulfate in the atmosphere.

In practice, only a limited number of processes involving several oxidising species take place at a rate sufficient to influence the atmospheric burden of sulfate. The rate of photochemical oxidation by the hydroxyl radical usually exceeds the rate of other pathways as investigated by Stockwell and Calvert [(23)]. The surface of carbonaceous particles and hygroscopic aerosols such as sodium chloride have also been associated with sulfur dioxide oxidation [(24)]. These oxidation processes can lead to highly acidic fogs. For example, pH values as low as 1.69 have been measured in coastal regions of southern California [(25)]. These high acidities, accompanied by high concentrations of other anions and cations, are likely due to the evaporation of water from fog droplets, leaving very high concentrations of ions in a strongly acidic liquid phase. Such acid fogs are a major health concern because the droplets are sufficiently small to be inhaled. Sulfuric acid, which after formation from SO_2 oxidation, can undergo binary nucleation with water under the following conditions: {1} High rate of gas phase oxidation of SO_2 and high H_2SO_4 formation rate; {2} High humidity; {3} Low pre-existing particle surface area available for condensation of newly formed H_2SO_4 and {4}

Low temperature. This gas to particle conversion may occur in the air outflowing from clouds, where these conditions are favourable [26],[27].

1.3.3.2 'Sulfurous acid' and Sulfites

Sulfurous acid (H_2SO_3) has never been characterised or isolated on Earth. This is related to the unfavourable conditions for the hydration product of SO_2 within the atmosphere. Such conditions (high temperature, water content and oxidation ability), however, can be found on the Jupiter moons Io and Europa [28]. Hydrated sulfur dioxide ($SO_2.H_2O$) is an important species as it represents the first intermediate in the overall oxidation of sulfur dioxide to sulfuric acid in the atmosphere. Equation 1-1 shows the initial facile interaction with water forming hydrogen sulfonate (HSO_3^-) and bisulfite ($OHSO_2^-$) ions, together termed as hydrogen sulfite (SHO_3^-).

$$SO_2 + H_2O \rightleftharpoons HSO_3^-, OHSO_2^- (SHO_3^-) + H^+ \qquad \textit{(1-1)}$$

$$K_a = 1.54 \times 10^{-2} \text{ L mol}^{-1}; \; pK_a = 1.81.$$

The hydrogen atom in the hydrogen sulfonate ion is bonded to the sulfur atom and not to an oxygen atom (e.g. bisulfite) as is more usual in the case of oxoanions. This has been shown in the solid state by x-ray crystallography and in aqueous solution by Raman spectroscopy (ν(S–H) = 2500 cm^{-1}). The hydrogen sulfonate-bisulfite tautomers are, however, acidic according to the following equilibrium:

$$SHO_3^- \rightleftharpoons SO_3^{2-} + H^+ \qquad \textit{(1-2)}$$

$$K_a = 1.02 \times 10^{-7} \text{ L mol}^{-1}; \; pK_a = 6.97.$$

At high concentrations of this ion in solution the equilibrium in Equation 1-3 becomes important; the equilibrium constant for dimerisation was measured to be $K_c = 8.8 \times 10^{-2}$ L mol^{-1} in 1 M $NaClO_4$ solution at 25 ºC [29].

$$2SHO_3^- \rightleftharpoons S_2O_5^{2-} + H_2O \qquad \textit{(1-3)}$$

The chemistry of aqueous solutions of SO_2 is surprisingly complicated and frequently misunderstood [30]. Some claim [31],[32] that sulfurous acid, H_2SO_3, is a product of the solvation of SO_2, others [33],[34] take the bisulfite ion, HSO_3^-, as the product of the primary dissociation of the system. In fact there is no experimental evidence for H_2SO_3 in water solution [35],[36] and the ion HSO_3^- could be less abundant than another isomer, $HOSO_2^-$, as studies of solutions of $NaHSO_3$ suggest [37]. A further relevant property of the SO_2 solution is its formation of the clathrate hydrate, $SO_2.7H_2O$, at 7 º C and a SO_2 pressure of 1 bar [38].

Early infrared studies found that the spectra of aqueous SO_2 solutions resemble the summation of the spectrum of liquid SO_2 and that of water [39]. Other reactions are also possible, as shown below, in a solution of SO_2 because they are suggested to take place in a solution of HSO_3^- containing salts [40].

$$HSO_3^- \leftrightarrow HOSO_2^- \qquad \textit{(1-4)}$$

$$HSO_3^- + HOSO_2^- \leftrightarrow [I] \quad = \text{Golding's Dimer (Figure 1.8)} \qquad \textit{(1-5)}$$

$$[I] \leftrightarrow H_2O + S_2O_5^{2-} \qquad \textit{(1-6)}$$

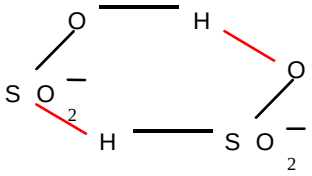

Figure 1.8: Golding's dimer (the red bonds between atoms represent hydrogen bonds).

This 'sulfurous acid' system from perspective of the $SO_2.H_2O$ complex will be discussed in Chapter 3 of this thesis.

1.3.3.3 Nitric acid and Nitrates

The formation of nitric acid (HNO_3) aerosols can be attributed to the presence of reactive nitrogen (abbreviated NO_y) in the atmosphere. Reactive nitrogen is traditionally defined as the sum of the simple oxides of nitrogen (NO_x) and their atmospheric products. The emission of reactive nitrogen to the troposphere occurs primarily as NO and NO_2. The important sources of NO_x are combustion of fossil fuel and biomass, lightning and biological activity. Nitric acid can be introduced to the atmosphere from sources of combustion such as industry and car exhausts but the amounts generated by these means are small. Nitric acid in the troposphere exists mainly due to its formation from free nitrogen. Figure 1.9 illustrates the various pathways associated with the formation of HNO_3 in the atmosphere.

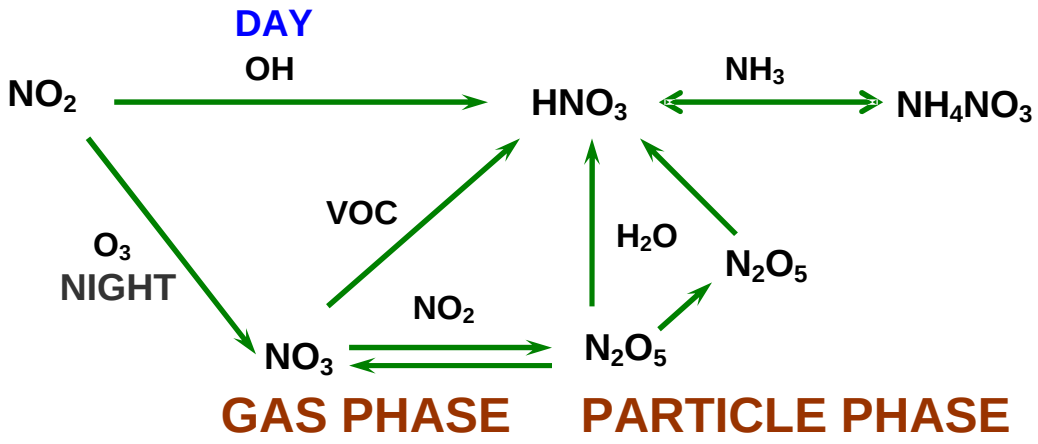

Figure 1.9: Schematic pathway illustrating the formation of nitric acid in the atmosphere.

The main production of nitric acid is based on reaction of NO_2 with the hydroxyl radical and ozone. The former takes place by day while the latter reactant forms the nitrate radical (NO_3) and occurs only at night time since the species is easily photolysed during the day. NO_3 can then react with hydrocarbons to produce HNO_3. The other main route, again involving NO_3, is through dinitrogen pentoxide (N_2O_5) and subsequent hydrolysis. In the upper troposphere, nitric acid constitutes the major component of NO_y and its main sink is thought to be provided by its uptake to cirrus cloud. However, uptake of HNO_3 is inefficient

and subsequently the nitric acid is lost from the atmosphere by precipitation, another cause of acid rain [41].

Nitric acid mixing ratios range between 100 and 2000 ppmv, in the upper troposphere, with the largest values influenced by fast vertical transport from the planetary boundary layer. The relatively high upper tropospheric nitric acid mixing ratio indicates a large rate for NO recycling from gaseous nitric acid, and possibly also an increased efficiency of aerosol activation, which may lead to an increased albedo of cirrus clouds [42].

Nitric acid is a 'sticky' molecule and readily absorbs to surfaces, particularly if there is water present, which is essentially always the case in the troposphere. Because of this, it undergoes dry and wet deposition rapidly with deposition velocities between 1 – 5 cm s^{-1}, at the highest end of the range of those measured for various gases in the troposphere.

1.3.3.4 Ammonia

Ammonia (NH_3), and its protonated form, the ammonium ion (NH_4^+), are important atmospheric components, NH_3 being the most abundant alkaline component in the atmosphere [43]. Ammonia is a key player in the partitioning of atmospheric sulfates and nitrates, and yet very few studies to date have been dedicated to elucidating its heterogeneous behaviour. The relevance of ammonia to the atmospheric environment lies not only in its contribution to N deposition to land surfaces and water bodies, which often leads to euthrophication and/or acidification [44]. It also has the capacity to neutralise atmospheric acids. A substantial part of the acid generated in the atmosphere, by the oxidation of sulfur dioxide (SO_2) and nitrogen oxides (NO_x), is neutralised by ammonia as attested by the high concentration of particulate ammonium in the troposphere [1]. Ammonium aerosols have a longer residence time in the atmosphere than gases and can be transported and dispersed over greater areas [45]. Gaseous NH_3 is very

stable as regards oxidation in the atmosphere and is extremely soluble in water. However, its lifetime is limited due to a very effective heterogeneous conversion to particulate matter in the form of the NH_4^+ ion. Gaseous NH_3 is removed from the atmosphere by the following three methods: wet deposition (remote sources), dry deposition (local sources), both of a non-chemical nature and reactions with acid species to form aerosols. Virtually all NH_3 and NH_4^+ (collectively termed NH_x) emission occurs in the form of NH_3, with NH_4^+ ion in the atmosphere originating from reactions of NH_3.

Gaseous ammonia is released at the Earth's surface primarily through the decomposition of organic matter, both from agricultural practices on land (80 – 90% of total NH_3 emissions in Europe [46] such as sludge spreading, sewage works, livestock and fertilisers and from ocean surface waters. Diurnal and seasonal variations in emission rates also occur. Direct industrial sources, including fossil fuel combustion, as well as natural processes in the soil, are probably relatively insignificant on a global scale [47]. Globally, a flux of 40×10^{12} g per year has been estimated for emissions from land as reported from oceanographic and geophysical sources [48],[49]. This gas therefore represents a significant pollutant in Ireland. These emissions are of the same order of magnitude as the NO_x-N emissions on both global and European scales. NH_3 emissions are estimated to have doubled since 1950. Recent tunnel studies have highlighted that an increasing contribution to ammonia emissions comes from petrol-engine vehicles equipped with three-way catalytic convertors, which generate ammonia as a by-product of the reaction between NO and H [50]. These findings have been confirmed by measurements of very high NH_3 concentrations in the urban area of Rome, Italy [51] and showed a close link between NH_3 and CO temporal patterns.

The role of ammonia in neutralising acidic aerosols has received considerable attention in literature concerning environmental acidification and the health effects of atmospheric aerosols [52]. If NH_3 is absorbed into aerosols, it raises the

pH of those aerosols, which enhances the rate of oxidation of dissolved sulfur dioxide (SO_2) by ozone (O_3) to form sulfate (SO_4^{2-}) [53]. High concentrations of NH_3 are also important for ammonium nitrate (NH_4NO_3) formation [54], although the affinity of sulfuric acid (H_2SO_4) for NH_3 exceeds that of nitric acid (HNO_3). The sulfur budget in particular is greatly affected, as both $(NH_4)HSO_4$ (acidic) and $(NH_4)_2SO_4$ (neutral) are stable [55]. In contrast ammonium nitrate tends to be shortlived and can re-evaporate into its original gas phase constituents (i.e. NH_3 and HNO_3). Although NH_3 can neutralise acidic species in the atmosphere, when NH_3 or NH_4^+ ions are deposited on ecosystems they have an acidifying effect [43]. Excessive deposition of these components can lead to the formation of nitric acid in the soil thus shifting plant species to more nitrophilic ones and exerting other ecological impacts.

The global percentages for conversion and deposition of primary emitted and oxidised secondary species of NH_x are presented in Figure 1.10.

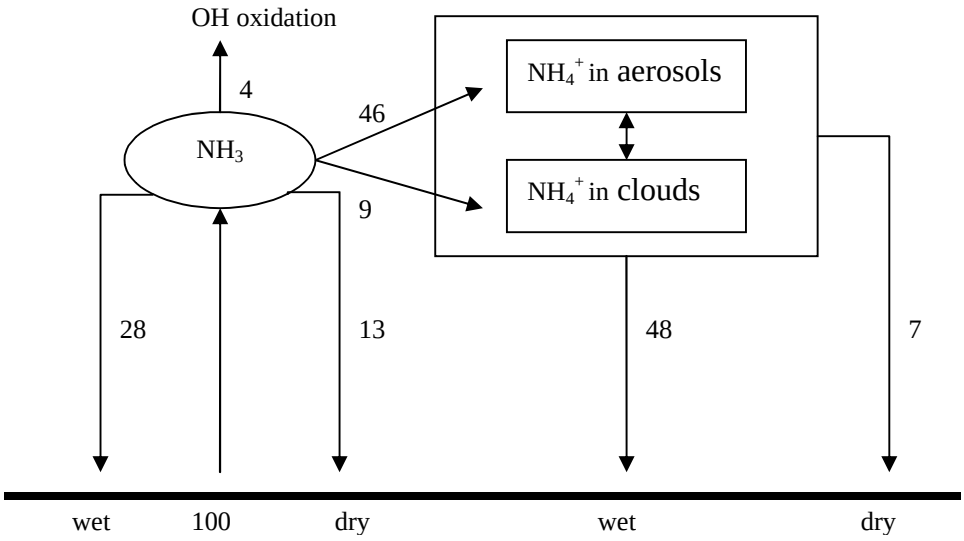

Figure 1.10: Fate of emitted NH_3, data in % of NH_3 emission [56].

These NH_x figures, based on global calculations using the Moguntia CTM (**M**odel **o**f the **G**lobal **Uni**versal **T**racer transport **I**n the **A**tmosphere, Chemical Tracer Model) [56], are virtually identical to those found for SO_2 dry (28%) and wet

deposition (12%). They are also relatively identical to the figures for SO_2 conversion to sulfate (60%), derived using a simple kinetic model [57]. This suggests a close relationship between NH_x and SO_x with regard to atmospheric conversion and deposition as ammonium sulfate. The presence of H_2SO_4/NH_4HSO_4 or $(NH_4)_2SO_4$, as a major component of ambient light scattering aerosols, has been established in a number of locations. $(NH_4)_2SO_4$ has been frequently observed in the Midwestern and southern United States [58], suggesting that there is often sufficient NH_3 present in ambient air to completely neutralise sulfuric acid aerosols. The ratio of NH_4^+ ions to SO_4^{2-} ions varied from 1.0 to 2.1 in particles collected at Meadview, Arizona, with an average value of 1.46 [59]. Consistent with this degree of neutralisation of the sulfuric acid was an average ratio of H^+ to SO_4^{2-} of 0.54.

1.3.3.5 Organics and Dicarboxylic acids

It has been long perceived that the major acids contributing to acid deposition in the troposphere were the inorganic sulfuric and nitric acids. However, there is an increasing recognition that organic acids may contribute significantly to the total acid burden and indeed may represent the majority of acidic species even in polluted urban environments. Organic material is a major component of natural and anthropogenic atmospheric aerosols [60]. In the past few decades, hundreds of organic species found in atmospheric particles have been identified, although the majority or organic aerosol mass often remains unspecified [60],[61],[62],[63]. Hence, there has been a renewed interest in the sources and fates of surface active organic molecules due to their potential impact on gas-aerosol interfacial chemistry. They also make an important contribution to the modification of radiative properties and indirect aerosol forcing [64]. However, the nature of the individual sources of these organic constituents and their relative contributions are not well established.

The major organic acids found in the gas-phase are formic acid (H_2CO_2) and acetic acid ($H_4C_2O_2$), with smaller contributions from aliphatic acids and

multifunctional acids such as pyruvic acid ($H_4C_3O_3$) and glyoxalic acid ($H_2C_2O_3$) [65]. Formic and acetic acids have sufficiently high vapour pressures that they are found almost exclusively in the gas-phase. A variety of dicarboxylic acids have been measured in air including, for example, oxalic acid ($H_2C_2O_4$), malonic acid ($H_4C_3O_4$) and succinic acid ($H_6C_4O_4$), as well as larger straight- and branched-chain carboxylic acids; unsaturated and aromatic acids such as phthalic acid are also observed in smaller concentrations [66]. Due to their lower vapour pressures, they are found predominantly in aerosol particles.

Low molecular weight dicarboxylic acids and their salts are highly water soluble and have been found in both the liquid (cloud, precipitation and fog) and particulate phases in the atmosphere [66]. Dicarboxylic acids are present in the atmosphere as gases, adsorbed on particles as well as being dissolved in rainwater and on snow crystals [67]. Of these dicarboxylic acids, oxalic is generally the most abundant succeeded by malonic and succinic acid in atmospheric aerosols ([68],[69]). These compounds are hygroscopic [70] and have recently received much attention due to their potential effects on direct cloud formation [71],[72]. The sodium salts of the dicarboxylic acids have been found to be as hygroscopic as NaCl and $(NH_4)_2SO_4$ salts [73] and can also potentially act as cloud condensation nuclei (CCN). Their presence alters the chemical and physical properties of atmospheric aerosols [74]. The effect is important, as the water soluble properties of organic aerosols indirectly control solar radiation of the Earth's atmosphere, thus cooling the Earth surface. Aerosols produced by anthropogenic activity could reduce the effect of global warming caused by greenhouse gases on a global scale [64]. Dicarboxylic acids can also reduce surface tension of particles to form CCN [67]. Oxalic acid is a likely end product of photochemical oxidation reactions between organic precursors of both anthropogenic and biogenic origin and can accumulate in the atmosphere [68]. It is very stable, existing in fine particulate matter form and hence, the only removal mechanism for it, is by wet deposition.

The sources of atmospheric dicarboxylic acids include direct emissions from fossil fuel combustion, oceanic emissions and photochemical oxidation of organic precursors of both anthropogenic and biogenic origin [75],[68],[66]. Oxalic acid is mainly produced from biomass burning, vehicle exhaust emissions and biogenic activity associated with plants and micro-organisms in the soil [76]. Although oxalate ions seem to engage in the metabolism and adaptation of animals, plants and fungi, their mechanism are far from being completely understood [77]. Plants can emit fatty acids which may be broken down to form oxalic acid in the atmosphere as a secondary pollutant as explained by Kawamura and Sakaguchi [78]. Soil metabolic processes can play a role in oxalic acid production through the hydrolysis of oxaloacetate from citric acid and the glyoxalate ions [79]. Anthropogenically, small diacids are directly emitted from combustion processing of fossil fuels and subsequent conversion to carboxylic acids and carbonyls in the atmosphere by photochemical oxidation of anthropogenic organic precursors such as aromatic hydrocarbons [1]. Very high concentrations of oxalic acid were detected in biomass burning plumes, suggesting that either oxalic acid is directly emitted or formed in the plume from biogenic precursors [80]. It has been shown that pyruvic acid and methylglyoxal, formed by the oxidation of isoprene, act as intermediates for the in-cloud formation of oxalic acid [81],[82]. Analysis of polar aerosols, in determining the gas/aerosol distribution of oxalic acid, recorded a gas-phase concentration of 23 ± 15 ng m^{-3} and aerosol concentration of 68 ± 40 ngm^{-3} [83]. In Hong Kong, urban aerosols collected and analysed, displayed levels of oxalate to be on average 370 ng m^{-3} and levels of malonate as ~ 90 ng m^{-3} [84].

Particles sampled from biomass burning and regional haze in Rondonia, Brazil, showed that dicarboxylic acids were mostly confined to the particulate phase, with oxalic acid, in particular, appearing as the major identified particulate organic species (mass concentrations of 3.8 μg m^{-3}). When organic acids were present as ammonium salts, their contribution to the total aerosol mass increased even more (e.g. 5.2 μg m^{-3} for oxalic acid as ammonium oxalate) [85]. A study looking at the similarity of the size distributions of oxalate and ammonium ions

suggested that ammonium oxalate aerosol may be directly formed from the gaseous precursors: ammonia and oxalic acid [86]. In agreement with other observations, the oxalate fraction in processed particles exceeds the fractions of other dicarboxylic acids, since it represents an end product in the oxidation of several organic gas-phase species [81].

Organics that have long chain non-polar groups attached to polar tails can form a surface film on droplets by lining up with the polar ends in the water and nonpolar, hydrophobic ends projecting into air [1],[86]. These organic films have the following effects: {1} Reduction of the rate of evaporation of water from the droplets; {2} Inhibition of the transport of stable molecules and of highly reactive free radicals such as OH and HO_2 from the gas phase into the droplet (possibly reducing their roles in atmospheric aqueous phase oxidations such as conversion of SO_2 to H_2SO_4 [87]) and {3} Reduction of the efficiency with which the particles are scavenged by larger cloud and rain droplets. Thus the presence of organic films may increase the lifetime of such particles in the atmosphere compared to those expected if the films were not present [88],[89].

Figure 1.11 is a typical example of an organic film structure.

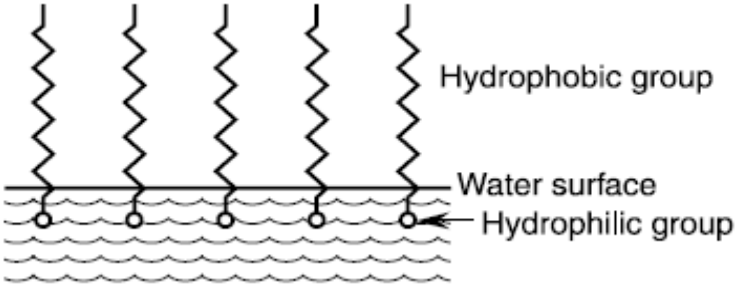

Figure 1.11: Basic structure of an organic film [1].

1.3.4 Kinetic parameters

The term ‘heterogeneous’, when applied to the atmosphere, refers to multiphase chemistry that occurs on or within condensed-phases which are in contact with the gaseous phase. Examples of condensed-phases found in the atmosphere are liquid aerosols, such as sulfuric acid, sea spray and cloud droplets, and solid atmospheric particulate such as soot, mineral dust or frozen water containing particles such as cirrus clouds. Heterogeneous chemistry, both in the troposphere and in the laboratory, involves a series of processes which combine to determine the overall rate of transport and chemical reaction between the gas- and condensed-phases [(90)]. These complex reactions take place at the gas-solid or gas-liquid interface and are made up of several elementary physico-chemical processes, such as gas-phase diffusion towards the surface of interest, determined by the gas-phase diffusion coefficient (D_g) and the gas-surface collision frequency given by the kinetic molecular theory, the mass accommodation rate, the desorption rate from the surface back to the gas-phase, the chemical reaction rate at the interface, ‘the fourth phase’, depending on particle surface area, the diffusion into the bulk of the condensed-phase and possible chemical reactions within the bulk condensed phase depending on particle surface volume. Any one process can act in a rate-determining way and equal rates of uptake and evaporation can occur in a dynamic equilibrium.

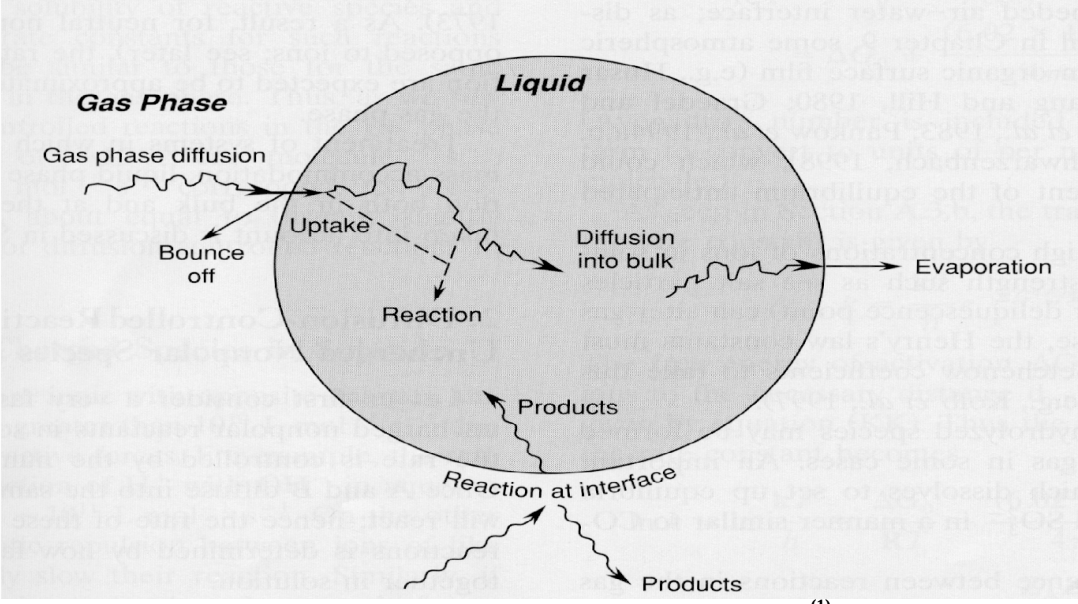

Figure 1.12: Processes occurring at the gas-solid or gas-liquid interface [(1)].

These processes are represented in Figure 1.12. Many parameters are employed to quantify heterogeneous interactions between the condensed-phase and gases. The main cited parameters are the mass accommodation coefficient, the reaction probability, and the net uptake coefficient [(1),(91)]. As used in this study, the mass accommodation coefficient, α, is defined as the fraction of gas- and condensed-phase collisions that result in reversible uptake and does not account for molecules that adsorb/condense and desorb/re-evaporate into the gas-phase over the timescale of an experiment. Mass accommodation coefficients of SO_2, HNO_3, NO_2 and NH_3 have been determined previously [(92)]. The reaction probability, γ_{rxn}, is the fraction of gas-and condensed-phase collisions that lead to irreversible uptake through chemical reaction. The net uptake coefficient, γ_{net} or γ_{meas}, is a measure of the net uptake of gas, normalised to the number of gas- and condensed-phase collisions. The net uptake coefficient depends on gas transport to the interface, mass accommodation and reaction probability.

The resistance model of gas uptake is a simplified representation based on an electrical circuit analogue shown schematically in Figure 1.13 [93]. Each process is expressed as a resistance term which represents its uptake-limiting effect, relative to the overall process. In employing this electrical circuit analogy, the processes can then be combined in series or in parallel to obtain the overall rate of the heterogeneous process.

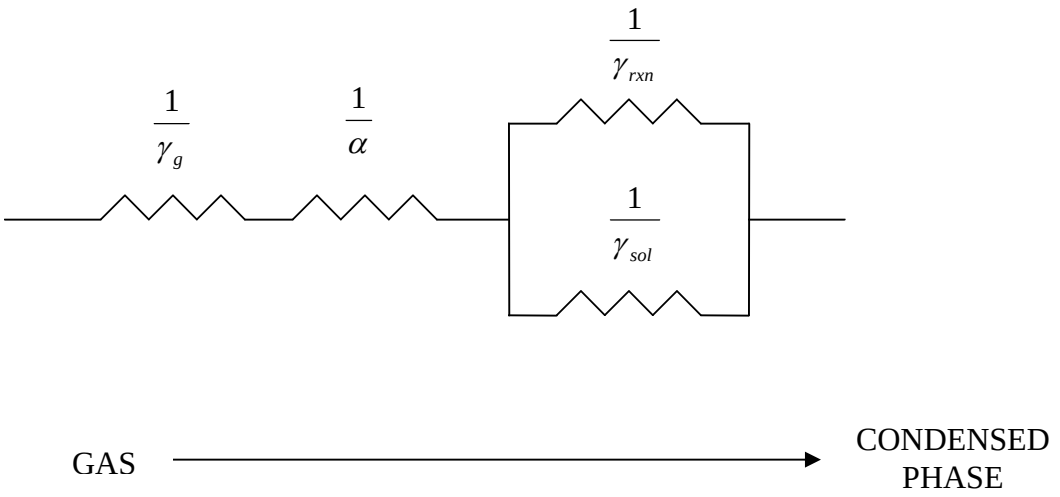

Figure 1.13: Simplified representation of the resistance model of gas uptake [93].

Referring to Figure 1.13, the resistances $1/\gamma_g$ and $1/\alpha$ represent the effect of gas transport and surface accommodation, respectively. The resistances $1/\gamma_{sol}$ and $1/\gamma_{rxn}$ are associated with liquid solubility and reaction, respectively. The overall resistance can be expressed as:

$$\frac{1}{\gamma_{meas}} = \frac{1}{\gamma_g} + \frac{1}{\alpha} + \frac{1}{(\gamma_{sol} + \gamma_{rxn})} \qquad \textit{(1-7)}$$

where resistances are expressed as dimensionless uptake coefficients. Inspection of (1.7) shows that γ_{meas} may approach the value of the mass accommodation coefficient, α depending on the relative sizes of γ_g, γ_{sol} and γ_{rxn}.

The mass accommodation coefficient, α, is the fundamental parameter that measures the rate at which molecules cross the interface between the gas- and condensed-phase.

$$\alpha = \frac{No.\ of\ gas\ molecules\ absorbed\ by\ the\ condensed\ phase / unit\ time}{No.\ of\ gas\ molecules\ collisions\ with\ the\ condensed\ phase / unit\ time} \qquad \textit{(1-8)}$$

The magnitude of α determines the maximum rate of mass transfer and is a measure of transport in one direction only. The *net* uptake of material by the condensed-phase is normally much smaller, due to evaporation from the surface. The rate of loss of a molecule to the surface, as a first-order term k_{het} (units: s^{-1}), is given by Equation 1-9 where <c> is the root-mean-square molecular velocity (units: cm s^{-1}) of the gas-phase molecules striking the surface, and S_a is the surface area of aerosol particles per unit volume of atmosphere.

$$k_{het} = 0.25\,\gamma\,\langle c \rangle\,S_a \qquad \textit{(1 -9)}$$

1.4 Thesis overview

The aim of this thesis is to elucidate some fundamental mechanistic understanding of the interactions between ammonia (trace gas) and acidic aerosols, namely sulfuric, 'sulfurous', nitric, oxalic, malonic and succinic aerosols, using a novel laboratory based flow-tube reactor. The current chapter outlines the principal issues facing atmospheric scientists today and how this thesis fits into the overall picture regarding the global compositional change phenomenon. Chapter 2 introduces the apparatus designed, developed and used to acquire the data presented in the subsequent chapters. Chapter 3 involves the study of 'sulfurous acid' with ammonia using FTIR spectroscopy, NO_x chemiluminescence and a scanning mobility particle sizer. Chapter 4 deals with the addition of oxalic acid to 'sulfurous acid' and ammonia. The three main dicarboxylic acids; oxalic, malonic and succinic acid are investigated with ammonia in Chapter 5. This is finally followed by the interaction of sulfuric acid with these organic aerosols in

Chapter 6. Reactions involving dicarboxylic acids and their interaction with inorganic acids and ammonia have not previously been investigated, a unique area of research undertaken in this study.

1.5 References

(1) Finlayson-Pitts, B. J.; Pitts Jr., J. N. *Chemistry of the Upper and Lower Atmosphere*; Academic Press, 2000.

(2) Singh, H. B. *Composition, Chemistry and Climate of the Atmosphere*; Van Nostrand Reinhold, 1995.

(3) Houghton, J. T. Y. Ding, D. J. Griggs, M. Noguer, P. J. van der Linden, X. Dai, K.; Maskell, A. C. A. J. "Climate Change 2001: The Scientific Basis. Contribution of Working Group I to the Third Assessment Report of the Intergovernmental Panel on Climate Change,' Cambridge University Press, 2001.

(4) Bowler, C.; Brimblecombe, P. *Journal of the Society of Archivists* **1992**, *13*, 136-142.

(5) Twomey, S. *Atmospheric Aerosols*; Elsevier, 1977.

(6) Tuohy, C. H.; Clarke, A. D.; Warren, S. G.; Radke, L. F.; Charlson R. J. *Journal of Geophysical Research* **1989**, *94*, 8623-8631.

(7) Kolb, C. E. D. R.; Worsnop, M. S.; Zahniser, P.; Davidovits, L. F.; Keyser, M.-T.; Leu, M. J.; Molina, D. R.; Hanson, A. R. R. L. R. Williams and M. A. Tolbert. *Progress and Problems in Atmospheric Chemistry*, 1994.

(8) Wayne, R. P. *Chemistry of Atmospheres*; Oxford University Press, 2000.

(9) Seinfeld, J. H.; Pandis, S. N. *Atmospheric Chemistry and Physics*; Wiley-Interscience, 1997.

(10) Reid, J.; Sayer, R. *Science Progress* **2002**, *85*, 263-296.

(11) Williamson, S. J. *Fundamentals of Air Pollution*; Addison-Wesley, 1973.

(12) Charlson, R. J.; Schwartz S. R., Hales, J. M.; Cess, R. D.; Coakley, J. A. Jr.; Hansen, J. E.; Hofmann, D. J. *Science* **1992,** *255***,** 423-430.

(13) Houghton, J. T.; Jenkins, G. T.; Ephraums, J. J. *IPCC (Intergovernmental Panel on Climate Change) 'The Scientific Assessment'*; Cambridge University Press, 1990.

(14) Kulmala, M.; Korhonen, P.; Napari, I.; Karlsson, A.; Berresheim, H.; O'Dowd, C. D. *Journal of Geophysical Research-Atmospheres* **2002**, *107*, 8111.

(15) Whitby, K. T.; Sverdrup, G. M. *Advanced Environmental Science & Technology* **1980**, *8*, 477-525.

(16) Heintzenberg, J. *Ambio* **1989**, *18*, 50-55.

(17) Fitzgerald, J. W. *Atmospheric Environment Part A-General Topics* **1991**, *25*, 533-545.

(18) Martin, S. T. *Chemical Reviews* **2000**, *100*, 3403-3453.

(19) Colberg, C. A.; Krieger, U. K.; Peter, T. *Journal of Physical Chemistry A* **2004**, *108*, 2700-2709.

(20) Weis, D. D.; Ewing, G. E. *Journal of Geophysical Research-Atmospheres* **1999**, *104*, 21275-21285.

(21) Pinnick, R. G.; Auvermann, H. J. *Journal of Aerosol Science* **1979**, *10*, 55-74.

(22) British National Research Council.

(23) Stockwell, W. R.; Calvert J. G. *Atmospheric Environment* **1983**, *17*, 2231.

(24) Harrison, R. M.; Van Grieken, R. E. *Atmospheric Particles*; John Wiley and sons, 1998.

(25) Jacob, D. J.; Hoffman, M. R. *Journal of Geophysical Research* **1983**, *88C*, 6611-6621.

(26) Hoppel, W. A.; Frick, G. M.; Fitzgerald, J. W.; Larson, R. E. *Journal of Geophysical. Research* **1994**, *99*, 14443-14458.

(27) Coffmann, D. J.; Hegg, D. A. *Journal of Geophysical Research* **1995**, *100*, 7147-7160.

(28) Voegele, A. F.; Loerting T.; Tautermann, C. S.; Hallbrucker, A.; Mayer E.; Liedl, K. R. *Icarus*, **2004,** *169***,** 242-249.

(29) Connick, R. E.; Tam, T. M; von Deuster, E. *Inorganic Chemistry*, **1982**, *21*, 103-107.

(30) Zhang, Z.; Ewing, G. E. *Spaectrochimica Acta. Part A* **2002**, *58* 2105-2113.

(31) Zumdahl, S. S.; Zumdahl, S. A. *Chemistry*; 5th Edition, 2000.

(32) Jones, L.; Aitkins, P. *Chemistry, Molecules, Matter and Change*; 4th Edition, 2000.

(33) Ebbing, D. D.; Gammon, S. D. *General Chemistry*; 6th Edition, 1999.

(34) Silberberg, M. S. *Chemistry, The Molecular Nature of Matter and Change*; 2th Edition, 2000.

(35) Falk, M.; Giguere, P. A. *Canadian Journal of Chemistry* **1958**, *36*, 1121.

(36) Davis, A. R.; Chatterjee, R. M. *Journal of Solution Chemistry* **1975** *4 (5)*, 399-412.

(37) Horner, D. A.; Connick, R. E. *Inorganic Chemistry* **1986**, *25*, 2414.

(38) Davidson, D. W. *Water: A Comprehensive Treatise* **1973**, *2*.

(39) Jones, L. H.; McLaren E. *Journal of Chemical Physics* **1958**, *28*, 995.

(40) Golding, R. M. J*ournal of the Chemical Society* **1960**, 3711.

(41) Brown, M. P.; Austin, K. *The New Physique*, **1997**, 25-40.

(42) Schneider, J.; Arnold, F.; Burger, V.; Droste-Franke, B.; Grimm, F.; Kirchner, G.; Klemm, M.; Stilp, T.; Wohlfrom, K. H.; Siegmund, P.; van Velthoven, P. F. J. *Journal of Geophysical Research* **1998**, *103*, 25337-25343.

(43) Asman, W. A. H.; Sutton, M. A.; Schjorring, J. K. *New Phytologist* **1998**, *139*, 27-48.

(44) Fowler, D.; Sutton, M. A.; Smith, R. I.; Pitcairn, C. E. R.; Coyle, M.; Campbell, G.; Stedman, J. *Environmental Pollution* **1998**, *102*, 337-342.

(45) Aneja, V. P.; Roelle, P. A.; Murray, G. C.; Southerland, J.; Erisman, J. W.; Fowler, D.; Asman, W. A. H.; Patni, N. *Atmospheric Environment* **2001**, *35*, 1903-1911.

(46) Perrino, C.; Catrambone, M. *Atmospheric Environment* **2004**, *38*, 6667-6672.

(47) Sutton, M. A.; Dragosits, U.; Tang, Y. S.; Fowler, D. *Atmospheric Environment* **2000**, *34*, 855-869.

(48) Wheeler, P. A.; Kirchman, D. L.; Landry, M. R.; Kokkinakis, S. A. *Limnology Oceanography* **1989**, *34*, 1025-1033.

(49) Dawson, G. A. *Journal of Geophysical Research* **1977**, *21*, 3125-3133.

(50) Kean, A. J.; Harley, R. A.; Littlejohn, D.; Kendall, G. R. *Environmental Science & Technology* **2000**, *34*, 3535-3539.

(51) Perrino, C.; Catrambone, M.; Di Bucchianico, A. D. M.; Allegrini, I. *Atmospheric Environment* **2002**, *36*, 5385-5394.

(52) Suh, H. H.; Spengler, J. D.; Koutrakis, P. *Environmental Science & Technology* **1992**, *26*, 2507-2517.

(53) Asman, W. A. H.; Janssen, A. J. *Atmospheric Environment* **1987**, *21*, 2099-2119.

(54) Russell, L. M.; Pandis, S. N.; Seinfeld, J. H. *Journal of Geophysical Research-Atmospheres* **1994**, *99*, 20989-21003.

(55) Brost, R. A.; Delany, A. C.; Huebert, B. J. *Journal of Geophysical Research-Atmospheres* **1988**, *93*, 7137-7152.

(56) Dentener, F. J.; Crutzen, P. J. *Journal of Geophysical Research-Atmospheres* **1993**, *98*, 7149-7163.

(57) Muller, J. F.; Brasseur, G. *Journal of Geophysical Research-Atmospheres* **1995**, *100*, 16445-16490.

(58) Weiss, R. E.; Waggoner, A. P.; Charslon, R. J.; Ahlquist, N. C. *Science* **1977**, *195*, 979-981.

(59) Turpin, B. J.; Saxena, P.; Allen, G.; Koutrakis, P.; McMurry, P.; Hildemann, L. *Journal of the Air & Waste Management Association* **1997**, *47*, 344-356.

(60) McMurry, P. H.; Woo, K. S.; Weber, R.; Chen, D. R.; Pui, D. Y. H. *Philosophical Transactions of the Royal Society of London Series A - Mathematical Physical and Engineering Sciences* **2000**, *358*, 2625-2642.

(61) Jacobson, M. C.; Hansson, H. C.; Noone, K. J.; Charlson, R. J. *Reviews of Geophysics* **2000**, *38*, 267-294.

(62) Andrews, E.; Saxena, P.; Musarra, S.; Hildemann, L. M.; Koutrakis, P.; McMurry, P. H.; Olmez, I.; White, W. H. *Journal of the Air & Waste Management Association* **2000**, *50*, 648-664.

(63) Turpin, B. J.; Saxena, P.; Andrews, E. *Atmospheric Environment* **2000**, *34*, 2983-3013.

(64) Huebert, B. J.; Bates, T.; Russell, P. B.; Shi, G.; Kim, Y. J.; Kawamura, K.; Carmicheal, G.; Nakajima, T. *Journal of Geophysical Research* **2003**, *108*, 8623.

(65) Kawamura, K.; Ng, L. L.; Kaplan, I. R. *Environmental Science and Technology* **1985**, *19*, 1082-1086.

(66) Kawamura, K.; Kasukabe, H.; Barrie, L. A. *Atmospheric Environment* **1996**, *30*, 1709-1722.

(67) Kawamura, K.; Kobayashi, M.; Tsubonuma, N.; Mochida, M.; Watanabe T.; Lee, M. *Geochemical Society* **2004**, *9*.

(68) Chebbi, A.; Carlier, P. *Atmospheric Environment* **1996**, *30*, 4233-4249.

(69) Saxena, P.; Hildemann, L. M. *Journal of Atmospheric Chemistry* **1996**, *24*, 57-109.

(70) Peng, C.; Chan, M. N.; Chan, C. K. *Environmental Science & Technology* **2001**, *35*, 4495-4501.

(71) Shulman, M. L.; Jacobson, M. C.; Carlson, R. J.; Synovec, R. E.; Young, T. E. *Geophysical Research Letters* **1996**, *23*, 277-280.

(72) Cruz, C. N.; Pandis, S. N. *Atmospheric Environment* **1997**, *31*, 2205-2214.

(73) Peng, C. G.; Chan, C. K. *Atmospheric Environment* **2001**, *35*, 1183-1192.

(74) Saxena, P.; Hildemann, L. M.; McMurray P. H.; Seinfeld, J. H. *Journal of Geophysical Research* **1995**, *100*, 18755-18770.

(75) Kawamura, K.; Kaplan, I. R. *Environmental Science & Technology* **1987**, *21*, 105-110.

(76) Yao, X.; Fang, M.; Chan C. K.; Ho, K. F.; Lee, S.C. *Atmospheric Environment* **2004**, *38*, 963-970.

(77) Claistan, M. *Turkish Journal of Zoology* **2000**, *24*, 103-106.

(78) Kawamura, K.; Sakaguchi, F. *Journal of Geophysical Research* **1999**, *104*, 3501-3509.

(79) Dutton, M.V.; Evans, C. S. *Canadian Journal of Microbiology* **1996**, *42*, 881-895.

(80) Jaffrezo, J. L.; Davidson, C. I.; Kuhns, H. D.; Bergin, M. H.; Hillamo, R.; Maenhaut, W.; Kahl, J. W.; Harris, J. M. *Journal of Geophysical Research-Atmospheres* **1998**, *103*, 31067-31078.

(81) Ervens, B.; Feingold, G.; Frost, G. J.; Kreidenweis, S. M. *Journal of Geophysical Research-Atmospheres* **2004**, *109*.

(82) Lim, H. J.; Carlton, A. G.; Turpin, B. *Journal of Environmental Science & Technology* **2005**, *39*, 4441-4446.

(83) Limbeck, A.; Puxbaum, H.; Otter, L.; Scholes, M. C. *Atmospheric Environment* **2001**, *35*, 1853-1862.

(84) Yao, X. H.; Fang, M.; Chan, C. K.; Ho, K. F.; Lee, S. C. *Atmospheric Environment* **2004**, *38*, 963-970.

(85) Falkovich, A. H.; Graber, E. R.; Schkolnik, G.; Rudich, Y.; Maenhaut, W.; Artaxo, P. *Atmospheric Chemistry and Physics* **2005**, *5*, 781-797.

(86) Lefer, B. L.; Talbot, R. W. *Journal of Geophysical Research-Atmospheres* **2001**, *106*, 20365-20378.

(87) Gill, P. S.; Graedal, T. E.; Weschler, C. J. *Journal of Geophysical Research. Space Physics* **1983**, *21*, 903.

(88) Chameides, W. L.; Davis, D. D. *Journal of Geophysical Research* **1982**, *87*, 4863.

(89) Toosoi, R.; Novakov, T. *Atmospheric Environment* **1985**, *19*, 125.

(90) Cox, R. A.; Plane, J. M. C. "An Introduction to Chemical Kinetics in the Atmosphere"; ERCA, 1996, Grenoble, France.

(91) Kolb, C. E. W. D.; Zahniser, M. S. ; Davidovits, P. ; Keyser L. F. et al. *Advanced Series of Physical Chemistry* **1995**, *3*, 771-875.

(92) Ponche, J. L.; George, Ch.; Mirabel, Ph. *Journal of Atmospheric Chemistry* **1993**, *16*, 1-21.

(93) Shi, Q.; Jayne, J. T.; Kolb, C. E.; Worsnop, D. R.; Davidovits, P. *Journal of Geophysical Research-Atmospheres* **2001**, *106*, 24259.

Chapter 2

Experimental Techniques and Methodology

2.1 Introduction

Heterogeneous reactions are those which occur between different phases such as gases and either solids or liquids. Reactions of this type have long been known to play a vital role in the chemistry of the atmosphere. Major developments in the experimental techniques employed in the study of these reactions have occurred as a result of the recognition of the importance of condensed- phases in the troposphere. For example the oxidation of SO_2 to sulfuric acid [(1)], leads to the detrimental sink known familiarly as 'acid rain' [(2)]. Although a significant amount of research has focused on heterogeneous chemistry over the last two decades, due to the complexities involved, this field is still in its infancy, especially when compared to the study of homogeneous gas-phase atmospheric chemistry.

The formation and growth of aerosols in the troposphere can impact climate change (coined popularly as 'global warming') and human health so it will become necessary to study these reactions in considerably more detail presently. For example the solubilities and fates of many trace gaseous species in aqueous and aqueous acid (principally sulfuric and nitric acid) aerosols and cloud droplets need to be addressed in relation to the atmospheric environment.

The next section describes the instrumentation employed in this particular study of heterogeneous reactions relevant to atmospheric chemistry, with flow-tube methods being of central interest to the studies presented in this thesis. A brief history of the instrumentation developed is initially given and following this, the aerosol flow-tube used here to study the interaction of trace gases with atmospherically relevant aerosols, is then described.

2.1.1 Experimental Methods

The increasing recognition of the importance of aerosols to our understanding of air pollution and climate change has resulted in rapid advances in the development of sophisticated instrumentation in recent years. The main objective of laboratory investigations is to 'mimic' the multiphase interactions in the atmosphere and to understand the kinetics and mechanisms of these processes at a molecular level. Data obtained include vapour pressures of multi-component condensed-phases, solubility coefficients and the kinetics of phase change in addition to the primary requirement of reaction data relevant to heterogeneous processing. The reaction rate at a surface is described in terms of the uptake coefficient, γ (as previously mentioned in Chapter 1), and measurement of this quantity in the laboratory provides a basis for quantitative treatment of heterogeneous reactions in atmospheric models. Also, when taken in conjunction with theoretical models of the reaction system, information on the mechanisms of the reactions can be deduced. If the fundamental parameters such as the Henry's law constants, diffusion coefficients and rate coefficients are known, extrapolation to the atmosphere can be carried out reliably and with reasonable accuracy.

The general approach to studying heterogeneous reactions is mainly related to the kinetic behaviour of gas-phase species upon varying total surface areas. This has led to the development of Knudsen cells, falling-droplet apparatus, bubble apparatus, liquid jet apparatus and aerosol chambers. For example, the uptake kinetics of methanesulfonic acid and glyoxal by aqueous solutions were studied as a function of temperature using the droplet train technique combined with mass spectroscopy and FTIR detection [(3)]. There are, however, techniques that focus on changes in the condensed-phase also, such as DRIFTS, electrodynamic balances and surface science apparatus. The instrumentation used in the current research work was the flow-tube, with a particular emphasis on chemical compositional change e.g. by varying concentrations and humidity of species in different phases. The path of

experimental development and its application to systems as a kinetic tool will now be discussed.

2.1.1.1 Flow-tubes

The first flow-tube kinetic measurements were made in the late 1920s to measure recombination of hydrogen atoms [4]. In the late 1950s and early 1960s several important advances were made that much of our present technology can be traced such as investigating afterglow reactions with oxygen and nitric oxide [5]. Flow-tubes were initially applied to obtain rate coefficients for a variety of homogeneous gas-phase reactions, such as the highly reactive radical intermediates Cl and OH. More recently, however, the same approach has been used in studying reactions of both solid and liquid surfaces. The gaseous phase is usually introduced through a sliding injector, allowing contact with different lengths/interaction times relative to the surface. The first-order rate coefficient (k) is determined by measuring the concentration of the gas- phase species at the downstream end of the reactor, as a function of exposure time. The low pressure at which flow-tubes operate and the continuous nature of the detection makes many detection schemes suitable. Mass spectrometry, laser induced fluorescence and chemiluminescence, which will be discussed briefly later, are the main detection techniques employed. However, FTIR spectroscopy was the main technique used in this research to identify speciations.

a) Coated-and wetted-wall flow-tubes

Coated- and wetted- wall flow-tubes were among the earliest techniques employed in measuring the uptake coefficients onto liquid and solid surfaces. The approach employed in these studies was to measure the first-order rate coefficient (k) for the removal of a gas-phase species to a solid or liquid surface (of greater concentration) located on the inside of the tubular flow reactor. The uptake coefficient can then be calculated from k using well established mass transport theory for such flow reactors, converting the reaction time into a distance measurement [6]. Uptake

coefficients (γ) in the range of 10^{-1} to 10^{-6} can be measured. At high uptake rates ($\gamma > 0.2$), the accuracy of the measurement is limited by the requirement of precise values of gas-phase diffusion coefficients. Creation of a radial gradient due to reactants near the tube centre traveling faster than those near the wall results in molecular diffusion.

To study uptake onto liquids, the inside wall of the reactor must be completely covered with a slow flowing film of the liquid of interest. Thus, the liquid surface is constantly renewed, so that the molecules absorb onto a fresh surface. In practice, the liquid surface becomes saturated quite quickly and the uptake rate is often limited by diffusion into or reaction within the liquid. If reaction in the liquid is fast, saturation effects are minimal (the desorption rate is zero) and γ approaches the true mass accommodation (striking) coefficient α [(7)]. This methodology is often inconvenient however, as only portions of the surface area may be reactive and formation of complex multilayers of crystalline grains occurs when studying solids.

b) Aerosol Flow-tube

Aerosol flow-tubes are used to examine the interaction of trace gases with airborne particles. An aerosol flow-tube is designed to continually supply fresh surface area with submicron particles. The surface area can be greatly increased over that available in a coated wall apparatus, allowing the observation of less efficient processes. Gas-phase analysis can be conducted using a chemiluminescence detector or chemical ionisation mass spectrometer; particles are sized and counted using an optical particle counter and/or IR scattering using an FTIR spectrometer. For example, a laminar flow reactor has been designed to measure the kinetics of reactive uptake of dinitrogen pentoxide by submicron sulfuric acid [(8)]. This apparatus consisted of a SO_3/H_2O reactor for aerosol production; an expansion aerosol counter; a UV transmission cell/laminar flow reactor; and a chemical ionisation mass spectrometer (CIMS) to monitor gas-phase species. A laminar flow-tube was also employed in studying N_2O_5 hydrolysis on sulfuric acid and

ammonium sulfate aerosols [9]. In this instance, a CIMS, for monitoring the gas-phase composition and an optical particle counter, for the determination of aerosol size and number density, was coupled to the flow-tube. Aerosols were generated using an ultrasonic nebuliser. Experiments were performed in a laminar flow reactor to measure the uptake of gas-phase ammonia onto sulfuric acid particles [10]. Gas-phase ammonia was detected with a CIMS and particle size distributions were monitored with a differential mobility analyser. An enclosed injector system, which prevents the introduction of contaminants into the flow reactor, for low temperature kinetic studies was designed and was employed in studies of N_2O_5 with sulfuric acid aerosols [11],[12].

One advantage of aerosol flow-tubes over coated/wetted wall flow-tubes and other techniques is that laboratory measurements on actual aerosol particles, rather than bulk liquids or thin films, provide data that are more representative of real atmospheric aerosol systems. The formation, growth and transformations of aerosols are more ideally mimicked rather than surface interactions involving bulk solutions and substrates. Useful information on the dependence of observed uptake coefficients upon aerosol size is also provided [13].

Although the general approach – the measurement of the loss of a gas-phase species upon aerosol distribution of varying concentration – is similar to other aerosol flow-tube experiments, the instrumental detection techniques that were used in this current study are somewhat different from those previously employed. The aerosol flow-tube configuration in this work employed a laminar flow-tube coupled to a FTIR spectrometer for monitoring the gas- and condensed-phase composition. Aerosol size and number density were determined using a Scanning Mobility Particle Sizer (SMPS). A chemiluminescence NO_x monitor was used in ammonia and ammonium ion (NH_3/NH_4^+) detection and two methods of aerosol generation were employed.

2.2 Apparatus

The apparatus designed to conduct the experiments was based on an aerosol flow-tube instrument adapted for NH_3-monitoring instrumentation. An aerosol flow-tube was used to obtain simultaneous optical and size distribution measurements as a function of relative humidity and aerosol composition. The system was devised mainly to study the interaction between acid containing aerosols with trace gases. A constant flow of mainly sub-micron particles (either acidic species or ionic salts) were generated, which closely resemble those found in the atmosphere. These were then passed through a vertically aligned laminar flow reactor, with gaseous species (ammonia in this case) introduced *via* a sliding injector. A variety of detection techniques were employed to monitor changes in the composition of both gas- and condensed-phase species. A schematic diagram of the flow reactor apparatus is shown in Figure 2.1. The apparatus has three main sections: {1} aerosol generation, {2} a reaction zone (i.e. a vertical flow-tube with several inlet and outlet ports) and {3} a detection region.

The following section describes the operational principles of the flow-tube, while section 2.3 explains the specific techniques employed. This section is in turn divided into {1} experimental conditions, {2} aerosol generation and {3} detection methods. Section 2.4 presents relevant results of those calibration experiments, which characterise the detection properties.

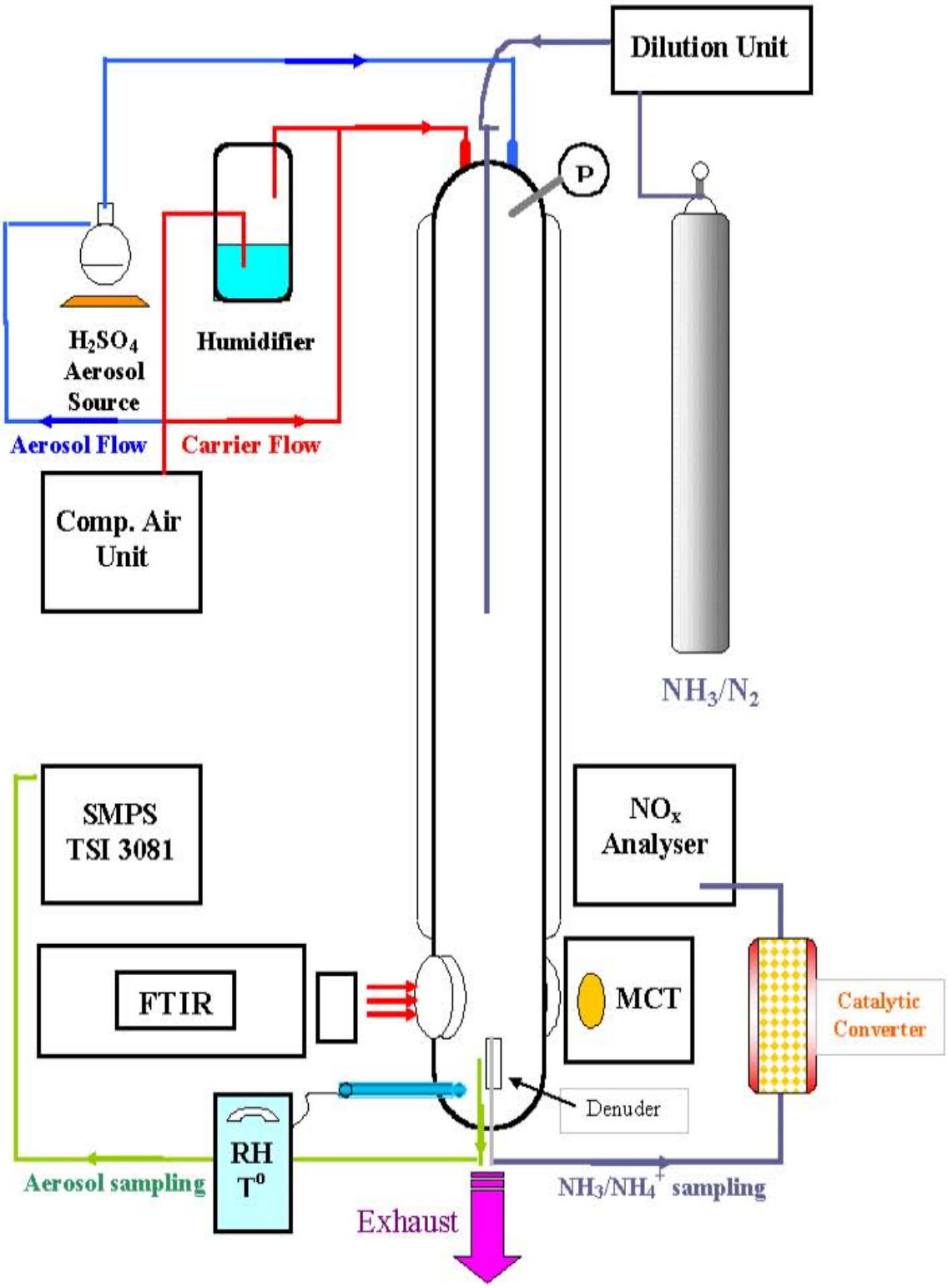

Figure 2.1: Schematic diagram of the Aerosol flow-tube apparatus.

2.2.1 Design

The aerosol flow reactor had been already designed and developed by the beginning of the project [14], its experimental function being to study the heterogeneous interactions between trace gases and aerosols, as illustrated by Figure 2.2.

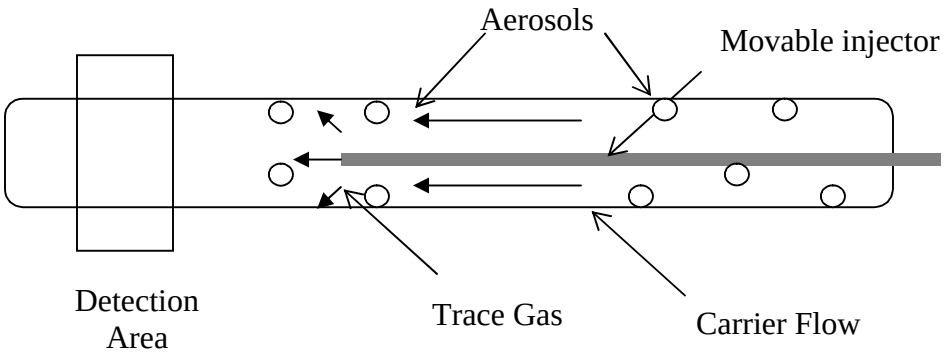

Figure 2.2: Outline of the flow-tube apparatus.

The flow-tube was limited to operate at atmospheric pressure because of the aerosol generation system employed in this study. The Constant Output Atomiser (COA) required a high flow rate (> 2500 standard cubic centimetre per minute, sccm) to generate particles. Therefore, in order to establish a reasonable interaction time (~ 100 s) between the trace gas and the aerosols, the flow-tube itself was designed to be of sufficient length (150 cm) to allow such an interaction time to be achieved.

Flow-tubes have been traditionally operated at low pressures (< 10 Torr of He) and the resulting calculations pertaining to uptake coefficients come to be termed as 'plug flow approximations', basically meaning that the effects of laminar flow and molecular diffusion are ignored and the flow velocity, directed along the tube axis, is assumed to be independent of both axial and radial positions [15]. The flow-tube kinetics approach was extended to pressures higher than those of the plug flow limit [16], which experimentally determined the axial/radial velocity and quantified flux divergence and chemical loss for any volume element in the flow-tube [17]. In assuming that a laminar flow within the flow-tube can be achieved, a number of

considerations were addressed, including those of gas composition, flow velocity and flow-tube diameter.

Flow-tube parameters

The Reynolds number (Re) is a non-dimensional parameter that determines if flow is laminar, transient or turbulent. Laminar flows occur when fluid particles move along straight parallel layers. The fluid particles of each layer do not mix with the fluid particles of other layers. Turbulent flow occurs when the particles of fluid move in all directions and fluid mixing occurs. Transition of laminar to turbulent flow may result due to roughness of the surface, abrupt changes in direction or size changes. The flow is:

- laminar if Re < 2300
- transient if 2300 < Re < 4000
- turbulent if Re > 4000

Equation 2.1 defines the dimensionless Reynolds number

$$\mathrm{Re} = \frac{\bar{\nu}\, d_f}{\gamma} \qquad \textit{(2-1)}$$

where d_f is the tube diameter in cm, $\acute{\upsilon}$ the average flow velocity in cm s^{-1}, γ the kinematic viscosity of air and is equal to 0.153 $cm^2\, s^{-1}$ at 298 K [18].

The flow velocity, $\acute{\upsilon}$, was calculated using the following equation [16]:

$$\bar{\nu} = \frac{760}{P}\,\frac{T}{273.2}\,\frac{F}{60\pi\, r_f^{\,2}} \qquad \textit{(2-2)}$$

where P is pressure (mg of Hg), T is temperature (K), r_f is the radius of the flow-tube (cm) and F is the flow rate (sccm). The flow rates passing through the flow-tube were derived from three separate sources: {1} filtered compressed air, {2} aerosol flow and {3} ammonia flow. The flow rate varied from 3500 and 1150 standard cubic centimetres per minute, (sccm), resulting in an average linear flow velocity of 1.47 and 0.48 cm s^{-1}, repectively. The flow-tube was operated at ambient

temperature and pressure conditions. The internal diameter, d_f, of the flow-tube measured 7.45 cm, giving an internal radius, r_f of 3.725 cm.

Flow-tube length

The entrance length, a term conventionally used to describe the point at which laminar flow is fully developed, may be estimated using (2-3):

$$l = 0.05 d_f \, \mathrm{Re} \qquad \textit{(2-3)}$$

This equation allowed calculation of the distance at which the central velocity of the flow reaches 1.99 times the value of the bulk velocity [17]. The Reynolds number, Re, for flow conditions in this work was typically between 90 and 100. As a result, this entrance length was in the order of 150 mm. To allow for sufficient interaction times between the trace gas and the aerosols, the reaction zone was determined to measure approximately 1000 mm. Figure 2.3 shows the turbulent and laminar regions of the flow-tube. Therefore, the length of the flow-tube was determined from the above calculations and was constructed to measure 1500 mm in total length.

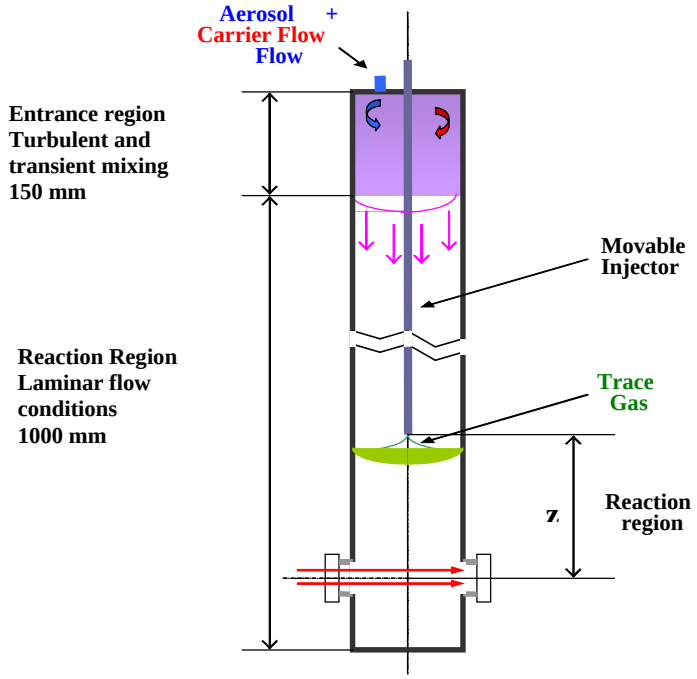

Figure 2.3: Turbulent and Laminar regions of the flow-tube.

Residence time

The trace gas used in the study to determine residence time was ammonia. The mixing time (the time to establish the diffusive profile) is given by [16]:

$$t_{mix} = \frac{r_f^2}{5D_g} \qquad \textit{(2-4)}$$

and was calculated to be approximately 11 seconds. D_g is the gas-phase diffusion coefficient and has been determined experimentally to be on average 0.25 atm cm^2 sec^{-1} [19],[20],[21].

Flow-tube kinetic measurements are usually calculated by varying the reaction zone length (Z), the distance to the detector from the point at which the two reactants are mixed. Varying the reaction zone length was accomplished by changing the position of the injector inlet. Ammonia was introduced to the flow-tube at distances between the detection region and the point of injection that were greater than 16 cm, (11 s × 1.47 cm s^{-1}). The injector rod had a centring device attached to it, to ensure that the ammonia introduced was in the centre of the laminar aerosol flow. The added ammonia was assumed to be thoroughly mixed with the carrier gas. The injector was varied over 4 positions in the reaction region of the flow-tube and these distances are given in Table 2.1. The flow velocity (*ύ*), for each flow rate was then used to calculate the residence times for ammonia at each of these positions.

Table 2.1: Residence times calculated for the injector positions for each flow velocity (ύ).

Injector Position	Reaction Lengths (cm)	Residence times (sec)	
		ύ: 1.47	ύ:0.48
Z_1	98	67	204
Z_2	75	51	156
Z_3	53	36	110
Z_4	30	20	63

The residence time in the flow reactor is a key experimental parameter. Laminar flow reactors have the disadvantage that air parcels at or near the centre much faster than those near the walls [22]. As a result there is a wide range of residence times at the reactor exit. This problem was solved by placing the denuder in the centre of the flow (by attaching a centring device) and sampling only a small fraction of the total flow at the centre line of the reactor as shown in Figure 2.1 [14]. The residence time for the sampled air was calculated by assuming the flow to be fully developed and laminar and by assuming that air was sampled symmetrically about the centre line. These assumptions were justified since, as previously shown, the Reynolds number was less than 100 and because the flow became fully developed within 15 cm downstream from the reactor entrance.

Kinetic treatment

The decay of reactive gases as a function of injector position are measured according to the following equation:

$$k = -\upsilon \frac{d \ln[C]}{dz} \qquad \textit{(2-5)}$$

where C is the reactant concentration and ύ is the average flow velocity. Varying the injector position in the flow-tube varied the interaction time between the reactive gas and the aerosol suspension. Because laminar flow conditions prevail in the reactor, the reaction time (*t*) is directly proportional to the distance, Z, between the tip of the injector and the detection/sampling point according to $t = Z / \upsilon$, where ύ is the flow velocity. The decays are converted to first-order rate coefficients (*k*) using the flow velocity and the standard correction for non-plug flow conditions [6]. The first order rate coefficients (*k*) are calculated from the slope of a linear least-squares fit to the experimental data.

The wall loss rate, k_w was measured in the absence of aerosol at varying relative humidities [14]. Figure 2.4 shows graphs of ($\ln[NH_3]_0/[NH_3]_t$) vs. time for the wall loss rate at various percentage relative humidity (%RH). Ammonia is adsorbed onto the walls of the flow-tube and greater absorption is observed at higher relative humidities. The values of k_w at each of the relative humidities were in the range of 2 to 3×10^{-3} s^{-1}.

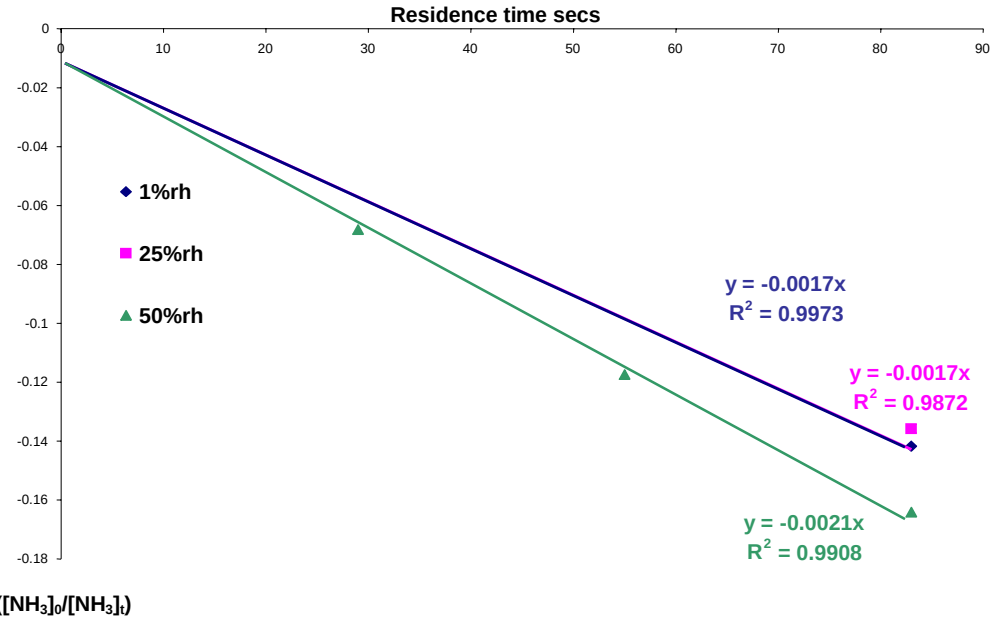

Figure 2.4: Wall-loss rates for ammonia as a function of relative humidity.

The uptake coefficient, γ, is then calculated from k using (2-6):

$$\gamma = \frac{4k}{S_a \langle c \rangle} \qquad \textit{(2-6)}$$

where S_a is the surface area of the aerosol suspension as measured by the SMPS (cm^2/cm^3) and <c> is the mean molecular speed of NH_3 under the experimental conditions (calculated to be 6×10^4 cm s^{-1}).

Denuder

The operating principle of a denuder is based on differences in the diffusion properties of gases compared to particles as a vital means of separation. A denuder, which was coated with oxalic acid, was required to selectively remove gaseous NH_3 from the air flow, sampled by the chemiluminescence monitor to facilitate the detection of ammonium ion formed in the condensed-phase. The length and diameter of the denuder were determined having considered all the equations and formulae from 2.1 to 2.4. The internal diameter, d_d of the denuder measured 10 mm, with the flow rate being established by the NO_x monitor to a value of 600 sccm. Using equation (2-2), the flow velocity was then calculated to be 0.14 cm s^{-1}, giving a Reynolds number of 92 (equation (2-1)). The flow rate through the denuder entered a turbulent region, before establishing a laminar flow profile, similar to the situation through the flow-tube. Therefore, the denuder was divided up into two regions: {1} a turbulent region where the denuder was left uncoated and {2} a laminar region where the denuder was coated with oxalic acid. The entrance length of the uncoated denuder was calculated to be 50 mm, from equation (2-3). The length of the coated region (l), that ensured the removal of all traces of ammonia from the air flow, was then determined using (2-7):

$$\frac{C}{C_o} = 0.819e^{-14.6272\Delta} \quad where\ \Delta = \frac{D_g l}{\gamma \,\mathrm{Re}\, d_d} \qquad \textbf{(2-7)}$$

An (l) value of 100 mm gave an $\frac{C}{C_o}$ equal to 0.06 which indicated that the majority of ammonia was absorbed by the denuder [14].

2.2.2 Assembly of the flow-tube

AGB, Dublin manufactured the flow reactor body. It consists of four Pyrex glass tubes, each with an internal diameter of 74.5 mm and with a combined length of 1500 mm as shown in Figure 2.5. Each individual Pyrex glass tube is flanged on open ends, to allow for assembly. They are joined together by house-built metal clamps, allowing them to be attached vertically onto a metal frame structure. Vacuum grease was used to ensure a tight seal between each of the flanges.

Tube 1 is the inlet and has four sample ports which allow the attachment of a trace gas injector, pressure gauge, carrier air flow inlet and an aerosol flow inlet. It also has a cooling jacket that can be used for temperature dependant studies. The flow profile in this region changes from turbulent to laminar. The main body of the flow reactor is tube 2 and is 1000 mm in length. It also has a cooling jacket. This is the reaction region of the flow-tube and laminar conditions prevail.

Tube 3 houses the optical windows for FTIR detection and the flow-tube is optically coupled to a Fourier Transform InfraRed spectrometer (BioRad Excalibur FTS 3000 coupled with external MCT detector), via re-entrant window mounts that hold the window surfaces a few centimetres away from the main gas flow. This ensures that the windows are not exposed to the aerosol flowing in the central core of the flow-tube and therefore, very little material condenses on them during the experiment. The barium fluoride (BaF_2) windows allow for *in situ* FTIR monitoring of both gas and condensed phase species. The FTIR pathlength through the flow-tube is approximately 250 mm.

Finally, tube 4 encases the oxalic acid coated denuder to allow sampling of particulate NH_4^+ ions. It also has two outlets that allow aerosol sampling. The final part of the flow-tube is the exhaust, which also houses the relative humidity and temperature sensor in the form of a digital hydrometer (Rotronic A2 Hygromer).

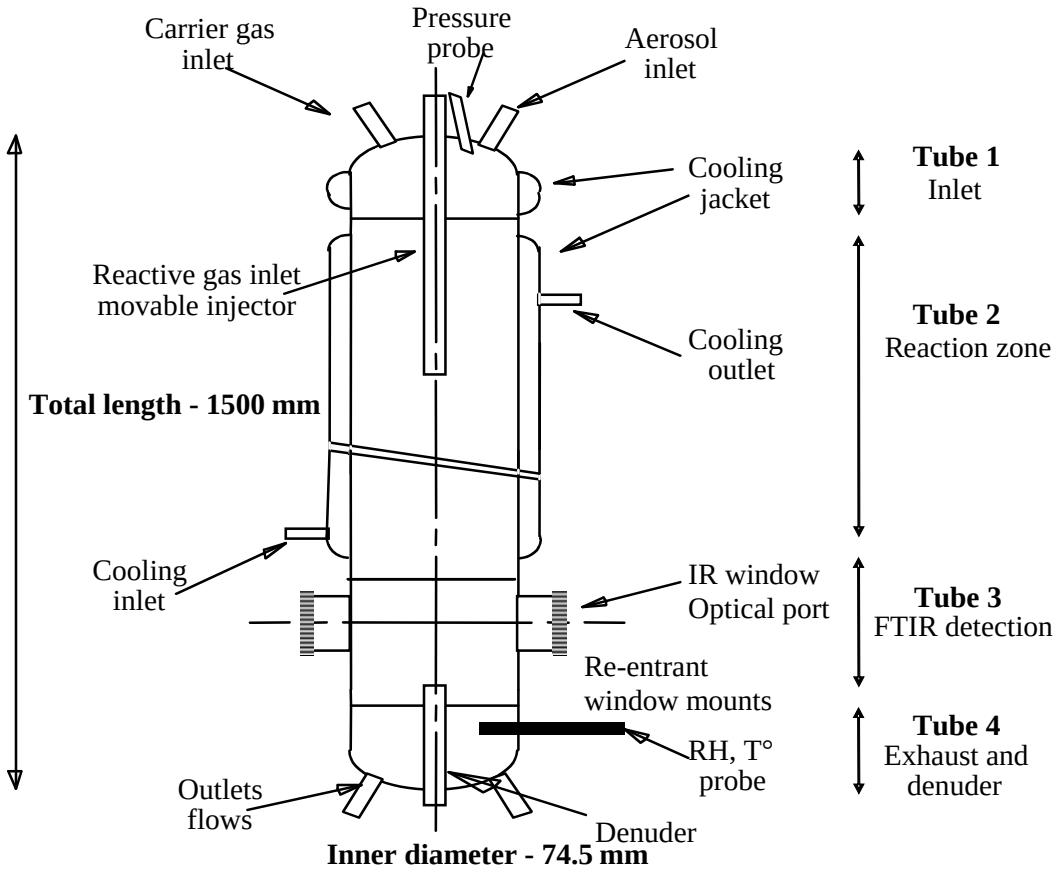

Figure 2.5: Pyrex glass Flow-tube.

2.3 Experimental Technique

2.3.1 Experimental Conditions

Table 2.2 lists the chemicals used in this study. They were used in accordance with the manufacturer's specifications, or alternatively prepared as described below.

Table 2.2: Chemicals used in this study.

Chemical	Formula	Purity	Manufacturer
Ammonia	NH_3	99.8%	BOC
Sulfuric acid	H_2SO_4	99.5%	BDH
Sodium sulfate	Na_2SO_4	99.5%	BDH
Sodium bisulfate	$NaHSO_4$	99.5%	BDH
Ammonium sulfate	$(NH_4)_2SO_4$	99.5%	BDH
Ammonium bisulfate	NH_4HSO_4	99.5%	BDH
Oxalic Acid	$H_2C_2O_4$	99.5%	BDH
Sodium oxalate	$Na_2C_2O_4$	99.5%	Sigma Aldrich
Ammonium oxalate monohydrate	$(NH_4)_2C_2O_4 .H_2O$	99.5%	Sigma Aldrich
'Sulfurous acid'	H_2SO_3 ($SO_2.H_2O$)	-	Sigma Aldrich
Sodium bisulfite	Na_2SO_3	99%	Sigma Aldrich
Sodium sulfite	$NaHSO_3$	98%	Sigma Aldrich
Nitric acid	HNO_3	90%	Sigma Aldrich
Sodium nitrate	$NaNO_3$	99.5%	BDH
Ammonium nitrate	NH_4NO_3	99.5%	BDH
Malonic acid	$H_4C_3O_4$	99%	Sigma Aldrich
Sodium malonate dibasic monohydrate	$Na_2H_2C_3O_4.H_2O$	99.5%	Sigma Aldrich
Succinic acid	$H_6C_4O_4$	99%	Sigma Aldrich
Sodium succinate	$Na_2H_4C_4O_4$	99%	Sigma Aldrich
Sulfosuccinic acid	$H_6C_4O_7S$	70%	Sigma Aldrich

The salts were dried in an oven for at least 24 hours prior to use in preparation of aqueous solutions. Masses were determined using an A&D Instruments EK-200G balance to an accuracy of ± 0.01 g, which equated to a maximum 0.1% error in mass measurements.

Concentrated aqueous acid solutions were prepared using standard volumetric apparatus, and stock solutions were at least 500 cm^3 for purposes of accuracy. Small volumes were handled with a calibrated 1 cm^3 Gilson Pro-pipette.

Ammonia was taken from a dilute (100 ppmv) mixture in nitrogen. A small flow of this mixture (typically in the range 100 – 300 sccm) was passed through the injector. The dilution of this flow by the main flow resulted in an average $[NH_3]_0$ in the flow reactor that was typically in the range of 1 – 3 ppmv. Introduction of acidic species to the flow-tube, using two different methods of aerosol generation is discussed later.

2.3.1.1 Flow controllers

Experimental flow conditions (typically 1000 – 3000 sccm), were achieved by using a series of MKS Type 247 mass flow controllers (3000, 500 and 20 sccm), and ensured that the necessary laminar flow conditions were always prevalent in the reactor ($Re < 100$).

2.3.1.2 Pressure

Pressure was monitored using an MKS Baratron Type 626A pressure gauge through an inlet port. The flow-tube was operated close to atmospheric pressures at all times. A slight increase in the pressure was noted on addition of the aerosols generated from the constant output atomiser technique.

2.3.1.3 Humidity

The relative humidity of the carrier flow (compressed air) through the flow-tube was tuned between 1 and 90% and monitored by a digital hydrometer (Rotronic A2 Hygromer). The humidity was increased by addition of water vapour to the air flow. The water vapour was entrained into the flow by bubbling at a known flow of compressed air through a humidifier of deionised water at room temperature. The exit of the humidifier was packed with glass wool to stop any droplets being entrained into the flow. This flow was then mixed within the conditioner with the aerosols. The dew point of the flow-tube effluent was monitored by the hydrometer.

2.3.2 Aerosol Generation

Aerosols were generated by two methods: {1} the constant output atomiser and {2} the heated reservoir technique.

2.3.2.1 The Constant Output Atomiser (COA)

Aerosol particles for many of these studies were generated by passing approximately 2500 sccm of dry filtered air through a Constant Output Atomiser (COA, TSI Model 3075) [23]. Aerosols of a given composition are formed from atomising solutions of liquids or suspensions of solids in liquids of the species of interest dissolved in water. The solution is entrained into a spray region, where droplets beyond a certain size (typically submicron) impact on a collector which in turn empties back into the reservoir. A range of particle sizes are produced initially but large particles are removed by impaction.

Drying the aerosols after its generation is an important factor in the final aerosol produced since this may alter both the physical and chemical nature of the particles. In experiments in which a low relative humidity (> 45 %RH) was desired, the

remaining droplets were passed through a house-built diffusion dryer (a tube of wire mesh surrounded by silica gel dessicant) to allow for complete recrystallisation of the salt dissolved in the droplets. As the air flow containing the aerosols passed through this tube, water vapour evaporated from the aerosols and was absorbed by the silica gel. The diffusion dryer was bypassed in experiments in which a high relative humidity (< 45 %RH) was desired. Once 'dried' or 'wetted', the particles were entrained into the apparatus for size selection, experimental processing, and detection. Reservoir solutions of 0.1 to 1 wt% concentration were sufficiently concentrated that the aerosol particle mass was high enough for FTIR observation yet sufficiently dilute that frequent obstruction of the atomiser did not occur. This type of particle generator produced particles that were well described by a log-normal distribution with a peak diameter typically in the region of 100 nm.

The aerosols generated by this technique were formed using salt solutions prepared from reagent grade material and doubly distilled deionised water as shown in Table 2.2. These included ammonium and sodium salts of sulfate, bisulfate, sulfite, bisulfite, nitrate, oxalate, malonate, and succinate. Sulfuric, 'sulfurous', nitric, oxalic, malonic, succinic and sulfosuccinic acid were the acids studied. Reservoir concentrations of these salts were in the region of 0.1 to 1 wt%. Mixtures of salts and acids were also prepared.

2.3.2.2 Heated Reservoir Technique

Acid particles were generated in a condensation-type particle generator where a flow rate of (~ 200 – 500 sccm) dry filtered air was passed over a small reservoir of liquid acid (~ 2 ml), at a temperature depending on the boiling point of the species; entraining a vapour saturated with acidic molecules [8]. These particles were then allowed to cool to room temperature in the conditioner. There are two fundamental processes involved in this method: {1} formation of a vapour phase by heating the liquid sample and {2} subsequent cooling to condense the vapour molecules. The nucleated particles then grow by two simultaneous mechanisms: condensation of

the remaining vapour molecules onto their surfaces, and coagulation among the particles themselves.

The optimum temperature of the reservoir bath was determined by recording the number concentration of particles formed at a range of temperatures. It was not possible to generate vapour at 415 K or above as the paraffin oil used in the reservoir bath began to produce smoke at a temperature of 420 K. Due to the low boiling point of sulfur dioxide dissolved in water (263 K) and high vapour pressure of nitric acid (48 Torr at 293 K), the experiments involving the heating reservoir technique were eventually deemed to be unreliable. Sulfuric acid on the other hand, has a very low vapour pressure (9.9×10^{-6} Torr at 296 K) so that it exists in the condensed- phase diluted with water to varying degrees.

Subsequent to their generation (by either method) the aerosols are passed through a conditioner, which allows the particles to reach equilibrium and ambient relative humidity with the surrounding air flow prior to their introduction into the flow-tube. Further changes in the relative humidity can be achieved by adding either a dry flow or a water saturated flow provided by a bubbler kept at room temperature. The total flow rate from these sources is approximately 2500 sccm. From the error estimates in the flows and temperature of the bubbler, the estimated error in the relative humidity in the conditioner is ± 1% and never greater than ± 2%. Assuming that the aerosols are in equilibrium with ambient flow conditions, this potential error in the relative humidity corresponds to an inaccuracy of no more than ± 2 wt% in the composition of the aerosols, based on the relationship between the relative humidity and the composition of the aerosols reported in the literature [(24),(25)].

2.3.3 Detection

This section provides an overview of detection techniques used in these studies, including the FTIR the SMPS (Scanning Mobility Particle Sizer) used for aerosol sizing, and the chemiluminescence NO_x monitor for ammonia and ammonium ion

(NH_3/NH_4^+) detection. After passing through the flow-tube, the reactant stream was channeled into both the electrostatic classifier of the SMPS and the denuder for NH_3/NH_4^+ detection, excess gas being vented into the exhaust hood.

2.3.3.1 FTIR Spectroscopy

This vital detection technique, characteristically associated with the 'fingerprints' of molecules, has been applied to ambient air measurements since the mid 1950s [26]. IR spectroscopy studies light in the infrared region absorbed by vibrating (stretching and bending mainly) chemical bonds within molecular structures. The conversion of the signal intensity as a function of optical path difference (the interferogram) into signal intensity as a function of wavelength (the infra red spectrum) requires applying a mathematical formalism known as Fourier Transform [27],[28]. FTIR can use of longer pathlengths and multiple reflections which enable an enormous increase in sensitivity, speed and improved data processing compared to dispersive instruments. In atmospheric studies, the latter is important as absorptions from known aerosol constituents can be subtracted leaving peaks due to unidentified particles relatively unobscured.

FTIR spectroscopy was used to monitor both gas- and aerosol-phase composition. The FTIR spectrometer (BioRad Excalibur) was coupled to an external mercury cadmium telluride (MCT) detector. In this set-up, collimated radiation from the FTIR spectrometer was directed through the probing path length, a distance measuring 250 mm. Barium fluoride windows mounted at both ends permitted a single passage of the IR beam. The transmitted radiation was focused by a zinc selenide lens onto the active area of the liquid nitrogen cooled MCT detector. The entire path length of the beam was purged with dry filtered air to reduce background signals and light was excluded to prevent degradation of the BaF_2 windows.

A background spectrum was taken while the flow-tube was fully purged with dry filtered air. Each spectrum represented the average of 512 scans recorded over the range 4000 – 750 cm^{-1} at 2 cm^{-1} resolution. The output flow from the aerosol generation system was then introduced and sample spectra were taken depending on the conditions of each particular experiment.

The software supplied with the spectrometer was Win-IR Pro, and it was used, in conjunction with Thermo Galactic's GRAMS/AI, to perform necessary manipulations on the spectra. These include baseline correction, spectral subtraction, integration and peak fitting. For example, Figure 2.6 shows a typical FTIR spectrum of 1 wt% sodium succinate aerosol at 90 %RH with 300 sccm ammonia.

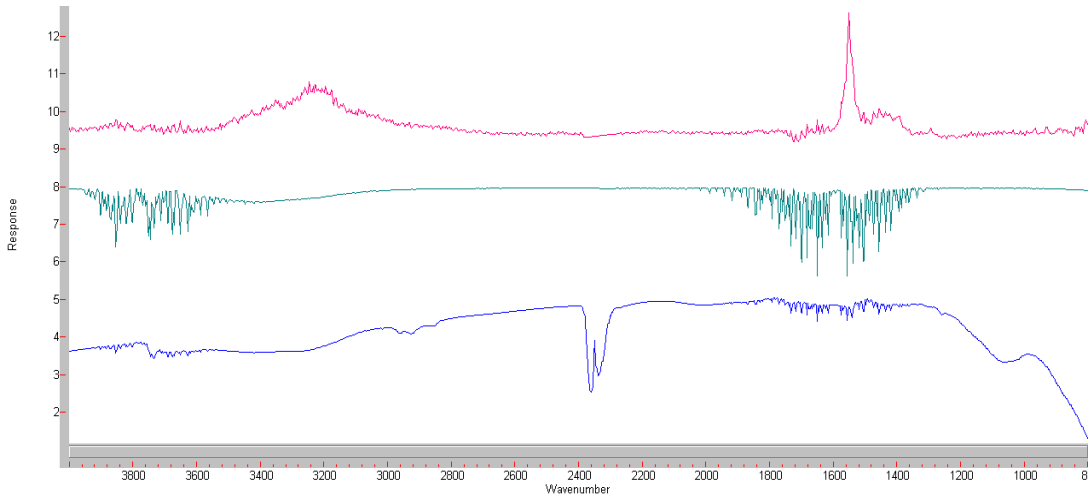

Figure 2.6: FTIR spectrum of 1 wt% sodium succinate aerosol at 90 %RH with (middle) and without (top) gas-phase H_2O absorption lines. The spectra have been offset for clarity. Absorption due to atmospheric CO_2 (at 2350 cm^{-1}) has been removed from both spectra. A background spectrum (bottom) is included to illustrate this absorption.

2.3.3.2 SMPS

The aerosol suspensions were characterised using a Scanning Mobility particle sizer (SMPS, TSI 3081) instrument, which determines key parameters such as mode (typically 100 nm for the atomiser technique), number distribution, surface area and

particulate mass by electrostatic means. The TSI SMPS consists of an electrostatic classifier (EC, TSI 3080), a differential mobility analyser (DMA, TSI 3011) and a condensation particle counter (CPC, TSI 3010).

Following passage through the flow-tube, particulate sampling was attained using the annular denuder sampling port. Sampling took place in the centre of the flow-tube, following FTIR spectroscopic measurement. The aerosol flow was then channeled into an electrostatic classifier (TSI 3080). After exposure to an ^{85}Kr bipolar charger, aerosol particles were selected according to their electrical mobility by the DMA as shown in Figure 2.7 [29]. The DMA is useful in defining the relative numbers of particles over a wide range of size intervals. Clean air flows down the central portion of the tube between the layer of ambient aerosol at the walls and the collection rod in the centre of the tube. A negative voltage is applied to the collection rod, causing the positively charged particles to move from the outer wall through the clean air to the collect ion rod. The relationship of the particle count at the detector to the voltage in the analyser is dependent on the particle mobility in the analyser, which depends on particle size. Thus size distributions can be obtained by studying the detector output as a function of collection rod voltage [30].

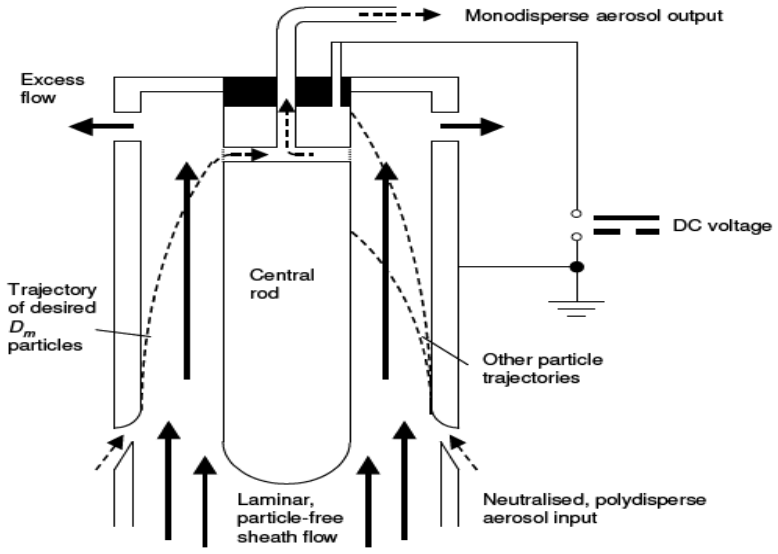

Figure 2.7: A schematic of the Differential Mobility Analyser, DMA.

By scanning the classifier voltage and measuring the particle sizes at those voltages, a particle distribution was obtained. Since particle separation depends on electrical mobility and not particle size, a correction to the particle distribution must be made to account for multiply-charged particles. The CPC was used to count the number density of particles using optical detection [31]. Particles passed between a light source and a detector sensing the particle's shadow. The CPC 3010 was sensitive to those particles having diameters greater than 10 nm. The particles were sampled within a region supersaturated in butanol vapour and grew by condensation before detection in the optical chamber of the device.

Typical size data of sodium bisulfite aerosol from this measurement technique is shown in Figure 2.8 and Table 2.3. From this information, a variety of properties of the aerosol can be calculated, including total particle density, surface area and number distribution. It should be noted that the calculation using SMPS software is based on the assumption that the aerosols are spherical.

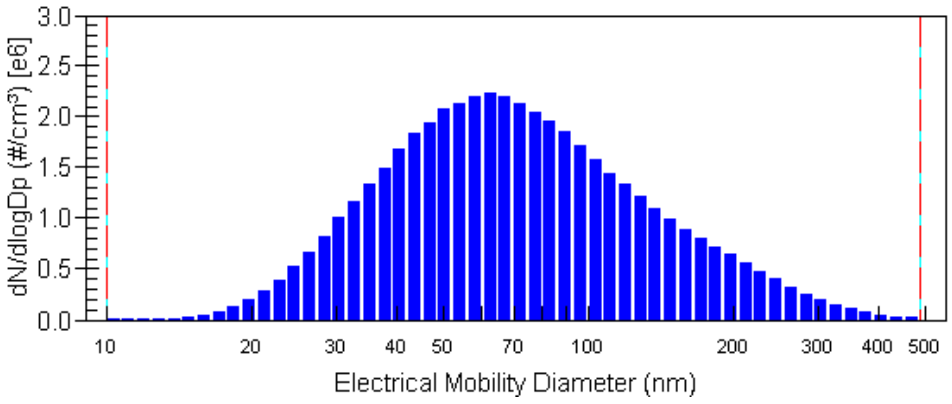

Figure 2.8: Typical size distribution of sodium bisulfite aerosols. Data shown are from 1 wt% at 20 %RH and are corrected for multiple charging of particles.

Table 2.3: Statistics Table containing properties of this aerosol.

	Number	Diameter	Surface Area	Volume
Median(nm)	67.4	97	143.3	208.1
Mean(nm)	81.9	118	168	225.1
Mode(nm)	67.3	96.5	138.2	305.1
Geo.St.Dev.	1.79	1.84	1.82	1.72
Total Conc.	1.5×10^{6}#/cm³	119.5 mm/cm³	4.4×10^{10} nm²/cm³	1.2×10^{12}nm³/cm³

Depending on the particles of interest, the SMPS was tuned, by varying the sheath and sample flow, to monitor large particles (in the range 20 – 898 nm) or smaller particles (in the range 10.7 – 470 nm). It was normally operated using sheath and aerosol sampling flows of 2000 and 200 sccm respectively, thus giving a particle range of 19 – 898 nm. Particle size and number concentration were measured with a time resolution of 2 to 3 minutes. The SMPS system was started prior to the introduction of reactants to confirm that no particles were present in the flow-tube before the aerosols were introduced.

To ensure that the aerosol size distribution measured after exposure to the flow-tube was the same as those generated during atomisation or reaction; tests were performed where the aerosol size distribution was measured at an entrance and the exit of the flow-tube under identical conditions. Measurements at the entrance of the flow-tube eliminate possible size changes occurring during transit, *i.e.* less residence time. In each case, the particle distribution showed less than 5% variation from each other. Thus, it can be concluded that aerosol loss or change in particle distribution in the absence of a chemical reaction within the reactor is negligible.

2.3.3.3 Chemiluminescence NO_x Monitor: Ammonia and Ammonium Ions Detection

FTIR spectroscopic detection of ammonia and ammonium ions is limited to the ppmv range and was found to be too insensitive at the low concentrations used in this study. The reason for this was that the cell path length was not long enough. Therefore, a novel method for detecting ammonia and ammonium ions was developed [(14)], using an Ostwald type reaction coupled with a chemiluminescence NO_x monitor. There are two stages in this new detection method:

- Catalytic oxidation of ammonia/ammonium to NO
- Chemilluminescent reaction in NO_x Monitor

This device allows the monitoring of NH_3/NH_4^+ species at low concentrations (down to ppbv levels) with accuracy (within 5%) and appropriate time response (within 3 minutes).

Catalytic oxidation of ammonia/ammonium to NO

Ammonia and oxygen gas react in the present of certain catalysts to form nitric oxide, as shown in (2-8), which is known as the Ostwald reaction [32].

$$4NH_3 + 5O_2 \xrightarrow{Cat,Heat} 4NO + 6H_2O \quad \textbf{(2-8)}$$

In the commercial process, the catalyst used is a platinum-rhodium metal gauze that is heated to about 1173 K. However, this catalyst is very expensive, so a suitable less expensive substitute was sought. It has been proven that lanthanide oxide systems are just as active at catalytic oxidation as platinum-rhodium systems [33], therefore the catalyst used in this work was a lanthanide oxide based catalyst doped with copper oxides (YPr(15%)Cu(20%)), operated at an optimum temperature of 1023 K. At the operational temperature of the catalyst, ammonium salts are found to decompose, releasing ammonia into the gas-phase. This in turn is converted to NO and detected in the chemiluminescence cell.

In order to determine the concentration of ammonium ions formed from the reaction of gas-phase ammonia with aerosols, a diffusion-denuder technique was employed. This allowed for the selective removal of gaseous ammonia from the mixed air-flow. Oxalic acid was chosen over citric acid as the denuder coating layer because previous studies showed that the citric acid coating displayed only a weak bond with ammonia, resulting in a release of the ammonia towards the air flow [34]. This coating was achieved by dissolving crushed oxalic acid (~ 5 g) in a minimum amount of acetone to produce a paste and pouring this mixture into the denuder. The denuder was rotated so that all internal surfaces were wetted, excess liquid was poured off and dry air was passed through to evaporate the thin film. The denuder

was designed and constructed to ensure that gas-phase ammonia was totally removed from the mixed air flow without affecting particle concentration (see Figure 2.9). A centring device was also fitted to the outside of the denuder to ensure that sampling always took place at the centre of the air-flow. The dimensions of the denuder have already been discussed in Section 2.2.1.

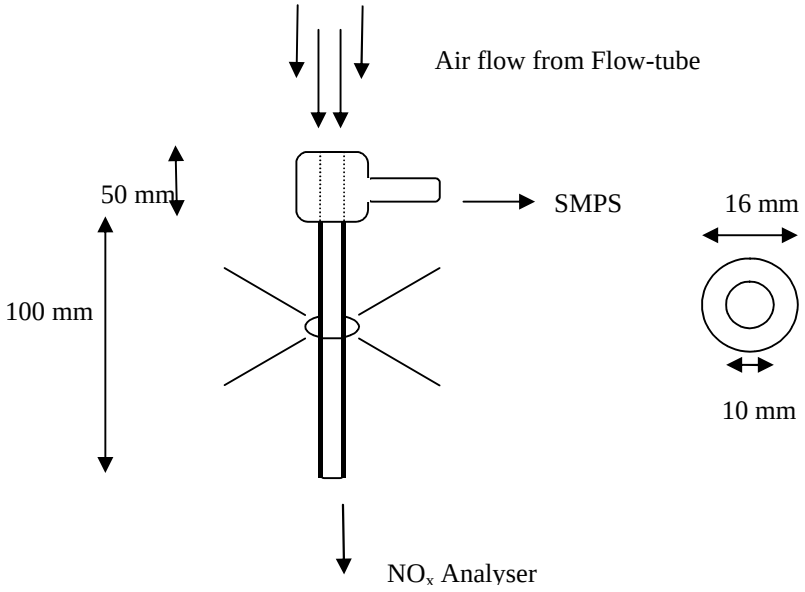

Figure 2.9: Diffusion denuder coated with oxalic acid for gaseous NH_3 removal. Also included are the centring device and the annular sampling port at the entrance of the denuder.

The first 5 cm of the denuder was left uncoated to allow for laminar flow conditions to be re-established inside the denuder tube before the ammonia was selectively removed. The entrance to the denuder tube was annular: it had an outer sampling port that was connected to the SMPS to ensure the sampled particles were similar in size and composition to those sampled by the NO_x analyser. The denuder was shown to be very effective at removing gaseous ammonia: tests performed on the flow-tube without the denuder present gave a NO_x signal of 820 ppbv for 1000 ppbv of NH_3 introduced [(14)].

Chemiluminescence NO_x Monitor

Analysis of NO by means of chemiluminescence is based on photon emission from an excited state of molecular NO_2, produced by a reaction between NO and O_3 in an evacuated chamber. NO molecules react with ozone to form the excited species (NO_2^*) according to the mechanism:

$$O_3 + NO \rightarrow NO_2^* + O_2$$
$$NO_2^* \rightarrow NO_2 + h\upsilon$$

NO_2^* has a short radiative lifetime, typically 115 μs, emitting light from 590 nm to 2800 nm – a region that is relatively easy and sensitively monitored using a photomultiplier. The molecule will emit light faster than collisional quenching by air molecules can occur. The effective concentration of the emitting species (and hence emitted light intensity) is proportional to the concentrations of the reactants.

Gas-phase ammonia was admitted into the flow-tube via a 6 mm diameter movable glass injector. From the 100 ppmv standard (NH_3/N_2 brand), the ammonia concentration was diluted down to the ppbv range using a range of mass flowmeters. The concentration of ammonia in the flow-tube was determined and subsequently compared to the NO_x levels. A calibration curve was set-up and a conversion factor was calculated [14].

As shown in Figure 2.10, the most effective catalyst was found to be YPr(15%)Cu20% giving a conversion factor of 0.8 ± 0.03 (NH_3 to NO_x) or 1.2 ± 0.03 (NO_x to NH_3).

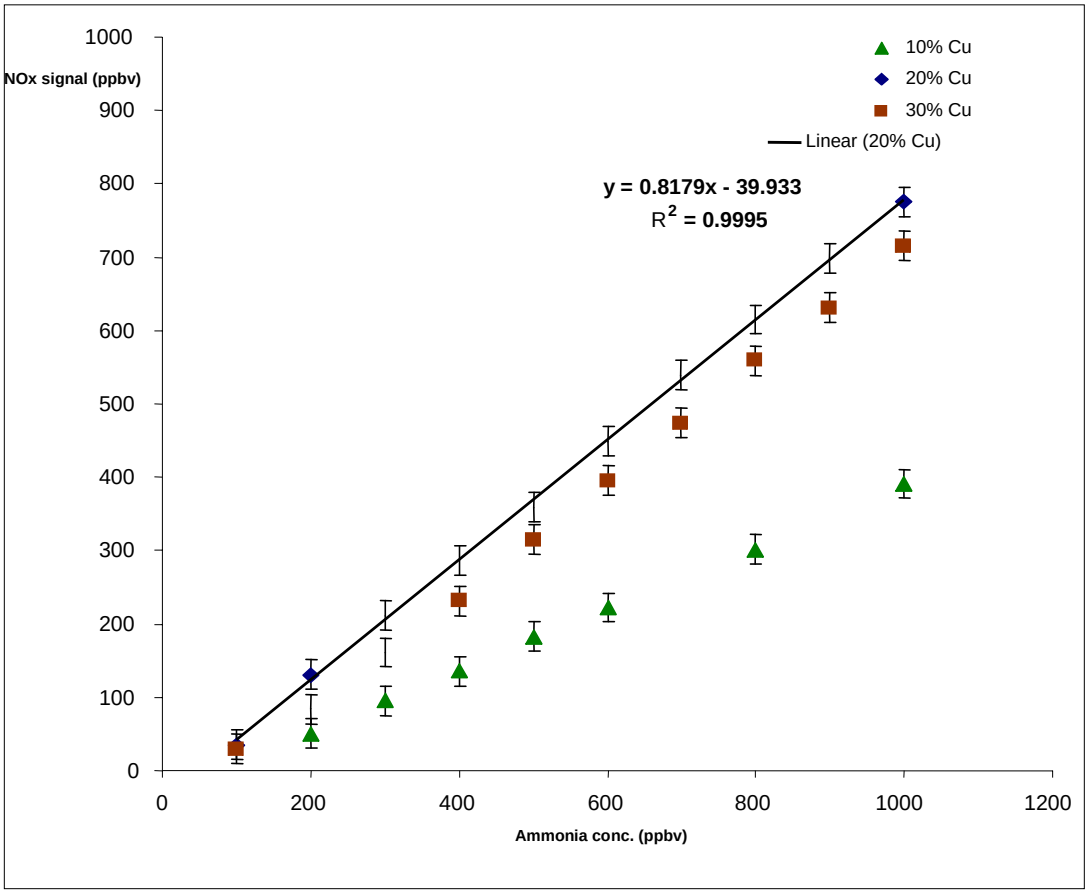

Figure 2.10: Calibration curves for each catalyst used. The catalyst with 20% Cu is the most effective [14].

Aerosols were analysed simultaneously by the SMPS, for particle mass, and the NO_x monitor, for NO_x concentration using the two sampling ports of the denuder. No significant difference was observed in the particle number and the NO_x signal, regardless of the port selected for sampling. A calibration curve was obtained between the particle mass and the NO_x signal [14]. There was a good correlation between the observed NO_x signal and the aerosol mass indicating that the particles are not affected by the oxalic acid coating on the denuder.

The interaction of ammonia with acidic aerosols resulted in the formation of ammonium ions. The concentration of ammonium ions was monitored using the NO_x monitor and all ammonium ion concentrations quoted in the results chapters have been converted from the NO_x signal, using the conversion factor of 1.2 ± 0.03. Therefore, these ammonium ion concentration values represent the NO_x signal converted to ammonia concentration with units of ppmv. The changes in ammonium ion concentration (by varying experimental conditions: humidity; aerosols concentration; ammonia concentration and interaction time) is of utmost importance to this study while the absolute value is of little concern.

$[NH_4]^+$ levels when studying nitric acid aerosol were hampered by the fact that a competition between the NO from ammonium ions and the NO_x gas from nitric acid exists. NO_2 levels were particularly high when the nitric acid was heated directly. As the humidity was increased, the $[NO_2]$ decreased and consequentially the [NO] increased. It was also noted that the [NO] increased dramatically on addition of ammonia to the HNO_3 system. Nebuliser generated aerosols did not produce much NO_2, however NO levels were consistently high both before and after ammonia addition. Humidity appeared to increase the amount of NO produced with and without ammonia and also when the flow concentration was lowered. The presence of nitrogen dioxide absorptions on the FTIR spectra correlated well with corresponding NO_x levels. An extra signal from nitric acid along with ammonia led to inevitably unreliable measurements. The catalytic convertor is likely to reduce nitric acid aerosols and ammonium nitrate aerosols. Nitric acid may be lost to the walls of the flow-tube before it even reaches the catalytic converter, because it appears to be a ‘stickier’ molecule than sulfuric acid for instance.

The resulting FTIR spectrum of ammonia in the gas-phase is well established and has four infrared active bands centring at 3444 cm^{-1} (v_3: degenerate asymmetric stretches), 3337 cm^{-1} (v_1: symmetric stretch), 1627 cm^{-1} (v_4: degenerate asymmetric deformations) and 950 cm^{-1} (v_2: symmetric deformation). This latter peak splits into two, resulting in peaks centring at 966 and 927 cm^{-1}. The NH_3 absorption line used in the current experiments to identify the presence of gaseous ammonia was the one centred at 966 cm^{-1} as shown in Figure 2.11. IR bands in crystalline ammonia appear at 3376, 3213, 1646 and 1060 cm^{-1} for v_3,v_1,v_4 and v_2, respectively [35].

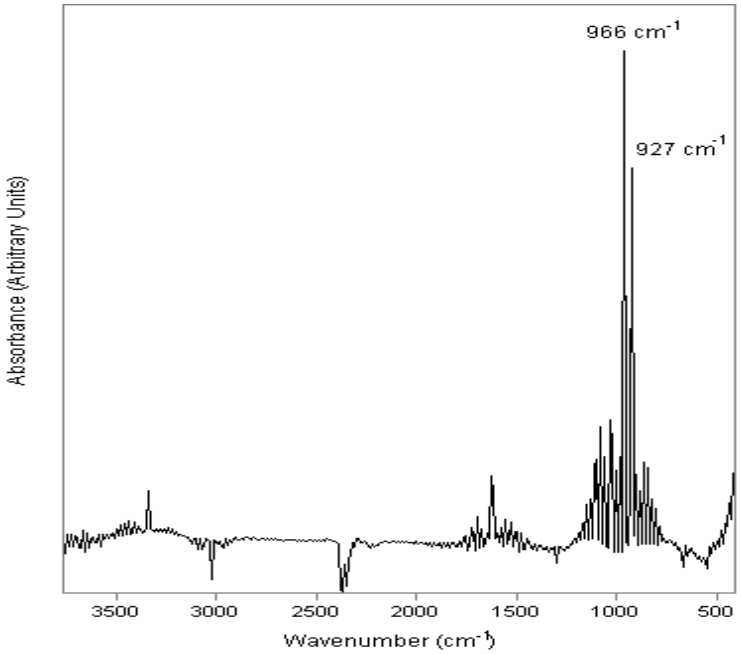

Figure 2.11: FTIR spectrum of 20 ppmv Ammonia gas in nitrogen.

The 'free' ammonium ion has T_d symmetry giving rise to four normal vibrational modes [36], represented as A_1 (v_1), E (v_2), and 2 x T_2 (v_3 and v_4). All the fundamentals are Ramon active, but only the triply-degenerate v_3 and v_4 modes are IR active. The observed frequencies for the free ammonium ion are:

v_1 = 3040 cm^{-1}, v_2 = 1680 cm^{-1}, v_3 = 3145 cm^{-1}, and v_4 = 1400 cm^{-1} [37]

In accordance with selection rules for T_d symmetry, the FTIR spectrum of $(NH_4)_2SO_4$, under ambient conditions, contains two intense absorption bands which can be assigned to the triply degenerate vibrations ν_3 (N-H stretching) and ν_4 (N-H-N bending) of the NH_4^+ ion. In typical cases, the first absorption band tends to be intense and broad (3300 – 3030 cm^{-1}), while the second exhibits medium to strong intensity and is narrow (1430 – 1390 cm^{-1}). Both often exist as multiple band structures, and this feature may be used to characterise individual compounds [38]. In addition, at the low-energy wing of the stretching band, ν_3, a combination mode $\nu_2 + \nu_4$ and the first overtone of the ν_4 bending mode are clearly visible. A decrease in the local symmetry of the ammonium ion may lead to a splitting of the former degenerate states, resulting in further bands [39]. This spectrum is shown in Figure 2.12.

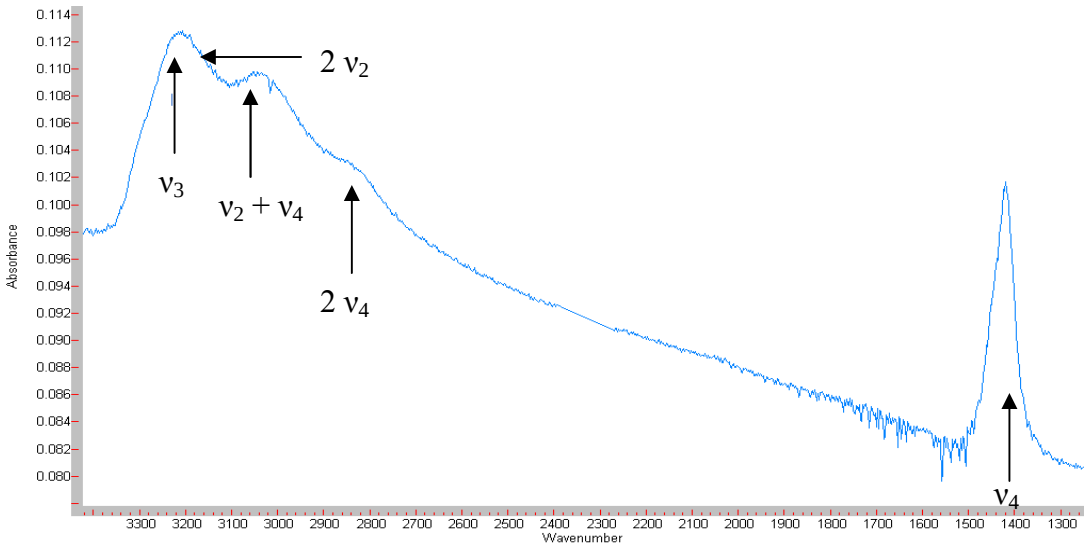

Figure 2.12: Normal modes, on the basis of T_d symmetry, in the FTIR spectrum of ammonium sulfate at 298 K.

Ammonium ion calibration:

Standard solutions of $(NH_4)_2SO_4$ were prepared and atomised using the constant output atomiser [14]. The concentration of the aerosol suspension was altered by varying the amount of carrier flow rate. Initially, the total flow rate, including the aerosol flow rate, was 3000 sccm, which was gradually increased to achieve a total

flow rate of 5500 sccm. Increasing the carrier flow rate dilutes the aerosol suspension, thereby decreasing the amount of ammonium ions reaching the catalytic converter, which in turn yields a lower NO_x signal.

Figure 2.13 illustrates the effects on the NO_x signal of an ever increasing carrier flow rate to aerosol flow rate.

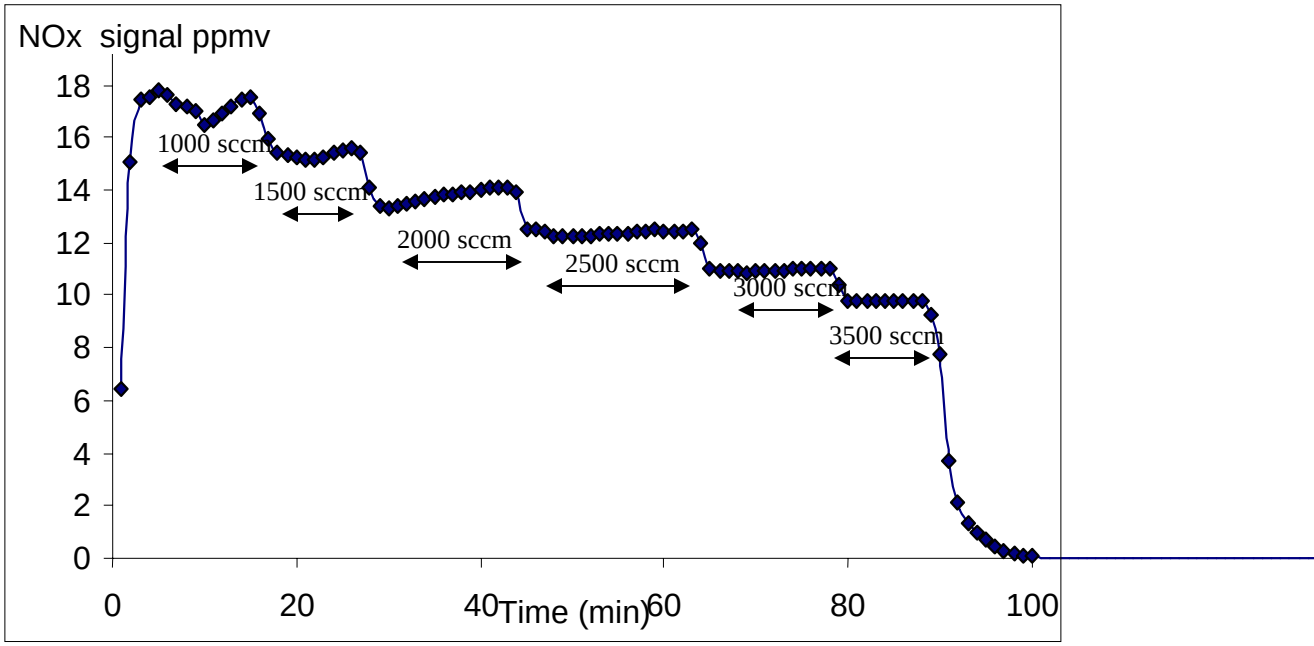

Figure 2.13: Diluting 1 wt% ammonium sulfate aerosol with additional flow (in sccm).

2.4 Typical experiment

2.4.1 Nitric acid aerosol generated by atomiser technique

As previously mentioned, particles were generated by two different methods in this study: {1} the atomiser technique and {2} the heated reservoir technique. Figure 2.14 shows plots of relative humidity, particle number concentration and peak area of the liquid water region (3620 – 2700 cm^{-1}), with respect to time, for aerosols generated from 1 wt% HNO_3 solution using the atomiser technique. Generating nitric acid aerosol by means of the nebuliser produced nitrate ion absorptions only, regardless of humidity, flow concentration and ammonia addition.

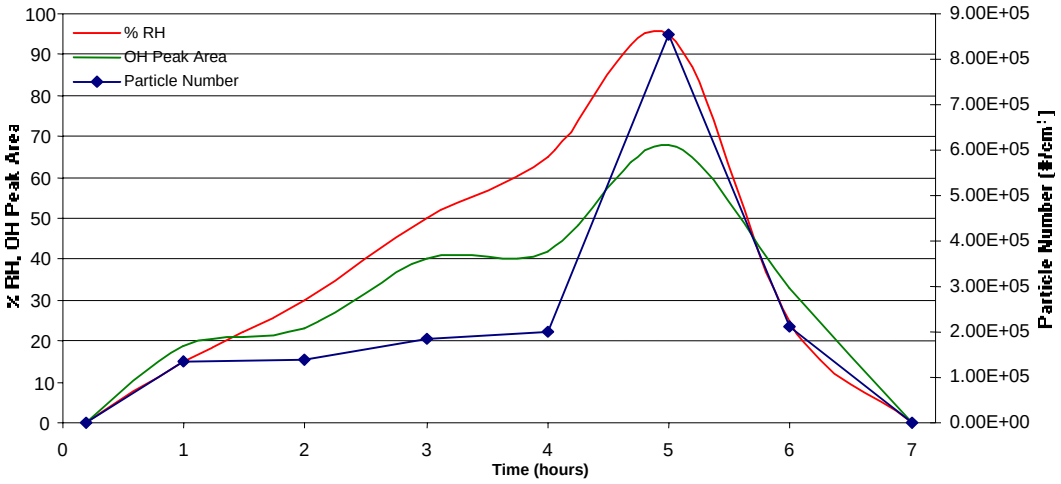

Figure 2.14: Particle concentration, relative humidity and liquid water absorption of nitric acid particles with respect to time.

The aerosols were admitted first into the reactor and allowed to fully equilibrate for several minutes after a background was recorded. The experiment took approximately 6½ hours to complete with a total flow of 2000 sccm. The aerosols, prior to introduction into the flow-tube, were 'dried' by passing the aerosol flow through the diffusion dryer. SMPS and FTIR spectroscopy were used to record the particle number concentration and the peak area, respectively. Initially, the dry carrier flow rate was the only two element to be introduced into the flow-tube. After

one hour, a wet carrier flow rate replaced the dry carrier flow rate. Finally, 6 hours after initiating the experiment, both the wet and the aerosol flow rates were substituted by a dry flow rate totalling 2000 sccm. For the first 2 – 3 minutes all readings from the instruments of detection measured approximately zero. Addition of the particles increased the humidity of the system. Analysis of the liquid water region of the spectra (3620 – 2700 cm^{-1}) provided information on how 'wet' or 'dry' the particles were. It was found that after approximately four minutes, the peak area started to increase, indicating that the particles consisted of either an aqueous solution containing aerosols, or a film of water surrounding an insoluble core. After one hour, the humidity of the system was increased further, by the introduction of a 500 sccm wet carrier flow rate. The particles absorbed more water vapour, leading to an increase in the liquid water region. A marginal increase in particle number was observed, on addition of this extra water vapour. After 6 hours, both the particle and the wet flow rates were turned off and substituted by dry air. The particle number concentration was seen to be the first to decrease in value, while a decrease in relative humidity and the peak area for liquid water was observed after a period of four minutes. This observation is due to the wet air (both particles and wet flow rate) being purged from the system. This takes a number of minutes to complete and therefore the relative humidity does not decrease until all of these contributing factors have been removed.

2.4.2 Nitric acid aerosol generated by heating technique

A second experimental setup was employed to generate nitric acid aerosols using the heated generator technique. They were generated by flowing 500 sccm of dry air through a heated reservoir containing liquid HNO_3. FTIR and SMPS were employed to record the peak areas and particle parameters, respectively. Figure 2.15 shows well characterised spectra obtained for nitric acid aerosols as the humidity of the system was changed from 2 to 90 %RH along with addition of ammonia. Particle number concentrations were observed to increase as the humidity was increased and as ammonia was introduced as seen in Figure 2.16.

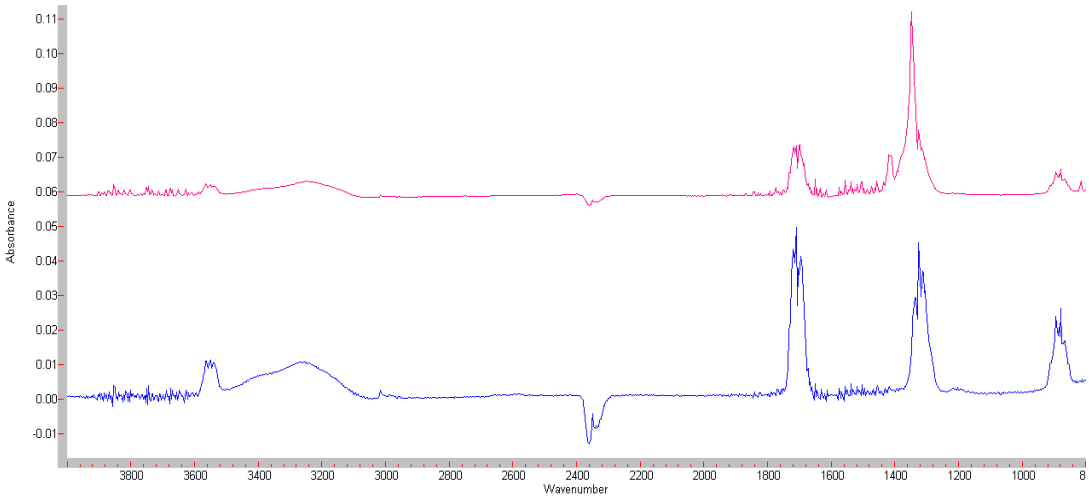

Figure 2.15: FTIR spectra of 1 wt% HNO_3 aerosol at 20 %RH (bottom) and at 90 %RH with 300 sccm NH_3 (top).

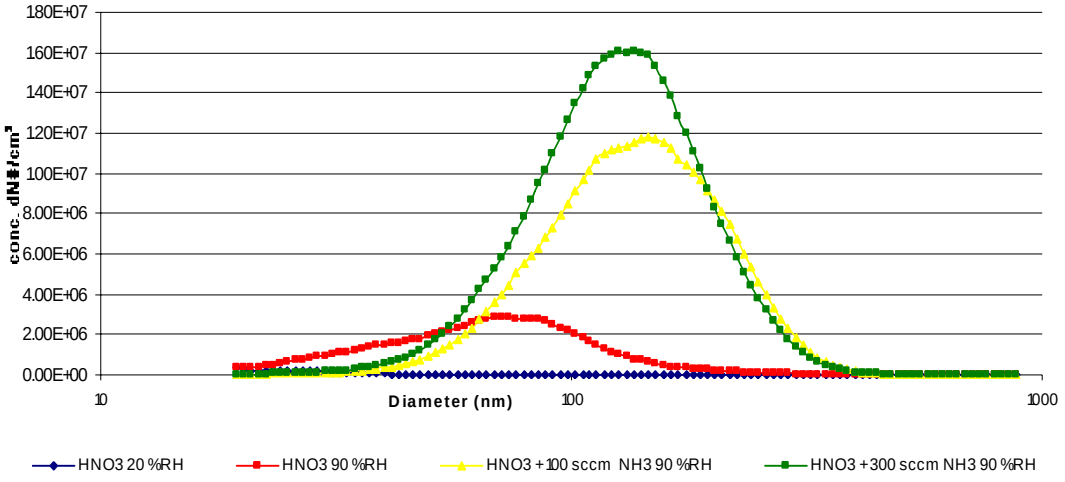

Figure 2.16: Typical size distributions for 1 wt% HNO_3 at various conditions.

When heating nitric acid directly (boiling point of 356 K), it was found that at low humidities, gaseous nitrogen dioxide was present. A brown gas was observed and the overall process is summarised by Equation (2-9).

$$4HNO_{3(g)} \rightarrow 4NO_{2(g)} + 2H_2O_{(g)} + O_{2(g)} \qquad \textit{(2-9)}$$

Nitrate ions either as a dissociated ion or in the form of ammonium nitrate (Equation (2-10)) [40], were observed in the aerosol and became more distinct in the FTIR spectra as the humidity was increased. This was achieved by either passing the main flow through the humidifier or reducing the flow concentration.

$$NH_{3\ (g)} + HNO_{3\ (g)} \rightleftharpoons NH_4NO_{3\ (s)} \qquad \textit{(2-10)}$$

Similar calibration experiments were performed initially when the flow-tube was designed [14].

2.4.3 Ammonia concentration

Varying the position of the injector, as ammonia (NH_3) was passed through it, had a direct effect upon the NO_x signal [14]. Figure 2.17 shows the NO_x signal as the injector is moved from position 1 (Z_1) to position 4 (Z_4). At Z_1, the position of longest residence time, the NO_x signal was measured to be at its weakest, as NH_3 was adsorbed onto the greatest surface area. In moving the injector, a shorter residence time within the flow-tube was achieved. The NO_x signal increased indicating that more NH_3 was being monitored.

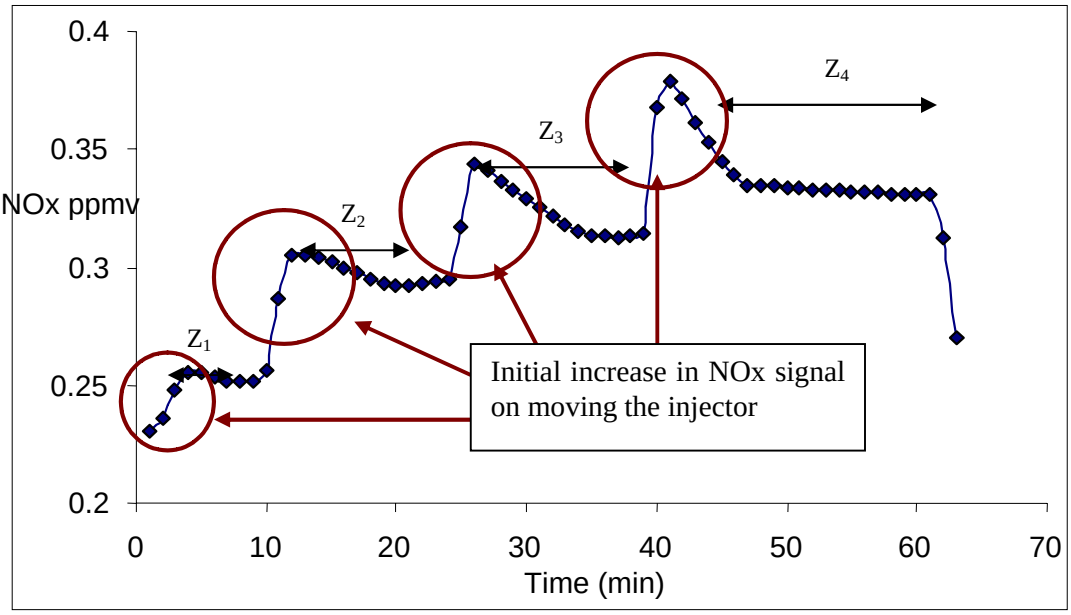

Figure 2.17: NO_x signal, which corresponds to an ammonia concentration of 400 ppbv, plotted against time at 25 %RH as the injector position is varied. The injector positions are shown as Z_1 (longest residence time) to Z_4 (shortest residence time). Red circles show the increase in the NO_x signal on moving the injector.

Another characteristic feature of this system became apparent on moving the injector (see red circles in Figure 2.17). A notable increase in NO_x signal was observed, but this quickly decreased before stabilising at a new value, somewhat higher than the previous one. NH_3 was absorbed onto the walls of the flow-tube and was in equilibrium with gaseous ammonia. When the injector was moved to a lower position, NH_3 quickly desorbed from the region of the flow-tube where the gaseous

ammonia had now ceased to flow. The result was an increase in concentration reaching the chemiluminescence monitor. A new equilibrium situation was reached and a stable NO_x signal was observed.

A kinetics run was performed by recording NO_x signals [14], the injector at first being positioned to give a long exposure of NH_3 to the particles (Z_1). Ever decreasing exposure to the particles was achieved by moving the injector in increments of 20 – 23 cm in the direction of the denuder. The injector was then moved in similar increments back towards its original position (Z_1). It was noted that the recorded data at long exposure (from the injector to the denuder region distances of 75 to 98 cm) was slightly higher at the end of a kinetic run than it was at the beginning. Figure 2.18 shows the recorded NO_x signal as the injector was moved firstly towards and then away from the denuder over time. This small increase in background signal was attributed to NH_3 desorbing from surfaces, especially from those surfaces in close proximity to the detection region. However, this effect was averaged out and was not expected to have any significant impact upon the value of the first-order rate coefficient *k*.

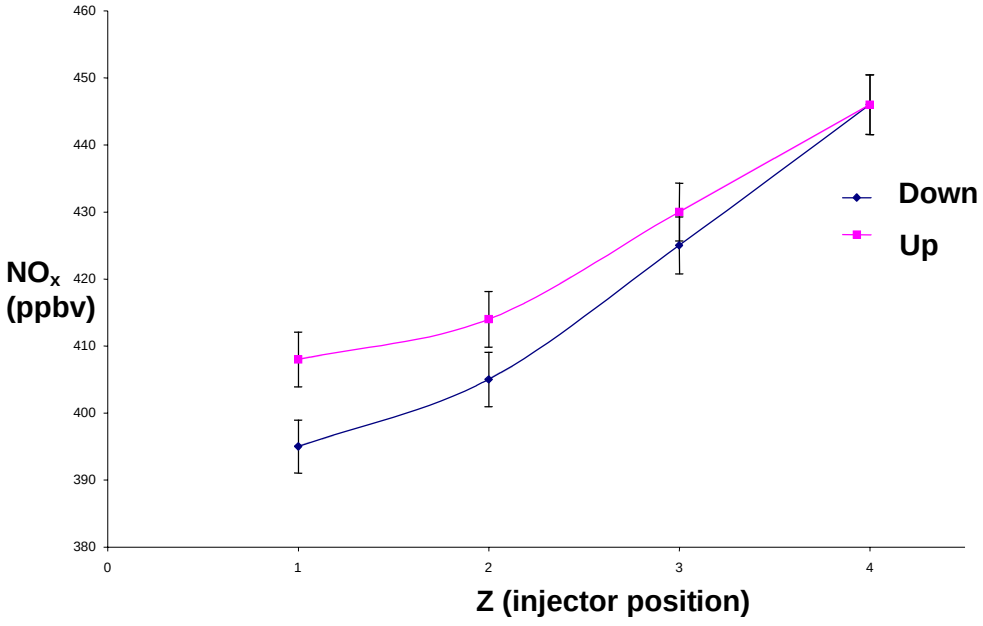

Figure 2.18: NO_x signal for 500 ppbv NH_3 as the injector is moved towards (blue line) and away from the denuder (pink line). The values shown at each injector position were calculated from an average of 10 experiments.

All ammonia experiments were performed at T = 293 ± 5 K and atmospheric pressure. The total flow rate was set to 2000 sccm (flow velocity ύ = 1 cm s^{-1}). The initial ammonia mixing-ratio was tuned to [NH_3] = 5 ppmv, mainly to keep within a concentration range suitable for detection by FTIR spectroscopy.

2.5 Summary

An improved understanding of heterogeneous atmospheric chemistry is dependent on a close interplay between laboratory experiments, field measurements, theoretical simulation of interfacial dynamics and atmospheric modelling. This is critical to elucidate fundamental processes and their relationship to each other. Attempts must be made to bridge these areas by using laboratory techniques to examine the dynamics of multicomponent and multiphase aerosols under conditions relevant to the atmosphere. In this work, a novel aerosol flow-tube system has been used to monitor the interactions between trace gases and tropospherically relevant aerosols. This apparatus is unique, in that it employed two aerosol generation methods and provided experimental set-ups to follow the size evolution of the aerosol particulate matter while simultaneously allowing detailed spectroscopic investigation of its chemical content. In addition, an Ostwald type reaction coupled with a chemiluminescence NO_x monitor was used. Also of interest is the possibility to vary the relative humidity of the system between 1 and 90 %RH, thus simulating conditions that are present in the atmosphere.

The aerosol flow-tube configuration, developed in this study, involved the employment of a laminar flow-tube, which was coupled to a FTIR spectrometer for monitoring the gas- and condensed-phase composition. Aerosol parameters were determined using a Size Mobility Particle sizer (SMPS). A chemiluminescence NO_x monitor was used to detect ammonia and ammonium ion (NH_3/NH_4^+). The system allowed a number of parameters to be observed, and, as a whole, proved extremely sensitive in detecting the various changes that occurred in relative humidity, aerosol composition and particle size for the ammonia-acid systems studied here.

2.6 References

(1) Pandis, S. N.; Seinfeld, J. H. *Journal of Geophysical Research-Atmospheres* **1989**, *94*, 12911-12923.

(2) Seinfeld, J. H.; Pandis, S. N. *Atmospheric Chemistry and Physics*; Wiley-Interscience, 1997.

(3) Schweitzer, F.; Magi, L.; Mirabel, P.; George, C. *Journal of Physical Chemistry* **1998**, *102*, 593-600.

(4) Smallwood, H. M. *Journal of the American Chemical Society* **1985** (**1929**), *51*.

(5) Kaufmann, F. *Proceeds of the Royal Society of London* **1958**, *247*, 123.

(6) Brown, R. L. *Journal of Research of the National Bureau of Standards* **1978**, *83*, 1-8.

(7) Utter, R. G.; Burkholder, J. B.; Howard, C. J.; Ravishankara, A. R. *Journal of Physical Chemistry* **1992**, *96*, 4973-4979.

(8) Lovejoy, E. R.; Hanson, D. R. *Journal of Physical Chemistry* **1995**, *99*, 2080-2087.

(9) Hu, J. H.; Abbatt, J. P. D. *Journal of Physical Chemistry A* **1997**, *101*, 871-878.

(10) Hanson, D.; Kosciuch, E. *Journal of Physical Chemistry A* **2003**, *107*, 2199-2208.

(11) Mozurkewich, M.; Henry, B.; Fried, A.; Fox, J.; Calvert, J. G. *Review of Scientific Instruments* **1994**, *65 (5)*, 1675-1678.

(12) Fried, A.; Henry, B. E.; Calvert, J. G.; Mozurkewich, M. *Journal of Geophysical Research* **1994**, *99*, 3517-3532.

(13) Hanson, D. R.; Lovejoy, E. R. *Science* **1995**, *267*, 1326-1328.

(14) Noonan, C. *'A Laboratory Study of Heterogeneous Chemistry between Ammonia and Acidic Particles relevant to the Troposphere'*, Ph.D Thesis: University College Cork, Ireland, 2007.

(15) Howard, C. J. *Journal of Physical Chemistry* **1979**, *83*, 3-9.

(16) Keyser, L. F. *Journal of Physical Chemistry* **1984**, *88*, 4750-4758.

(17) Abbatt, J. P. D.; Demerjian, K. L.; Anderson, J. G. *Journal of Physical Chemistry* **1990**, *94*, 4566-4575.

(18) Weast, R. C. *CRC Handbook of Physics and Chemistry*; CRC: Florida, 1979.

(19) Shelley, T. J. The Development And Application Of Tungsten Oxide Surfaces For The Preconcentration Of Ammonia And Nitric Acid In Air", Thesis: University of South Florida, Tampa**,** 1986.

(20) Coulson, J. M.; Richardson, J. F. *Chemical Engineering,* Pergamon Press: Oxford England, 1954; Vol. 1.

(21) Logan, B. E. *Environmental Transport Processes*, 1st ed.; John Wiley & Sons, New York, 1999.

(22) McMurry, P. H.; Takano, H.; Anderson, G. R. *Environmental Science and Technology* **1983**, *17*, 347-352.

(23) TSI Model 3075/3076 Constant Output Atomiser, Instrument Manual. August 1998; Vol. F.

(24) Perry, R. H. C. C. H. *Chemical Engineers' Handbook*; McGraw-Hill: New York, 1973.

(25) Zaytsev, I. D. A. G. G. *Properties of Aqueous Solutions of Electrolytes*; CRC Press: New York, 1992.

(26) Stephens, E. R. *Society for Applied Spectroscopy* **1958,** *12,* 80-84.

(27) Hollas, J. M. *Modern Spectroscopy*, Second ed.; John Wiley; 1992.

(28) Murrell, J. N.; Kettle, S. F.; Tedder, J. M. *The chemical bond,* 2 ed.; Wiley: New York, 1985.

(29) TSI Model 3080 Electrostatic Classifier, Instrument Manual. August 1998; Vol. F.

(30) Lundgren, D. A.; Harris, F. S.; Marlow, W. H.; Lippmann, P.; Clark, W. E.; Durham, W. E. *Aerosol Measurement,* **1979**.

(31) TSI Model 3010 Condensation Particle Counter, Instrument Manual. July 2000, Vol E.

(32) Cotton, F. A.; Wilkinson, G. *Advanced Inorganic Chemistry*, 5th ed.; Wiley: New York, 1988.

(33) Morris, M. A. Oxidation Catalysts. In *ICI PLC*; Patent, Martin Fowles: GB, 1994; Vol. EC: BO1J23/10.

(34) Perrino, C.; Gherardi, M. *Atmospheric Environment* **1999**, *33*, 4579-4587.

(35) Clapp, M. L.; Miller, R. E. *Icarus* **1993**, *105*, 529 - 536.

(36) Herzberg, G. *Infra-red and Raman Spectra of Polyatomic Molecules*; Van Nostrand: New York, 1955.

(37) Nakamoto, K. *Infrared and Raman Spectra of Inorganic and Coordination Compounds*; John Wiley and Sons Inc.: New York, 1997; Vol. 2.

(38) Coates, J. P. *Encyclopedia of Analytical Chemistry*; John Wiley & Sons Ltd: Chichester, 2000.

(39) Wagner, L.; Hornig, D. F. *Journal of Chemical Physics* **1950**, *18*, 296-304.

(40) Townsend, T; Sodeau, J.R. *Nucleation and Atmospheric Aerosols:Conference Proceedings, Galway: National University of Ireland* **2007**, 802-808.

Chapter 4

Heterogeneous interactions between ammonia and multi-component ‘sulfurous acid’/oxalic acid aerosols

4.1 Introduction

It has become evident that real atmospheric aerosols, present in the troposphere, are chemically complex and consist of both inorganic and mixed inorganic/organic species. Sulfur dioxide and water mixtures as discussed in Chapter 3 of this thesis are important species as they are responsible for the atmospheric formation of sulfuric acid by homogeneous and heterogeneous oxidation processes. Oxalic acid, present in the troposphere, is the most abundant dicarboxylic acid in aerosols in both urban and remote atmospheres, and is often a significant contributor to the overall particulate organic mass. Ammonia is a predominant airborne gaseous base and, as such, holds an important place in atmospheric chemistry neutralisation. Hence, aerosols consisting of mixtures of 'sulfurous' and oxalic acid were studied by the complementary FTIR and SMPS techniques and their interaction with ammonia analysed.

4.1.1 Atmospheric context

4.1.1.1 Sulfur (IV) Chemistry in the Troposphere

The troposphere consists of a variety of multiphase, complicated systems. For example, evolution of both inorganic and organic components of aerosol during a Saharan dust episode were observed in the French Alps [(1)]. The radical-driven oxidation of S(IV) species to S(VI), even after a great deal of research in the last one hundred years, still constitutes an extensive research topic in its own right [(2)]. Open questions exist with regards to the dependencies of elementary reaction rate coefficients on temperature and also to ionic strengths and ionic composition of solution. Aqueous-phase processing studies have turned more and more towards investigating the effects of organic compounds on S (IV) oxidations. Organic chemistry in cloud water may influence the rate of S(IV) oxidation in droplets [(3)], alter the pattern of precipitation composition, and may also lead to the production of harmful substances [(4)].

As well as the S(IV) to S(VI) oxidation process, another important in-cloud reaction involving S(IV) is the formation of hydroxymethane sulfonate (HMSA), an adduct (Figure 4.1) resulting from the reaction between formaldehyde (HCHO) and S(IV) in solution (Equation 4-1).

Fig 4.1: Hydrated formaldehyde and hydroxymethane sulfonate structures.

$$HCHO + HSO_3^- \rightleftharpoons CH_2(OH)SO_3^- \qquad \textit{(4-1)}$$

Formaldehyde is a ubiquitous compound in the atmosphere [5] and the adduct formation leads to total concentrations of both HCHO and S(IV) in solution that are far greater than those predicted by Henry's Law. HMSA can therefore serve as a reservoir for both HCHO and S(IV) in solution, since bound S(IV) is stable towards oxidation. Another potentially very interesting coupling of sulfur chemistry to organic chemistry exists in the area of multiphase dimethyl sulfide (DMS) oxidation. Recent laboratory experiments have shown that OH radicals can react with HMSA quite rapidly. The major reaction appears to be abstraction of a hydrogen atom from the carbon. In the presence of oxygen, the major products are sulfate and formic acid, but more than one sulfate ion is formed for each OH radical consumed. This suggests the occurrence of an aqueous chain oxidation reaction carried by either OH or SO_4 radicals. Both are capable of abstracting a hydrogen atom from hydroxymethane sulfonate. It has also been shown that the presence of organic material in ammonium sulfate aerosols can lower their deliquescence relative humidity (DRH) [6] and can alter their hygroscopic growth [7]. The presence of these compounds can also affect the ability of the particles to take up water and to form ice crystals in the atmosphere.

Acidic aerosols are found in the atmosphere mainly as a result of atmospheric reactions between emissions from a variety of fossil fuel combustion sources,

including power plants, industrial and commercial facilities, hazardous waste storage and treatment facilities. There is a size – pH dependency due to differing particulate chemical content as discussed below. For example, at three locations in Bavaria (Central Europe), aerosol particles were collected in five size fractions and the water soluble part of each fraction was analysed for both major ions and strong, weak or neutralising acidities [8]. This study revealed a distinct difference in amount and character of the acidity between fine (particle diameter, denoted $D_p < 1.35$ μm) and coarse ($D_p > 4.05$ μm) particles. Fine particles always reacted in an acidic fashion with their acidity mainly resulting from the presence of strong acids. Concentrations were highest in polluted urban air, where weak, organic acids were also present in the fine particles. The *in situ* pH values for these particles were calculated, and found to range between 1 – 2 at all sampling sites. Coarse particles were only slightly acidic, with mean *in situ* pH values between 5.5 – 6.5. Their acidity was mainly caused by weak acids, especially hydroxylated metal ions dominated by aluminium. Another field study investigated the aerosols in the Hawaiian marine boundary layer and found that the pH ranged from 4.5 to 5.4 (median 5.1) for super-μm (primarily sea-salt) size fractions and 2.6 to 5.3 (median 4.6) for sub-μm (primarily sulfate) fractions [9]. The *in situ* free acid concentration and pH of atmospheric aerosols has also been investigated in Hong Kong where it was found that the particles were highly acidic in general, and that the pH of sub-micron acidic sulfate aerosols was significantly below 3 [10].

4.1.1.2 Ammonia in the Troposphere

Ammonia is the predominant airborne gaseous base, and, as such, holds an important place in atmospheric chemistry. The total global NH_3 emission has been estimated to be of the order 50 Mt N yr^{-1} [11]. The average global ammonia concentration in the atmosphere ranges from 0.3 to 15 ppbv [12], with concentration orders of magnitude higher in the vicinity of agricultural or industrial regions. For example, near some types of livestock areas, the local atmospheric concentration has been reported to be as high as 47 ppmv [13]. Since it is the only soluble base

found in the atmosphere in significant quantities, it plays a principal role in neutralising acidic aerosols converting them to new non-volatile aerosol particles. This process of neutralisation influences the aqueous oxidation rates of S(IV) species and the formation of new aerosols.

Ammonia reacts readily with sulfuric, nitric, hydrochloric and carbonic acids to form ammonium sulfate ($(NH_4)_2SO_4$), letovicite ($(NH_4)_3H(SO_4)_2$), ammonium bisulfate (NH_4HSO_4), ammonium nitrate (NH_4NO_3), ammonium chloride (NH_4Cl) and ammonium carbonate ($(NH_4)_2CO_3$) aerosols, respectively, as attested by the high concentrations of particulate ammonium sampled throughout the troposphere. The sulfate budget in particular is greatly affected by the availability of gaseous ammonia, as $(NH_4)HSO_4$, $(NH_4)_3H(SO_4)_2$ and $(NH_4)_2SO_4$ are stable. In contrast, ammonium nitrate tends to be shortlived and re-evaporates into its original gas-phase constituents of NH_3 and HNO_3. From a variety of measurements, the lifetime of ammonium-containing aerosols has been determined to be of the order of ~ 4 days [(14)].

Although there is a large variation from country to country, about 80% of the agricultural ammonia emissions in Europe are attributed to contributions from animal manure, the remaining 20% are assigned to the use of fertilisers. The contribution of road traffic to non-agricultural ammonia emissions has been considered to be rather small. However, ammonia emissions from road traffic are expected to be increasing in future as a result of the introduction of vehicles equipped with catalytic convertors [(15),(16)]. Consequently, road traffic might soon become an important source of ammonia in urban areas [(17)]. Gaseous ammonia has a relatively short atmospheric lifetime and is deposited fairly close to its source [(18)]. When dissolved in water droplets, ambient ammonia can form secondary aerosol particles, such as ammonium nitrate and ammonium sulfate, which may remain airborne for longer times, and therefore, can be transported over longer distances [(19)]. In order to account for the complex impacts of ammonia to the environment, reduction targets for ammonia were set by the protocol to the Convention on Long-

Range Transboundary Air Pollution in Europe. The member countries of the Convention accepted an obligation to reduce ammonia emissions to the agreed national emission ceilings by 2010 [20].

Primary sources of ammonia are located at the Earth's surface and are mainly attributed to biological or agricultural activities. Ammonia has a relatively short atmospheric lifetime (generally 24 hours) and undergoes dry deposition to wet surfaces and vegetation very efficiently [14]. Ammonia that is not deposited is available for reaction, but gas- phase reactions involving NH_3 tends to be slow. Its tropospheric lifetime for reaction with the OH radical for example, is ~ 2.5 months. As a result, the heterogeneous chemistry of NH_3 plays an important role in determining its eventual fate in the atmosphere.

Ammonia has a high solubility in water (89.9 g/100 ml at 0 ^{o} C [21]). Therefore, depending on the extent of neutralisation and relative humidity, atmospheric aerosol particles containing NH_3 may exist in a completely dissolved, partially dissolved or crystalline state. Full consideration of atmospheric ammonia should then include the effects of partitioning on the chemistry associated with the aqueous- and particle-phases as well as the gas-phase. In all three phases ammonia is the major neutralising agent for acid vapours, acid aerosols and acids dissolved in cloud- and fog-water.

4.1.2 Previous atmospheric studies

It has become evident that atmospheric aerosols are chemically complex, with both organic and mixed inorganic/organic aerosols widely present in the troposphere. Given the chemically mixed nature of aerosols, it is therefore important to understand and quantify the effect of organic chemicals on the phase transition behaviour of model inorganic tropospheric aerosols. To date, several studies have examined mixtures of dicarboxylic acids and inorganic salts with respect to phase transitions or water uptake. These include a study of the deliquescence relative

humidities of ternary bulk solutions [25] and the water cycles of dicarboxylic acids with both sodium chloride and $(NH_4)_2SO_4$ using an electrodynamic balance (EDB) technique [26]. Four tandem differential mobility analyser (DMA) studies have been performed. For example, mixtures of glutaric acid and $(NH_4)_2SO_4$ were examined [27] while water uptake of $(NH_4)_2SO_4$-dicarboxylic mixtures at three compositions were studied [28]. In addition, $(NH_4)_2SO_4$ was studied in the presence of several dicarboxylic acids [29]. Finally, the interaction between water vapour and aerosol particles, containing various amounts of inorganic salts ($(NH_4)_2SO_4$, NH_4NO_3 and NaCl) and three organic compounds (levoglucosan, succinic acid and fulvic acid) was studied at different relative humidities [30]. Lightstone et al. [31] focused on the potential heterogeneous effect of succinic acid cores on the effloresence RH of mixed ammonium nitrate-succinic acid particles.

Fe-catalysed photochemical oxidation of dissolved sulfur dioxide in the presence of oxalate ions has been studied under conditions typical for acidified water. The presence of oxalate strongly inhibits Fe(III)-catalysed S(IV) oxidation due to the formation of Fe(III) oxalate complexes both in the dark and under UV-Visible light [32]. Elevated concentrations of S(IV) and formaldehyde were observed in fog and cloudwater at sites in California. Equilibrium computations indicate that high concentrations of S(IV) cannot be achieved without the formation of S(IV) adducts [33]. Liquid sulfur dioxide reacts with aqueous NR_4OH (R = Et, Bu, or n-pentyl) solutions to form the corresponding bisulfite [34]. The preparative method used is that which leads to the formation of tetramethylammonium pyrosulfide when tetramethylammonium hydroxide is treated with sulfur dioxide. Tetra-n-propylammonium hydroxide on treatment with sulfur dioxide, yields tetra-n-propylammonium pyrosulfide. The deliquescence and crystallisation of ammonium sulfate particles internally mixed with water-soluble organic material have been studied, but restricted to an organic mass fraction of less than 0.6. The organic species used were malonic acid, glycerol, levoglusan and Suwannee River fulvic acid [35].

A detailed study of the water activity, phase transitions and growth of dicarboxylic acid-inorganic salt-water bulk solutions and aerosols has also been completed [36]. Saturated bulk solutions of up to five dicarboxylic acids with ammonium nitrate, ammonium sulfate and sodium chloride have also been examined [37]. Thermodynamic properties of mixed organic/inorganic particles have been modelled [38]. These authors note that there is a need for an improved knowledge of the physical properties of the organic component in the aerosol. Few studies have been performed but it has been shown that the presence of organic compounds may alter the deliquescence point [39],[29], the rate of deliquescence [40], and the hygroscopic behaviour [41],[29],[27] of inorganic particles. A study in the Great Smoky Mountains (USA) indicated excess water increased with increasing mass fraction of organics in particles, implying that the organic fraction of the aerosol was somewhat hygroscopic [42]. This study also showed that the amount of organic-associated water was considerably less than sulfate-associated water at high relative humidity with respect to water (RH_w), but was comparable or greater at low RH_w. Another study showed that organics can alter the water uptake behaviour of inorganic aerosol both positively (non-urban) and negatively (urban), depending on location [43].

No prior studies on correlating speciation and size behaviour of dicarboxylic acids in the presence of 'sulfurous' acid (and ammonia) have been performed.

4.1.3 Kinetic Treatment

As mentioned in Chapter 2, the kinetics of NH_3 loss in the flow-tube was measured by changing the position of the sliding injector to vary the contact time between the NH_3 and the aerosol, monitoring the formation of NH_4^+ ions simultaneously. As laminar flow conditions prevail within the flow-tube, the reaction time (t) is directly proportional to the distance (Z) between the tip of the injector and the detection/sampling point, expressed in the equation t = Z / ύ, where ύ represents

flow velocity. The linear flow velocity was 2.2 cm s^{-1} and the mixing of both flows (aerosol and ammonia) was accomplished after approximately 5 seconds [22]. Kinetic data were collected for contact times of 27 – 86 seconds.

The NH_4^+ product concentration was measured at the end of the flow-tube for a range of reaction zone lengths corresponding to reaction time (t) and the first order rate coefficient (k) was determined from plots of $\ln([NH_4^+]_0/[NH_4^+]_t)$ vs. t. The first order loss rate coefficients were corrected for diffusion and wall losses under non-plug flow conditions, using a method employed by Brown 1978. In the corrections, the gas-phase diffusion coefficient, D_g, for NH_3 was assumed to be 0.25 atm cm^2 s^{-1}. The corrected first order rate coefficient was then used to determine the uptake coefficient.

The first-order decay rate for ammonia is given by Equation 4-2:

$$\frac{d[NH_3]}{dt} = -k[NH_3] \qquad \textit{(4-2)}$$

where $k = k_w + k_r$, with k_w accounting for ammonia loss to the wall of the flow-tube, and k_r the effective reaction rate coefficient. By plotting $(\ln[NH_3]_0/[NH_3]_t)$ vs. time, the value of k can be calculated. The wall loss rate coefficient, k_w, was measured in the absence of aerosol at varying relative humidities [23].

Figure 4.2 shows graphs of ($\ln[NH_3]_o/[NH_3]_t$) vs. time for the wall loss rate at various %RH. Ammonia is adsorbed onto the walls of the flow-tube and greater adsorption is observed at higher relative humidities. The values of k_w at each of the relative humidities were in the range of 2 to 3×10^{-3} s^{-1}.

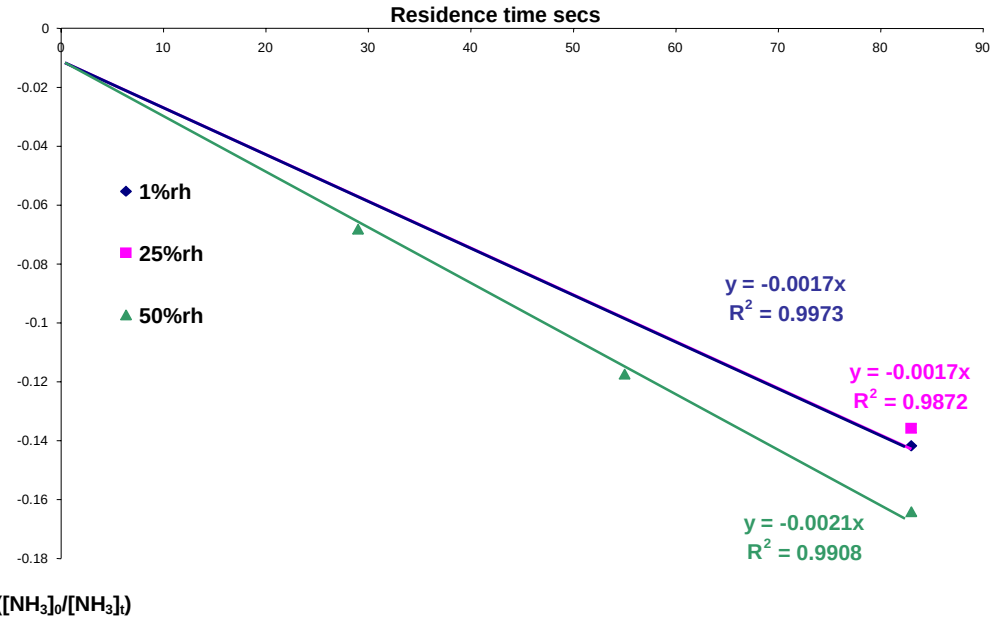

Figure 4.2: Wall-loss rates for ammonia as a function of relative humidity.

In the presence of aerosols, however, the gas-phase ammonia concentration cannot be measured directly because of interference generated by ammonium ion formation. This topic was previously addressed in Chapter 2. Hence, if the monitoring of ammonium ion concentration formed as a function of time is taken into consideration, k_r (the effective reaction rate coefficient) can be calculated using Equation 4-3:

$$\frac{d[NH_4^+]}{dt} = k_r[NH_3] = -\frac{d[NH_3]}{dt} \qquad \textit{(4-3)}$$

where $[NH_4^+]$ expresses the hypothetical ammonium concentration detected as NH_3/NO_x subsequent to pyrolysis/conversion on the catalyst.

The ammonia concentration is given by:

$$[NH_3] = [NH_3]_0 + [NH_3]_r + [NH_3]_w \qquad \textbf{(4-4)}$$

This can be substituted into Equation 4-3 to give:

$$\frac{d[NH_4^+]}{dt} = k_r([NH_3]_0 + [NH_3]_r + [NH_3]_w) \qquad \textbf{(4-5)}$$

The term $[NH_3]_w$ indicates ammonia that is lost to the wall and is given by:

$$[NH_3]_w = [NH_3]_0 e^{-k_w t} \qquad \textbf{(4-6)}$$

The ammonia that has reacted is equal to the ammonium ions formed which is made up of absorbed ammonia and reacted ammonia and is given by:

$$-[NH_3]_r = +[NH_4^+] = [NH_3]_r + [NH_3]_{abs} \qquad \textbf{(4-7)}$$

Assuming the only processes affecting the initial ammonia concentration $[NH_3]_o$ are established by the dilution unit, Equation 4-8, in conjunction with equations 4-6 and 4-7, can be written in the form:

$$\frac{d[NH_4^+]}{dt} = k_r[NH_4^+] + k_r[NH_3]_o(1 - e^{k_w t}) \qquad \textbf{(4-8)}$$

As the wall loss rate coefficient (k_w) is practically negligible (Figure 4.4), it is possible to ignore the second term in the equation and thereby obtain k_r by plotting $\ln([NH_4^+]_0/[NH_4^+]_t)$ vs. time.

The reaction probability γ is then calculated from k_r using Equation 4-9:

$$\gamma = \frac{4k_r}{S_a\langle c\rangle} \qquad \textbf{(4-9)}$$

where S_a is the surface area of the aerosol suspension as measured by the SMPS (cm^2/cm^3) and <c> is the mean molecular speed of NH_3 under the experimental conditions (calculated to be 6×10^4 cm s^{-1}).

As a short pathlength was imposed by the flow-tube geometry, it was not possible to rely, with confidence, on spectroscopic detection for quantitative measurements. Therefore, the primary use of the FTIR spectrometer in this current study was in the area of product characterisation, with the chemiluminescence technique being applied for quantitative analysis, as described below.

A linear correlation was observed between the NO_x ($NO + NO_2$) signal and increasing NH_3 concentration, with a calibration factor of 1.2 ± 0.03, which was subsequently applied to NO_x values pertaining to gaseous ammonia (see Figure 4.3) [23].

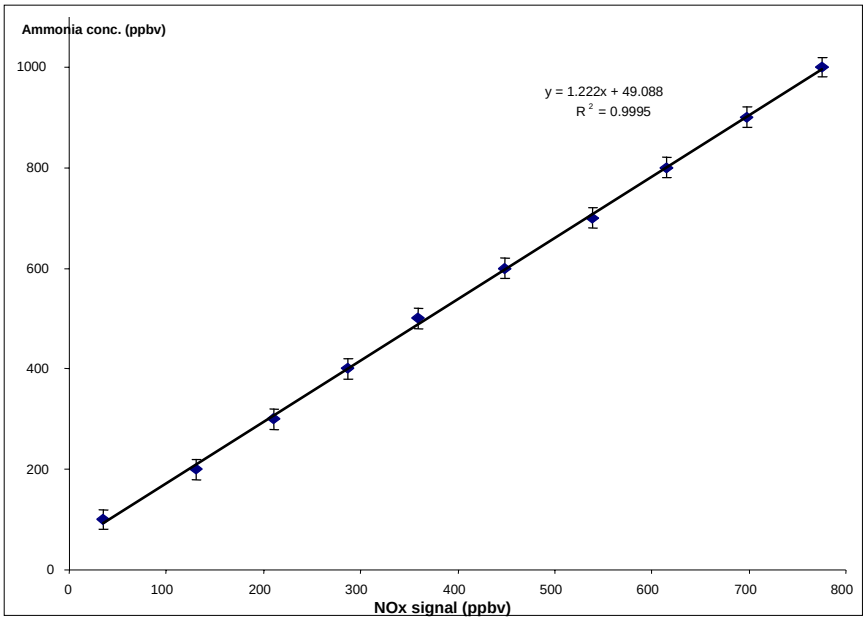

Figure 4.3: Calibration curve for NO_x signal vs. ammonia concentration giving a calibration factor of 1.2 ± 0.03.

Ammonia was admitted into the flow-tube *via* the sliding injector and the flow rate was varied from 100 to 200 to 300 sccm, resulting in a concentration range of 4.3 to 8.7 to 13 ppmv, respectively.

The interactions between ammonia gas and 'sulfurous'/oxalic containing aerosols were then examined. The general procedure was similar for each aerosol suspension studied. Firstly, the aerosol suspension, generated from either the constant output atomiser, was admitted into the reactor and was allowed to fully equilibriate for several minutes during which time background data were recorded. Once the relative humidity and the aerosol suspension were well established and had reached equilibrium, ammonia was then introduced via the injector. After approximately five minutes, the NO_x signals were found to rise to a new equilibrium value, indicative of the amount of ammonium ions formed: the reaction time being in direct relation to the injector position. The obtained value was then corrected for background noise and the injector was moved to a new position. The purpose of this experimental procedure was to determine a first order coefficient (k) for NH_3. This was achieved by altering the position of the sliding injector to vary the contact time (27 ─ 86 seconds) between the aerosol and the ammonia, while also monitoring the formation of NH_4^+ ions. Ammonia that is taken up diffuses throughout these small particles very rapidly. An approximate time scale for diffusion of a species with diffusion coefficient D_l in a particle of radius a is given by a^2/D_l. For a ~ 100 nm and D_l ~ 10^{-6} cm^2 s^{-1}, this time is ~ 10^{-4} s [24]. Similar sets of experiments were conducted at three relative humidity values, 32, 55 and 80 %RH, respectively, to probe the role of water (liquid or adsorbed vapour) in promoting the uptake of ammonia at the particle interface. The phase of the aerosol at each relative humidity was an aqueous saline solution.

The reaction between ammonia and the aerosols leads to the formation of condensed-phase ammonium ions, but adsorption of ammonia onto the particles (without chemical reaction) is also possible. As previously discussed in Chapter 2, the oxalic acid coated denuder removes all trace of gaseous ammonia from the aerosol supply which is sampled by the chemiluminescence monitor. However, this detection technique can be described as destructive rather than passive and the uptake products are ultimately converted back to gaseous ammonia by catalytic oxidation, resulting in the NO_x monitor being unable to distinguish between

ammonium ions formed and adsorbed ammonia. The availability of water appears to control the uptake of ammonia and the possibility that ammonia is lost to the surface, by some adsorption process involving hydrogen bonding of ammonia with water molecules present at the surface of the particles, cannot be disregarded. It must be stated however, that evidence of ammonium ion formation, in the reaction of ammonia and the aerosols, is also given by FTIR measurements. Spectra recorded in the presence of ammonia show the appearance of ammonium ion modes (NH_4^+ deformation 1457 and 1401 cm^{-1}) as shown in Figure 4.4.

Gaseous ammonia is visible in the FTIR spectrum when the injector is at position Z_4 (short residence time). This observation is to be expected as ammonia has a short interaction time with the aerosols. Quantification of materials in the condensed-aerosol phase using FTIR spectroscopy is quite complex and the possibility that both ammonia adsorption and ammonium ion formation are occurring concurrently cannot be excluded.

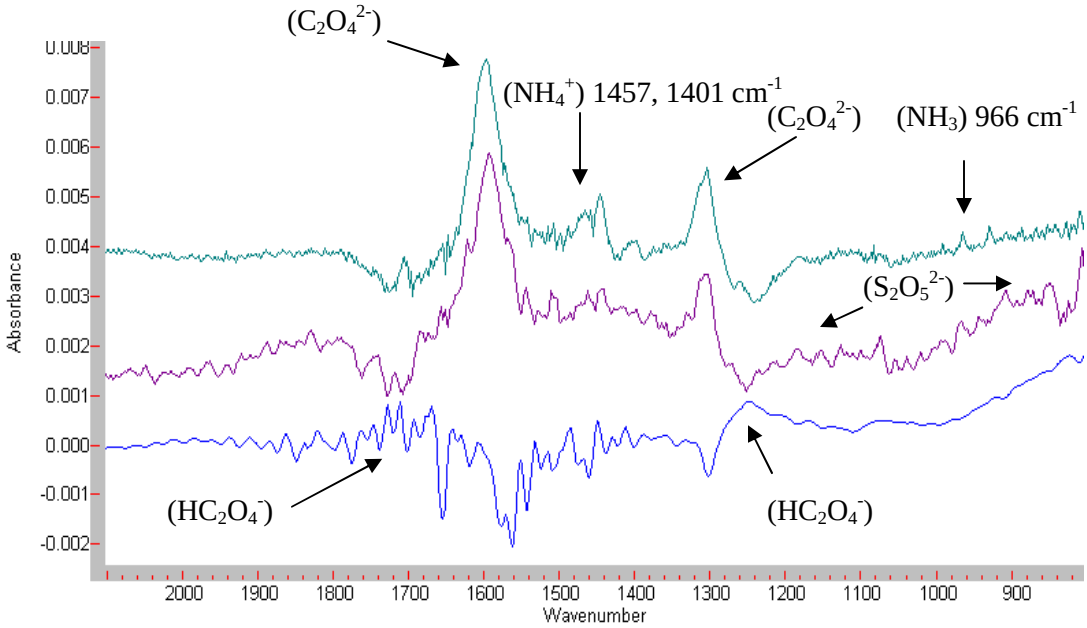

Figure 4.4: FTIR spectra of 0.5 wt% $SO_2.H_2O$ + 0.5 wt% $C_2H_2O_4$ (bottom), NH_3 + 0.5 wt% $SO_2.H_2O$ + 0.5 wt% $C_2H_2O_4$ at Z_1 (middle) and NH_3 + 0.5 wt% $SO_2.H_2O$ + 0.5 wt% $C_2H_2O_4$ at Z_4 (top). NH_3 gas is visible in the top spectrum only.

The addition of 300 sccm NH_3 to this aerosol suspension reduces the particle concentration from Z_1 to Z_4. The smaller interaction time between ammonia and the particles results with smaller particle concentrations and size distributions along with new particle formation. The particle diameter also decreases as shown in Figure 4.5.

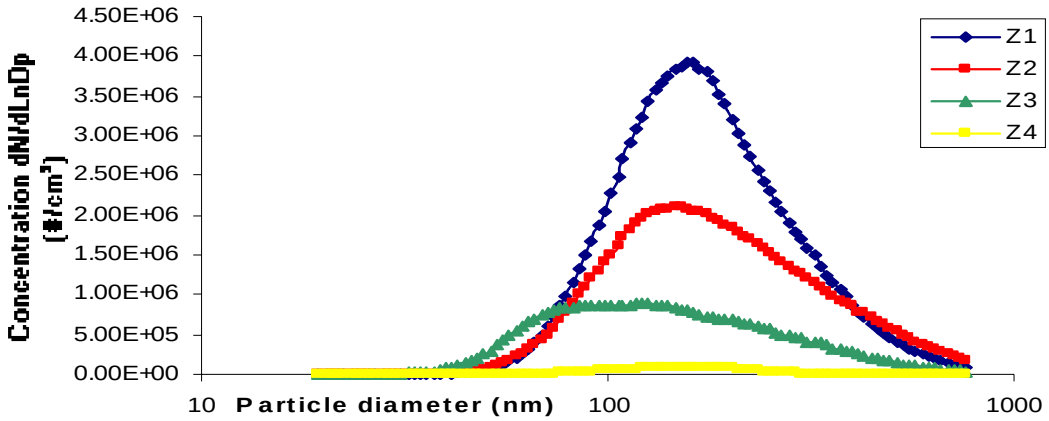

Figure 4.5: Particle number distribution for 0.5 wt% $SO_2.H_2O$ + 0.5 wt% $C_2H_2O_4$ with 300 sccm NH_3 at the four different interaction times; z_1, z_2, z_3 and z_4.

The ammonium ion concentrations were observed to decrease as the injector was moved from Z_1 to Z_4 as shown later in Figure 4.23; a direct result of the shortening of the interaction time between ammonia and the aerosol.

4.1.4 Aim and Chapter Overview

It is important to understand in detail simple binary organic-water systems before complex mixed inorganic-organic systems are considered. In reality such mimics are certainly too simplistic but they do represent good foundations. Therefore, mixtures of oxalic and 'sulfurous' acid aerosols and their interaction with ammonia gas were investigated by the complimentary FTIR and SMPS techniques. 'Sulfurous' aerosols were initially characterised in this current study as discussed in Chapter 3 and are, therefore, easily identified as their spectroscopic and physical characteristics have been well established. Investigating sulfate ion formation, by a possible S(IV) to S(VI) oxidation pathway, with the aid of an organic component,

was also a main purpose of this research. The chemistry of these reactions is discussed and likely mechanisms relevant to the troposphere are proposed.

4.2 Results and Discussion

4.2.1 Oxalic acid and 'sulfurous acid' aerosols with ammonia

Three different types of oxalic acid aerosols with 'sulfurous acid' were analysed: 0.25, 0.5 and 0.75 wt% oxalic acid and 0.25, 0.5 and 0.75 wt% $SO_2.H_2O$. The aerosols were generated using a commercially available constant output atomiser (COA, TSI Model 3075). Prior to injection into the flow-tube, the aerosols were diluted with dry or wet air, depending on the experimental conditions (20 and 50 %RH). Aqueous oxalic and 'sulfurous acid' dispersions of particles consist of a mixture of hydrogenoxalate, oxalate, hydrogensulfite tautomers, sulfite and disulfite ions in addition to oxalic and 'sulfurous acid'. Oxalic acid is a weak acid and does not dissociate in solution, while 'sulfurous acid' is composed of sulfur dioxide dissolved in gas ($SO_2.H_2O$) and the acid itself (H_2SO_3) cannot exist under normal atmospheric conditions as discussed previously. The potential chemical ionisations occurring within aerosols composed of a mixture of 'sulfurous' and oxalic acids are summarised in Table 4.1.

Table 4.1: Chemical reactions occurring in atmospheric aerosols containing only $SO_2.H_2O$, $H_2C_2O_4$ and water.

$SO_2.H_2O \leftrightarrow H^+ + SHO_3^-$
$SHO_3^- \leftrightarrow H^+ + SO_3^{2-}$
$2SHO_3^- \leftrightarrow H_2O + S_2O_5^{2-}$
$H_2C_2O_4 \leftrightarrow H^+ + HC_2O_4^-$
$HC_2O_4^- \leftrightarrow H^+ + C_2O_4^{2-}$
$2H_2O \leftrightarrow H_3O^+ + OH^-$

4.2.1.1 FTIR data

The following FTIR data show the spectra for interactions of 'sulfurous acid' with oxalic acid along with ammonia addition and also with varying humidity. Spectra were difficult to obtain for studies involving oxalic acid and 'sulfurous acid' at equal concentrations without ammonia. It was even more difficult to obtain spectra for oxalic acid at 0.75 wt% and 'sulfurous acid' at 0.25 wt% at both low humidity and without ammonia. This indicates the strong relationship between oxalic acid and ammonia, particularly at high humidities, especially in comparison with aqueous solutions of 'sulfurous acid'.

As an overview, the IR peaks seen range from a weak absorption at 1705 cm^{-1} (carbonyl group stretching vibration of hydrogenoxalate), to a small shoulder at 1655 cm^{-1} occasionally associated with oxalate, to a main absorption at 1594 cm^{-1} (oxalate, stretching vibration of the weakened carbonyl group). In the 1400 cm^{-1} centred region, the absorption is split suggesting ammonium ions present with hydrogenoxalate, oxalate, hydrogensulfite tautomers and disulfite ions. A medium split peak at 1314 cm^{-1} (oxalate, carboxylate group stretching formation), a medium absorption at 1265 cm^{-1} (stretching vibration of the C-OH group in the oxalic component, hydrogenoxalate) and finally an absorption at 1230 cm^{-1} representing the S-O stretch in $S_2O_5^{2-}$) are also observed. Hydrogen sulfite tautomers are present below 1200 cm^{-1}, attributed by S-O stretching vibration bands in predominantly 'sulfurous' solutions and a disulfite absorption at 950 cm^{-1} indicating the symmetric stretching of the S-O bond. Sulfur dioxide absorptions were present (the centred 1350 cm^{-1} region indicating asymmetric fundamentals of the molecule) in solutions containing a larger proportion of 'sulfurous' component. Detection of the OH group of water and the bisulfite tautomer is also noted at 3000 cm^{-1} and above. Explanations are given in Chapters 3 and 5 regarding the individual absorptions of both oxalic acid and 'sulfurous acid'. Table 4.6 at the end of this chapter summarises the observed absorptions and their assignments.

In Figure 4.6, the spectrum of 0.75 wt% $SO_2.H_2O$ and 0.25 wt% $C_2H_2O_4$ at 20 %RH (blue spectrum) and 60 %RH (green spectrum) is shown. The only clear band is the characteristic absorptions for sulfur dioxide which decrease in intensity as the humidity increases. Such an observation is also made with $SO_2.H_2O$, as explained in Chapter 3.

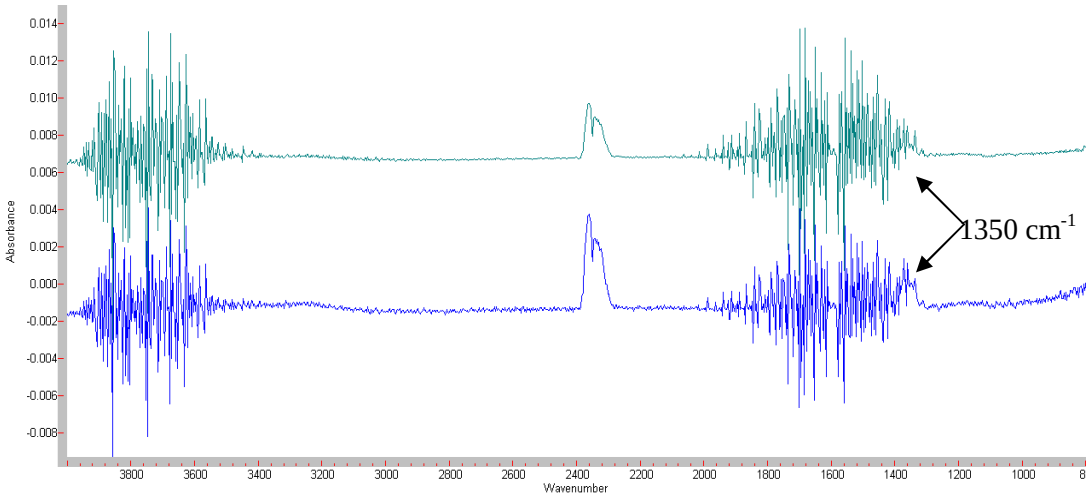

Fig 4.6: 0.75 wt% $SO_2.H_2O$ and 0.25 wt% $C_2H_2O_4$ at 20 %RH (blue) and at 60 %RH (green). Absorption of gas phase CO_2 can be seen between 2200 and 2400 cm^{-1}.

Figure 4.7 shows typical spectra obtained for 0.75 wt% $SO_2.H_2O$ and 0.25 wt% $C_2H_2O_4$ at 20 %RH and at 50 %RH with 300 sccm NH_3. Sulfur dioxide absorptions are observed in both of these spectra, however it can also be observed that the symmetric stretches of sulfur dioxide at 1350 cm^{-1} are inverted in the ammonia case indicating loss of this species and production of sulfur (IV) ions. Other absorptions associated with the 'sulfurous' component are hydrogensulfite/disulfite ions at 1200 cm^{-1} (which was deconvoluted in Chapter 3, Figure 3.15) and the S-O symmetric stretching of the disulfite ion at 950 cm^{-1}. Gaseous ammonia peaks in the latter absorption are also observed indicating neutralisation of the sulfur (IV) species. An inverted absorption at 1260 cm^{-1} is observed indicating loss of hydrogenoxalate species. The CO_2 stretching absorptions representing oxalate at 1600 and 1300 cm^{-1} are not as distinct as other oxalate absorptions in spectra with higher concentrations of oxalic acid which are discussed later. The ammonium deformation band is located at 1420 cm^{-1} which implies the formation of ammonium disulfite, with ammonium hydrogensulfite in trace amounts. The ammonium oxalate ion, which has been diagnosed at higher wavenumbers (1450 cm^{-1}), is not present at this concentration. The composition of the aerosol is a mixture of hydrogen sulfite, disulfite and oxalate ions, all of which are neutralised by ammonium ions.

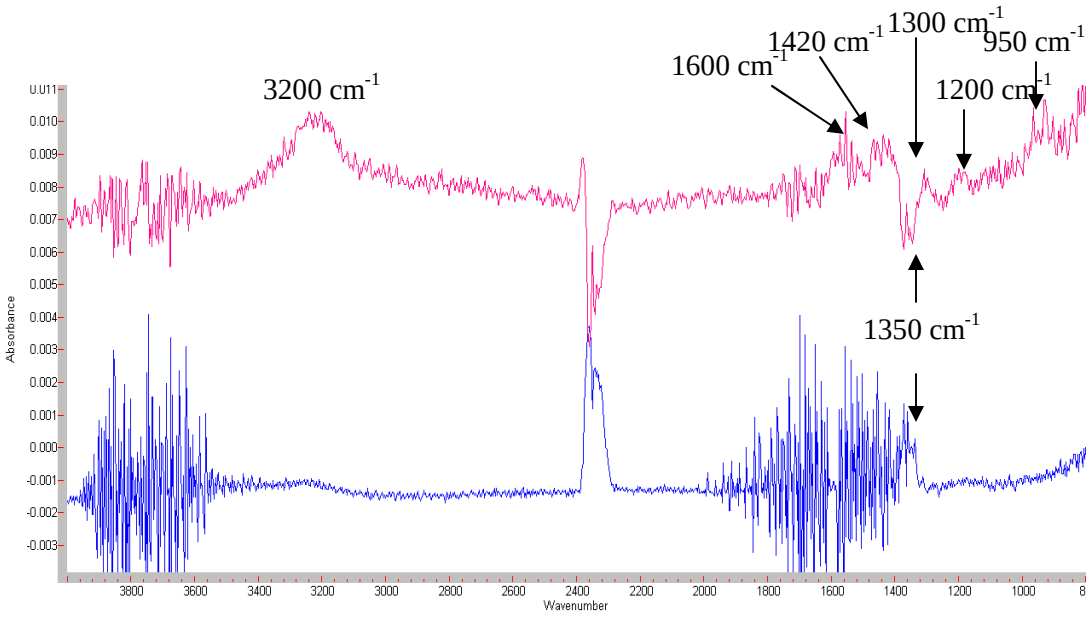

Fig 4.7: 0.75 wt% $SO_2.H_2O$ and 0.25 wt% $C_2H_2O_4$ at 20 %RH (blue) and at 50 %RH and 300 sccm ammonia (red).

Figure 4.8 displays the FTIR spectra for 0.5 wt% 'sulfurous acid' and oxalic acid at various conditions. At 15 %RH, the presence of disulfite ions (1230 cm^{-1}), which was not identified in solely 'sulfurous' acid studies, and hydrogenoxalate ions (1280 cm^{-1}) are observed. The oxalate peaks at 1300 and 1600 cm^{-1} are barely evident implying the low absorbance of these species at low humidities. After addition of ammonia at this humidity, the oxalate absorptions become clearer and more intense along with the presence of ammonium absorptions at 1400 and 1450 cm^{-1}. This indicates the presence of different types of ammonium ion pairs, specifically with oxalate, and hydrogenoxalate ions (1450 cm^{-1}) and disulfite (1420 cm^{-1}) on a minor level. The 1450 cm^{-1} is partially fragmented implying the presence of both ammonium oxalate and hydrogenoxalate. The emergence of an absorption at 1700 cm^{-1} indicates the presence of hydrogenoxalate, which is absent for studies involving only oxalic acid and ammonia at high humidities (see Chapter 5). The peaks area differences of the oxalate and ammonium absorptions range from 0.035 ± 0.001 to 0.65 ± 0.01 (1600 cm^{-1}), 0.019 ± 0.001 to 0.18 ± 0.01 (1450 cm^{-1}) and 0.005 ± 0.0001 to 0.35 ± 0.01 (1300 cm^{-1}). These spectra can be related to the SMPS data in Figure 4.16.

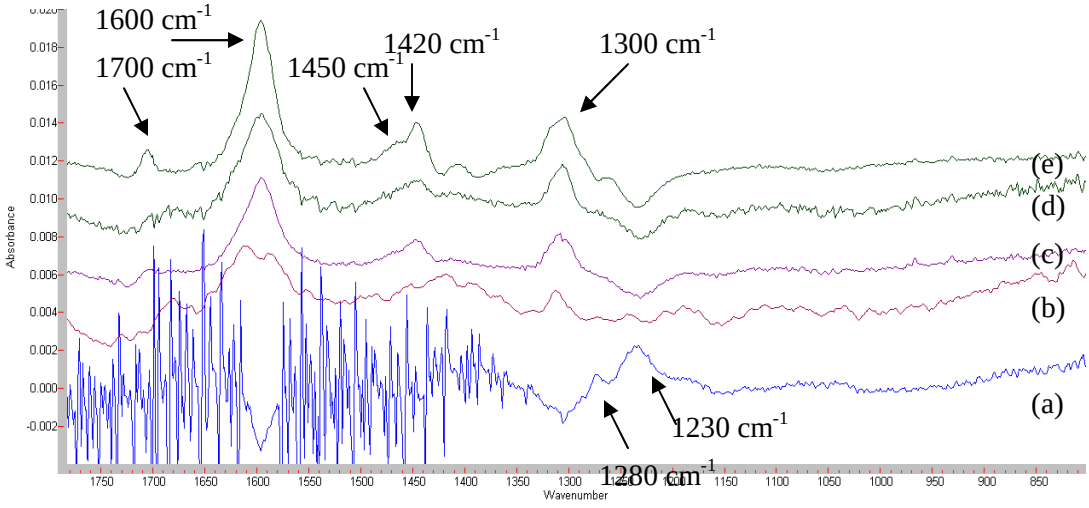

Figure 4.8: FTIR spectra of 0.5 wt% oxalic acid and 0.5 wt% 'H_2SO_3' aerosols with added ammonia 100 sccm (spectrum b), 200 sccm (spectrum c) and 300 sccm (spectrum d) at 15 %RH. Spectrum a is before ammonia is added and spectrum e is at 30 %RH with ammonia added.

Studies were undertaken involving mixtures of sulfuric acid and oxalic acid which will be discussed in more detail in Chapter 6 [23] and are shown here for comparison and contrast. FTIR spectra recorded for aerosols consisting of 1 wt% oxalic acid and 1 wt% sulfuric acid at 20 and 50 %RH are shown in Figure 4.9 (spectra a and b respectively). At 20 %RH the dominant features of spectrum (a) are the HSO_4^- ion absorption bands at *ca*. 1210, 1055 and 890 cm^{-1} and hydrogenoxalate ion absorption band at 1723 cm^{-1}. Spectral deconvolution of the peak at 1210 cm^{-1}, yields three peaks at 1242, 1216 and 1157 cm^{-1} (assigned to $HC_2O_4^-$, HSO_4^- and SO_4^{2-} ions, respectively). Increasing the humidity to 50 %RH promotes the formation of oxalate ions with the peak at *ca.* 1631 cm^{-1} assigned to oxalate ion. The broad peak centred at 1109 cm^{-1} consists of both "free" and "bonded" SO_4^{2-} ions. Therefore, at 50 %RH, the aerosols consist of a mixture of hydrogenoxalate, oxalate and sulfate ions. In comparison to 'sulfurous acid'-oxalic acid studies, the more ionised form is promoted by increasing humidity.

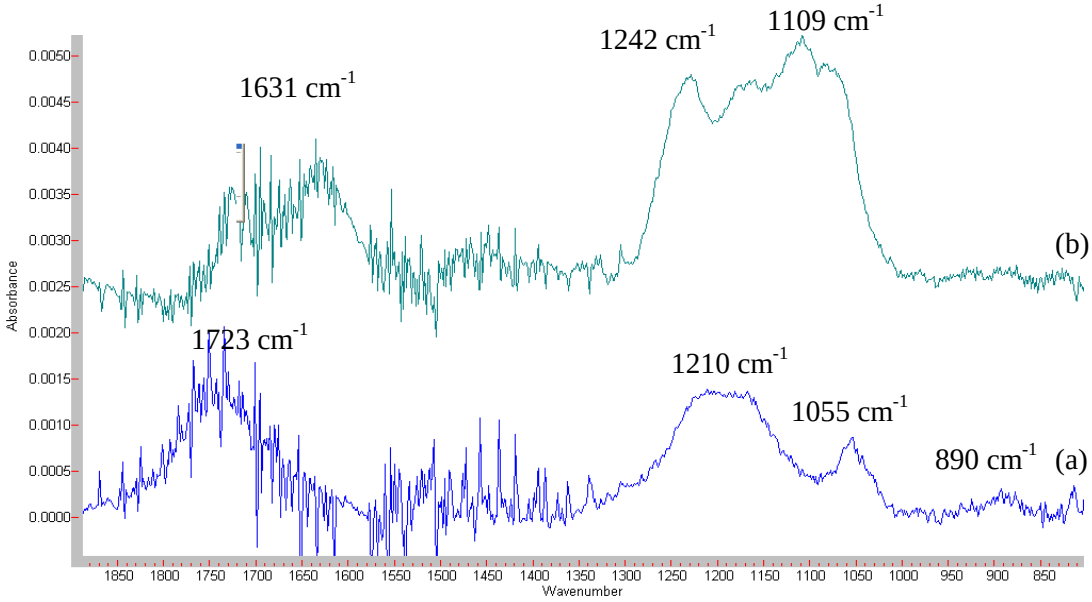

Figure 4.9: FTIR spectra of 1 wt% oxalic acid aerosols with 1 wt% H_2SO_4 spectrum (a) at 20 %RH and spectrum (b) at 50 %RH.

Figure 4.10 shows the FTIR spectra of 1 wt% oxalic acid and 1 wt% H_2SO_4 aerosols with added 100, 200 and 300 sccm NH_3 (spectra a, b and c respectively) at 20 %RH.

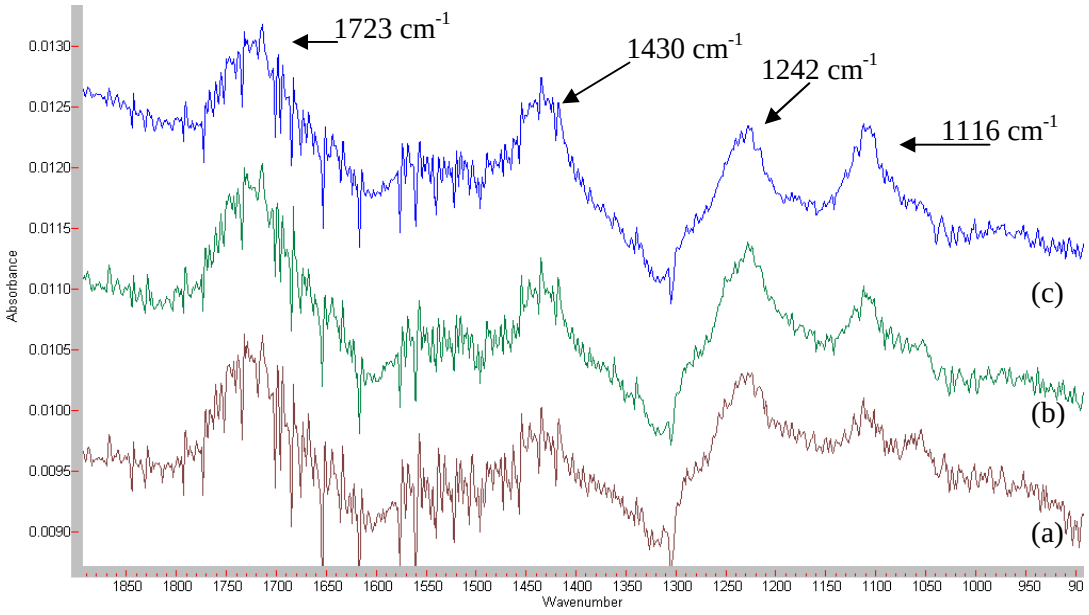

Figure 4.10: FTIR spectra of 1 wt% oxalic acid and 1 wt% H_2SO_4 aerosols with added ammonia 100 sccm (spectrum a), 200 sccm (spectrum b) and 300 sccm (spectrum c) at 20 %RH.

The composition of these acid aerosols consists of mainly bisulfate and hydrogenoxalate ions prior to the introduction of ammonia. The presence of an FTIR absorbance band at 1116 cm^{-1} indicates the formation of sulfate ions while a peak at 1430 cm^{-1} indicates a NH_4^+ ion. However this peak is asymmetrical and spectral deconvolution yields two peaks at 1438 and 1421 cm^{-1}. The latter of these peaks is attributable to the NH_4^+ ion in ammonium sulfate while the former can be assigned to the NH_4^+ ion in ammonium hydrogenoxalate. FTIR absorbances due to the hydrogenoxalate ion are at 1723 and 1242 cm^{-1}. Further additions of ammonia lead to an increase in the intensity of the NH_4^+ ion peak and SO_4^{2-} ion peak, while little change is observed for the $HC_2O_4^{2-}$ ion peaks. It can be observed here that the hydrogenoxalate ion is in abundance compared to the current studies involving

oxalic acid with 'sulfurous acid' This is due to the greater acidic strength of sulfuric acid which promotes the formation of the hydrogenoxalate ion.

At higher humidities (50 %RH), the FTIR spectra for 1 wt% oxalic and sulfuric acid aerosols with the addition of 100, 200 and 300 sccm NH_3, as represented by spectra a, b and c respectively, are shown in Figure 4.11. These aerosols are primarily composed of $HC_2O_4^-$, $C_2O_4^{2-}$ and SO_4^{2-} ions prior to the addition of ammonia.

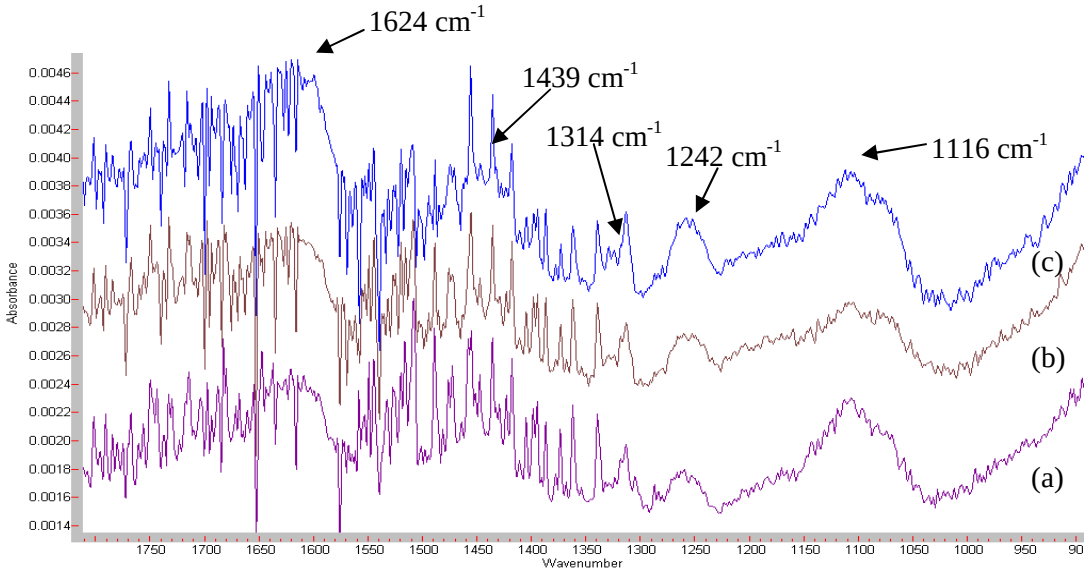

Figure 4.11: FTIR spectra of 1 wt% oxalic acid and 1 wt% H_2SO_4 aerosols with added ammonia 100 sccm (spectrum a), 200 sccm (spectrum b) and 300 sccm (spectrum c) at 50 %RH.

A number of different compounds are formed on addition of ammonia including ammonium sulfate, ammonium oxalate and ammonium hydrogenoxalate. Spectra a, b and c show a number of distinctive features at 1624 cm^{-1}, 1439 cm^{-1}, 1314 cm^{-1}, 1242 cm^{-1} and 1116 cm^{-1} and are absorption bands, corresponding to (i) ν_{as} C=O stretch (ii) ν_4 (NH_4^+) deformation mode (iii) ν_s C=O stretch (iv) ν_s C-O stretch, and (v) the ν_3 (SO_4^{2-}) mode, respectively. In addition, spectral deconvolution of the ν_4 (NH_4^+) absorbance at 1439 cm^{-1} produces three peaks at 1446, 1438 and 1421 cm^{-1}. Therefore, the addition of ammonia to mixed 1 wt% oxalic-sulfuric acid aerosols at 50 %RH results in the formation of ammonium hydrogenoxalate, ammonium

oxalate and ammonium sulfate. This is similar to the 'sulfurous acid' and oxalic acid studies in that the oxalate ions are more dominant at high humidities. However, in contrast, there is also the presence of ammonium hydrogenoxalate due to the presence of sulfuric acid which is a stronger acid than $SO_2.H_2O$.

Figure 4.12 shows spectra of 0.75 wt% $C_2H_2O_4$ and 0.25 wt% $SO_2.H_2O$ at different humidities. At 20 %RH, hydrogenoxalate and 'sulfurous ions' are mainly present. As the humidity is increased the oxalate ion absorptions are favoured.

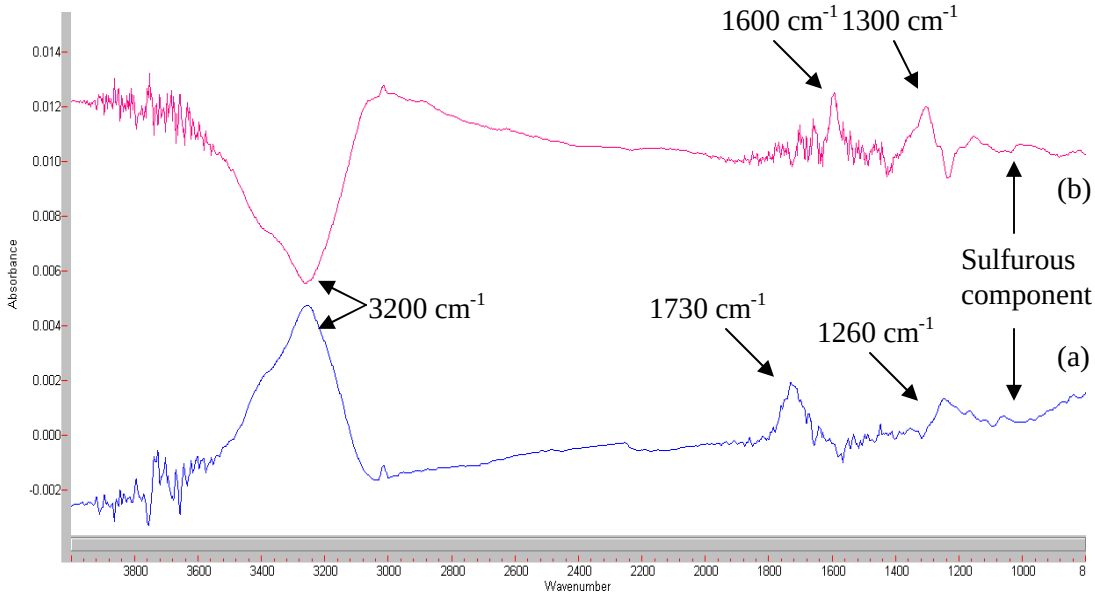

Figure 4.12: FTIR spectra of 0.75 wt% oxalic acid and 0.25 wt% 'H_2SO_3' aerosols at 20 %RH (spectrum (a)) and at 50 %RH (spectrum (b)).

There is an expected increase in the intensity of the characteristic hydrogenoxalate and oxalate ions on increasing the concentration of oxalic acid to 0.75 wt% and decreasing the concentration of the 'sulfurous acid' to 0.25 wt% as seen in Figure 4.13 which involves the addition of ammonia. The main NH_4^+ ion absorption is at 1450 cm^{-1} indicating ammonium oxalate. This band is quite sharp compared to the band at the same location in Figure 4.8 indicating the absence of ammonium hydrogenoxalate under these conditions. The peaks representing the 'sulfurous' component are not readily observable and gaseous ammonia peaks are not present. The composition of the aerosol is now a mixture of mainly hydrogenoxalate and oxalate ions.

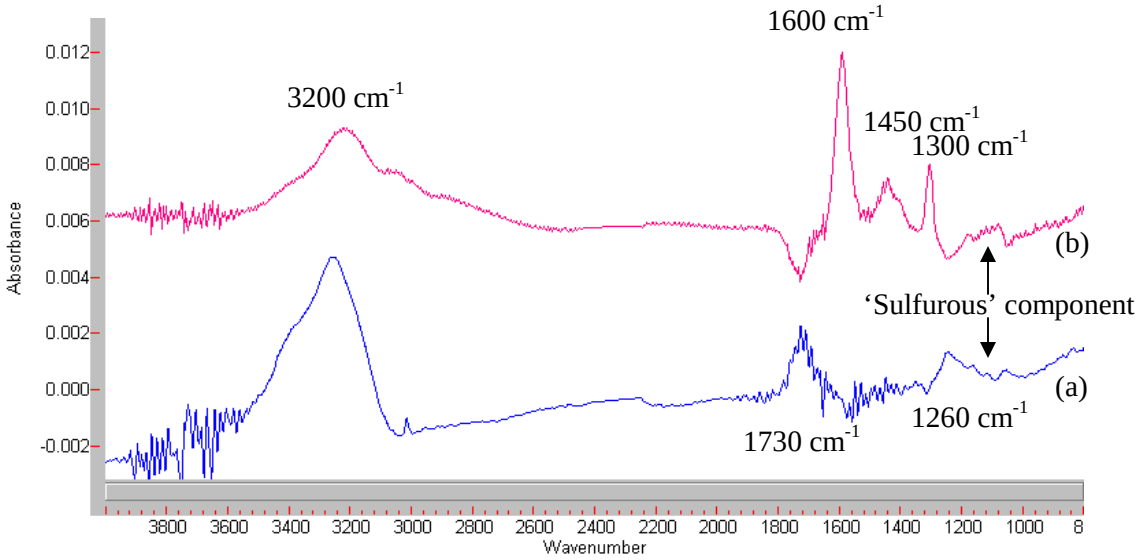

Figure 4.13: FTIR spectra of 0.75 wt% oxalic acid and 0.25 wt% 'H_2SO_3' aerosols at 20 %RH (blue) and at 50 %RH with 300 sccm NH_3 (red).

Figure 4.14 compares the spectra for each of the three concentrations at 50 %RH and 300 sccm. Gaseous ammonia peaks at 954 and 966 cm^{-1} are present in the spectrum containing an abundance of 'sulfurous acid' indicating the weakness of this acid and thus lack of reactivity with ammonia. These peaks are absent in the other spectra however indicating the affinity of ammonia for oxalic acid and subsequent generation of ammonium oxalate. The oxalate absorptions are stronger in compositions containing more organic component. Equal concentrations of each acid exhibit two distinct ammonium ions at 1420 cm^{-1} and 1450 cm^{-1} representing ammonium disulfite and ammonium oxalate respectively. The latter absorption is split indicating the presence of both hydrogenoxalate and oxalate forms of ammonium. Figures 4.15 and 4.17 relate the SMPS data for these spectra.

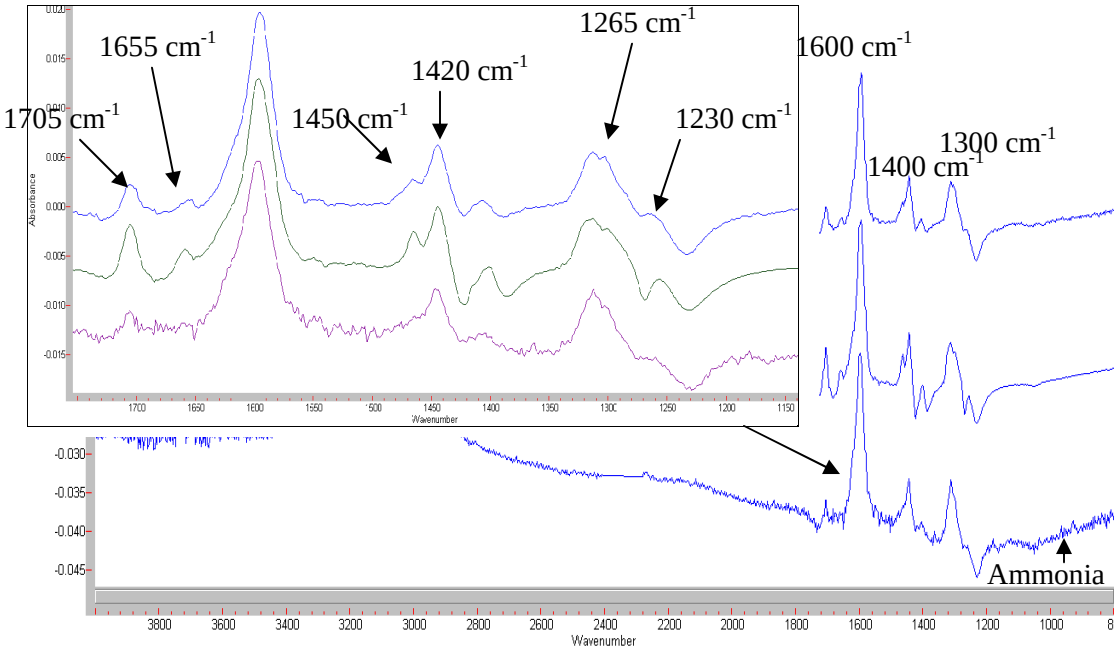

Fig 4.14: 0.75 wt% and 0.25 wt% (bottom), 0.5 wt% + 0.5 wt% (middle) and 0.25 wt% + 0.75 wt% (top) $SO_2.H_2O$ + $C_2H_2O_4$ at 50 %RH and 300 sccm ammonia. The CO_2 absorption has been removed for clarity.

4.2.1.2 SMPS data

Size measurements of the species discussed above produced contrasting results due to differences in concentration ratios. When studying this binary system with the sulfurous counterpart being dominant, both the particle number and mode increases upon increasing the humidity; the mode further increases upon introduction of ammonia. For 0.75 wt% oxalic acid-0.25 wt% 'sulfurous acid' solutions, a substantial increase of mode and number is observed due to a greater presence of organic constituent. The particle number drops and the mode becomes broader with humidity implying that water is incorporated by the organic component followed by complete ionisation to the oxalate component. The particle distribution is also broader and addition of ammonia results in an increase in particle number and a more Gaussian distribution. Figure 4.15 compares the two different concentrations and their particle distributions.

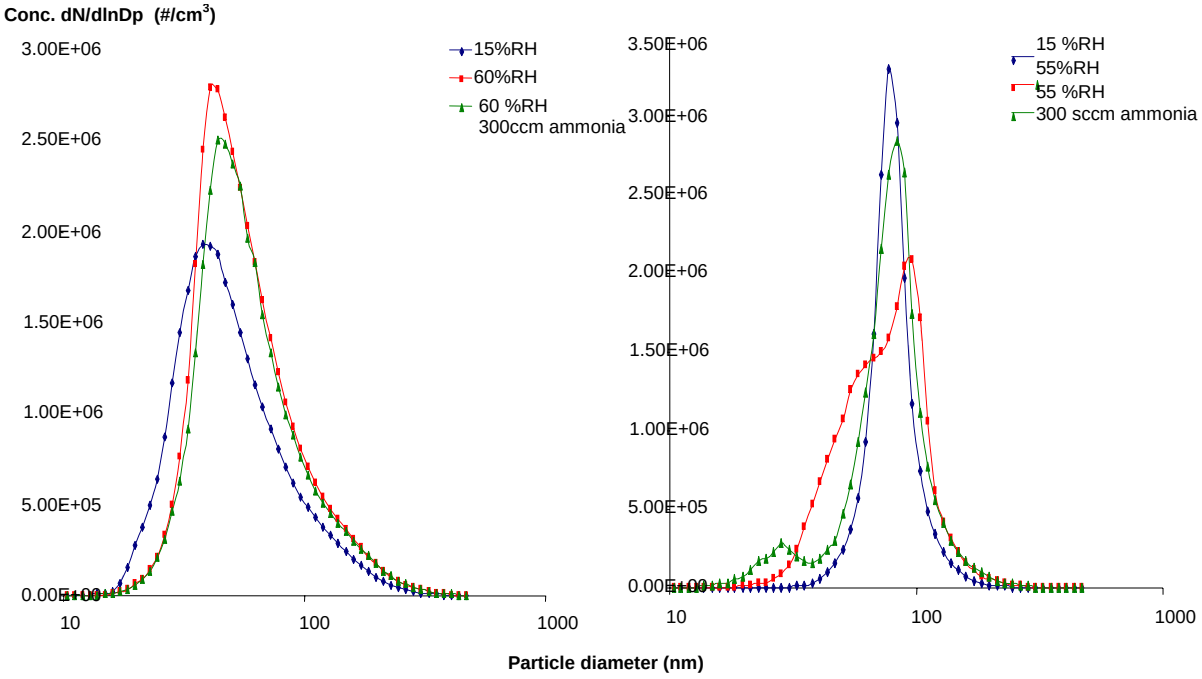

Figure 4.15: Resulting size distributions for this solution, modes of 37, 40 and 47 for 0.75 wt% 'sulfurous acid' aerosols with added 0.25 wt% oxalic acid, (blue boxes 15 %RH, red triangles: 60 %RH and green diamonds: 60 %RH + 300 sccm ammonia). Modes of 77, 96 (main mode) and 83 are seen here for 0.75 wt% oxalic acid aerosols with added 0.25 wt% 'sulfurous' acid, (blue boxes 15 %RH, red triangles: 55 %RH and green diamonds: 55 %RH + 300 sccm ammonia).

Bimodal distributions are very clearly observed in Figure 4.16 which shows the addition of ammonia to 0.5 wt% sulfurous and oxalic acid at 15 %RH suggesting the formation of two modes. The modes of roughly 40 and 100 nm vary in size distribution with increasing ammonia concentration. The smaller mode increases in particle number as ammonia is increased while the larger mode simultaneously decreases in particle number. The smaller mode at 40 nm represents the 'sulfurous' component while the oxalate component is larger as previously explained. This humidity indicates the preference of the 'sulfurous' component composed of hydrogen sulfite, sulfite and disulfite ions. These results can be linked with the FTIR spectrum 4.8.

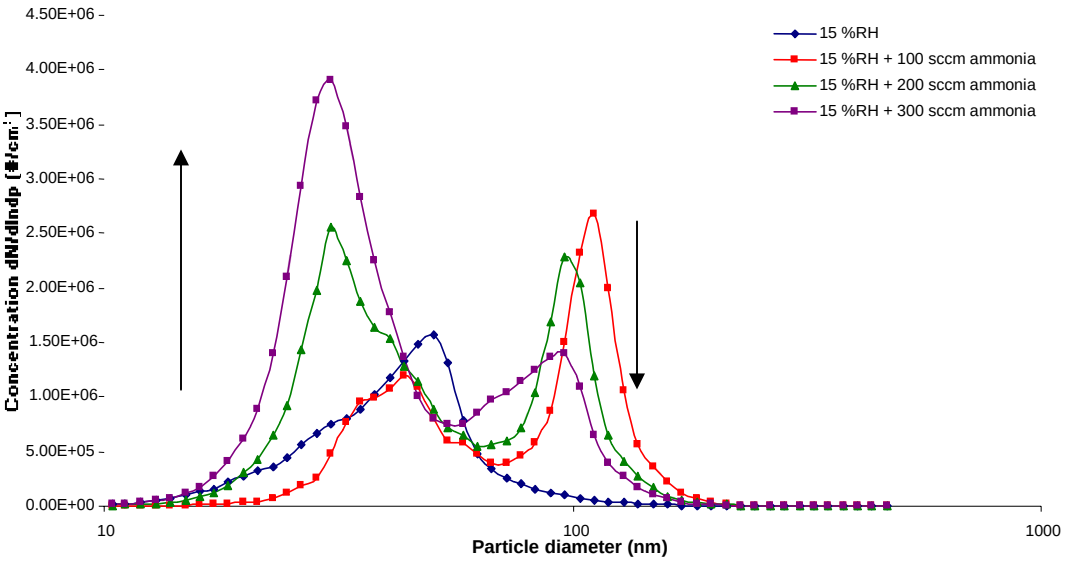

Figure 4.16: 0.5 wt% 'sulfurous acid' and oxalic acid at various conditions.

Figure 4.17 illustrates the change in particle number and concentration upon addition of ammonia at higher humidities to equal concentrations of these two acids. There is a dramatic reduction in particle mode from 54 to 28 nm as humidity is increased, implying complete ionisation of the species present. This component is oxalate due to its abundance at high humidities. The addition of ammonia results in a dramatic increase in particle mode and concentration of 103 nm and 1×10^8 particles cm^{-3} respectively. Further additions of ammonia result in a decrease in the mode and concentration and a more Gaussian distribution indicating incorporation of ammonia into these aerosols and their subsequent contraction.

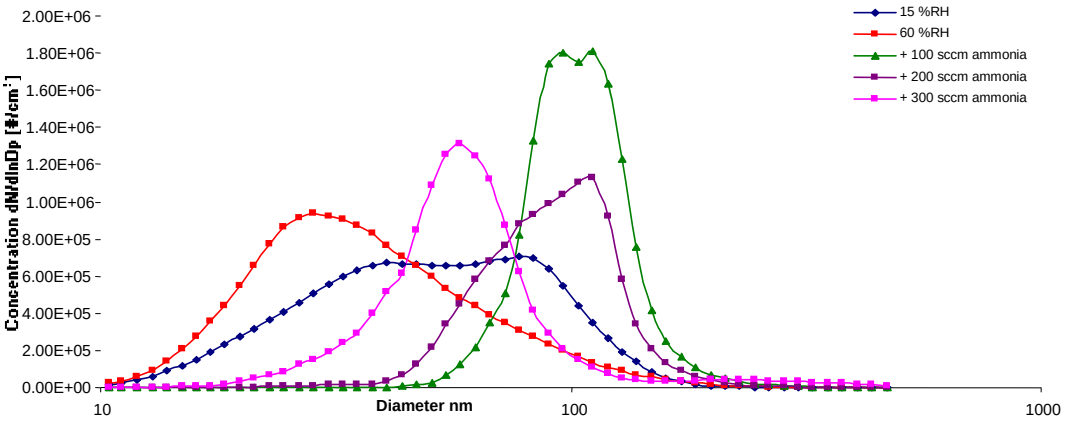

Figure 4.17: 0.5 wt% 'sulfurous acid' and oxalic acid at various conditions.

In comparison with SMPS data for equal weight fractions of oxalic and sulfuric acid, there is not a distinct change in particle diameter, concentration or distribution under various conditions (Figure 4.18).

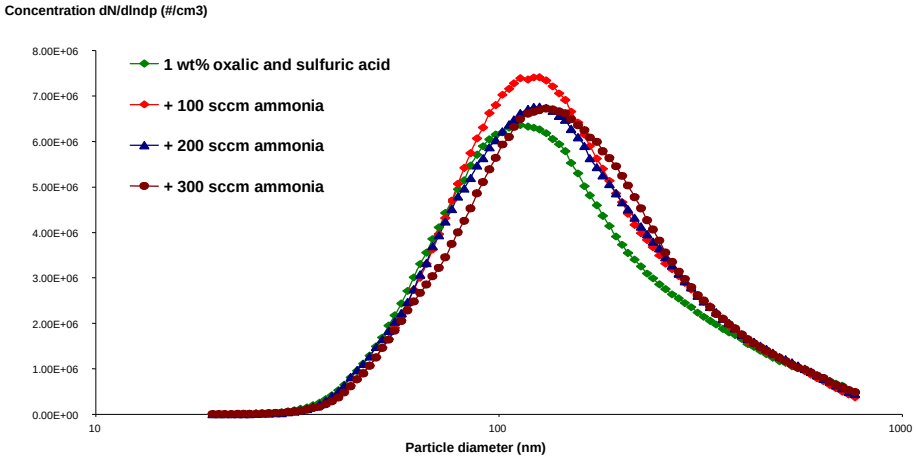

Figure 4.18: Particle distributions for 1wt% oxalic and sulfuric acid aerosols with added ammonia, as shown in the legend, at 50%RH.

Figure 4.19 shows the dramatic change in particle distribution of both of these acids when flow concentration of the generated aerosols is reduced. There are less particles present in the system due to a decrease in the velocity of the particles. From a change of 2 L min^{-1} to 1 L min^{-1}, the particle diameter increases due to more interaction time between the aerosols. However, reducing the flow concentration further results in a decrease in the size of the particles due to particle 'shrinking'.

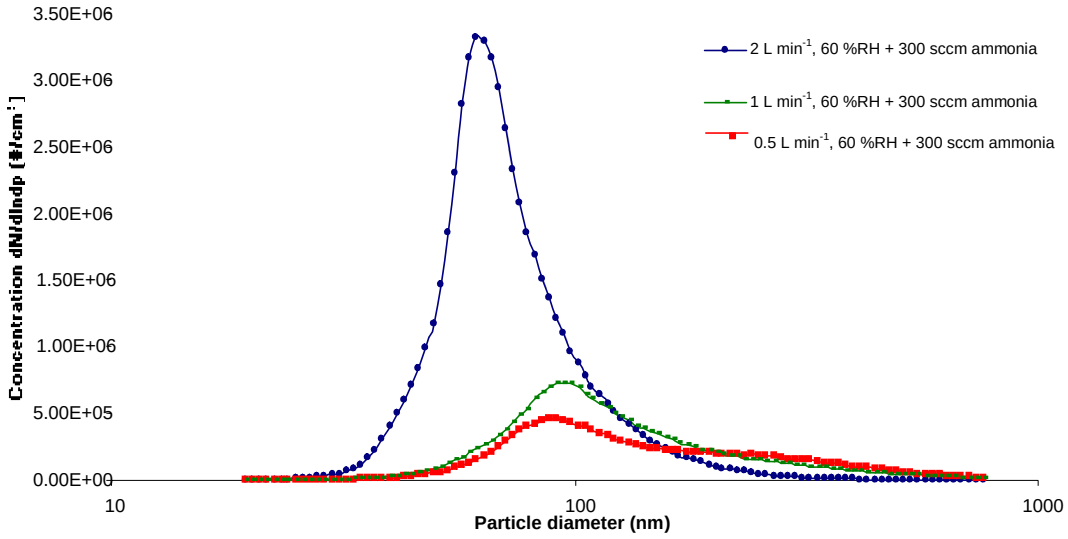

Figure 4.19: 0.5 wt% 'sulfurous acid' and oxalic acid at various conditions.

4.2.1.3 NO_x Data

The NH_4^+ ion concentrations for the three mixtures of 'sulfurous' and oxalic acid at various ammonia flow rates, were calculated from the NO_x data using the calibration factor of 1.2, as discussed in Chapter 2. Inspection of this NH_4^+ ion concentration value, as discussed below, leads to the conclusion that increasing the concentration of oxalic acid has a direct, positive effect on the amount of ammonium ions formed, as illustrated in Figure 4.20. There were different observations recorded for the three concentrations of 'sulfurous'-oxalic acid mixtures used (75:25, 50:50 and 25:75 'sulfurous' and oxalic respectively).

The only significant increase was for the solution containing oxalic acid as the dominant component ranging from 0.164 to 0.192 ppmv with 100 to 300 sccm NH_3 respectively as illustrated in Figure 4.20. As will be discussed in Chapter 5, increasing the oxalic acid concentration increases the amount of ammonium ions formed. In addition, increasing the relative humidity increased the ammonium ion concentration. The solubility of oxalic acid increases at higher humidities, resulting in more oxalic acid dissociating to produce hydrogenoxalate and oxalate ions. Therefore, more ammonia reacts with these ions, thereby, increasing the amount of ammonium ions being formed.

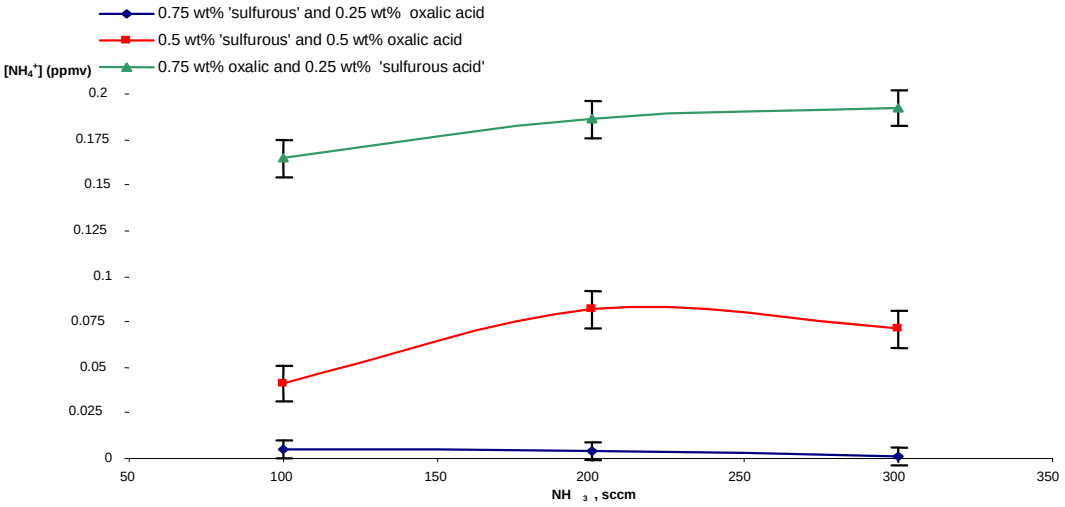

Figure 4.20: Ammonia flow rate vs. ammonium ion concentration at 65 %RH for various concentrations as shown in the legend.

Figure 4.20 illustrates the effect of oxalic acid on ammonium ion formation. The solution containing equal amounts of each acidic species highlights the fact that there is a slight drop in ammonium ion production with humidity; a hydrogen bond between water and the 'sulfurous' species is responsible for this. Addition of water vapour to these species changes the speciation to mainly oxalate and sulfite/disulfite ions while diluting the acid concentration. Therefore, less ammonium ions are formed from the reaction of ammonia with these less concentrated acidic aerosols. This observation is similar to the decrease in ammonium ion production measured by sulfuric acid with increasing humidity as explained in Chapter 3. Further additions of ammonia do not increase the concentration of ammonium ions formed indicating that the aerosol is completely neutralised. There is no distinct increase in ammonium ion formation at 0.75 wt% $SO_2.H_2O$-0.25 wt% $C_2H_2O_4$ again indicating the weak acidity of this sulfur (IV) species.

As a comparison, Figure 4.21 illustrates the effect of ammonia on concentrations of oxalic acid and sulfuric acid. Sulfuric acid is a much stronger acid than its 'sulfurous' counterpart and this is indicated by the formation of a greater amount of ammonium ion. However, there is a decreases in $[NH_4^+]$ with increasing humidity due to dilution of the acid concentration as previously mentioned.

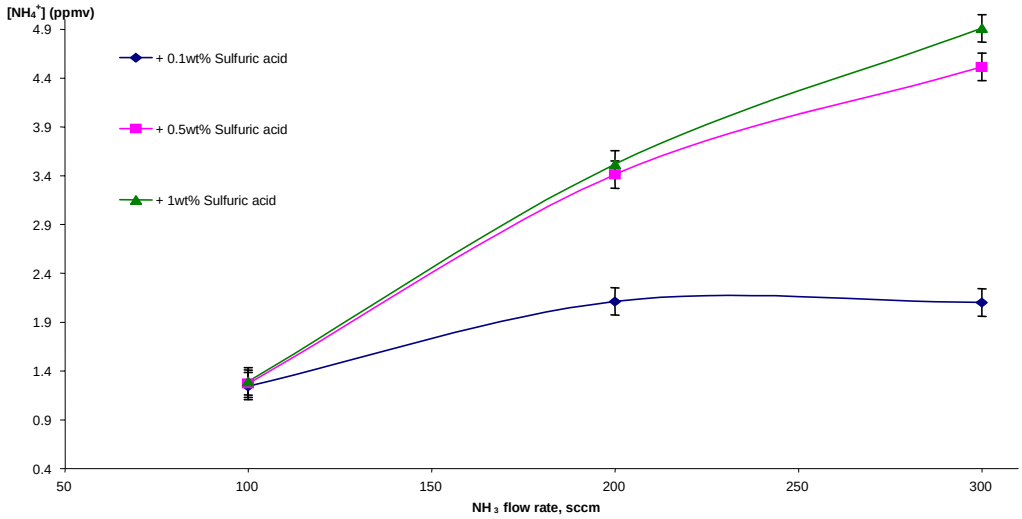

Figure 4.21: Ammonia flow rate vs. ammonium ion concentration at 20 %RH, for 0.1 wt% oxalic acid aerosols with added sulfuric acid as shown in the legend.

Different observations were noted when adding ammonia firstly to these species before increasing the humidity. There was a slight change for the 0.75 wt% sulfurous-0.25 wt% oxalic acid solution which cannot be quantified as the ammonium ion concentration was beyond the detection limit of the NO_x technique, but then it decreased as the humidity rose due to a hydrogen-type bonding between ammonia and water (as already explained). At drier conditions the sulfurous component is responsible for ammonia uptake. The same trend emerges for the 50:50 mixture of both these acids, but with higher ammonium levels (in the region of 0.05 ppmv), due to the presence of more oxalic component. Higher humidities favour a greater uptake of ammonia by oxalic acid at 0.75 acid weight fraction (Fig. 4.22). The generation of the oxalate anion and increased proton stabilisation is responsible for the ammonium ion formation. A linear increase in ammonium ion production with increasing humidity was not noted due to the apparatus set-up.

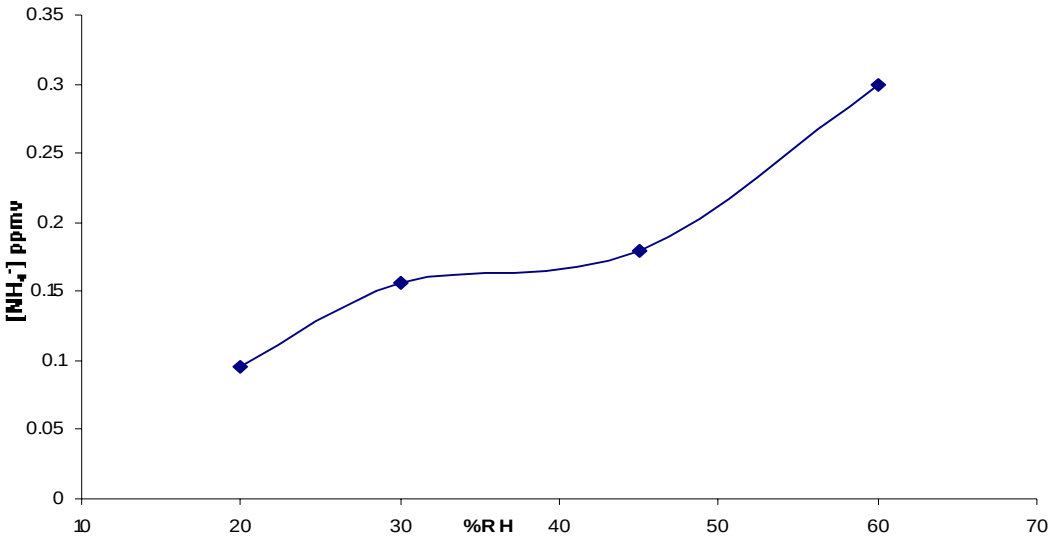

Figure 4.22: Effect of humidity on ammonium levels for 0.75 wt% $C_2H_2O_4$ + 0.25 wt% $SO_2.H_2O$ at 300 sccm NH_3.

When reducing the flow concentration, the ammonium ion production is found to rise dramatically as seen in Table 4.2. For the other concentrations, there is a greater production at 0.75 wt% $C_2H_2O_4$; 0.75 %wt 'H_2SO_3' dominant solution shows $[NH_4]^+$ increases at lower humidities only. The NO_x data presented here are related to the SMPS data in Figure 4.19 where particle distributions, numbers and diameters become smaller due to reduced flow concentration.

Table 4.2 Effect of flow concentration on 0.5 wt% compositions of both acids.

Flow L min^{-1}	$[NH_4^+]$ (ppmv)	Humidity %RH
2	0.124	60
1	0.584	95
0.5	0.896	95

Varying the interaction times between the ammonia and the aerosols (0.75 wt% $C_2H_2O_4$ + 0.25 wt% $SO_2.H_2O$) gave consistent $[NH_4]^+$ values. The more interaction time, the greater the ammonium ion production is as can be seen from Figure 4.23. These studies are related to the FTIR spectrum Figure 4.4, where gaseous ammonia is visible at Z_4, and the SMPS diagram in Figure 4.5, where smaller size distributions are observed with less interaction time. Consistent measurements were obtained also for the other concentration ratios. It can also be clearly seen that there is a substantial difference between Z_3 and Z_4 indicating a significant limit of interaction between the acidic aerosols and gaseous ammonia.

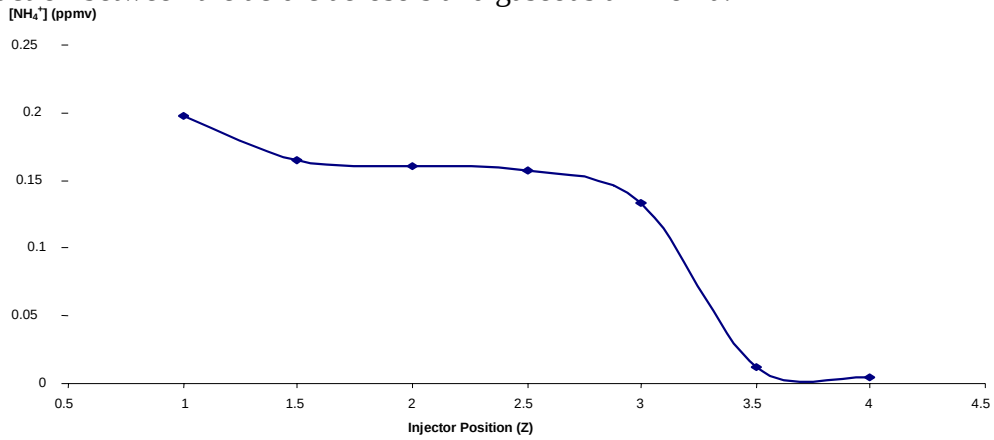

Figure 4.23: Effect of interaction time on ammonium production for 0.5 wt% $C_2H_2O_4$ + 0.5 wt% $SO_2.H_2O$ at 300 sccm NH_3 at 70 %RH.

Figure 4.24 shows plots of $\ln([NH_4^+]_0/[NH_4^+]_t)$ vs. residence time. The amount of NH_4^+ ions formed decreases as the injector is moved between the positions identified as Z_1 (long residence time) and Z_4 (short residence time). It is apparent from these plots that the loss of NH_3 is characteristic of a first order process.

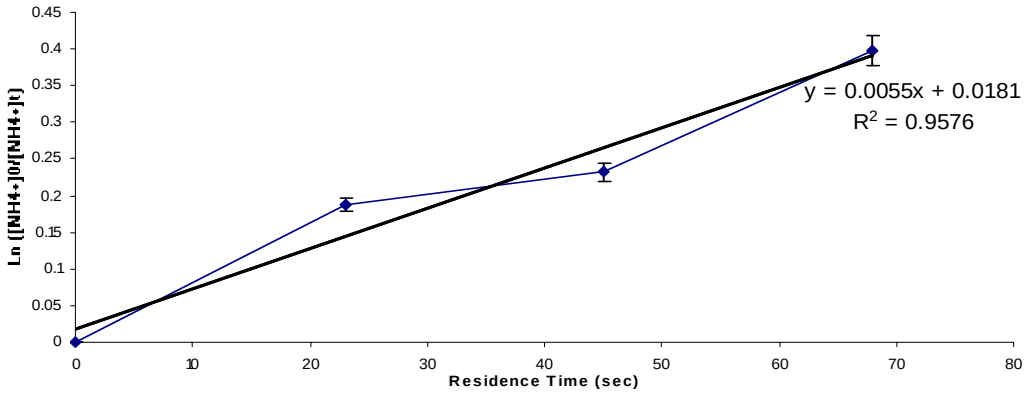

Figure 4.24: Plot of $\ln([NH_4^+]_0/[NH_4^+]_t)$ vs time for the reaction between 0.5 wt% $C_2H_2O_4$ + 0.5 wt% $SO_2.H_2O$ and 300 sccm NH_3 at 70 %RH. These plots were used in the calculation of k_r, the first order rate coefficient.

The slope of each of these plots is equal to the first order rate coefficient, k_r. Table 4.3 displays k_r, surface area (S_a) and the reaction probability (γ) obtained for the reaction between ammonia and equal concentrations of $SO_2.H_2O$ and $C_2H_2O_4$ aerosols. Equation 4-10 allowed the reaction probability to be calculated from the k_r value obtained.

Table 4.3: Uptake coefficient for the reaction of ammonia on 0.5 wt% $C_2H_2O_4$ + 0.5 wt% $SO_2.H_2O$ aerosols (errors for γ are quoted as ($\pm 2 \times 10^{-6}$)).

%RH	k_r (s^{-1})	S_a (cm^2/cm^3)	γ
70	5.5×10^{-3}	6.6×10^{-2}	5.5×10^{-6}

$$\gamma = \frac{4k_r}{S_a \langle c \rangle} \qquad \textit{(4-10)}$$

4.2.2 Summary

Table 4.4 shows the peaks observed in these studies for the interactions of mixtures of 'sulfurous' acid and oxalic acid with ammonia and their corresponding assignment. With varying concentration, different absorptions were noted. Sulfur dioxide (before ammonia addition), hydrogen sulfite and disulfite absorptions (after ammonia addition) were particularly evident with 'sulfurous' dominated mixtures. Equal concentrations of both acids resulted in hydrogenoxalate and disulfite ions at 20 %RH, the latter absorption is a noticeable difference between studies of only 'sulfurous acid'. Oxalic acid absorptions are only seen upon addition of ammonia due to its affinity with alkalinity. For dominant oxalic acid concentrations, hydrogenoxalate and oxalate peaks are mainly observed with oxalate ions being present only after ammonia addition at 50 %RH.

Table 4.4: Observed absorptions and their assignments.

FTIR Shift / cm^{-1}	Vibration*	Species	Reference
1705	$\nu_{as}(CO_2)$	$HC_2O_4^-$	Previous Studies
1610	$\nu_{as}(CO_2)$	$C_2O_4^{2-}$	Previous Studies
1442	δN-H	NH_4	Previous Studies
1330	$\nu_a(SO_2)$	$SO_{2(aq)}$	[44,45]
1310	$\nu_s(CO_2)$	$C_2O_4^{2-}$	Previous Studies
1240	$\nu_s(CO_2)$	$HC_2O_4^-$	Previous Studies
1200	νS-O	$S_2O_5^{2-}$	[44,46]
1200	νS-O	$HOSO_2^-$	GRAMS/AI
1200	$\nu_{as}(SO_3)$	HSO_3^-	GRAMS/AI, [45,46]
1148	$\nu_s(SO_2)$	$SO_{2(aq)}$	[44,.45]
1122	δS-H	HSO_3^-	GRAMS/AI, [45]
1086	ν(S-OH)	$HOSO_2^-$	[45,46]
1067	$\nu_s(SO_2)$	$S_2O_5^{2-}$	GRAMS/AI, [46]
1050	$\nu_s(SO_2)$	$HOSO_2^-$	GRAMS/AI
1022	$\nu_s(SO_3)$	HSO_3^-	[45,46]
950	ν_sS-O	$S_2O_5^{2-}$	[44,46]

*** Notation of vibrational modes: ν, stretching; δ, bending; s, symmetric; a, asymmetric.**

Table 4.5 shows the particle diameter and number concentration for 1 wt% $SO_2.H_2O$ and 1 wt% oxalic acid aerosols with their interaction to each other at different quantities. As previously explained in Chapter 3, hydrogensulfite and disulfite are the main components in 'sulfurous' dominant studies whereas hydrogenoxalate and oxalate are the main components in 'oxalic' dominant studies (discussed in Chapter 5). There is a general increase in particle number and decrease in particle mode with increasing humidity implying ionisation and mainly oxalate formation which is a smaller ion in particular. The mode and concentration increase universally for all aerosol compositions with addition of ammonia. It can also be clearly seen that the oxalic component is larger in diameter and particle concentration. 'Sulfurous acid' studies as previously explained were more difficult to reproduce due to the various phases of the $SO_2.H_2O$ complex.

Table 4.5: Particle statistics for 0.1 wt% oxalic and 'sulfurous' acid aerosols at 20, 50 %RH and 50 %RH with 300 sccm NH_3.

	20 %RH	**50 %RH**	**50 %RH + 300 sccm NH_3**
Aerosol Composition	**Diameter, Concentration (nm, × 10^6 cm^{-3})**	**Diameter, Concentration (nm, × 10^6 cm^{-3})**	**Diameter, Concentration (nm, × 10^6 cm^{-3})**
1 wt% $SO_2.H_2O$	50, 0.4	48, 1.2	52, 2.5
1 wt% $H_2C_2O_4$	70, 0.6	55, 0.9	128, 3.2
0.75 wt% $SO_2.H_2O$ + 0.25 wt% $H_2C_2O_4$	37, 1.9	40, 2.8	47, 2.5
0.5 wt% $SO_2.H_2O$ + 0.5 wt% $H_2C_2O_4$	54, 0.7	28. 0.9	55, 1.3
0.25 wt% $SO_2.H_2O$ + 0.75 wt% $H_2C_2O_4$	77, 3.3	96, 2.0	83, 2.8

Table 4.6 lists the NH_4^+ ion concentrations for interactions between 'sulfurous acid' and oxalic acid aerosols with an added 300 sccm of ammonia at both 20 and 50 %RH. The interactions of these acids individually are also shown as a comparison. Increasing the oxalic acid concentration increased the amount of ammonium ion formed. Increasing the relative humidity also increased the ammonium ion concentration. Addition of water vapour to these aerosols changes the speciation to mainly oxalate and hydrogensulfite/disulfite ions. Sulfite and disulfite ions are known to favour alkaline conditions and increased ionisation would result in more ammonium ion formation. Mixtures of these acids tend to increase the ammonium concentration with increasing humidity particularly for oxalic dominated compositions. 'Sulfurous' dominated compositions favour ammonia uptake at lower humidities. With higher humidities, a hydrogen type bond with ammonia and water emerges for the 'sulfurous' component. It is also apparent that 'sulfurous acid' is a weaker acid than its oxalic acid counterpart. Reducing the flow concentration and increasing the interaction time results in more ammonium ion formation and the kinetic measurements are characteristic of a first order process.

Table 4.6: Ammonium ion concentrations, ppmv, recorded as a result of the interaction of 300 sccm ammonia gas with oxalic acid aerosols, both with 1 wt% sulfuric acid, at 20 and 50%RH.

Aerosol Composition	20%RH	50%RH
1 wt% $SO_2.H_2O$	0.10	0.11
1 wt% $H_2C_2O_4$	0.50	4.64
0.75 wt% $SO_2.H_2O$ + 0.25 wt% $H_2C_2O_4$	0.03	0.03
0.5 wt% $SO_2.H_2O$ + 0.5 wt% $H_2C_2O_4$	0.08	0.06
0.25 wt% $SO_2.H_2O$ + 0.75 wt% $H_2C_2O_4$	0.10	0.28

Table 4.7 summarises the composition of the 'sulfurous' and oxalic acid aerosols on addition of water vapour and ammonia. The acid weight fraction of oxalic acid was varied between 0.25 to 0.75 wt% in addition to the 'sulfurous acid' weight fraction. It was observed that speciation within the tertiary acid systems shifted towards the most ionised form as the relative humidity was increased because of increasing proton stabilisation. At low relative humidities (20 %RH) the less ionised form of each acidic species (hydrogenoxalate ($HC_2O_4^-$) for oxalic acid and sulfur dioxide (SO_2) for $SO_2.H_2O$) was more prominent. At higher relative humidities the more ionised form was evident (oxalate ($C_2O_4^{2-}$) and more aqueous sulfur dioxide absorptions were also observed. With the introduction of ammonia, oxalate was again observed as well as hydrogensulfite, hydrogenoxalate (both in trace amounts) and disulfite ions. Disulfite ions are observed without the addition of ammonia, which is not the case with solely 'sulfurous acid'.

Table 4.7: Sulfurous acid' and oxalic acid compositions at various conditions.

Aerosol Composition	**20 %RH**	**50 %RH**	**50 %RH + 300 sccm NH_3**
1 wt% $SO_2.H_2O$	SO_2	$SO_2.H_2O$	SHO_3^-, $S_2O_5^{2-}$
1 wt% $H_2C_2O_4$	$HC_2O_4^-$	$C_2O_4^{2-}$	$C_2O_4^{2-}$
0.75 wt% $SO_2.H_2O$ + 0.25 wt% $H_2C_2O_4$	Mainly SO_2 $HC_2O_4^-$	$SO_2.H_2O$	SHO_3^-, $S_2O_5^{2-}$ $C_2O_4^{2-}$
0.5 wt% $SO_2.H_2O$ + 0.5 wt% $H_2C_2O_4$	$S_2O_5^{2-}$ $HC_2O_4^-$	$S_2O_5^{2-}$ $C_2O_4^{2-}$	$S_2O_5^{2-}$ $HC_2O_4^-$, $C_2O_4^{2-}$
0.25 wt% $SO_2.H_2O$ + 0.75 wt% $H_2C_2O_4$	$S_2O_5^{2-}$ Mainly $HC_2O_4^-$	$C_2O_4^{2-}$	$S_2O_5^{2-}$ $HC_2O_4^-$, $C_2O_4^{2-}$

4.2 Conclusion

The interaction of oxalic and ‘sulfurous’ acid (and with ammonia) has not been previously investigated, therefore the results here are new for the field of trophospheric aerosol chemistry. Aqueous oxalic and ‘sulfurous acid’ dispersions of particles consist of a mixture of hydrogenoxalate, oxalate, hydrogensulfite tautomers, sulfite and disulfite ions in addition to oxalic and ‘sulfurous acid’. As the concentration of oxalic acid is increased and the concentration of ‘sulfurous acid’ is decreased, the speciation changes from sulfur dioxide to disulfite and hydrogenoxalate ions; the latter being only present in higher proportions of oxalic acid. As humidity is increased, the more ionised species from oxalic acid is mainly present i.e. the oxalate ion. With addition of ammonia, the disulfite ion is abundant in ‘sulfurous acid’ dominated solutions. Hydrogen sulfite isomers are found on a minor level. As the oxalic acid is increased in concentration, and with addition of ammonia, oxalate ions are produced, particularly at high humidities. The ammonium ion is also present, being mainly associated with the oxalate ion in comparison to the weaker aqueous sulfur (IV) ions. The effects of oxalic and ‘sulfurous’ acid are debatable. The interesting question is: do they lead to sulfate formation and a viable oxidation pathway? A possible intermediate is an oxalic-sulfonate type structure ($C_2HO_3SO_3^-$) generated by in-cloud multiphase mechanisms as shown in Figure 4.25.

Figure 4.25: Structure of oxalic acid and possible structure of oxalic sulfonate.

Atmospheric aerosols are a mixture of many inorganic and organic compounds. It is currently not clear how these combinations of compounds interact to impact the particle growth, the cloud condensation ability of the particle and the catalytic behavior of the particle towards heterogeneous reactions. As ‘sulfurous acid’ represents the first step in the overall oxidation of sulfur dioxide to sulfuric acid and

oxalic acid is the major dicarboxylic acid present in tropospheric aerosols, the interaction between these two compounds is important and was therefore investigated. It was observed that speciation within the tertiary acid systems shifted towards the most ionised form as the relative humidity was increased because of increasing proton stabilisation. Addition of ammonia led to more reaction with oxalic acid aerosols, mainly at high humidites, however interaction with ammonia and the ‘sulfurous’ component were observed more at low humidities, albeit with lower ammonium ion production.

More data on the individual reaction channels and rate coefficients are needed for a critical assessment of this oxidation process. For a more systematic understanding of multiphase sulfur oxidation, the broader solution phase chemistry needs to be better characterised in laboratory studies, with results implemented into tropospheric multiphase chemistry models. These, subsequently, have to be coupled to microphysical models, to be tested in field experiments with regards to their ability to describe measured gas phase trace gas and oxidant concentrations, cloud water constituent concentrations and chemical aerosol composition in the tropospheric multiphase system. However this work does indicate some possible speciations for further study.

4.4 References

(1) Aymoz, G.; Jaffrezo, J. L.; Jacob, V.; Colomb, A.; George, C. *Atmospheric Chemistry and Physics* **2004**, *4*, 2499-2512.

(2) Hermann, H.; Ervens, B.; Weise, D. IGAC Newsletter Issue 23, Institut für Troposphärenforschung, Leipzig, Germany, 2001.

(3) Warneck, P.; Mirabel, P.; Salmon, G. A.; Van Eldik, R.; Vinckier, C.; Wannowius, K. J.; Zetzsch, C. *Heterogeneous and Liquid Phase Processes* **1996**, 140-145.

(4) Luttke, J.; Scheer, V.; Levsen, K.; Wunsch, G.; Cape, J. N.; Hargreaves, K.; Storetonwest, R. L.; Acker, K.; Wieprecht, W.; Jones, B. *Atmospheric Environment* **1997**, *31*, 2637-2648.

(5) Warneck, P. *Chemistry of the Natural Atmosphere*: Academic Press; San Diego, 1988.

(6) Wexler, A.; Seinfield, J. H. *Atmospheric Environment* **1991**, *25*, 2731-2748.

(7) Saxena, P. L.; Hildemann, L. M.; McMurray, P. H.; Seinfield, J. H. *Journal of Geophysical Research* **1995**, *100*, 18755-18770.

(8) Ludwig, J.; Klemm, O. *Water Air and Soil Pollution* **1990**, *49*, 35-50.

(9) Pszenny, A. A. P.; Moldanov, J.; Keene, W. C.; Sander, R.; Maben, J. R.; Martinez, M.; Crutzen, P. J.; Perner, D.; Prinn, R. G. *Atmospheric Chemistry and Physics* **2004**, *4*, 147-168.

(10) Pathak, R. K.; Louie, P. K. K.; Chan, C. K. *Atmospheric Environment* **2004**, *38*, 2965-2974.

(11) Asman, W. A. H.; Sutton, M. A.; Schjorring, J. K. *New Phytologist* **1998**, *139*, 27-48.

(12) Yamamoto, N.; Nishiura, H.; Honjo, T.; Ishikawa, Y.; Suzuki, K. *Atmospheric Environment* **1995**, *29*, 97-103.

(13) Lewandowska, A.; Falkowska, L. *Oceanologia* **2004**, *46*, 175-184.

(14) Adams, P. J.; Seinfeld, J. H.; Koch, D. M. *Journal of Geophysical Research-Atmospheres* **1999**, *104*, 13791-13823.

(15) Moeckli, M. A.; Fierz, M.; Sigrist, M. W. *Environmental Science and Technology* **1996**, *30 (9)*, 2864-2867.

(16) Sutton, M. A.; Dragositis, U.; Tang, Y. S.; Fowler, D. *Atmospheric Environment* **2000**, *34 (6)*, 855-869.

(17) Perrino, C.; Catrambone, M.; Di Bucchianico, A. D. M.; Allegrini, I. *Atmospheric Environment* **2002**, *36 (34)*, 5385-5394.

(18) Asman, W. A. H. *Atmospheric Environment* **1998**, *32 (3)*, 415-421.

(19) Berge, E.; Bartnicki, J.; Olendrzynski, K.; Tsyro, S. G. *Journal of Environmental Management* **1999**, *57 (1)*, 31-50.

(20) Schilt, S.; Thevenaz, L.; Nikles, M.; Emmenegger, L.; Huglin, C. *Spectrochimica Acta Part A* **2004**, *60*, 3259-3268.

(21) Weast, R. C. *CRC Handbook of Physics and Chemistry*; CRC: Florida, 1979.

(22) Hallquist, M.; Stewart, D. J.; Baker, J.; Cox, R. A. *Journal of Physical Chemistry A* **2000**, *104*, 3984-3990.

(23) Noonan, C. *'A Laboratory Study of Heterogeneous Chemistry between Ammonia and Acidic Particles relevant to the Troposphere'*, Ph.D Thesis: University College Cork, Ireland, 2007.

(24) Hanson, D.; Kosciuch, E. *Journal of Physical Chemistry A* **2003**, *107*, 2199-2208.

(25) Brooks, S. D.; Wise, M. E.; Cushing, M.; Tolbert, M. A. *Geophysical Research Letters* **2002**, *29*.

(26) Choi, M. Y.; Chan, C. K. *Environmental Science & Technology* **2002**, *36*, 2422-2428.

(27) Cruz, C. N.; Pandis, S. N. *Environmental Science & Technology* **2000**, *34*, 4313-4319.

(28) Prenni, A. J.; De Mott, P. J.; Kreidenweis, S. M. *Atmospheric Environment* **2003**, *37*, 4243-4251.

(29) Hameri, K.; Charlson, R.; Hansson, H. C. *Aiche Journal* **2002**, *48*, 1309-1316.

(30) Svenningsson, B.; Rissler, J.; Swietlicki, E.; Mircea, M.; Bilde, M.; Facchini, M. C.; Decesari, S.; Fuzzi, S.; Zhou, J.; Monster, J.; Rosenorn, T. *Atmospheric Chemistry and Physics* **2006**, *6*, 1937-1952.

(31) Lightstone, J. M.; Onasch, T. B.; Imre, D.; Oatis, S. *Journal of Physical Chemistry A* **2000**, *104*, 9337-9346.AA

(32) Zuo, Y.; Zhan, J. *Atmospheric Environment* **2005**, *39*, 27-37.

(33) Munger, J. W.; Jacob, D. J.; Hoffmann, M. R. *Journal of Atmospheric Chemistry* **1984**, *1*, 335-350.

(34) Maylor, R.; Gill, J. B.; Goodall, D. C. *Journal of the Chemical Society, Dalton Transactions: Inorganic Chemistry* **1972**, *18*, 2001-2003.

(35) Parsons, M. T.; Knopf, D. A.; Bertram, A. K. *Journal of Physical Chemistry* **2004**, *108*, 11600-11608.

(36) Wise, M. E.; Surratt, J. D.; Curtis, D. B.; Shilling, J. E.; Tolbert, M. A. *Journal of Geophysical Research-Atmospheres* **2003**, *108*.

(37) Marcolli, C.; Luo, B. P.; Peter, T. *Journal of Physical Chemistry A* **2004**, *108*, 2216-2224.

(38) Clegg, S. L.; Seinfeld, J. H.; Brimblecombe, P. *Journal of Aerosol Science* **2001**, *32*, 713-738.

(39) Andrews, E.; Larson, S. M. *Environmental Science & Technology* **1993**, *27*, 857-865.

(40) Wagner, J.; Andrews, E.; Larson, S. M. *Journal of Geophysical Research-Atmospheres* **1996**, *101*, 19533-19540.

(41) Hansson, H. C.; Rood, M. J.; Koloutsou-Vakakis, S.; Hameri, K.; Orsini, D.; Wiedensohler, A. *Journal of Atmospheric Chemistry* **1998**, *31*, 321-346.

(42) Dick, W. D.; Saxena, P.; McMurry, P. H. *Journal of Geophysical Research-Atmospheres* **2000**, *105*, 1471-1479.

(43) Saxena, P.; Hildemann, L.M.; McMurray, P. H.; Seinfeld, J. H. *Journal of Geophysical Research* **1995**, *100*, 18755-18770.

(44) Zhang, Z.; Ewing, G. E. *Spaectrochimica Acta. Part A.* **2002**, *58*, 2105-2113.

(45) Damian Risberg, E.; Eriksson, L.; Mink, J.; Petterson, L. G. M.; Skripkin, M. Y.; Sandstroem, M. *Inorganic Chemistry* **2007**, *46*, 8332-8348.

(46) Herlinger, A. W.; Long, T. V. *Inorganic Chemistry* **1969**, *8 (12)*, 2661-2665.

Chapter 6

Heterogeneous interactions between ammonia and multi-component sulfuric/dicarboxylic acid aerosols

6.1 Introduction

It has become evident that real atmospheric aerosols, present in the troposphere, are chemically complex and consist of both inorganic and mixed inorganic/organic species. For example sulfuric acid plays an important role in the formation and growth of aerosol particles due to its low vapour pressure and ammonia is a predominant airborne gaseous base and, as such, holds an important place in atmospheric chemistry neutralisation. However, as previously mentioned in Chapter 5, dicarboxylic acids also make up a huge proportion of the organic mass contributing to condensed phase particles. Hence, ammonia containing aerosols consisting of mixtures of malonic and sulfuric acid or succinic and sulfuric acid, were studied here by the complementary FTIR and SMPS techniques. Oxalic and sulfuric acid aerosol studies were previously undertaken and were used as a comparison [(1)].

6.1.1 Atmospheric context

6.1.1.1 Effects of organic species on aerosols

It is evident that atmospheric aerosols are chemically very complex, with both organic and mixed inorganic/organic aerosols widely present in the troposphere. Therefore, given the chemically mixed nature of aerosols, it is important to understand and quantify the effect of organic chemicals on the phase transition behaviour of model inorganic tropospheric aerosols. Organic compounds may play an important role in altering the characteristics of the inorganic particles and, hence, altering their cloud nucleating ability. For example, it has been shown that the presence of organic material in ammonium sulfate aerosols can lower their deliquescence relative humidity (DRH) [(2)] and can alter their hygroscopic growth [(3)]. The presence of these compounds can also affect the ability of these particles to take up water and to form ice crystals in the atmosphere.

Organic compounds may affect the kinetics of reaction of ammonia with water and aqueous droplets in the atmosphere. Rubel and Gentry [4] showed that organic compounds capable of forming a film on the surface of water may have a significant effect on the rate of mass transfer and reaction of atmospheric ammonia with water and aqueous solutions. They found that covering an acid droplet with a monolayer of solid hexadecanol decreases the accommodation coefficient of ammonia by a factor of ten. As the monolayer expands, i.e. as the area per monolayer molecule increases, the monolayer experiences a phase transition from solid to liquid state. The accommodation coefficient decreases further until the monolayer collapses as it contracts because of increasing layer cohesion. When the monolayer collapses a rapid increase in accommodation coefficient is observed. These observations suggest that film-forming organic compounds in the atmosphere are likely to impede the dissolution of ammonia in water and its reaction with acid aerosols.

6.1.1.2 Effect of ammonia on aerosols

The role of ammonia in neutralising acidic aerosols has received considerable attention in the literature concerning environmental acidification and the health effects of atmospheric aerosols [5],[6],[7],[8]. Although the results of epidemiological studies are not definitive, there is evidence that exposure to acid aerosols (defined as having pH > 4.3) has a more significant deleterious impact upon human health than exposure to neutral aerosols of the same size distribution [6]. However, this apparent neutralising environmental benefit is offset by the role NH_3 plays in enhancing aerosol formation. NH_3 can be absorbed into aerosols which raises their pH, thereby enhancing the rate of oxidation of dissolved sulfur dioxide (SO_2) by ozone (O_3) to form sulfate (SO_4^{2-}) ions [9],[10]. Sulfuric acid has a high affinity towards NH_3 and forms ammonium bisulfate before forming ammonium sulfate [11]. These latter aerosols are stable once formed.

In addition, incorporation of NH_3 into acid aerosols:

(i) Enhances light scattering by producing $(NH_4)_2SO_4$, $(NH_4)_3H(SO_4)_2$ and NH_4HSO_4. The light extinction coefficient of 0.5 μm diameter $(NH_4)_2SO_4$, is approximately 1.5 times that for H_2SO_4 over the visible light range [12].

(ii) Leads to more complex hygroscopic behaviour for SO_4^{2-} containing aerosols. H_2SO_4 absorbs and releases water more readily with changing relative humidity than $(NH_4)_2SO_4$, which exhibits strong hysteresis and displays deliquescence at relative humidities of approximately 80% [13]. This also has implications for the light scattering efficiency of aerosols and hence visibility degradation [14].

Ammonia, partly or totally, neutralises acidic aerosols, forming dry ammonium sulfate salts or NH_3-H_2SO_4-H_2O solutions depending on relative humidity. If excess NH_3 is available beyond that required to neutralise H_2SO_4, then HNO_3 can condense to form a NH_3-H_2SO_4-HNO_3-H_2O aerosol or a separate NH_4NO_3 aerosol [15]. In concentrated acidic solutions, at tropospheric temperatures, HNO_3 is present in trace quantities only [16],[17]. In the upper troposphere, for example, with a typical temperature of 220 K and a HNO_3 concentration of 100 pptv, a 40 wt% H_2SO_4 aerosol contains 3×10^{-5} wt% HNO_3 [18]. Measurements taken at a range of sites located in the USA indicate that aerosols, in general, are fully neutralised, except in the industrial midwest and the northeast [19]. The principal alkaline materials identified were NH_3 and crustal $CaCO_3$. In contrast, sulfate aerosols in marine air are usually acidic [20]. Models suggest that free tropospheric aerosol should be highly acidic, due to efficient wet deposition of NH_3 and soil dust [21]. However, recent aircraft measurements indicate that the aerosol is frequently neutralised up to the tropopause, with NH_4^+ and Ca^{2+} as the dominant alkaline cations present in the aerosol [22]. Knowledge of whether an aerosol is 'dry' or aqueous is essential in modelling its chemical behaviour. Hence, a number of laboratory studies have

investigated the phase properties of H_2SO_4-HNO_3-NH_3-H_2O aerosols and their components as a function of relative humidity.

Ammonium nitrate is one of the most important constituents of atmospheric aerosols and accounts for 10 − 20% of the fine aerosol mass [23]. It often coexists with ammonium sulfate and has important environment impacts such as visibility, degradation, radiative forcing and climate change [24]. The emission of NO_x, one of the precursors of atmospheric nitrate, has been predicted in the future to triple while SO_2 emission is expected to decline slightly [25]. Hence, the importance of ammonium nitrate in atmospheric aerosols will likely increase substantially in the future. However, NH_4NO_3 is unstable under atmospheric conditions, existing in reversible phase equilibria with the gaseous precursors, nitric acid and ammonia. The dissociation constants of the equilibria depend not only on the concentrations of acidic gases and ammonia, but also heavily on the chemical composition of the particles, their temperatures and RH [26]. Zhang et al. showed that most NH_4^+ was neutralised by SO_4^{2-} and existing as ammonium sulfate in the less polluted periods. While, in more polluted periods, when ammonium ions were more abundant and the %RH was high, then more NH_4^+ was neutralised by NO_3^- and existing as ammonium nitrate [27]. It is found that the efficiency of heterogeneous conversion increases with an increase in humidity during polluted periods.

The pH of atmospheric aqueous solutions in equilibrium with the current concentration of carbon dioxide is approximately 5.6, assuming other species such as ammonia are not available to neutralise the acids formed when CO_2 dissolves in water (the bicarbonate ion (HCO_3^-) and carbonate ion (CO_3^{2-}) are formed as aquated CO_2 reacts) [28]. However, over the past three decades, starting in Europe and particularly for the Scandinavian countries, the formation of rains, clouds and fogs with much higher acidities has been widely recognised. Rain with pH of 4.5 is common worldwide, and even more acidic precipitation has been measured in many areas. Clouds with pH around 2.5 and fogs with a pH as low as 1.69 have also been observed [29],[30]. The apparent increase in acidity in going from rain to clouds to fog

likely reflects the different liquid water contents, i.e. in essence, the effects of concentration and dilution.

6.1.2 Previous laboratory studies

To date, several studies have examined mixtures of dicarboxylic acids and inorganic salts with respect to phase transitions or water uptake. These include a study of the deliquescence relative humidities of ternary bulk solutions [31] and the water cycles of dicarboxylic acids with both sodium chloride and $(NH_4)_2SO_4$ using an electrodynamic balance (EDB) technique [32]. Four tandem differential mobility analyser (DMA) studies have been performed. For example, mixtures of glutaric acid and $(NH_4)_2SO_4$ have been examined [33] while water uptake of $(NH_4)_2SO_4$-dicarboxylic mixtures at three compositions were undertaken [34]. In addition, $(NH_4)_2SO_4$ mixtures have been investigated with several dicarboxylic acids [35]. The interaction between water vapour and aerosol particles, containing various amounts of inorganic salts ($(NH_4)_2SO_4$, NH_4NO_3 and NaCl) and three organic compounds (levoglucosan, succinic acid and fulvic acid) was studied at different relative humidites [36]. Lightstone et al. focused on the potential heterogeneous effect of succinic acid cores on the effloresence relative humidity (ERH) of mixed ammonium nitrate-succinic acid particles [37].

Laboratory experiments have also shown that the nucleation of sulfuric acid is considerably enhanced in the presence of aromatic acids. Theoretical calculations have identified the formation of an unusually stable aromatic acid-sulfuric acid complex, which likely leads to a reduced barrier [18]. The deliquescence and crystallisation of ammonium sulfate particles internally mixed with water-soluble organic material have also been studied, but restricted to an organic mass fraction of less than 0.6. The organic species used were malonic acid, glycerol, levoglusan and Suwannee River fulvic acid [38]. Phase transitions of aerosol composed of ternary mixtures of ammonium sulfate and malonic acid using infrared extinction spectroscopy have also been studied [39].

A detailed study of the water activity, phase transitions and growth of dicarboxylic acid-inorganic salt-water bulk solutions and aerosols has been completed [40]. Saturated bulk solutions of up to five dicarboxylic acids with ammonium nitrate, ammonium sulfate and sodium chloride have also been examined [41]. Thermodynamic properties of mixed organic/inorganic particles have been modelled [42]. The authors of the latter publication note that there is a need for an improved knowledge of the physical properties of the organic component in the aerosol. Few studies have been subsequently performed but it has been shown that the presence of organic compounds may alter the deliquescence point [43],[38], the rate of deliquescence [44], and the hygroscopic behaviour [45],[33] of inorganic particles. A study made in the Great Smoky Mountains (USA) indicated excess water increased with increasing mass fraction of organics in particles, implying that the organic fraction of the aerosol was somewhat hygroscopic [46]. This study also showed that the amount of organic-associated water was considerably less than sulfate-associated water at high relative humidity with respect to water (RH_w), but was comparable or greater at low RH_w. Another study showed that organic species can alter the water uptake behaviour of inorganic aerosol both positively (non-urban) and negatively (urban), depending on location [47]. Furthermore, a model study suggests that the presence of water-soluble organic compounds can significantly increase cloud condensation nuclei in marine, rural, and urban environments [48].

Rubel and Gentry [6] also measured the accommodation coefficient for water as well as ammonia on acid droplets coated with heaxadeconal. The water accommodation coefficient decreased from 8×10^{-3} as the alcohol coverage increased, i.e. as the degree of compression of the organic film increased, to 4×10^{-4}, with a sharp change at the point that the film underwent a phase transition from the liquid to the solid condensed state. Similarly, Daumer et al [49] showed that coating a sulfuric acid aerosol with straight chain organics retarded the rate of neutralisation by ammonia, whereas branched molecules did not, presumably because the

permeability of the films was much larger. Figure 6.1 exhibits the basic structures for adsorbed dicarboxylic acids.

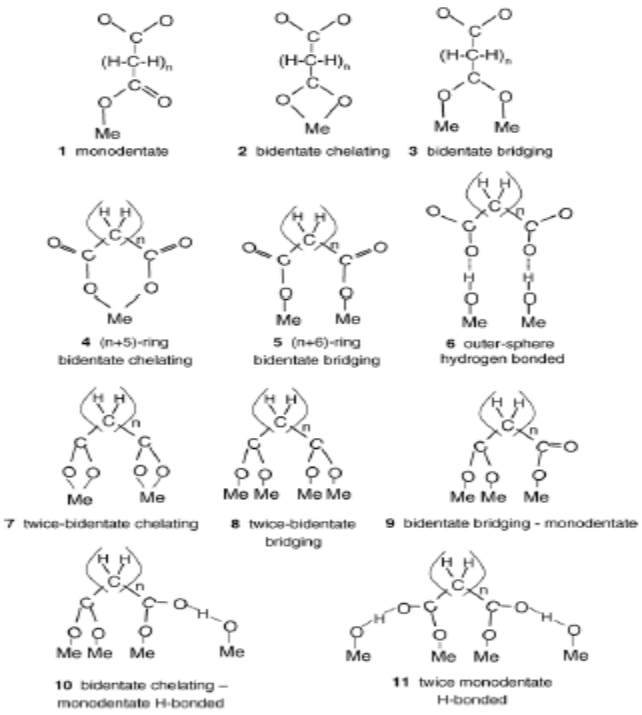

Figure 6.1: Basic surface structures for adsorbed dicarboxylic acids [50].

Rate coefficients for a series of alcohols, ethers and esters toward the sulfate radical (SO_4) have been directly determined using a laser photolysis set-up in which the radical was produced by the photodissociation of peroxodisulfate anions [51]. The sulfate radical concentration was monitored by following its optical absorption by means of time-resolved spectroscopy techniques. Bimolecular rate coefficients for the reactions of the nitrate radical, NO_3, with organics have also been measured using a similar experimental approach [52].

No prior studies on correlating speciation and size behaviour of dicarboxylic acids in the presence of sulfuric acid (and ammonia) have been performed.

6.1.3 Aim and Chapter Overview

It is important to understand in detail simple binary organic-water systems before complex, mixed inorganic-organic systems are considered. In reality such mimics are certainly too simplistic but they do represent good foundations. Hence, included in this chapter are results and discussions of the interactions between both malonic and succinic acid with sulfuric acid, along with the addition of ammonia. Comparison with oxalic acid, sulfuric acid and ammonia studies, which were initially analysed, are also discussed as a basis for real atmospheric aerosols. FTIR spectroscopy, SMPS and NO_X measurements were again used as tools for the characterisation of the physio-chemical properties of these highly complicated ternary/quaternary systems.

6.2 Results and Discussion

Three different types of aerosols with either malonic or succinic acid plus sulfuric acid were analysed: 1 wt% oxalic acid and 0.1 wt% H_2SO_4, 0.5 wt% oxalic acid and 0.5 wt% H_2SO_4 and 1 wt% oxalic acid and 0.1 wt% H_2SO_4. The aerosols were generated using a commercially available constant output atomiser (COA, TSI Model 3075). Prior to injection into the flow-tube the aerosols were diluted with dry or wet air (20 and 50 and 90 %RH). As a short pathlength was imposed by the flow-tube geometry, it was not possible to rely, with confidence, on spectroscopic detection for quantitative measurements. Therefore, the primary use of the FTIR spectrometer in this current study was in the area of product characterisation, with the chemiluminescence technique being applied for more quantitative chemical analysis, as described below.

Aqueous dicarboxylic and sulfuric acid dispersions of particles consist of a mixture of dicarboxylate, hydrogencarboxylate, bisulfate and sulfate ions in addition to dicarboxylic and sulfuric acid. Dicarboxylic acids are weak acids and do not readily dissociate in solution, while sulfuric acid completely dissociates in solution as

discussed in previous chapters. The chemical reactions occurring within aerosols composed of a mixture of sulfuric and dicarboxylic acids are summarised in Table 6.1.

Table 6.1: Chemical reactions occurring in atmospheric aerosols containing only H_2SO_4, $H_{2,4,6}C_{2,3,4}O_4$ and water.

$H_2SO_4 \leftrightarrow H^+ + HSO_4^-$
$HSO_4^- \leftrightarrow H^+ + SO_4^{2-}$
$H_{2,4,6}C_{2,3,4}O_4 \leftrightarrow H^+ + H_{1,3,5}C_{2,3,4}O_4^-$
$H_{1,3,5}C_{2,3,4}O_4^- \leftrightarrow H^+ + C_{2,3,4}O_4^{2-}$
$2H_2O \leftrightarrow H_3O^+ + OH^-$

6.2.1 Oxalic and sulfuric acid aerosols with ammonia

6.2.1.1 FTIR data

Figure 6.2 shows typical FTIR spectra obtained for 1 wt% oxalic acid with 0.1 wt% H_2SO_4 at 20 and 50 %RH (spectrum a and b respectively).

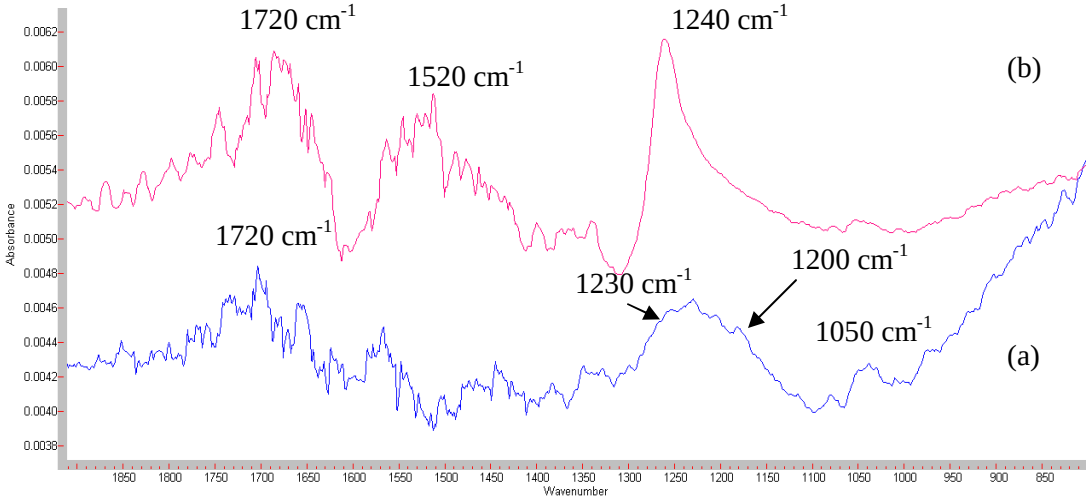

Figure 6.2: FTIR spectra of 1 wt% oxalic acid aerosols and 0.1 wt% H_2SO_4 at 20 %RH (spectrum (a)) and 50 %RH (spectrum (b)).

As can be seen, spectrum (a) consists essentially of three bands at 1720, 1230, 1050 cm^{-1} originating from both oxalic acid and sulfuric acid species. However, the band at 1230 cm^{-1} is asymmetrical and represents a HSO_4^- ion absorption band at 1200 cm^{-1} and a hydrogenoxalate ion peak at 1240 cm^{-1}. The peak at 1720 cm^{-1} is also assigned to the stretching vibration of the C=O of the hydrogenoxalate ion. The peak at 1050 cm^{-1} originates from the HSO_4^- ion. The composition of the aerosol is, therefore, a mixture of bisulfate and hydrogenoxalate ions. Increasing the humidity, removes the bisulfate component and the aerosol changes to a primarily hydrogenoxalate composition (spectrum b). The absorption at 1520 cm^{-1} suggests a derivative from the hydrogenoxalate species.

Figure 6.3 displays the FTIR spectra for 1 wt% oxalic acid and 0.1 wt% sulfuric acid with added ammonia at 50 %RH after water subtraction.

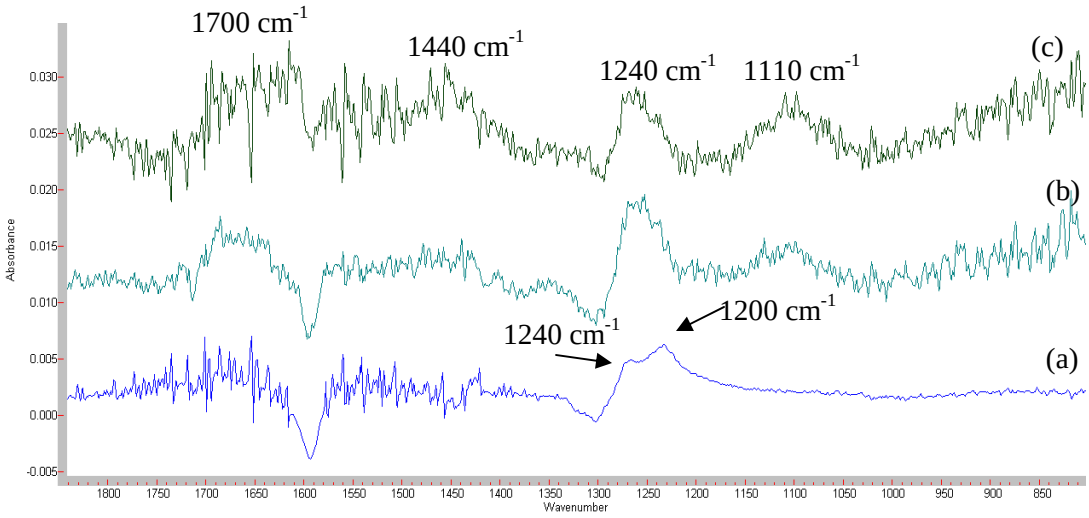

Figure 6.3: FTIR spectra of 1 wt% oxalic acid aerosols with 0.1 wt% H_2SO_4 at 50 %RH (spectrum (a)), plus 100 sccm ammonia (spectrum (b)) plus 300 sccm ammonia (spectrum(c)).

As previously mentioned, hydrogenoxalate absorptions (1700 and 1240 cm^{-1}) and a bisulfate absorption (1200 cm^{-1}) are observed at 50 %RH. With the introduction of ammonia, an ammonium deformation band and a sulfate stretching absorption emerge at 1440 and 1110 cm^{-1} respectively. The ammonium band is indicative of the formation of both ammonium hydrogenoxalate and ammonium sulfate. As

discussed later, the ammonium hydrogenoxalate mode vibrates at a slightly higher wavenumber than its sulfate counterpart. There is no indication of oxalate or bisulfate ions under these conditions for this concentration ratio.

FTIR spectra recorded for aerosols consisting of 0.1 wt% oxalic acid and 0.1 wt% sulfuric acid with addition of ammonia at 20 %RH are shown in Figure 6.4. At 20 %RH the dominant features of spectrum (a) are the HSO_4^- ion absorption bands at *ca*. 1210, 1050 and 890 cm^{-1} and a hydrogenoxalate ion absorption band centred at 1700 cm^{-1}. Spectral deconvolution of the peak at 1210 cm^{-1}, yields two components at 1240 and 1200 cm^{-1} (assigned to $HC_2O_4^-$ and HSO_4^- ions, respectively) as previously explained. With increasing additions of ammonia, oxalate ion absorptions emerge at 1600 and 1300 cm^{-1} and are assigned to the asymmetric and symmetric stretching modes of the carboxylate group respectively. A sulfate ion mode is located at 1110 cm^{-1}.

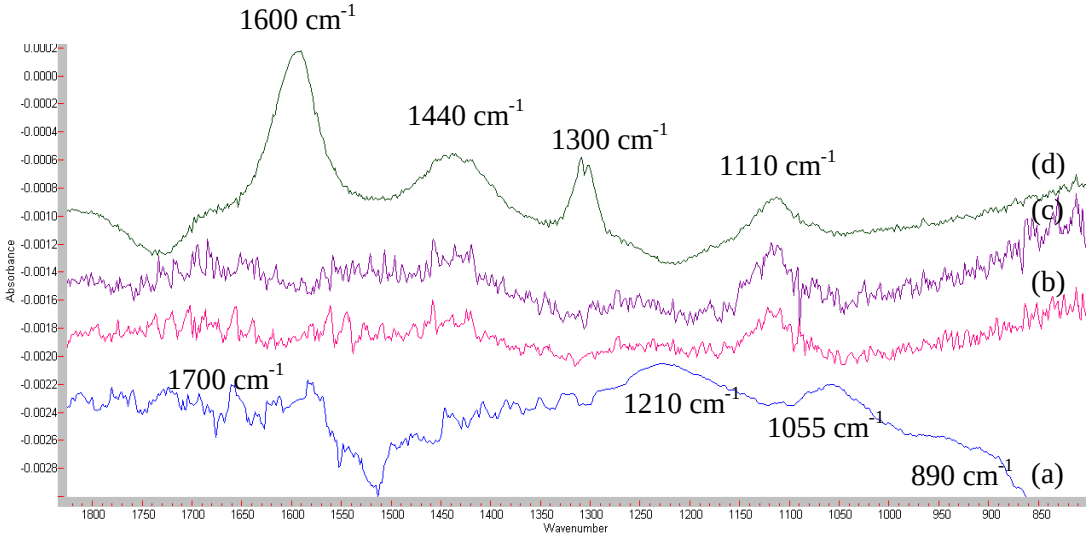

Figure 6.4: FTIR spectra of 0.1 wt% oxalic acid aerosols and 0.1 wt% H_2SO_4 at 20 %RH (spectrum (a)) and with 100 (spectrum (b)), 200 (spectrum (c)) and 300 sccm ammonia (spectrum (d)).

A broad peak at 1440 cm^{-1} is attributable to the NH_4^+ ion formation of oxalate. GRAMS/AI spectral deconvolution of this broad absorption in Figure 6.5 yields two components at 1446 and 1421 cm^{-1}. The former of these two peaks is associated with the NH_4^+ ion in ammonium oxalate while the latter is associated with ammonium sulfate. The position of the ammonium ion absorption peak can therefore be used as a diagnostic of what type of aerosol is generated. Tables 6.3 and 6.4 shown later in this chapter outlines in more detail the various spectral locations for each of the ammonium ions detected.

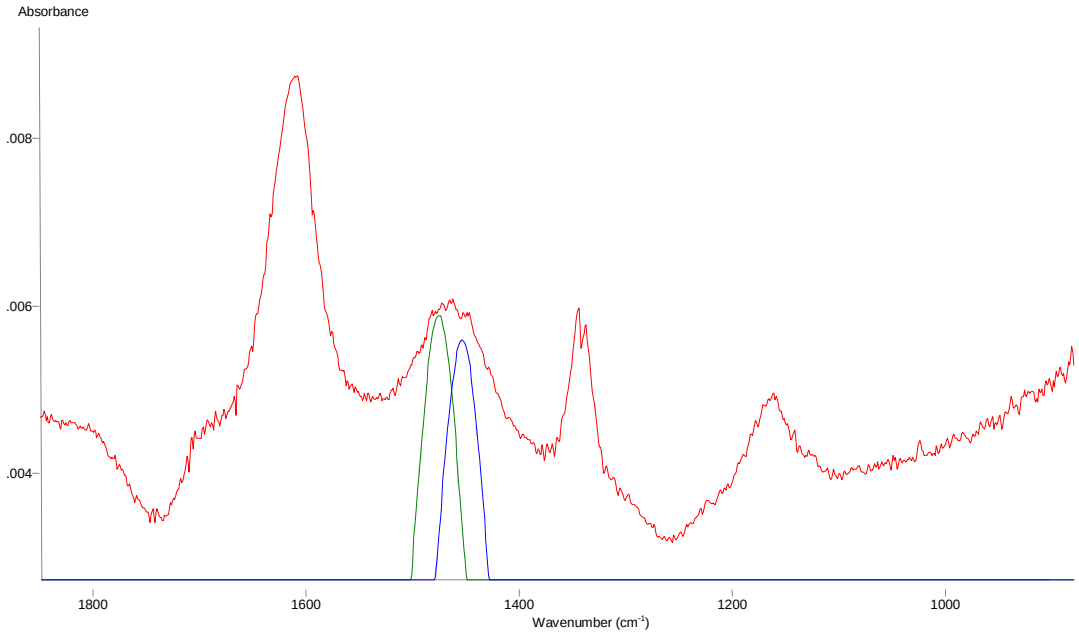

Figure 6.5: Deconvolution of the FTIR spectrum of 0.1 wt% $C_2H_2O_4$ + H_2SO_4 and 300 sccm NH_3 at 20 %RH. The red curve is the source spectrum and the green (ammonium oxalate) and blue (ammonium sulfate) curves are the deconvolution peaks.

Figure 6.6 shows the FTIR spectra of 0.1 wt% $C_2H_2O_4$ and H_2SO_4 aerosols with the addition of 100, 200 and 300 sccm NH_3 (spectra c, d and e respectively) at 50 %RH. Oxalic-sulfuric acid aerosols at 50 %RH are composed of a mixture of $HC_2O_4^-$, $C_2O_4^{2-}$ and HSO_4^- ions. Addition of ammonia results in the formation of ammonium sulfate and ammonium oxalate. The oxalate ions peaks are at 1596 and 1314 cm^{-1}, while the SO_4^{2-} peak is at 1110 cm^{-1}.

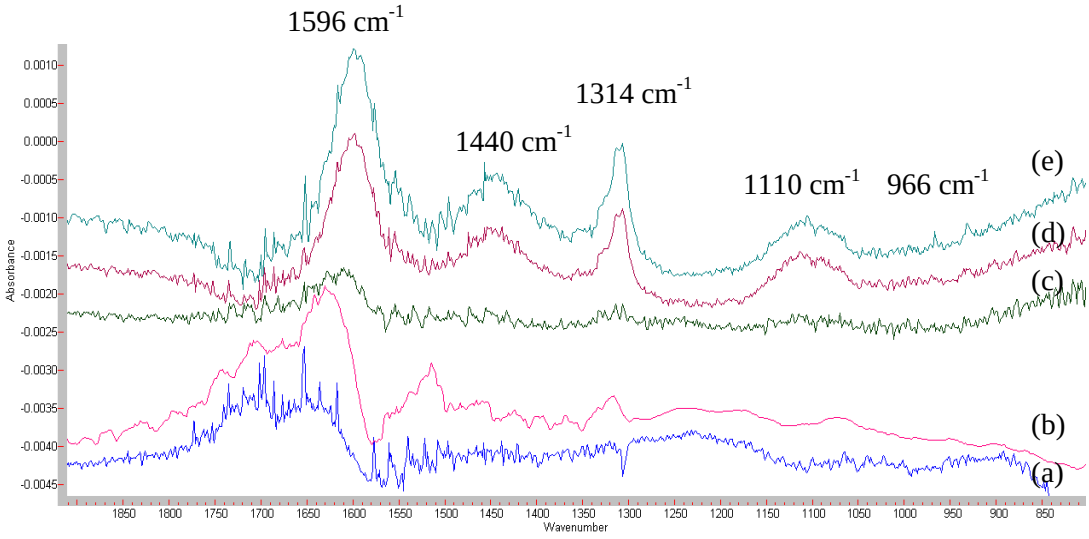

Figure 6.6: FTIR spectra of 0.1 wt% oxalic acid and 0.1 wt% H_2SO_4 aerosols at 20 (spectrum (a)) and 50 %RH (spectrum (b)) plus with added ammonia 100 sccm (spectrum (c)), 200 sccm (spectrum (d)) and 300 sccm (spectrum (e)) at 50 %RH.

Further additions of ammonia lead to an increase in the intensity of the SO_4^{2-} ion and oxalate until no further increases are observed and IR absorbance due to gaseous ammonia is visible in spectrum (e). No ammonium bisulfate or ammonium hydrogenoxalate were formed. These ammonia peaks are clearer to see at 50 %RH than at 20 %RH indicating that less ammonia reacts with these aerosols at this humidity due to dilution of the system, a fact which is further explained in the consideration of $[NH_4^+]$ data.

Figure 6.7 illustrates the effect of a higher humidity (90 %RH) on this acid composition. The seven main absorptions can be assigned to ammonium hydrogenoxalate, ammonium oxalate and ammonium sulfate species. The speciation shows that at higher humidities, ammonium hydrogenoxalate is formed in abundance along with the already fully ionised oxalate and sulfate ions. The peak at 1613 cm^{-1} indicates a partial hydrogenoxalate/oxalate ion which was a rare peak discovered. Two distinct ammonium ions are also observable at 1470 and 1430 cm^{-1} representing both the oxalic and sulfuric acid components.

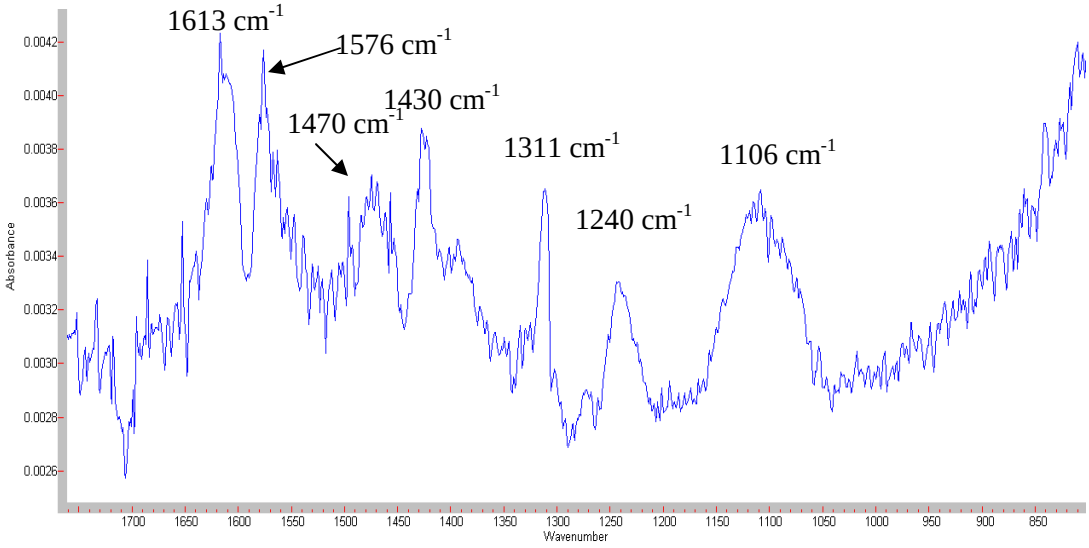

Figure 6.7: FTIR spectra of 0.1 wt% oxalic acid aerosols and 0.1 wt% H_2SO_4 with 300 sccm ammonia at 90 %RH.

Figure 6.8 shows the FTIR spectra of 0.1 wt% oxalic acid and 1 wt% H_2SO_4 aerosols with varying humidity.

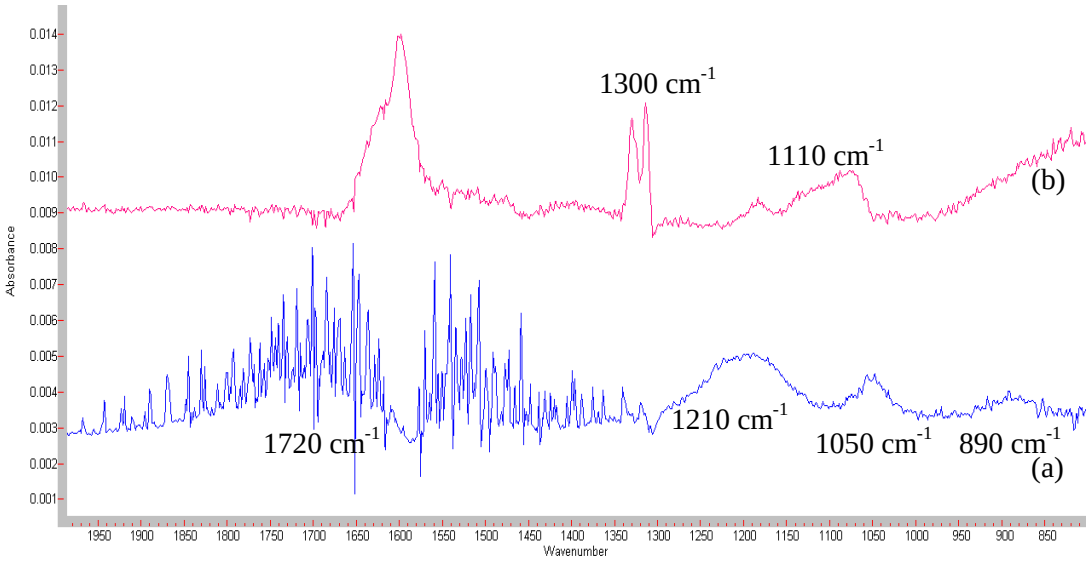

Figure 6.8: FTIR spectra of 0.1 wt% oxalic acid and 1 wt% H_2SO_4 aerosols at 20 %RH (spectrum (a)) and 50 %RH (spectrum (c)).

The composition is mainly bisulfate and hydrogenoxalate ions prior to an increase in humidity. The band at 1210 cm^{-1} is representative of both a hydrogenoxalate and bisulfate species as previously mentioned. A marked difference occurs with humidity change. The broad peak centred at 1109 cm^{-1} can be considered to consist of SO_4^{2-} ions. FTIR absorbances due to the oxalate ion are present at 1600 and 1300 cm^{-1}. At 50 %RH the aerosols consist of a mixture of oxalate, bisulfate and sulfate ions.

The FTIR spectra for the aerosols at 50 %RH with the addition of 100 and 300 sccm NH_3, as represented by spectra a, b and c respectively, are shown in Figure 6.9. These aerosols are primarily composed of $HC_2O_4^-$ and HSO_4^- ions before the addition of ammonia. With addition of ammonia, the aerosol speciation again dramatically changes to oxalate and sulfate. Spectrum (c) show a number of distinctive features at 1600 cm^{-1}, 1430 cm^{-1}, 1300 cm^{-1} and 1115 cm^{-1} and are absorption bands, corresponding to (i) ν_{as} C=O stretch (ii) ν_4 (NH_4^+) deformation mode (iii) ν_s C=O stretch and (iv) the ν_3 (SO_4^{2-}) mode, respectively. The ammonium peak is asymmetrical and yields two peaks at 1438 and 1421 cm^{-1}. The latter of these peaks is attributable to the NH_4^+ ion in ammonium sulfate while the former can be assigned to the NH_4^+ ion in ammonium oxalate. Further additions of ammonia lead to an increase in the intensity of the NH_4^+ ion peak and SO_4^{2-} ion peak, while little change is observed for the oxalate ion peaks.

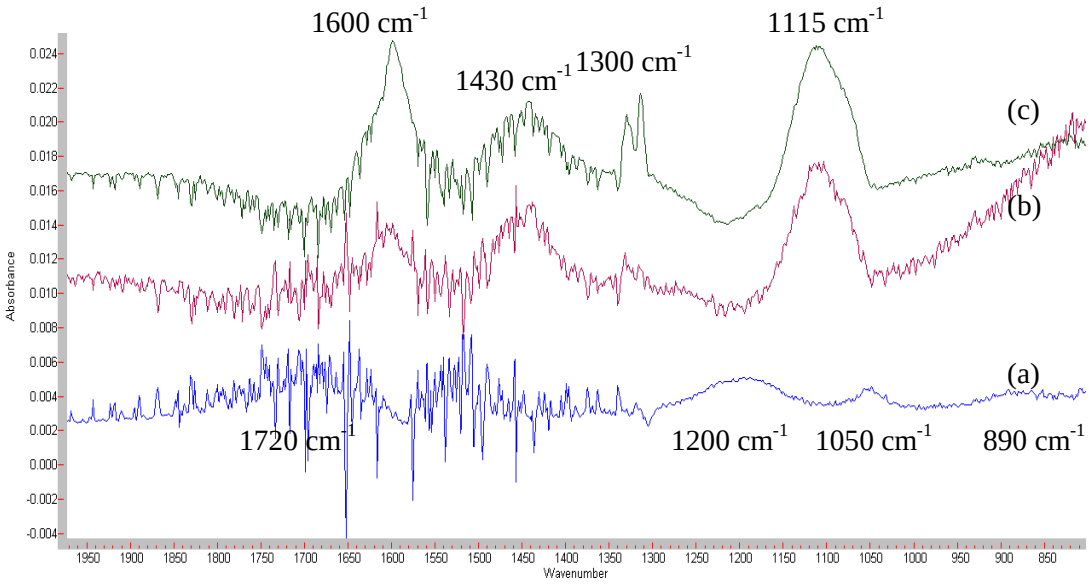

Figure 6.9: FTIR spectra of 0.1 wt% oxalic acid and 1 wt% H_2SO_4 aerosols at 50 %RH (spectrum (a)), and with 100 sccm (spectrum (b)) and 300 sccm added ammonia (spectrum (c)).

6.2.2 Malonic and sulfuric acid aerosols with ammonia

6.2.2.1 FTIR data

As with the studies of malonic acid alone (Chapter 5), spectra were not obtainable at low humidities or in the absence of ammonia for the solubility reasons already discussed. Bacterial growth was not evident in preserved solutions, however, due to the presence of sulfuric acid [53]. The following FTIR spectra were obtained for 1, 0.5 and 0.1 wt% malonic acid with 0.1, 0.5 and 1 wt% H_2SO_4 respectively at 20 to 95 %RH and with 300 sccm NH_3.

Figure 6.10 displays a typical spectra of 1 wt% malonic acid and 0.1 wt % sulfuric acid at 20 and 50 %RH with 300 sccm ammonia.

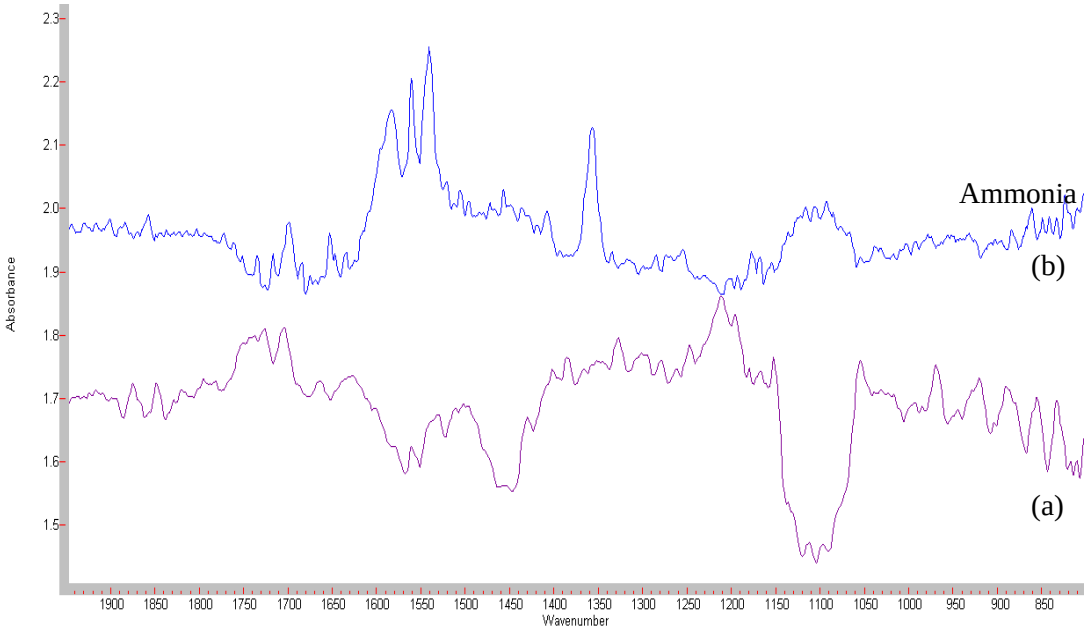

Figure 6.10: FTIR spectra of 1 wt% malonic and 0.1 wt% sulfuric acid aerosols at 20 %RH and 300 sccm ammonia (spectrum (a)) and 50 %RH and 300 sccm ammonia (spectrum (b)).

As can be seen, the spectrum consists essentially of six bands at 1720, 1560, 1440, 1350, 1230 and 1110 cm^{-1} originating from both malonic acid and sulfuric acid species. The absorptions at 1720 cm^{-1} and 1320 cm^{-1} are assigned to the stretching

vibrations of the C=O of the hydrogenmalonate ion. The absorptions at 1560 cm^{-1} and 1350 cm^{-1} represent the $C_3H_2O_4^{2-}$ ion. The sulfate absorption is at 1110 cm^{-1} and in addition, the ν_4 (NH_4^+) absorbance measured at 1440 cm^{-1} is attributable to both malonic and sulfuric components. The composition of the aerosol is, therefore, a mixture of sulfate, malonate and hydrogenmalonate ions. It is observed that at the lower humidities, hydrogenmalonate is the main ion, however at high humidities with ammonia, ammonium malonate and ammonium sulfate are the main components. Gaseous ammonia absorptions are weakly apparent in the spectra indicating that a maximum interaction between $C_3H_4O_4$ and NH_3 has been reached. Figure 6.11 provides a clearer observation of these absorptions at 50 %RH and with increasing additions of NH_3. The ammonium deformation band at 1440 cm^{-1} is again unclear which indicates the inefficient formation of ammonium ions by malonic acid because of its weak acidity. This interpretation is supported by the very apparent gaseous ammonia absorptions at 950 and 964 cm^{-1}.

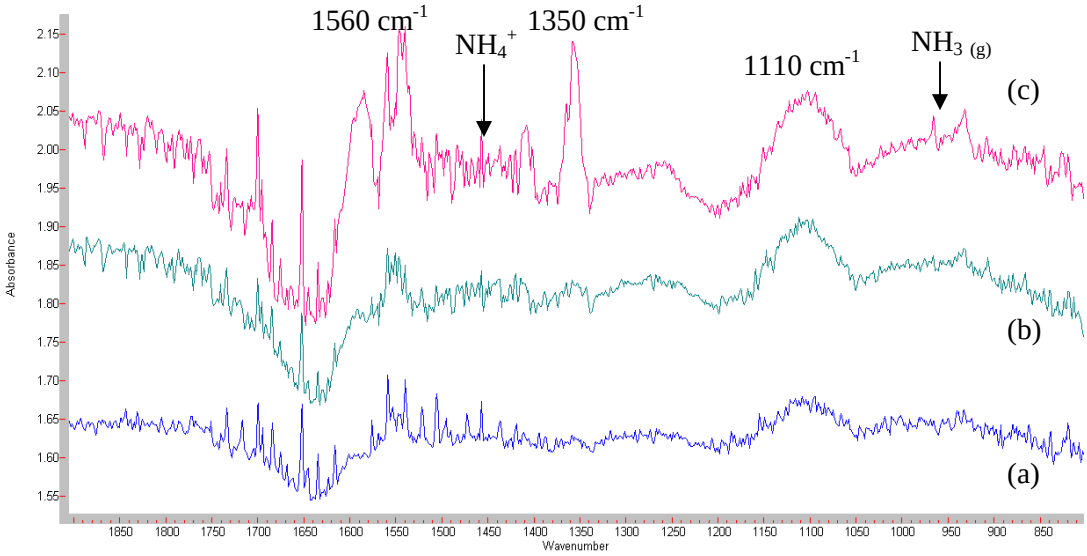

Figure 6.11: FTIR spectra of 1 wt% malonic and 0.1 wt% sulfuric acid aerosols at 50 %RH and 100 sccm ammonia (spectrum (a), 200 sccm ammonia (spectrum (b)) and 300 sccm ammonia (spectrum (c)).

Figure 6.12 shows a typical spectrum obtained using equal concentrations of malonic and sulfuric acid. As previously stated, the spectra for this solution were difficult to obtain at low humidities and without ammonia. The sulfate absorption at 1100 cm^{-1} is stronger with this concentration and the malonate peaks at 1560 cm^{-1} and 1340 cm^{-1} are also observed at 50 %RH and 300 sccm ammonia. The band centred at 1440 cm^{-1} is an indication of the formation of ammonium ions for both the malonate and sulfate cases. A baseline corrected version of this spectrum is seen in Figure 6.13.

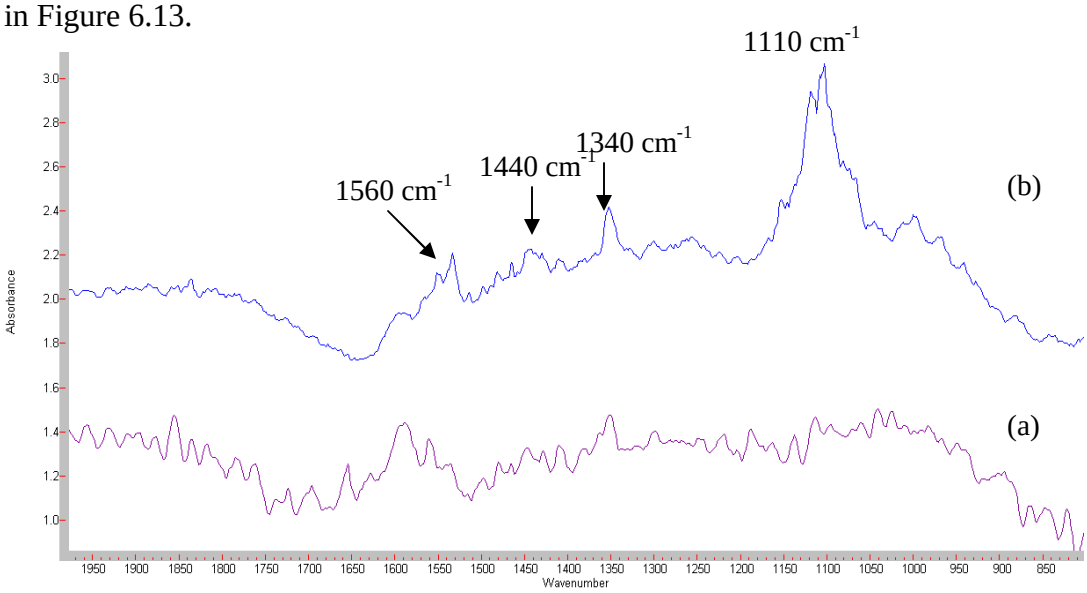

Figure 6.12: 0.5 wt% malonic and 0.5 wt% sulfuric acid at 20 %RH (spectrum (a)) and at 50%RH with 300 sccm ammonia (spectrum (b)).

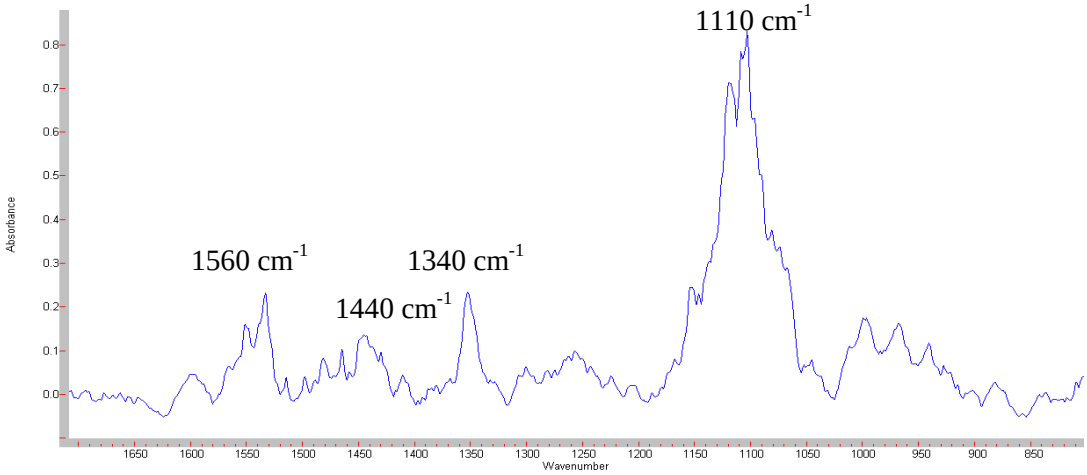

Figure 6.13: 0.5 wt% malonic and 0.5 wt% sulfuric acid at 50 %RH and 300 sccm ammonia, this is a baseline corrected version of the above spectrum (b) of Figure 6.12.

Figure 6.14 shows a typical spectrum for equal concentrations of malonic and sulfuric acid at 95 %RH with 300 sccm ammonia. The bands at 1643 cm^{-1} indicates a partial hydrogenmalonate ion which is observed for conditions of 95 %RH with 300 sccm NH_3. This species is lost from the system with increasing humidity and the aerosol changes primarily to malonate and sulfate. The ν_4 (NH_4^+) band centred at 1442 cm^{-1} produces two peaks at 1439 and 1421 cm^{-1} representing ammonium oxalate and ammonium sulfate. This behaviour is similar to the results obtained for the deconvolutions undertaken for mixtures of oxalic and sulfuric acid. The OH stretching band for water is also observed at 3400 cm^{-1}.

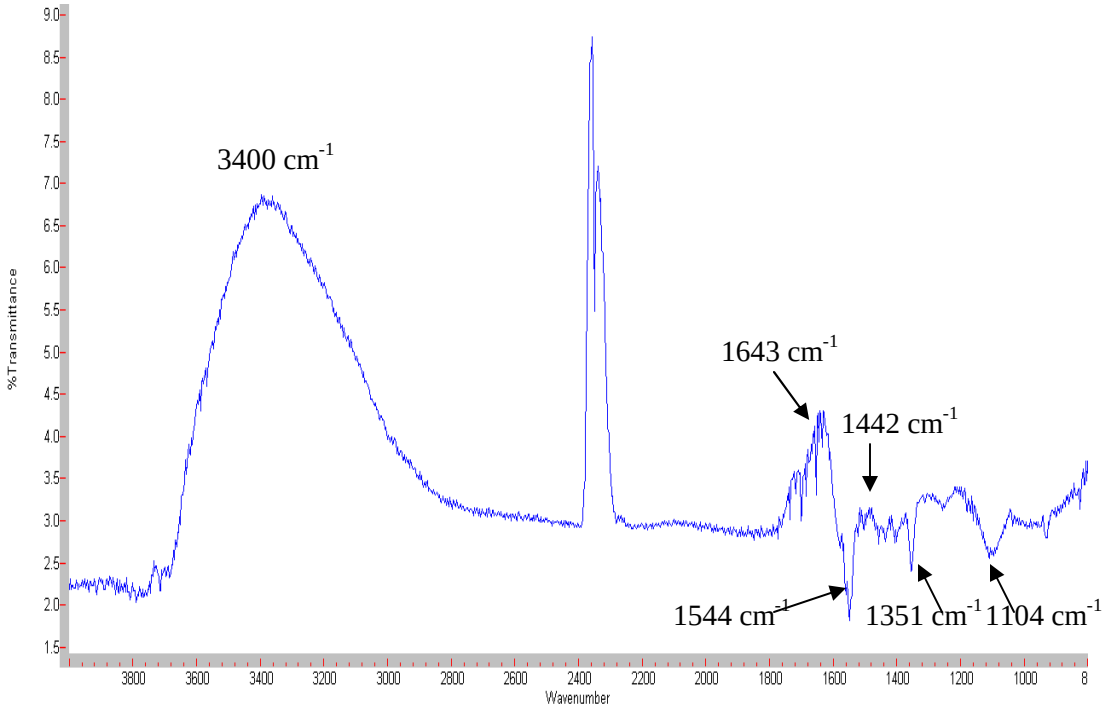

Figure 6.14: FTIR spectrum of 0.5 wt% malonic and 0.5 wt% sulfuric acid at 95 %RH and 300 sccm ammonia, the peak at 2300 cm^{-1} indicates CO_2.

Figures 6.15 and 6.16 show typical spectra of a 0.1 wt% malonic acid and 1 wt% sulfuric acid. Increasing the sulfuric acid weight fraction further, removes the distinct presence of both malonate or hydrogenmalonate ions. Bisulfate absorption bands are possibly formed but weak at 20 %RH with 300 sccm ammonia. Such bands should be obtained at 1210 and 1055 cm^{-1}. Increasing the humidity leads to ammonium sulfate formation with absorptions at 1420 and 1105 cm^{-1}. The composition of the aerosol is, therefore mainly a mixture of ammonium and sulfate ions with possible contribution from bisulfate ions.

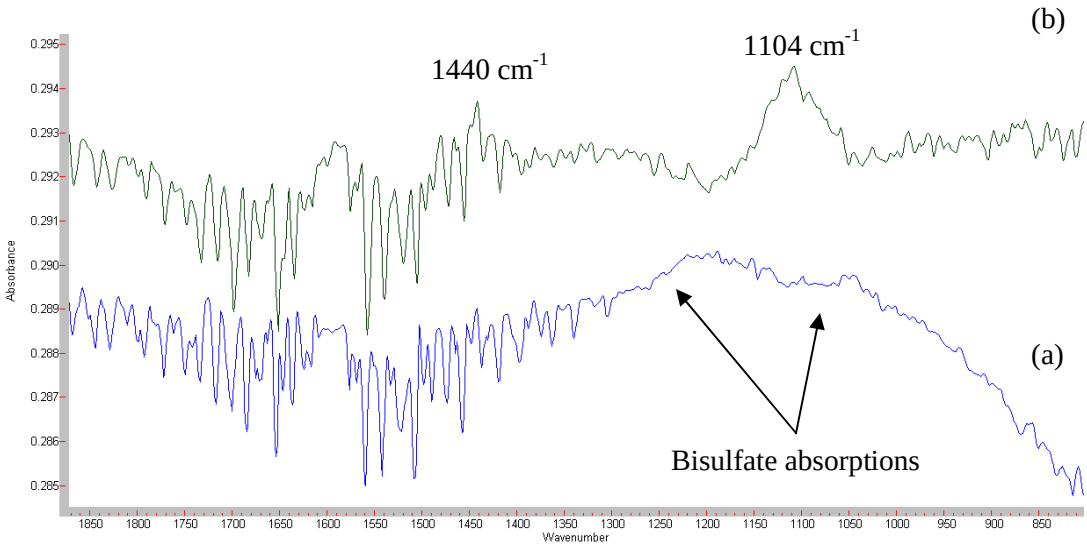

Figure 6.15: FTIR spectra of 0.1 wt% malonic and 1 wt% sulfuric acid aerosols with 300 sccm ammonia at 20 %RH (spectrum a) and at 50 %RH (spectrum b).

The malonate absorption at 1560 cm^{-1}, as assigned to the asymmetric stretching of the carboxylate group, is evident in Figure 6.16. This represents a more established spectrum for this acid weight fraction ratio at 50 %RH and 300 sccm NH_3. The other malonate absorption which has been previously located at 1340 cm^{-1} is not clear. This spectrum therefore shows the decreasing strength of malonic acid at this concentration. In contrast, the sulfate absorption at 1110 cm^{-1} is intense. The ammonium deformation absorption at 1440 cm^{-1} is also strong compared with previous spectra at other concentration ratios indicating the stronger acidity of sulfuric acid compared to malonic acid. This conclusion is further enhanced by the absence of gaseous ammonia peaks.

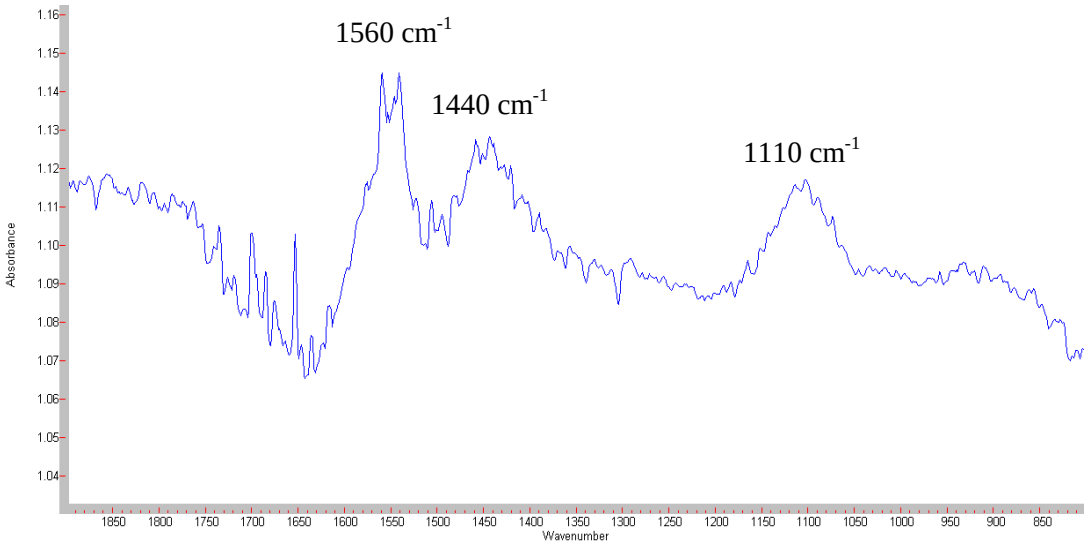

Figure 6.16: FTIR spectra of 0.1 wt% malonic and 1 wt% sulfuric acid aerosols with 300 sccm ammonia at 50 %RH.

FTIR spectra, adapted from Braban and Abbatt [39], of five compositions of ammonium sulfate-malonic acid solutions at < 1 %RH (Figure 6.17) and > 80 %RH (Figure 6.18) are shown. Firstly, regarding the ammonium sulfate component, absorptions are seen between 2800 − 3000 cm^{-1}, 1420 − 1450 cm^{-1}, 1115 cm^{-1} and 620 cm^{-1} corresponding to N-H stretch modes, NH_4^+ deformation mode and two sulfate bands, respectively [54]. These features are present as the fraction of malonic acid is increased until f_{MA} = 0.90, where the ammonium sulfate features are not discernable. The NH_4^+ mode in Figure 6.17 present at 1420 cm^{-1} is indicative of ammonium sulfate in the crystalline-phase. The corresponding mode in Figure 6.17 at 1455 cm^{-1} is indicative of the salt being in solution. As the fraction of malonic acid is increased, the ammonium sulfate modes are broader and the NH_4^+ mode is shifted to higher wavenumbers (Figure 6.17 C) and there is also a side peak evident on the broadened mode at 1105 cm^{-1}. This is thought to show that the ammonium sulfate component is aqueous rather than crystalline. Condensed phase H_2O features can be seen between 2500 − 3500 cm^{-1}, ~1600 cm^{-1} and < 1000 cm^{-1} and are assigned to the OH stretch, the H-O-H bending mode and the H-bonding vibrations respectively.

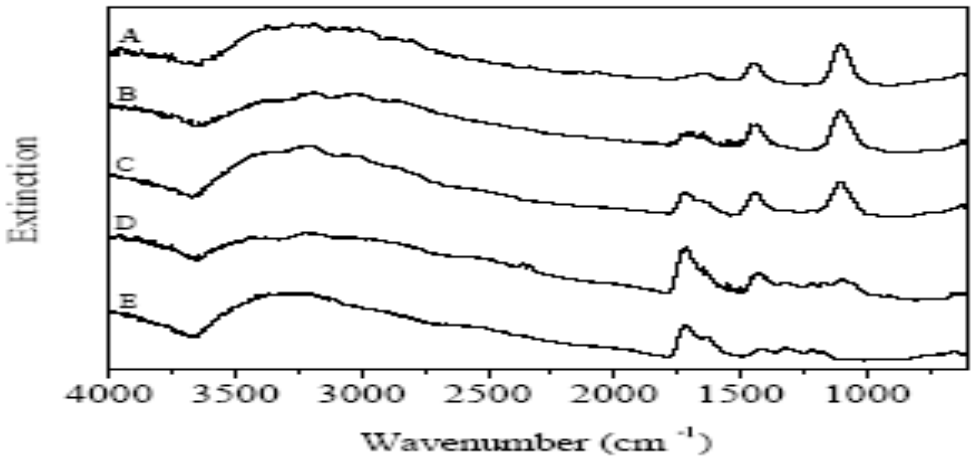

Figure 6.17: Infrared spectra of five compositions of ammonium sulfate (AS) – malonic acid (MA) solutions at < 1 %RH . Compositions as dry fraction of MA (f_{MA}): A: 0.10; B: 0.25; C: 0.49; D:0.75; E: 0.90 [34].

Figure 6.18 C the carbonyl stretch at ~ 1720 cm^{-1} is possibly observable but it is not clear. However as the fraction of malonic acid is increased, this mode increases in intensity and other IR features due to malonic acid become apparent between 2000 and 1000 cm^{-1}. In Braban and Abbatts' previous aerosol studies, the carbonyl resolves into the two peaks at 1749 cm^{-1} and 1686 cm^{-1} when the malonic acid is dry and crystalline [55]. Also, features between 1500 and 1000 cm^{-1} are sharp and well resolved, and the modes at 912 and 630 cm^{-1} are present. In a solution containing ammonium sulfate and malonic acid, it is possible that other salts including ammonium bisulfate, letovicite and ammonium hydrogen malonate could form if partial dissociation of aqueous malonic acid occurs.

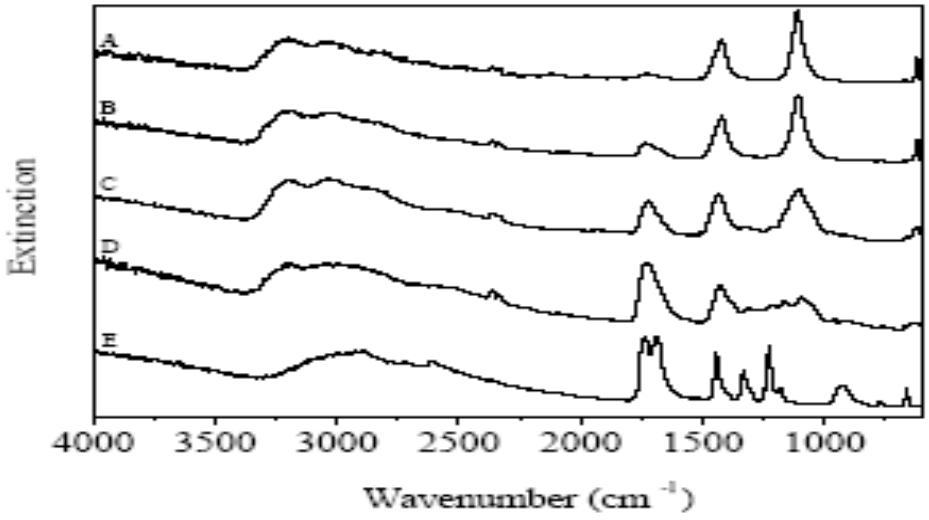

Figure 6.18: Infrared spectra of five compositions of ammonium sulfate (AS) – malonic acid (MA) solutions at > 80 %RH. Compositions as dry fraction of MA (f_{MA}): A: 0.10; B: 0.25; C: 0.49; D:0.75; E: 0.90 [34].

6.2.3 Succinic and sulfuric acid aerosols with ammonia

6.2.3.1 FTIR data

The succinic acid FTIR data obtained was comparable to the oxalic acid results due to its similar solubility in water [31]. Spectra were obtainable at low humidities and without ammonia in contrast to the malonic acid case. The following figures show typical FTIR spectra obtained for 1, 0.5 and 0.1 wt% succinic acid with 0.1, 0.5 and 1 wt% H_2SO_4 respectively with varying humidities and also varying ammonia additions.

Figure 6.19 displays a spectrum of 1 wt% succinic acid and 0.1 wt % sulfuric acid at low humidity (spectrum (a)), high humidity (spectrum (b)) and high humidity plus ammonia (spectrum (c)).

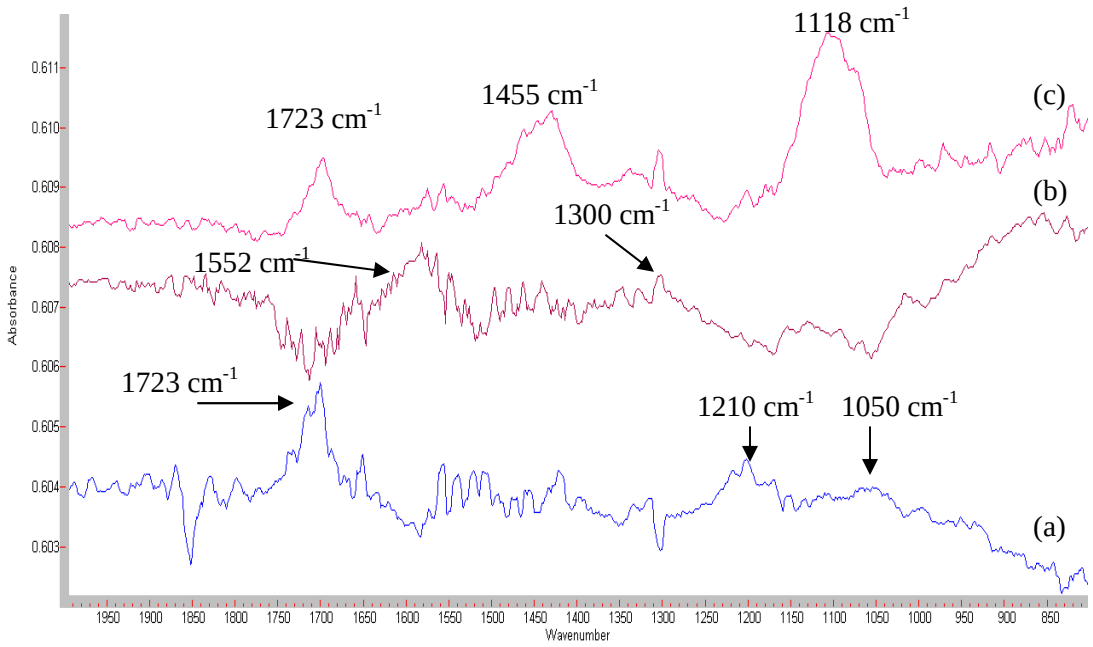

Figure 6.19: 1 wt% succinic and 0.1 wt% sulfuric acid at 20 %RH (spectrum (a)), 50 %RH (spectrum (b)) and with 300 sccm ammonia at 50 %RH (spectrum (c)).

Spectrum (a) exhibits a hydrogensuccinate absorption at 1723 cm^{-1} indicating the asymmetric stretching of the hydrogencarboxylate ion. The other characteristic

hydrogensuccinate ion mode which was observed in previous studies is not present. Weak bisulfate absorptions are observable at 1210 and 1050 cm^{-1}. These absorptions are expected to be weak due to the low concentration of sulfuric acid used to generate these spectra (0.1 wt%). As humidity is increased, the succinate species emerge and there is a decrease in the absorbance of the hydrogensuccinate absorption. The bisulfate absorptions are observed to be inverted indicating that they are used up at high humidities. On addition of ammonia, the spectra dramatically changes. The hydrogensuccinate ion re-emerges at 1723 cm^{-1} and the sulfate ion is observable as a peak at 1118 cm^{-1}. This is a notable difference compared to the malonic and sulfuric acid studies for this concentration ratio. The absorption at 1455 cm^{-1} is assigned to the ammonium ion of both succinate and sulfate. Ammonium hydrogensuccinate is also formed without H_2SO_4 (Chapter 5).

At 90 %RH however, there are changes in aerosol composition in the FTIR data. The succinate ion is now the dominant species with a characteristic absorption at 1560 cm^{-1}. There is a loss of the hydrogensuccinate absorption at 1720 cm^{-1} and there is little or no indication of the sulfate ion at 1115 cm^{-1}. The ammonium deformation band is split at 1455 cm^{-1} and 1415 cm^{-1} representing ammonium succinate and sulfate respectively. Thus, at very high humidities, ammonium succinate appears to be the mainly favoured speciation.

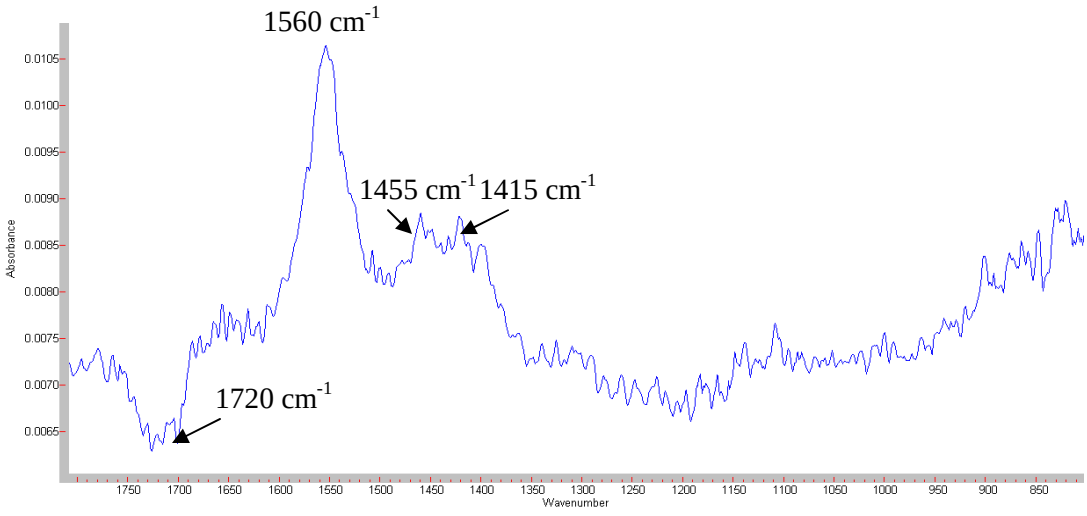

Figure 6.20: FTIR spectrum of 1 wt% succinic and 0.1 wt% sulfuric acid at 90 %RH with 300 sccm ammonia.

Figure 6.21 shows spectra of succinic and sulfuric acid at equal concentrations with increasing additions of ammonia at 50 %RH. The symmetric stretching mode of the succinate ion at 1340 cm^{-1} is now more clearly observed in this figure as well as the other characteristic absorptions for the succinate, sulfate and ammonium ions. Ammonia absorptions are also observed with 300 sccm NH_3 addition indicating that the aerosol is fully neutralised at this stage of this experiment. A closer inspection of the spectrum is shown in Figure 6.22.

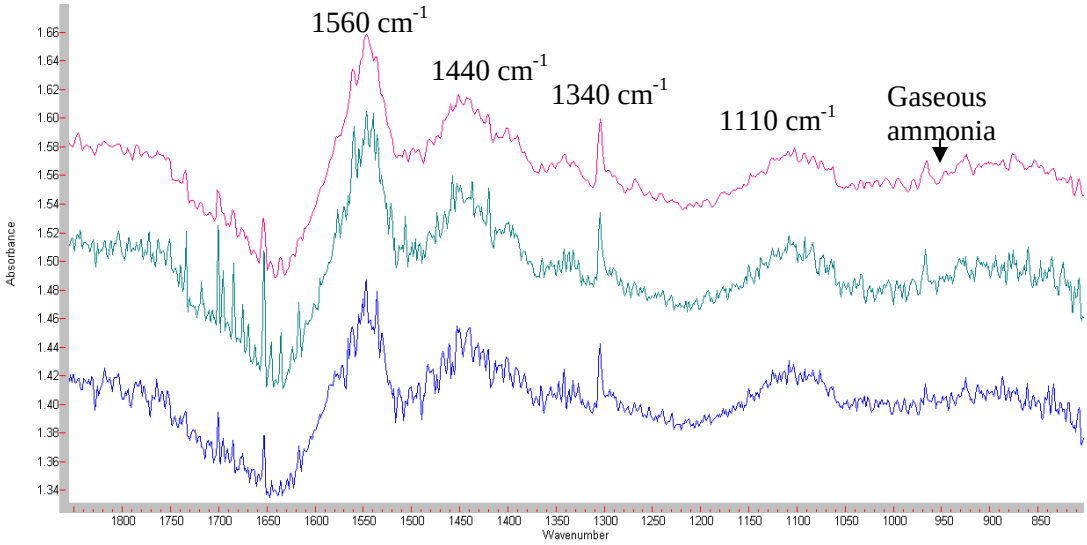

Figure 6.21: 0.5 wt% succinic and sulfuric acid with 100 (spectrum (a)), 200, (spectrum (b)) and 300 sccm ammonia (spectrum (c)) at 50 %RH.

Figure 6.22: 0.5 wt% succinic and sulfuric acid with 300 sccm ammonia at 50 %RH (a magnification of the previous spectrum).

Figure 6.23 shows an established spectrum at equal concentrations of $C_4H_6O_4$ and H_2SO_4. The succinate absorption is located at 1552 cm^{-1} and the hydrogensuccinate absorptions at 1723 and 1230 cm^{-1} are clearly lost from the system. The aerosol changes primarily to one containing succinate and sulfate (1118 cm^{-1}) ions. The ν_4 (NH_4^+) band at 1440 cm^{-1} produces two peaks at 1455 and 1425 cm^{-1} indicating the formation of two ammonium ions coordinated to succinate and sulfate respectively. The OH band centred at 3200 cm^{-1} is also observed.

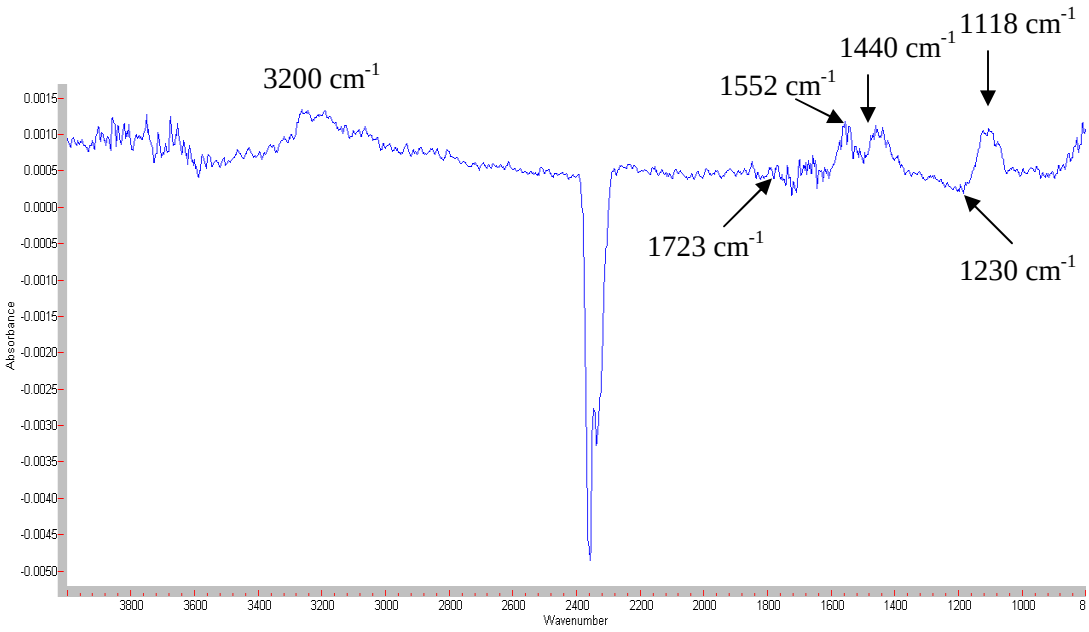

Figure 6.23: FTIR spectrum of 0.5 wt% succinic and sulfuric acid with 300 sccm ammonia at 50 %RH.

Figure 6.24 shows typical spectra of a 0.1 wt% succinic acid and 1 wt% sulfuric acid under various conditions of humidity and ammonia content. Increasing the sulfuric acid weight fraction further, removes the clear presence of both succinate or hydrogensuccinate at 20 %RH. Bisulfate absorptions are now clear at 20 %RH, at 1210 and 1055 cm^{-1}. As humidity is increased, the succinate component is more observable and the bisulfate absorptions are inverted and removed from the system. Addition of ammonia leads to ammonium sulfate formation with absorptions at 1420 and 1105 cm^{-1}, there are no traces of either hydrogensuccinate or succinate ions. The aerosol composition finally becomes mainly composed of ammonium sulfate.

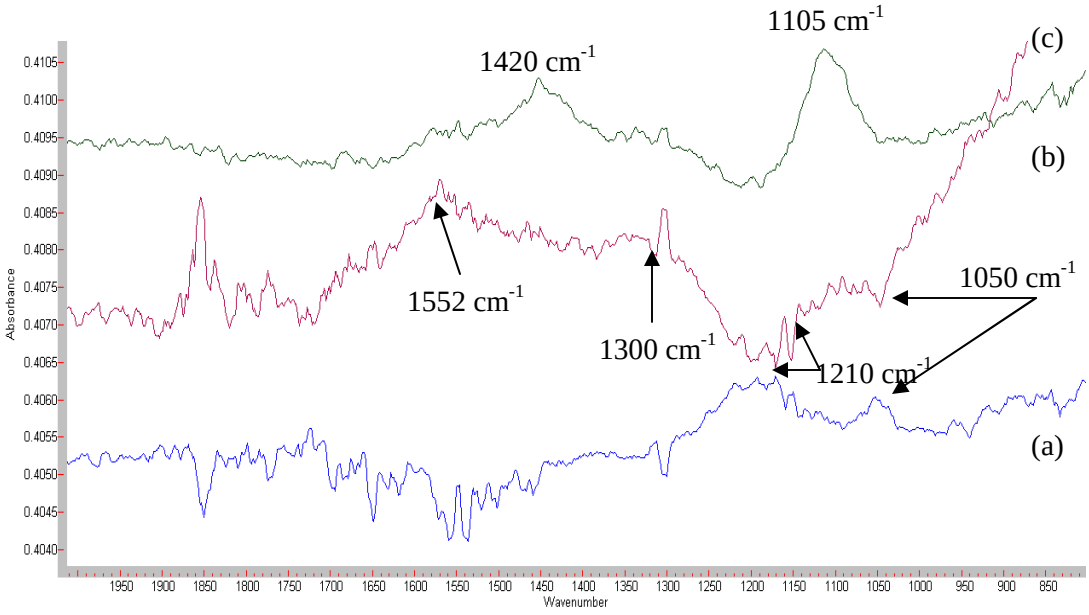

Figure 6.24: 0.1 wt% succinic and 1 wt% sulfuric acid at 20 %RH (spectrum (a), 50 %RH (spectrum (b) and at 50 %RH plus 300 sccm ammonia (spectrum (c)).

Figure 6.25 is a spectrum of this concentration mixture with 300 sccm ammonia at 90 %RH. It again highlights the formation of sulfate at 1100 cm^{-1} and the loss of hydrogensuccinate/succinate ions at 1630 and 1560 cm^{-1}.

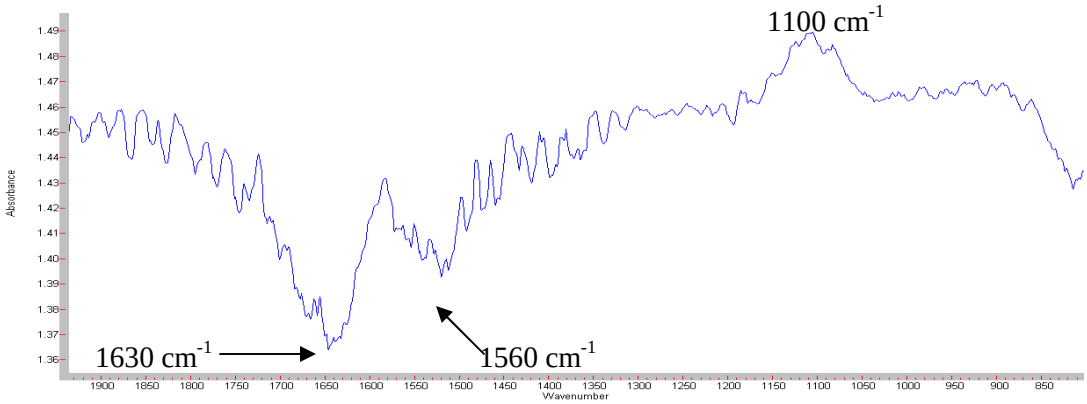

Figure 6.25: FTIR spectrum showing 0.1 wt% succinic and 1 wt% sulfuric acid with 300 sccm ammonia at 50 %RH.

Sulfosuccinic acid was studied as a reference salt to investigate spectra that contains a sulfonate and organic component. The following FTIR spectrum (Figure 6.27) shows the absorption bands obtained on directly heating the molecule which is in liquid form at room temperature (boiling point, 373 K). The succinic constituent is represented by the characteristic carboxylate absorptions previously discussed at 1637, 1541 and 1370 cm^{-1} whereas the sulfonate constituent provides sharp peaks at 1257, 1094, 1029 and 815 cm^{-1}. From studies previously undertaken with sulfuric acid [(1)], and as shown in Table 6.4, the bisulfate absorptions are found at 1257, 1029 and 815 cm^{-1}. The 1257 cm^{-1} band may also account for the formation of molecular sulfuric acid. One sulfate absorption band is apparent at 1094 cm^{-1}. The absorption at 1040 cm^{-1} in Figure 6.28, which is part of a spectrum obtained using the nebuliser method of aerosol generation, is associated with sulfocarboxylic compounds [(56)]; this absorption was not present in the separate studies of succinic and sulfuric acid suggesting that the ions are free and uncoordinated in the experiments undertaken. Succinate ions are the main aerosol component before ammonia is introduced (1643 and 1228 cm^{-1}). With ammonia addition, speciation changes occur to make hydrogensuccinate ions (1719 and 1230 cm^{-1}) and ammonium sulfate (1418 and 1170 cm^{-1}).

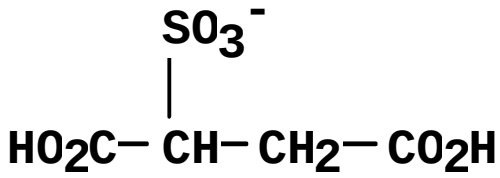

Figure 6.26: Molecular structure of sulfosuccinic acid.

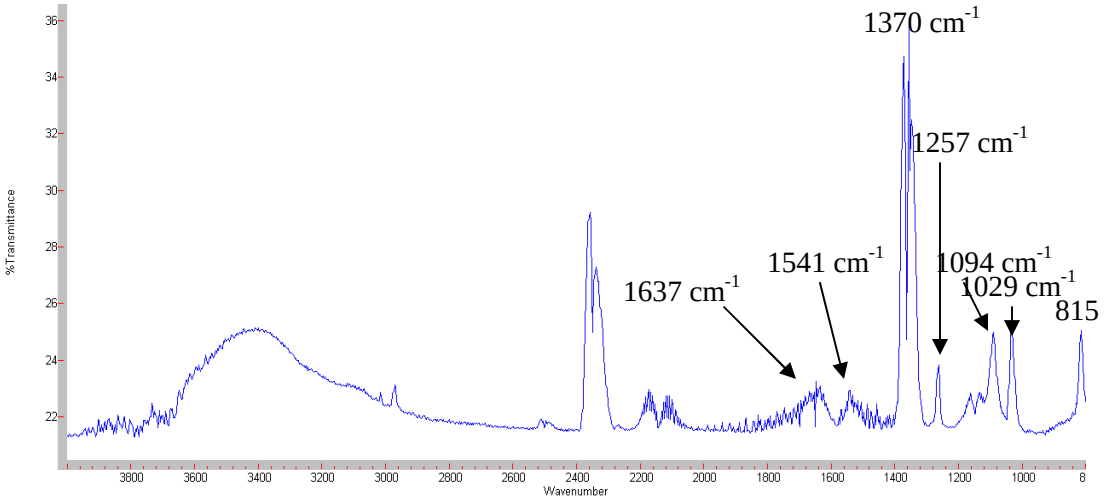

. **Figure 6.27: FTIR spectrum obtained when heating 1 wt% sulfosuccinic acid.**

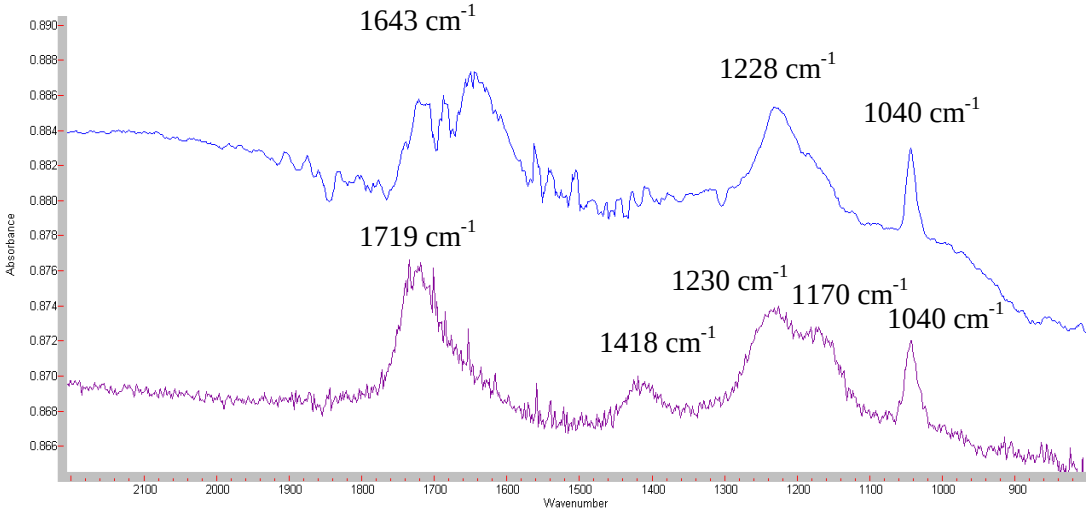

Figure 6.28: 1 wt% sulfosuccinic acid with (bottom) and without (top) ammonia by nebuliser.

6.2.4 Summary of FTIR data

The main FTIR peaks attributed to hydrogendicarboxylate, dicarboxylate, bisulfate, sulfate and ammonium ion aerosol species for oxalic, malonic and succinic acid with sulfuric acid and ammonia are summarised in Table 6.2. Hydrogenoxalate and bisulfate are the species present at low humidities for mixtures of oxalic and sulfuric acid. Oxalate is the prevalent ion at high humidities. With the introduction of ammonia, ammonium oxalate and ammonium sulfate are the species produced. Ammonium sulfate is favoured more at low humidities whereas ammonium oxalate is the dominant species at high humidities. Increasing the concentrations of oxalic acid, ammonium hydrogenoxalate is also found to be present.

Table 6.2: Absorption positions (cm^{-1}) of hydrogendicarboxylate, dicarboxylate, sulfate and ammonium ions for oxalic, malonic and succinic acid aerosols with sulfuric acid and ammonia.

Aerosol	$H_{1,3,5}C_{2,3,4}O_4^-$	$C_{2,3,4}O_4^{2-}$	NH_4^+	HSO_4^-	SO_4^{2-}
Oxalic acid	1723, 1242	~	~	1216, 1055	~
+ Sulfuric acid	1723, 1242	1605, 1317	1439	~	1116
+ Ammonia					
Malonic acid	~	~	~	~	~
+ Sulfuric acid	1723, 1643	1544, 1351	1442	1210, 1050	1104
+ Ammonia					
Succinic acid	1723, 1240	~	~	1210, 1050	~
+ Sulfuric acid	1723, 1240	1552, 1340	1435	~	1105
+ Ammonia					

FTIR spectra of malonic and sulfuric acid were not obtainable without the addition of ammonia, particularly at low humidities. Hydrogenmalonate and bisulfate were the main absorptions at low humidities whereas at conditions of 50 %RH or higher, malonate and sulfate were favoured being coordinated to ammonium ions. No spectra indicated the formation of ammonium hydrogenmalonate. However, the malonic component was also difficult to observe in sulfuric dominated concentrations. Succinic and sufuric acid studies were more recordable however with similar trends in the ion speciations observed in terms of humidity and

ammonia addition. The less ionised species was formed at low humidities whereas the fully deprotonated form was found at high humidities and with addition of ammonia. A unique difference was the observation of hydrogensuccinate at high humidities.

The main FTIR peaks attributed to hydrogendicarboxylate, dicarboxylate and ammonium ion aerosol species for oxalic, malonic and succinic acid and ammonia are summarised in Table 6.3. The main differences due to the addition of sulfuric acid is the presence of ammonium hydrogendicarboxylate and the absence of any observable C-H and C-C stretches.

Table 6.3: Peak positions (cm^{-1}) of hydrogendicarboxylate, dicarboxylate and ammonium ions for oxalic, malonic and succinic acid aerosols.

Aerosol	$H_{1,3,5}C_{2,3,4}O_4^-$ (mainly low humidities)	$C_{2,3,4}O_4^{2-}$ (mainly high humidities)	NH_4^+
Oxalic acid	1720, 1240	1600, 1320	~
+ Ammonia	~	1600, 1310	1450
Malonic acid	1720, 1630, 1328, 1415	1560, 1360	~
+ Ammonia	~	1560, 1340	1440
Succinic acid	1700, 1420, 1335, 1200	1630, 1310, 1420, 1205	~
+ Ammonia	~	1550, 1310	1430

The main IR peaks representing sulfate, bisulfate and ammonium ion aerosol species for the sodium and ammonium salts are summarised in Table 6.4 as a useful comparison. It is worth mentioning that bisulfate peaks were mainly observed without the addition of ammonia but the sulfate absorption is only present with the addition of ammonia when using the nebuliser method of generation regardless of humidity. This observation is also reflected in the studies made here for sulfuric acid with the dicarboxylic acids.

Table 6.4: Peak positions (cm^{-1}) of sulfate and bisulfate for ammonium and sodium bisulfate and sulfate salts along with sulfuric acid and ammonia.

Aerosol	**HSO_4^-**	**SO_4^{-2}**			**HSO_4^-**	**HSO_4^-**	**NH_4^+**
$NaHSO_4$	1233	1172			883	883	
Na_2SO_4		1173	1152	1112			
NH_4HSO_4	1213		1164		876	876	1422
$(NH_4)_2SO_4$				1116			1436
H_2SO_4	1216		1157		888	888	
$H_2SO_4 + NH_3$			1110				1422

6.2.5 SMPS data of dicarboxylic acids and sulfuric acid with ammonia

Table 6.5 shows the particle diameter and number concentration for 0.1 wt% oxalic acid aerosols with the addition of sulfuric acid. As shown previously, 0.1 wt% oxalic acid aerosols consist of hydrogenoxalate ions at 20 %RH, while at 50 %RH, oxalate ions are more prominent.

Table 6.5: Particle statistics for 0.1 wt% oxalic and sulfuric acid aerosols at 20 and 50 %RH

	20 %RH		50 %RH	
Aerosol Composition	**Diameter (nm)**	**Concentration ($\times 10^6$ cm^{-3})**	**Diameter (nm)**	**Concentration ($\times 10^6$ cm^{-3})**
0.1 wt% $H_2C_2O_4$	70	0.6	55	0.9
+ 0.1 wt% H_2SO_4	91	1.7	71	2.3
+ 0.5 wt% H_2SO_4	95	2.7	88	3.4
+ 1 wt% H_2SO_4	131	4.0	102	5.1

The particle diameter for aerosols composed of oxalate ions is smaller than that for hydrogenoxalate ions. Addition of sulfuric acid (0.1 wt%) to these aerosols resulted in the formation of a mixture of hydrogenoxalate and bisulfate ions while at higher sulfuric acid concentrations (1 wt%) only bisulfate ions were present. Increasing the humidity decreases the particle diameter as the aerosol composition changes from hydrogenoxalate to oxalate ions at low concentrations of sulfuric acid with no bisulfate/sulfate ions. However, at higher concentrations of sulfuric acid, a mixture of oxalate, bisulfate and sulfate ions are present in the aerosols. Inspection of Table 6.5 clearly shows that addition of sulfuric acid leads to a larger particle diameter, while the addition of water vapour promotes the formation of the more ionised species for both oxalic and sulfuric acid; oxalate and sulfate ions, respectively. As

previously shown, the particle diameter for aerosols composed mainly of sulfate ions is smaller than that observed for bisulfate ions.

Addition of water vapour has a clear effect on particle number distributions. As seen in Table 6.5, the particle number for various concentrations of added sulfuric acid increased with changing relative humidity while the mean particle diameter decreased, as illustrated in Figure 6.29. The particle distributions shown in Figure 6.29 are related to the FTIR spectra shown in Figures 6.2 and 6.8.

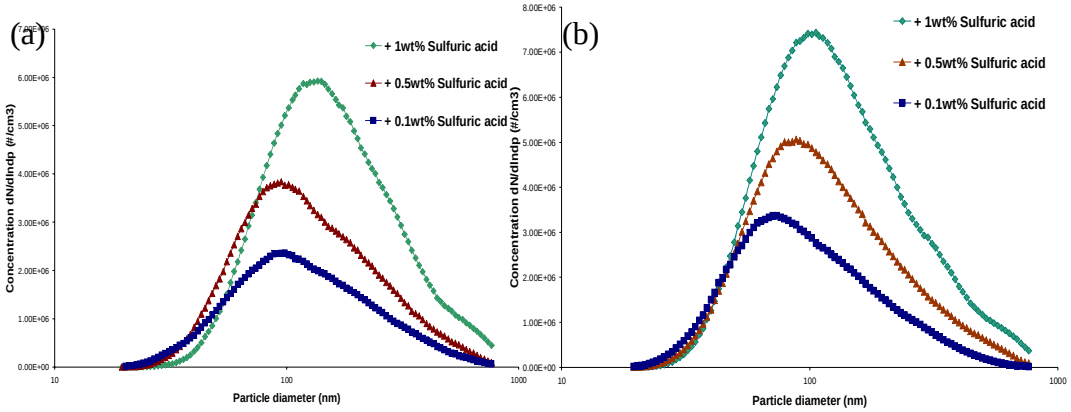

Figure 6.29: Particle distributions for 0.1 wt% oxalic acid aerosols with added sulfuric acid, (blue boxes: 0.1 wt%, red triangles: 0.5 wt% and green diamonds: 1 wt%) at 20 %RH (a) and 50 %RH (b).

At higher relative humidities (50 %RH), little change in the particle distribution was observed on addition of ammonia to oxalic acid aerosols with varying amounts of sulfuric acid. The particle distribution for the interaction between 0.1 wt% oxalic and 0.1 wt% sulfuric acid aerosols with ammonia at 50 %RH is plotted in Figure 6.30. The particle number concentration increased from 2.4 to 3.4×10^6 particles cm^{-3} on addition of 300 sccm NH_3.

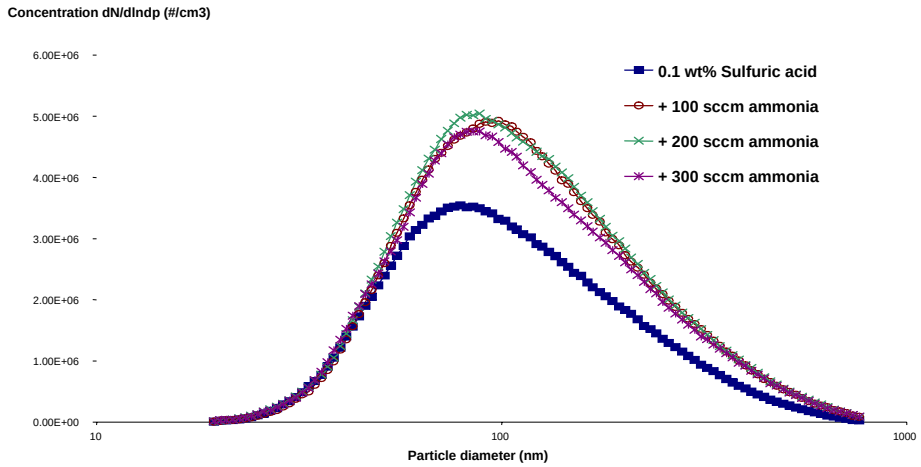

Figure 6.30: Particle distributions for 0.1 wt% oxalic and 0.1 wt% sulfuric acid aerosols with added ammonia, as shown in the legend, at 50 %RH.

Tables 6.6 and 6.7 shows the particle diameter and number concentration for malonic and succinic acid aerosols with the addition of sulfuric acid. As discussed previously in Chapters 3 and 5, the less ionised form is prevalent at low humidities (i.e. hydrogencarboxylate and bisulfate), while the more ionised form is prevalent at high humidities (i.e. carboxylate and sulfate).

Table 6.6: Particle statistics for malonic and sulfuric acid aerosols at 20 and 50 %RH.

	20 %RH		50 %RH	
Aerosol Composition	**Diameter (nm)**	**Concentration ($\times 10^6$ cm^{-3})**	**Diameter (nm)**	**Concentration ($\times 10^6$ cm^{-3})**
0.1wt% $H_4C_3O_4$	82	1.8	73	1.7
1 wt% $H_4C_3O_4$	102	4.1	98	3.8
1 wt% $H_4C_3O_4$ + 0.1 wt% H_2SO_4	102	5.2	88	5.4
0.5 wt% $H_4C_3O_4$ + 0.5 wt% H_2SO_4	109	6.3	102	7.0
0.1 wt% $H_4C_3O_4$ + 1 wt% H_2SO_4	109	6.3	98	6.6

Table 6.7: Particle statistics for succinic and sulfuric acid aerosols at 20 and 50 %RH.

	20 %RH		50 %RH	
Aerosol Composition	**Diameter (nm)**	**Concentration ($\times 10^6$ cm^{-3})**	**Diameter (nm)**	**Concentration ($\times 10^6$ cm^{-3})**
0.1wt% $H_6C_4O_4$	82	1.4	79	1.5
1 wt% $H_6C_4O_4$	98	4.6	88	5.2
1 wt% $H_6C_4O_4$ + 0.1 wt% H_2SO_4	102	4.3	106	1.0
0.5 wt% $H_6C_4O_4$ + 0.5 wt% H_2SO_4	88	5.7	92	4.8
0.1 wt% $H_6C_4O_4$ + 1 wt% H_2SO_4	82	5.7	98	3.7

Regarding malonic acid, increasing the humidity decreases the particle diameter as the aerosol composition changes along with a decrease of particle concentration. As previously explained, the particle concentration decreases due to the water solubility of malonic acid. Inspection of Table 6.6 clearly shows that addition of sulfuric acid leads to a larger particle diameter, while the addition of water vapour promotes the formation of the more ionised species for both malonic and sulfuric acid: malonate and sulfate ions, respectively. These ions have been previously discussed and shown to possess smaller diameters. The particle concentration is also noted to increase with addition of sulfuric acid and subsequent raising of the humidity.

However, regarding succinic and sulfuric acid (Table 6.7), the opposite trend tends to occur compared to the studies involving only succinic acid. There is an increase in particle diameter and a decrease in particle concentration when increasing the humidity. The reason for this difference is due to the increased chain length of this dicarboxylic acid, which forms larger sized but fewer particles. The succinate ion also may not be formed at 50 %RH, a similar occurrence for SMPS data of succinic acid as discussed in Chapter 5. The presence of sulfuric acid is also important for this process to occur. Particle concentrations increase dramatically and the particle diameter decreases possibly due to lack of interaction between the acidic aerosols which go on to form many particles of small diameters.

Addition of water vapour has a clear effect on particle number distributions. The particle number for various concentrations with sulfuric acid increased with changing relative humidity, while the mean particle diameter decreased, as illustrated in Figure 6.31.

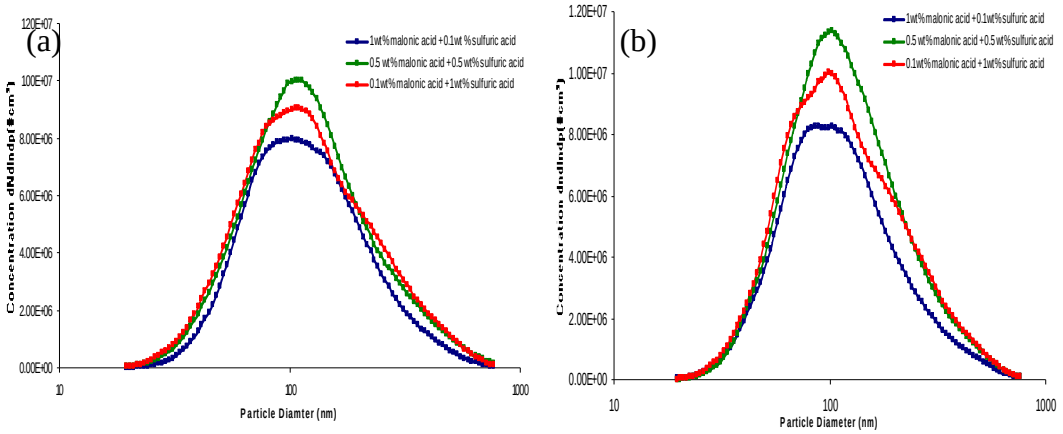

Figure 6.31: Particle distributions for malonic acid aerosols with sulfuric acid, blue boxes: 1 wt%:0.1 wt%, red triangles: 0.5 wt%:0.5 wt% and green diamonds: 0.1 wt%:1 wt%) at 20 %RH (a) and 50 %RH (b).

Figure 6.32 shows the particle distribution of 0.5 wt% malonic and 0.5 wt% sulfuric acid aerosols at 55 %RH with added NH_3 (100, 200 and 300 sccm). The particle number concentration was observed to increase from 6.4 to 7.6 x 10^6 particles cm^{-3} on addition of 300 sccm NH_3. Addition of NH_3 resulted in a more Gaussian distribution of the particle number concentration. The mean particle diameter was in the region of 106 nm. These size distributions are connected to the FTIR spectrum displayed in Figure 6.12.

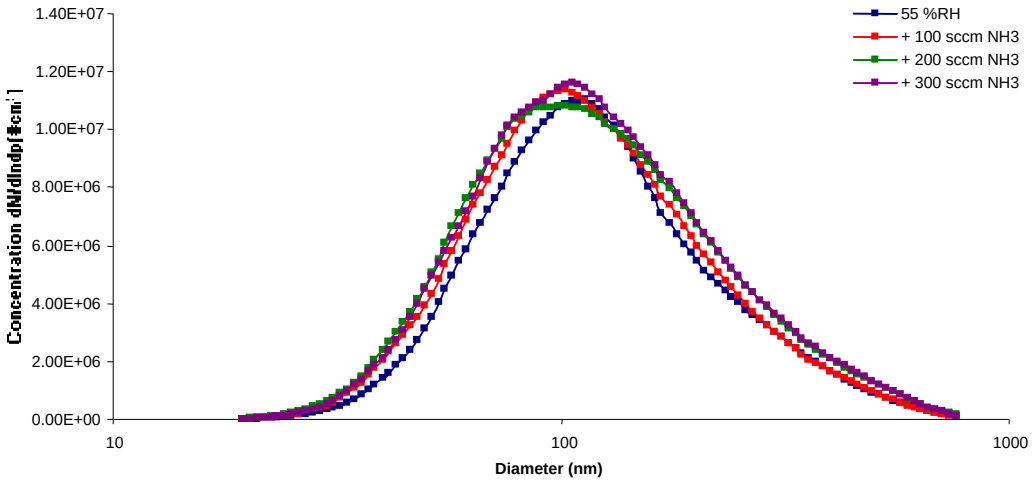

Figure 6.32: Particle distributions for 0.5 wt% malonic and 0.5 wt% sulfuric acid aerosols at 55 %RH with added ammonia as shown in the legend.

Figure 6.33 shows the particle distribution of 0.5 wt% succinic and 0.5 wt% sulfuric acid aerosols with added NH_3 (300 sccm) at 20 %RH and increasing humidity to 50 %RH.

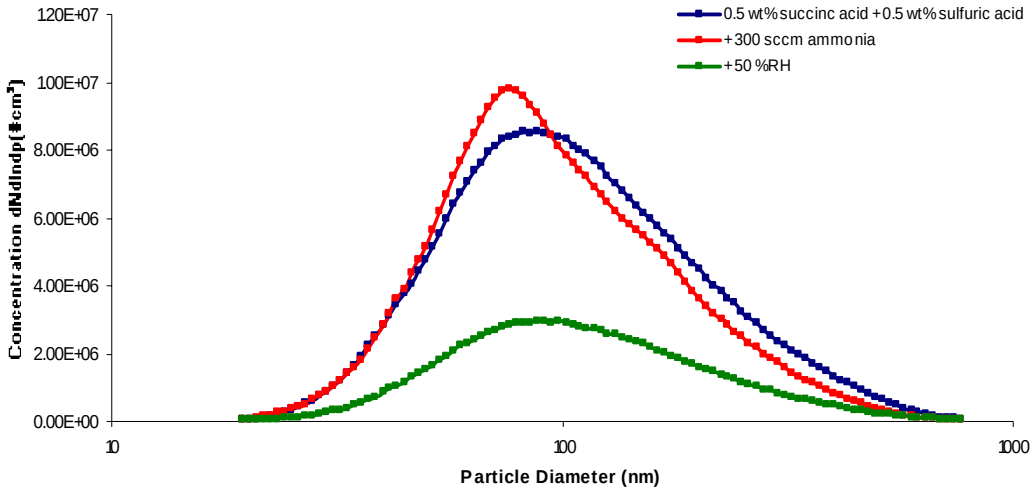

Figure 6.33: Particle distributions for 0.5 wt% succinic and 0.5 wt% sulfuric acid aerosols at 20 RH with added ammonia and increasing %RH, as shown in the legend.

The particle number concentration for 0.5 wt% succinic and 0.5 wt% sulfuric acid aerosols was observed to increase from 8.5 to 9.8 × 10^6 particles cm^{-3} on addition of 300 sccm NH_3. Addition of NH_3 results in a larger particle diameter due to the ammonium ion diameter being larger than the H^+ counterpart. Increasing the humidity, once again increased the particle diameter, yet dramatically reduced the particle concentration. This behaviour for succinic acid is in contrast to the data obtained for oxalic and malonic acid and is due to the increased chain length of this dicarboxylic acid, forming less larger sized particles. The hydrogensuccinate ion is possibly formed aswell at 50 %RH resulting in a larger diameter and reduction of ammonium succinate content. Ammonium and sulfate ions are the other species also present.

6.2.6 NO_x chemiluminescence data for dicarboxylic acids and sulfuric acid with ammonia

The NH_4^+ ion concentrations for 0.1 wt% oxalic acid with varying sulfuric acid weight fractions, at various ammonia flow rates, were calculated from the NO_x data using the calibration factor of 1.2, as discussed in Chapter 2. Inspection of this NH_4^+ ion concentration value leads to the conclusion that increasing the concentration of sulfuric acid concentration has a direct, positive effect on the amount of ammonium ions formed, as illustrated in Figure 6.34.

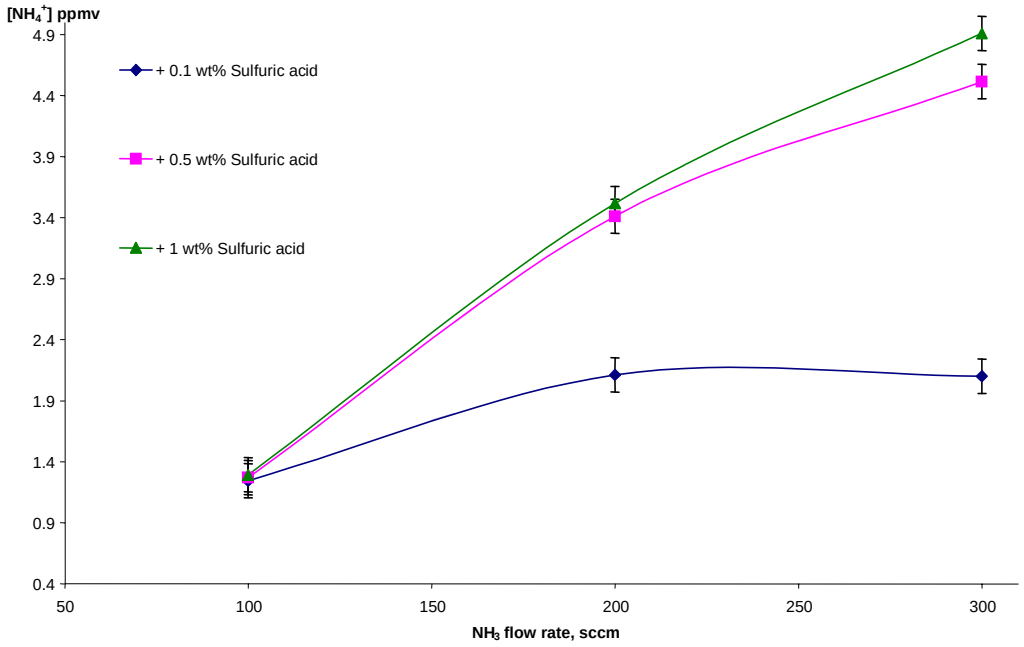

Figure 6.34: Ammonia flow rate vs. ammonium ion concentration at 20 %RH, for 0.1 wt% oxalic acid aerosols with added sulfuric acid as shown in the legend.

In addition, increasing the NH_3 concentration in the flow system increases the ammonium ion concentration. Addition of 100 sccm ammonia to low concentration oxalic-sulfuric aerosols (both at 0.1 wt%) leads to the formation of both $(NH_4)_2SO_4$ and $(NH_4)_2C_2O_4$. Further additions of ammonia do not increase the concentration of ammonium ions formed indicating that the aerosol is completely neutralised (blue line, Figure 6.34). In contrast, at higher sulfuric acid weight fractions (1 wt%) with 0.1 wt% oxalic acid, the addition of ammonia results in the formation of

predominately $(NH_4)_2SO_4$. The ammonium ion concentration increases on the addition of more ammonia (green line, Figure 6.34).

Table 6.8 lists the NH_4^+ ion concentrations obtained for interactions between oxalic acid aerosols with an added 100 sccm of ammonia at both 20 and 50 %RH. Increasing the oxalic acid concentration increased the amount of ammonium ion formed. In contrast, increasing the relative humidity decreased the ammonium ion concentration. For example, on addition of 100 sccm NH_3 to 0.1 wt% oxalic and sulfuric acid aerosols, the NH_4^+ ion concentration was 1.0 ppmv at 50 %RH, while at 20 %RH it was observed to be 1.2 ppmv. The oxalic acid weight fraction was varied from 0.1 to 1 wt% while the sulfuric acid concentration remained at 1 wt%. Addition of water vapour to these aerosols changes the speciation to mainly oxalate and sulfate ions while diluting the acid concentration. Therefore, less ammonium ions are formed from the reaction of ammonia with these less concentrated acidic aerosols. The opposite observation occurs for oxalic acid which were studied as a separate system. Due to its greater solubility at higher humidities, more of the acid is deprotonated forming more ammonium ions.

Table 6.8: Ammonium ion concentrations, ppmv, recorded due to the interaction of 100 sccm ammonia gas with oxalic acid aerosols, both with 1 wt% sulfuric acid, at 20 and 50 %RH.

%wt Oxalic acid	20 %RH	50 %RH
0.1	1.2 ppmv	1.0 ppmv
1	3.3 ppmv	3.2 ppmv

Inspection of the NH_4^+ ion concentration value of malonic and succinic acid leads to the conclusion that increasing the concentration of sulfuric acid has a direct, positive effect on the amount of ammonium ions formed as illustrated in Tables 6.9 and 6.10. These tables illustrate the amount of ammonia uptake with these dicarboxylic acids separately both at a low and at a high humidity. Increasing the relative humidity decreased the ammonium ion concentration. For example, on addition of 300 sccm NH_3 to 0.5 wt% malonic and sulfuric acid aerosols, the NH_4^+ ion concentration was 0.166 ppmv at 20 %RH, while at 50 %RH it was observed to

be 0.066 ppmv. Addition of water vapour to these aerosols changes the speciation to mainly malonate and sulfate ions while obviously diluting the acid concentration. Therefore, less ammonium ions are formed from the reaction of ammonia with less concentrated acidic aerosols. The opposite trend took place for 0.5 wt % succinic and sulfuric acid solutions. 0.230 ppmv was observed at 20 %RH whereas at 50 %RH, 0.420 ppmv ammonium ion was produced. Increased carbon chain length is a possible reason to why this phenomenon occurs. Thus more solubility would occur with increasing humidity resulting in more deprotonation followed by more ammonium ion production. Discrepancies in the NO_x chemiluminesence detection limit for these weaker acidic dicarboxylic acids also cannot be ignored. It should be noted too that direct comparisons with the oxalic acid results are not facile because these set of experiments were carried out using a different calibration set-up.

Table 6.9: Ammonium ion concentrations, ppbv, ppmv, recorded as a result of the interaction of 300 sccm ammonia gas with malonic acid aerosols with sulfuric acid, at 20 and 50 %RH.

Malonic/Sulfuric wt% ratio	20 %RH	50 %RH
1 / 0.1	34 ppbv	41 ppmv
0.5 / 0.5	166 ppbv	66 ppmv
0.1 / 1	210 ppbv	64 ppmv

Table 6.10: Ammonium ion concentrations, ppbv, recorded as a result of the interaction of 300 sccm ammonia gas with succinic acid aerosols with sulfuric acid, at 20 and 50 %RH.

Succinic/Sulfuric wt% ratio	20 %RH	50 %RH
1 / 0.1	247 ppbv	200 ppbv
0.5 / 0.5	230 ppbv	420 ppbv
0.1 / 1	274 ppbv	508 ppbv

Table 6.11 shows the effect of 90 %RH when 300 sccm ammonia was reacted with varying concentrations of malonic or succinic acid with sulfuric acid. In relation to studies of these two dicarboxylic acids with ammonia at lower humidities, it is concluded that increasing humidity has a positive effect on ammonium ion production. Malonic acid interacts more with ammonia than its succinic counterpart at this humidity. These results are comparable to the previous oxalic acid and sulfuric acid studies (Table 6.8) and illustrate that the effect of acid strength decreases with increasing carbon content of the dicarboxylic acids. The pK_a also coincides with ammonium ion formation for each respective dicarboxylic acid in a similar fashion to studies involving dicarboxylic acid studies without the presence of sulfuric acid (Chapter 5). The frequent presence of gaseous ammonia absorptions in the FTIR spectra of malonic and succinic acid also reinforces this point. As evidenced by the FTIR spectra also, ammonium malonate and succinate are the main aerosols formed along with ammonium sulfate. Ammonium hydrogensuccinate also occurs with dominant concentrations of succinic acid at high humidities only.

Table 6.11: Ammonium ion concentrations, ppmv, recorded as a result of the interaction of 300 sccm NH_3 gas with 0.5 wt% malonic and succinic acid aerosols, each with 0.5 wt% sulfuric acid, at 95 %RH.

Aerosol Composition	95 %RH
1 wt % malonic acid + 0.1 wt% sulfuric acid	236 ppmv
0.5 wt % malonic acid + 0.5 wt% sulfuric acid	780 ppmv
0.1 wt% malonic acid + 1 wt% sulfuric acid	1176 ppmv
1 wt% succinic acid + 0.1 wt% sulfuric acid	140 ppmv
0.5 wt% succinic acid + 0.5 wt% sulfuric acid	515 ppmv
0.1 wt% succinic acid + 1 wt% sulfuric acid	970 ppmv

6.2.7 Summary of SMPS and NO_x data

Table 6.12 shows the particle diameter and number concentrations for sulfuric and dicarboxylic acid aerosols both individually and as mixtures. Sulfuric acid is observed to have the largest particle diameter and concentration compared to the dicarboxylic acids. Increasing the relative humidity caused a reduction in the particle diameter and an increase in particle concentration. This observation can be attributed to a change in the particle composition from the partially deprotonated ions to the fully deprotonated ions. There is a change in hygroscopicty of the ions. Deviations resulted for succinic acid as full deprotonation only occurs at humidities higher than 50 %RH. When ammonia is introduced, there is generally an increase in both particle diameter and particle concentration due to the formation of the ammonium ion. Mixtures of a dicarboxylic acid and sulfuric acid resulted in a general increase in particle diameter and concentration. These trends are also reflected in the particle distributions of these species.

Table 6.12: Particle statistics for sulfuric and dicarboxylic acids.

	20 %RH	**50 %RH**	**50 %RH + 300 sccm NH_3**
Aerosol Composition	**Diameter, Concentration (nm, × 10^6 cm^{-3})**	**Diameter, Concentration (nm, × 10^6 cm^{-3})**	**Diameter, Concentration (nm, × 10^6 cm^{-3})**
1 wt% H_2SO_4	168, 1.3	113, 3.3	126, 4.11
1 wt% $H_2C_2O_4$	60, 0.9	48, 1.3	126, 3.2
1 wt% $H_4C_3O_4$	102, 4.1	98, 3.8	126, 8.2
1 wt% $H_6C_4O_4$	98, 4.6	88, 5.2	141, 2.9
0.1 wt% $H_2C_2O_4$ + 0.1 wt% H_2SO_4	91, 1.7	71, 2.3	98, 4.3
0.5 wt% $H_4C_3O_4$ + 0.5 wt% H_2SO_4	109, 6.3	102, 7.0	106, 11.1
0.5 wt% $H_6C_4O_4$ + 0.5 wt% H_2SO_4	88, 5.7	92, 4.8	98, 3.5

It is clear that sulfuric acid is a stronger acid than the dicarboxylic acids due to the amount of ammonium ion concentration formed as shown in Table 6.13. The addition of ammonia to these acid compositions had a direct, positive effect on ammonium ion concentration. There is less reaction of ammonia with the malonic and succinic mixtures and hence less ammonium ion formation in comparison to oxalic acid. This coincides with the decrease in acidity strength of these organic species and the increase in carbon chain length. There is a marked contrast for oxalic acid species with sulfuric acid at high humidities. Increasing the humidity decreases the ammonium concentration of oxalic and sulfuric acid compositions due to dilution. The opposite observation occurs for oxalic acid studies, as a separate system. As a result of its greater solubility at higher humidities, more of the acid is deprotonated forming more ammonium ion. There is, however, a slight increase for malonic and succinic acid with sulfuric acid, particularly at humidities of 95 %RH. This is possibly due to the increased chain length of these dicarboxylic acids and more stabilisation of the deprotonated form with increasing humidity. This may lead to more reaction with ammonia but discrepancies in the NO_x chemiluminesence detection limits cannot be ignored here.

Table 6.13: Ammonium ion concentrations, ppmv, recorded as a result of the interaction of 300 sccm ammonia gas with sulfuric and dicarboxylic acid aerosols, both separately and as compositions at 20 and 50 %RH.

Aerosol Composition	20 %RH	50 %RH	95 %RH
1 wt% H_2SO_4	5.2 ppmv	5.2 ppmv	5.2 ppmv
1 wt% $H_2C_2O_4$	0.49 ppmv	4.64 ppmv	0.88 ppmv*
1 wt% $H_4C_3O_4$	-	0.16 ppmv	0.37 ppmv
1 wt% $H_6C_4O_4$	-	0.14 ppmv	0.16 ppmv
1 wt% $H_2C_2O_4$ + 1 wt% H_2SO_4	3.3 ppmv	3.2 ppmv	-
0.5 wt% $H_4C_3O_4$ + 0.5 wt% H_2SO_4	0.17 ppmv	0.66 ppmv	0.78 ppmv
0.5 wt% $H_6C_4O_4$ + 0.5 wt% H_2SO_4	0.23 ppmv	0.42 ppmv	0.52 ppmv

***This measurement was taken with a different calibration to the other [NH_4^+] values.**

Table 6.14 summarises the composition of the dicarboxylic acid aerosols on addition of water vapour and ammonia with various concentrations of sulfuric acid. The acid weight fraction of dicarboxylic acid was varied between 0.1 to 1 wt% in addition to the sulfuric acid weight fraction. It was observed that speciation within the tertiary acid systems shifted towards the most ionised form as the relative humidity was increased because of increasing proton stabilisation. At low relative humidities (20 %rh) the less ionised version of each acidic species (hydrogendicarboxylate($H_{1,3,5}C_{2,3,4}O_4^-$) for oxalic/malonic/succinic acid and bisulfate (HSO_4^-) for sulfuric acid) was more prominent while at higher relative humidities the more ionised form was evident (dicarboxylate ($C_{2,3,4}O_4^{2-}$) and sulfate (SO_4^{2-})). On addition of ammonia, ammonium dicarboxylate and ammonium sulfate are the prominent species observed. However with higher concentrations of the organic species, the hydrogendicarboxylate is also present, a notable difference compared to those made within individual dicarboxylic acids. Ammonium sulfate is the dominant ion in compositions containing more sulfuric acid component.

Table 6.14: Dicarboxylic acid aerosol composition at various additions of sulfuric acid at 20, 50 %RH and at 50 %RH with 300 sccm NH_3.

Aerosol	Composition 20 %RH	Composition 50 %RH	Composition 50 %RH+300 sccm NH_3
1 wt% $H_2C_2O_4$ + 0.1 wt% H_2SO_4	mainly $HC_2O_4^-$	HC_2O_4 $C_2O_4^{2}$ + SO_4^{2-}	NH_4^+ $HC_2O_4^-$ $C_2O_4^{2-}$ + NH_4^+ SO_4^{2-}
0.1 wt% $H_2C_2O_4$ + 1 wt% H_2SO_4	mainly HSO_4^-	$C_2O_4^{2-}$ + HSO_4^- SO_4^{2-}	NH_4^+ $C_2O_4^{2-}$ + NH_4^+ SO_4^{2-}
1 wt% $H_4C_3O_4$ + 0.1 wt% H_2SO_4	-	-	NH_4^+ $H_5C_3O_4^-$ $H_4C_3O_4^{2-}$ + NH_4^+ SO_4^{2-}
0.1 wt% $H_4C_3O_4$ + 1 wt% H_2SO_4	mainly HSO_4^-	-	NH_4^+ SO_4^{2-}
1 wt% $H_6C_4O_4$ + 0.1 wt% H_2SO_4	$H_5C_4O_4^-$ + HSO_4^-	$H_5C_4O_4^{2-}$ + SO_4^{2-}	NH_4^+ $H_5C_4O_4^-$ $H_4C_4O_4^{2-}$ + NH_4^+ SO_4^{2-}
0.1 wt% $H_6C_4O_4$ + 1 wt% H_2SO_4	mainly HSO_4^-	$H_5C_4O_4^{2-}$ + SO_4^{2-}	NH_4^+ SO_4^{2-}

6.3 Conclusion

The interactions between dicarboxylic and sulfuric acids (and with ammonia) has not previously been investigated. Therefore the results presented here are novel to the field of tropospheric aerosol chemistry.

Table 6.15 lists the possible reactions occurring in the novel atmospheric aerosols studied.

Table 6.15: Chemical reactions occurring in aerosols containing $H_xC_xO_4$, NH_3 and water.

$H_{2,4,6}C_{2,3,4}O_4 \leftrightarrow H^+ + H_{1,3,5}C_{2,3,4}O_4^-$
$H_{1,3,5}C_{2,3,4}O_4^- \leftrightarrow H^+ + H_{2,4}C_{2,3,4}O_4^{2-}$
$NH_3 + H_{2,4,6}C_{2,3,4}O_4 \leftrightarrow NH_4\ H_{1,3,5}C_{2,3,4}O_4$
$2NH_3 + H_{2,4,6}C_{2,3,4}O_4 \leftrightarrow (NH_4)_2\ C_{2,3,4}O_4$
$NH_4\ H_{1,3,5}C_{2,3,4}O_4 \leftrightarrow NH_4^+ + H^+ + C_{2,3,4}O_4^{2-}$
$(NH_4)_2\ C_{2,3,4}O_4 \leftrightarrow 2NH_4^+ + C_{2,3,4}O_4^{2-}$

Bisulfate aerosols at low humidity (20 %RH) prevailed while dicarboxylate type particles were dominant at higher humidities (50 %RH). Inspection of the mean particle diameter showed that it decreased on addition of water vapour. This, also, indicated the change in the particle composition from bisulfate to dicarboxylate. At low concentrations of these acids, the composition of the aerosol was primarily a mixture of bisulfate and hydrogendicarboxylate ions. The aerosol composition changed from a mixture of bisulfate ions and hydrogendicarboxylate ions to primarily bisulfate on increasing the sulfuric acid weight fraction.

The reaction of these aerosols with ammonia resulted in the formation of two main products: ammonium sulfate ($(NH_4)_2SO_4$) and ammonium dicarboxylate ($(NH_4)_2C_{2,3,4}O_4$) at 20 %RH. Increasing the sulfuric acid weight removed the

hydrogendicarboxylate and dicarboxylate ion species and the predominant aerosol consisted of ammonium sulfate. Increasing the sulfuric acid fraction also increased the concentration of ammonium ions. With a greater dicarboxylic acid concentration, particularly at high humidities, ammonium hydrogendicarboxylate was a unique species observed. This chemistry does not readily occur in the bulk phase and is usually perceived as an intermediate step.

Such original and complex systems involving organic and inorganic species are important mimics of current tropospheric aerosol chemistry. Organics that have long chain non-polar groups attached to polar tails can form a surface film on droplets by lining up with the polar ends in the water and non-polar, hydrophobic ends projecting into air as shown in Figure 1.11 [(1),(58)] and Figure 6.35. These organic films have the following effects; {1} Reduction of the rate of evaporation of water from the droplets, {2} Inhibition of the transport of stable molecules and of highly reactive free radicals such as OH and HO_2 from the gas phase into the droplet (possibly reducing their roles in atmospheric aqueous phase oxidations such as conversion of SO_2 to H_2SO_4 [(59)]) and {3} Reduction of the efficiency with which the particles are scavenged by larger cloud and rain droplets. Thus the presence of organic films may increase the lifetime of such particles in the atmosphere compared to those expected if the films were not present [(60),(61)].

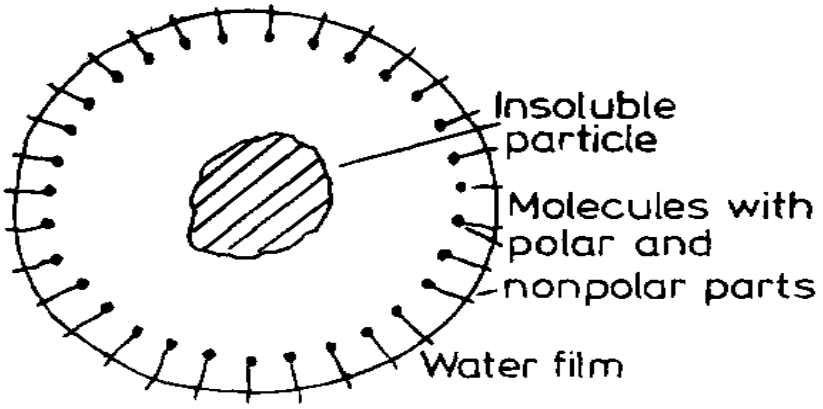

Figure 6.35: Depicting the formation of an organic film in aged atmospheric aerosols [(57)].

6.4 References

(1) Noonan, C. '*A Laboratory Study of Heterogeneous Chemistry between Ammonia and Acidic Particles relevant to the Troposphere'*, Ph.D Thesis: University College Cork, Ireland, 2007.

(2) Wexler, A.; Seinfield, J. H. *Atmospheric Environment* **1991**, *25*, 2731-2748.

(3) Saxena, P. L.; Hildemann, L. M.; McMurray, P. H.; Seinfield, J. H. *Journal of Geophysical Research* **1995**, *100*, 18755-18770.

(4) Rubel, G. O.; Gentry, J. W. *Journal Aerosol Science* **1985**, *16*, 571-574.

(5) Brauer, M.; Koutrakis, P.; Spengler, J. D. *Environmental Science & Technology* **1989**, *23*, 1408-1412.

(6) Suh, H. H.; Spengler, J. D.; Koutrakis, P. *Environmental Science & Technology* **1992**, *26*, 2507-2517.

(7) Tidy, G.; Cape, J. N. *Atmospheric Environment Part A - General Topics* **1993**, *27*, 2235-2237.

(8) Wilson, W. E.; Suh, H. H. *Journal of the Air & Waste Management Association* **1997**, *47*, 1238-1249.

(9) Asman, W. A. H.; Janssen, A. J. *Atmospheric Environment* **1987**, *21*, 2099-2119.

(10) Bauer, S. E.; Balkanski, Y.; Schulz, M.; Hauglustaine, D. A.; Dentener, F. *Journal of Geophysical Research-Atmospheres* **2004**, *109*.

(11) Brost, R. A.; Delany, A. C.; Huebert, B. J. *Journal of Geophysical Research-Atmospheres* **1988**, *93*, 7137-7152.

(12) Horvath, H. *Atmospheric Environment Part A-General Topics* **1993**, *27*, 293-317.

(13) Tang, I. N.; Munkelwitz, H. R. *Atmospheric Environment Part A - General Topics* **1993**, *27*, 67-473.

(14) Sisler, J. F.; Malm, W. C. *Atmospheric Environment* **1994**, *28*, 851-862.

(15) Jacob, D. J. *Atmospheric Environment* **2000**, *34*, 2131-2159.

(16) Carslaw, K. S.; Clegg, S. L.; Brimblecombe, P. *Journal of Physical Chemistry* **1995**, *99*, 11557-11574.

(17) Tabazadeh, A.; Toon, O. B. *Geophysical Research Letters* **1998**, *25*, 1379-1382.

(18) Zhang, R. Y.; Wooldridge, P. J.; Molina, M. J. *Journal of Physical Chemistry* **1993**, *97*, 8541-8548.

(19) Altwicker, E. R.; Johannes, A. H. *Atmospheric Environment* **1987**, *21*, 129-135.

(20) Vong, R. J. *Atmospheric Environment Part A - General Topics* **1990**, *24*, 1007-1018.

(21) Talbot, R. W.; Dibb, J. E.; Loomis, M. B. *Geophysical Research Letters* **1998**, *25*, 1367-1370.

(22) Adams, P. J.; Seinfeld, J. H.; Koch, D. M. *Journal of Geophysical Research-Atmospheres* **1999**, *104*, 13791-13823.

(23) Brown, M. P; Austin, K. *Applied Physical Letters* **1994**, *65*, 2503-2504.

(24) Wang, R.T. *Classic Physiques* **1997**, 212-213.

(25) Smith, C. D.; Jones, E. F. AIP *Conference Proceedings 429, New York: American Institute of Physics* **1998**, 651-654.

(26) Matsumoto, K.; Tanaka, H. *Atmospheric Environment* **1996**, *30*, 639-648.

(27) Zhang et al. "Properties of nitrate, sulfate and ammonium in typical polluted atmospheric aerosols (PM10) in Beijing" Article in Press.

(28) Finlayson-Pitts, B. J.; Pitts Jr., J. N. *Chemistry of the Upper and Lower Atmosphere*; Academic Press: San Diego, **2000**.

(29) Aneja, V. P.; Kim, D. S. *Air Waste* **1993**, *43*, 1074-1083.

(30) Jacob, D. J.; Hoffman, M. R. *Journal of Geophysical Research* **1983**, *88C*, 6611-6621.

(31) Brooks, S. D.; Wise, M. E.; Cushing, M.; Tolbert, M. A. *Geophysical Research Letters* **2002**, *29*.

(32) Choi, M. Y.; Chan, C. K. *Environmental Science & Technology* **2002**, *36*, 2422-2428.

(33) Cruz, C. N.; Pandis, S. N. *Environmental Science & Technology* **2000**, *34*, 4313-4319.

(34) Prenni, A. J.; De Mott, P. J.; Kreidenweis, S. M. *Atmospheric Environment* **2003**, *37*, 4243-4251.

(35) Hameri, K.; Charlson, R.; Hansson, H. C. *Aiche Journal* **2002**, *48*, 1309-1316.

(36) Svenningsson, B.; Rissler, J.; Swietlicki, E.; Mircea, M.; Bilde, M.; Facchini, M. C.; Decesari, S.; Fuzzi, S.; Zhou, J.; Monster, J.; Rosenorn, T. *Atmospheric Chemistry and Physics* **2006**, *6*, 1937-1952.

(37) Lightstone, J. M.; Onasch, T. B.; Imre, D.; Oatis, S. *Journal of Physical Chemistry A* **2000**, *104*, 9337-9346.

(38) Parsons, M. T.; Knopf, D. A.; Bertram, A. K. *Journal of Physical Chemistry A* **2004**, *108*, 11600-11608.

(39) Braban, C. F.; Abbatt, J. P. D. *Atmospheric Chemistry and Physics* **2004**, *4*, 1451-1459.

(40) Wise, M. E.; Surratt, J. D.; Curtis, D. B.; Shilling, J. E.; Tolbert, M. A. *Journal of Geophysical Research-Atmospheres* **2003**, *108*.

(41) Marcolli, C.; Luo, B. P.; Peter, T. *Journal of Physical Chemistry A* **2004**, *108*, 2216-2224.

(42) Clegg, S. L.; Seinfeld, J. H.; Brimblecombe, P. *Journal of Aerosol Science* **2001**, *32*, 713-738.

(43) Andrews, E.; Larson, S. M. *Environmental Science & Technology* **1993**, *27*, 857-865.

(44) Wagner, J.; Andrews, E.; Larson, S. M. *Journal of Geophysical Research-Atmospheres* **1996**, *101*, 19533-19540.

(45) Hansson, H. C.; Rood, M. J.; Koloutsou-Vakakis, S.; Hameri, K.; Orsini, D.; Wiedensohler, A. *Journal of Atmospheric Chemistry* **1998**, *31*, 321-346.

(46) Dick, W. D.; Saxena, P.; McMurry, P. H. *Journal of Geophysical Research-Atmospheres* **2000**, *105*, 1471-1479.

(47) Saxena, P.; Hildemann, L. M.; McMurray, P. H.; Seinfeld, J. H. *Journal of Geophysical Research* **1995**, *100*, 18755-18770.

(48) Mircea, M.; Facchini, M. C.; Decesari, S.; Fuzzi, S.; Charlson, R. J. *Tellus Series B-Chemical and Physical Meteorology* **2002**, *54*, 74-81.

(49) Daumer, B.; Niessner R.; Klockow, D. *Journal Aerosol Science* **1992**, *23*, 315-325.

(50) Hug, S. J.; Bahnemann, D. *Journal of Electron Spectroscopy and Related Phenomena* **2006**, *150*, 208-219.

(51) George, Ch.; El Rassy, H.; Chovelon, J. M. *International Journal of Chemical Kinetics* **2001**, *33*, 539-547.

(52) Rousse, D.; George, Ch. *Physical Chemistry Chemical Physics* **2004**, *6*, 3408-3414.

(53) Dimroth, P.; Hilbi, H. *Molecular Microbiology* **1997**, *25(1)*, 3-10

(54) Czizio, D. J.; Abbatt, J. P. D. *Journal of Geophyscial Research-Atmospheres* **1999**, *104*, 13781-13790.

(55) Braban, C. F.; Carroll, M. F.; Styler, S. A.; Abbatt, J. P. D. *Journal of Physical Chemistry A* **2003**, *107*, 6594-6602.

(56) Tember, G. A; Panaeva, S. A; Volkov, Y. M. *Infra red spectra of sulfocarboxylic and sulfosuccinic acids – Journal written in Russian* **1973**, *12*, 52-54.

(57) Brandt, C.; van Eld, R. *Chemical Reviews* **1995**, *95*, 119-190.

(58) Lefer, B. L.; Talbot, R. W. *Journal of Geophysical Research-Atmospheres* **2001**, *106*, 20365-20378.

(59) Gill, P. S., Graedal, T. E.; Weschler, C. J. *Review of Geophysical Space Physics* **1983**, *21*, 903.

(60) Chameides, W. L.; Davis, D. D. *Journal of Geophysical Research* **1982**, *87*, 4863.

(61) Toosoi, R; Novakov, T. *Atmospheric Environment* **1985**, *19*, 125.

Chapter 7

Summary

7.1 Overview

This chapter provides a summary of the main experiments and results of this thesis which are of direct relevance to processes occurring within the field of tropospheric chemistry. An improved understanding of heterogeneous aerosol chemistry is dependent on a close collaboration between laboratory experiments, field measurements and atmospheric modelling. Attempts must be made to bridge the gap between these areas by using laboratory techniques to examine the dynamics of multi-component and multiphase aerosols under conditions relevant to the atmosphere. By doing so, the research community will be a in a position to view the 'bigger picture' and to put these results into context with the current state of knowledge of atmospheric chemistry.

Although the general approach – the measurement of the loss of a gas-phase species upon aerosol distribution of varying concentration – is similar to other aerosol flow-tube experiments, the instrumental detection techniques that were used in this current study are somewhat different from those previously employed. The apparatus designed to conduct the experiments was based on an aerosol flow-tube instrument adapted for NH_3-monitoring instrumentation. This instrument was used to obtain simultaneous optical and size distribution measurements using FTIR spectroscopy and SMPS measurements respectively as a function of relative humidity and aerosol composition. The system was undertaken mainly to study the interaction between acid containing aerosols with trace gases as opposed to bulk solutions. Constant flows of sub-micron particles (either acidic species or ionic salts) were generated and closely resemble those found in the atmosphere. These were then passed through a vertically aligned laminar flow reactor, with gaseous species (ammonia in this case) introduced *via* a sliding injector. This apparatus is unique, in that it employed two aerosol generation methods and included instrumentation to follow the size evolution of the aerosol particulate matter while simultaneously allowing detailed spectroscopic investigation of its chemical content. In addition, an Ostwald type reaction coupled with a chemiluminescence

NO_x monitor was used to quantify ammonium species. Also of interest is the fact that it was possible to vary the relative humidity of the system between 1 and 90 %RH, thus simulating conditions that are present in the atmosphere.

7.2 Discussion

The notion that human activities may endanger the Earth's environment has emerged as a leading societal concern in the post-industrial era. Under the ever increasing pressures of population growth and economic development, the problems of air pollution have now become matters of both local and global concern. Although the Earth's atmosphere is predominantly gaseous, with 90% of the atmosphere's bulk residing in the troposphere [(1)], the observations of such phenomena as acid rain and photochemical smog confirm the role of aerosols in mediating important atmospheric chemical reactions [(2)]. Heterogeneous chemistry, both in the troposphere and in the laboratory, involves a series of processes which combine to determine the overall rate of transport and chemical reaction between the gas and condensed phases. Condensed-phase reactions in the bulk of an aerosol particle and heterogeneous reactions on the particle surface can provide alternative reaction pathways to those that can occur in the homogeneous gas phase.

Sulfurous acid (H_2SO_3) has never been characterised or isolated on Earth. This is related to the unfavourable conditions for the hydration product of SO_2 within the atmosphere [(3)]. $SO_2.H_2O$ is an important species as it represents the first intermediate in the overall oxidation of sulfur dioxide to sulfuric acid in the atmosphere. Aqueous sulfur (IV) solutions are ubiquitous in the atmosphere due to the large anthropogenic emissions of sulfur dioxide gas. In this study, dissolved suspensions of sulfur dioxide in deionised water were employed to produce gaseous, aqueous and aerosol SO_2.With the addition of ammonia, the main species produced were hydrogen sulfite tautomers (hydrogen sulfonate and bisulfite) and disulfite (pyrosulfite) which were more prevalent at high humidities enhancing the aqueous nature of sulfur (IV) species. At high concentrations of ammonia (300

sccm) and at low humidities (20 %RH), however, gaseous ammonia was present suggesting the weak acidity of these anions. The weak acidic nature is further enhanced regarding the [NH_4^+]. When increasing the humidity for the $SO_2.H_2O$ and NH_3 systems, the ammonium concentration decreased indicating the hygroscopicity of these aerosols and the uptake of water on the aerosol causing dilution.

Tropospheric chemical studies have turned more and more towards investigating the effects of organic compounds on the oxidation of S(IV) ions. No prior studies on correlating speciation and size behaviour of dicarboxylic acids in the presence of 'sulfurous' acid (and ammonia) have been performed. Aqueous oxalic and 'sulfurous acid' dispersions of particles consist of a mixture of hydrogenoxalate, oxalate, hydrogensulfite tautomers, sulfite and disulfite ions in addition to oxalic and 'sulfurous acid'. Hydrogensulfite and disulfite are the main components in 'sulfurous' dominant studies whereas hydrogenoxalate and oxalate are the main components in 'oxalic' dominant studies. It was observed that speciation within the tertiary acid systems shifted towards the most ionised form as the relative humidity was increased because of increasing proton stabilisation. At low relative humidities (20 %RH) the less ionised form of each acidic species (hydrogenoxalate ($HC_2O_4^-$) for oxalic acid and sulfur dioxide (SO_2) for $SO_2.H_2O$) was more prominent while at higher relative humidities the more ionised form was evident (oxalate ($C_2O_4^{2-}$). More aqueous sulfur dioxide absorptions were also observed, a notable difference to the independent $SO_2.H_2O$ studies. With the introduction of ammonia, oxalate was again observed as well as hydrogensulfite and disulfite ions, the latter species being more prevalent. Increasing the oxalic acid concentration and the relative humidity increased the amount of ammonium ion formed. Addition of ammonia led to more reaction with oxalic acid aerosols, mainly at high humidities, however interactions with ammonia and the 'sulfurous' component were observed more at low humidities, albeit with lower ammonium ion production.

Ammonia (NH_3), and its reaction product, ammonium ion (NH_4^+), are important atmospheric components, NH_3 being the most abundant alkaline component in the

atmosphere [4]. Ammonia is a key player in the partitioning of atmospheric sulfates and nitrates, and yet very few studies to date have been dedicated to elucidating its heterogeneous behaviour. The relevance of ammonia to the atmospheric environment lies mainly in its contribution to N deposition to land surfaces and water bodies, which often leads to euthrophication and/or acidification [5]. However, it also has the capacity to neutralise atmospheric acids. A substantial part of the acid generated in the atmosphere, by the oxidation of sulfur dioxide (SO_2) and nitrogen oxides (NO_x), is neutralised by ammonia as attested by the high concentration of particulate ammonium in the troposphere [6]. Ammonia is the predominant airborne gaseous base, and, as such, holds an important place in atmospheric chemistry. Since it is the only soluble base found in the atmosphere in significant quantities, it plays a principal role in neutralising acidic aerosols converting them to new non-volatile aerosol particles. This process of neutralisation influences the aqueous oxidation rates of S(IV) species and the formation of new aerosols. From a variety of previous measurements, the lifetime of ammonium aerosol has been determined to be of the order of ~ 4 days, in which time it can travel 100 – 1000 km.

There is an increasing recognition that organic acids may contribute significantly to the total acid burden and indeed may represent the majority of acidic species even in polluted urban environments. The sources of dicarboxylic acids include direct emissions from fossil fuel combustion and photochemical oxidation of organic precursors of both anthropogenic and biogenic origin. They make an important contribution to the modification of radiative properties and indirect aerosol forcing. These compounds are hygroscopic and have recently received much attention due to their potential effects on direct cloud formation and can also potentially act as cloud condensation nuclei (CCN). Of these dicarboxylic acids, oxalic is generally the most abundant succeeded by malonic and succinic acid in atmospheric aerosols [7]. Hydrogendicarboxylate ions are observed at 20 %rh. Increasing the humidity to 50 and 70 %RH changes the speciation of the aerosols to a mainly dicarboxylate ion composition with some hydrogendicarboxylate ions remaining. With addition of ammonia, ammonium dicarboxylate ions were formed. Gaseous ammonia

absorptions were regularly seen in malonic acid FTIR experiments and the ammonium deformation absorption was absent suggesting a lack of interaction between ammonia with malonic acid; Ammonium malonate was found to be present at extremely high humidities only. Succinic acid studies compare to oxalic acid rather than malonic acid due to their similar solubilities. However in contrast; the hydrogensuccinate ion was found to be present with addition of ammonia at higher humidities (60 %RH). Higher humidities were needed for ammonium succinate to form. A change was also observed in the particle composition from the partially deprotonated ions to the fully deprotonated ions. This behaviour is due to the change in hygroscopicty of the ions. Increasing the dicarboxylic acid concentration increased the amount of ammonium ion formed. In addition, increasing the relative humidity increased the ammonium ion concentration. As previously mentioned, the solubility of dicarboxylic acid increases at higher humidities, resulting in more acid dissociating to produce hydrogencarboxyalate and the fully deprotonated ion. There is less reaction between ammonia with the deprotonated malonic and succinic species and hence less ammonium ion formation (in comparison to the oxalic acid case). These observations coincide with the decrease in acidic strength of these organic species and the increase in carbon chain length.

The interaction between dicarboxylic acids and sulfuric acid has not been previously investigated. Therefore the results presented here are novel to the field of tropospheric chemistry. Hydrogendicarboxylate and bisulfate are the main species present at low humidities for mixtures of oxalic and sulfuric acid. Dicarboxylate ions are the prevalent species at high humidities. With the introduction of ammonia, ammonium dicarboxylate and ammonium sulfate are the main species observed. However with increasing concentrations of dicarboxylic acid, ammonium hydrogendicarboxylate is also present. Ammonium sulfate is favoured more at low humidities whereas ammonium oxalate is the dominant species at high humidities. It is clear that sulfuric acid is the stronger acid due to the greater increases of $[NH_4^+]$. In addition, increasing the relative humidity decreased the ammonium ion concentration for oxalic-sulfuric acid studies (a marked difference to oxalic acid

studies as a separate system), yet there were minor changes for malonic and succinic acid with sulfuric acid. With a greater dicarboxylic acid concentration, particularly at high humidities, ammonium hydrogendicarboxylate was a unique species observed. This process does not readily occur in the bulk phase and is usually perceived as an intermediate step.

On a final note, heterogeneous chemistry needs to be better characterised in laboratory studies, with results implemented into multiphase chemistry models. These, subsequently, have to be coupled to microphysical models, to be tested in field experiments with regards to their ability to describe measured gas phase trace gas and oxidant concentrations, cloud water constituent concentrations and chemical aerosol composition in the tropospheric system. Novel laboratory research into atmospheric chemistry can then make progressive steps to understanding the environmental issues in our world.

7.3 References

(1) Seinfeld, J. H.; Pandis, S. N. *Atmospheric Chemistry and Physics*; Wiley-Interscience., 1997.

(2) Reid, J.; Sayer, R. *Science Progress* **2002**, *85*, 263-296.

(3) Voegele, A.F.; Loerting T.; Tautermann, C.S.; Hallbrucker, A.; Mayer E.; Liedl, K.R. *Icarus* **2004**, *169*, 242-249.

(4) Asman, W. A. H.; Sutton, M. A.; Schjorring, J. K. *New Phytologist* **1998**, *139*, 27-48.

(5) Fowler, D.; Sutton, M. A.; Smith, R. I.; Pitcairn, C. E. R.; Coyle, M.; Campbell, G.; Stedman, J. *Environmental Pollution* **1998**, *102*, 337-342.

(6) Finlayson-Pitts, B. J.; Pitts Jr., J. N. *Chemistry of the Upper and Lower Atmosphere.*; Academic Press, 2000.

(7) Chebbi, A.; Carlier, P. *Atmospheric Environment*, **1996**, 30, 4233-4249.